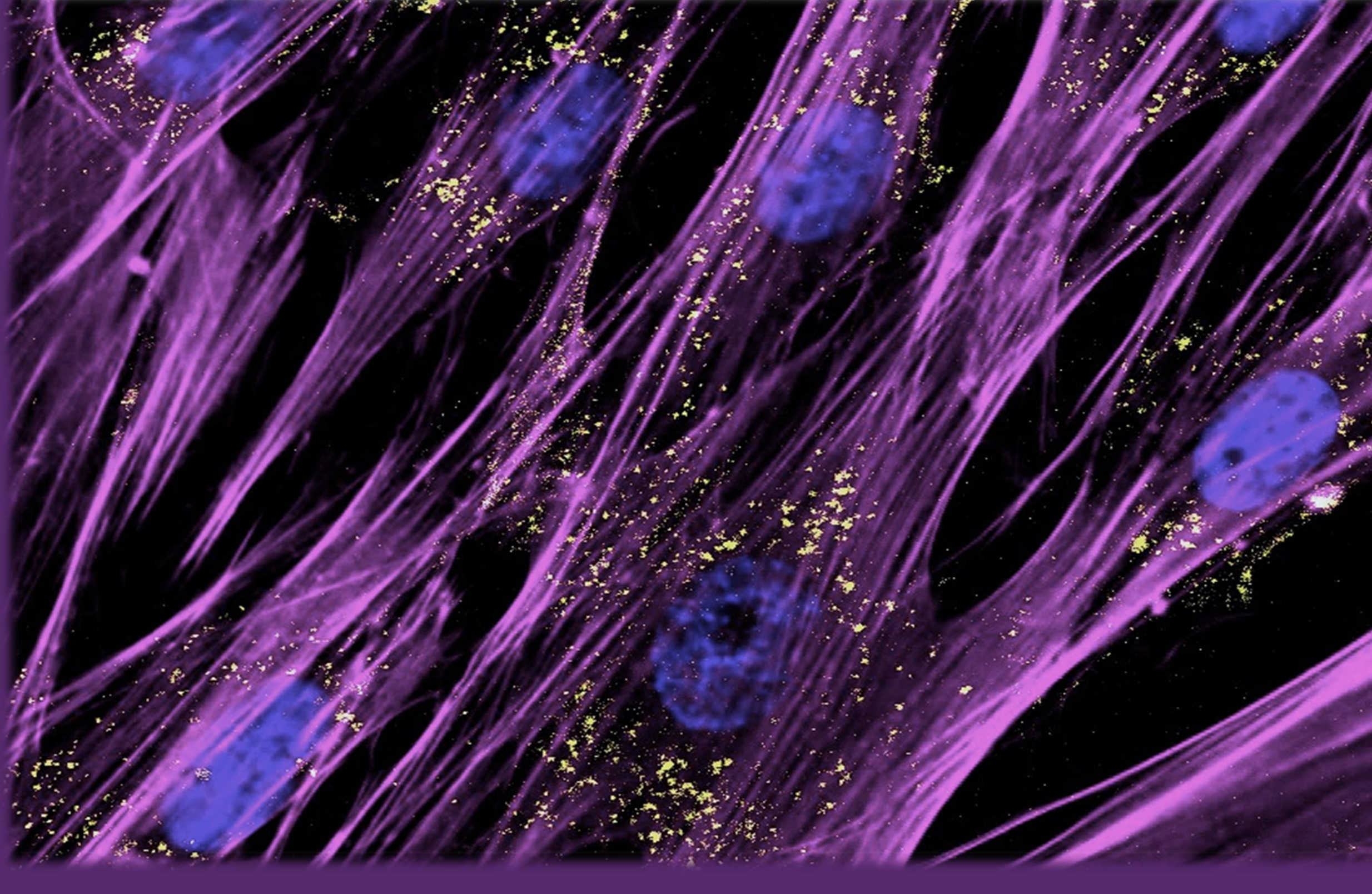

TESIS DOCTORAL

PROGRAMA DE DOCTORADO EN BIOCIENCIAS MOLECULARES
Departamento de Biología Molecular
Facultad de Ciencias
Universidad Autónoma de Madrid

Therapeutic applications of dendritic nanosystems against viral infections: Human Immunodeficiency Virus Type 1, Herpes Simplex Virus Type 2 and Human Cytomegalovirus

Elena Royo Rubio

Madrid, 2022

Universidad Autónoma de Madrid

Departamento de Biología Molecular
Facultad de Ciencias
Universidad Autónoma de Madrid

TESIS DOCTORAL

Therapeutic applications of dendritic nanosystems against viral infections: Human Immunodeficiency Virus Type 1, Herpes Simplex Virus Type 2 and Human Cytomegalovirus.

Memoria presentada por la graduada en Biotecnología
Elena Royo Rubio

Directores de tesis
Dra. Mª Ángeles Muñoz Fernández
Dr. José Luis Jiménez Fuentes

Lugar de realización
Sección de Inmunología
Laboratorio de Inmuno-Biología Molecular
Hospital General Universitario Gregorio Marañón

Madrid, 2022

Los doctores José Luis Jiménez Fuentes y Mª Ángeles Muñoz Fernández, Jefe de Sección del Servicio de Inmunología y directora del BioBanco VIH de Hospital General Universitario Gregorio Marañón,

CERTIFICAN QUE,

El trabajo de investigación y la redacción de la Tesis Doctoral titulada: **"Therapeutic applications of dendritic nanosystems against viral infections: Human Immunodeficiency Virus Type 1, Herpes Simplex Virus Type 2 and Human Cytomegalovirus"** ha sido realizado por Elena Royo Rubio bajo nuestra dirección. Revisado el trabajo, consideramos éste como satisfactorio y autorizamos su presentación y defensa para optar al grado de Doctor por la Universidad Autónoma de Madrid.

Y para dar constancia de ello, firmamos el presente documento.
Madrid, 13 de junio de 2022

Fdo. Dr José Luis Jiménez Fuentes

Fdo. Dra. Mª Ángeles Muñoz Fernández

ACKNOWLEDGEMENTS

En primer lugar quería agradecer a la Dra. Mª Ángeles Muñoz Fernández la confianza que me dio hace cuatro años de unirme al grupo y la oportunidad que me concedió, menos de un año después, para que realizase esta tesis doctoral bajo su dirección. También quería agradecerle al Dr. José Luís Jiménez Fuentes que haya sido el codirector de este trabajo, muchas gracias por tu apoyo durante este tiempo; te hemos echado mucho de menos.

En segundo lugar quiero agradecer a todos mis compañeros del laboratorio por toda la ayuda que me han prestado desde que comencé. Quiero dar gracias especialmente y por orden alfabético, para que no se enfade nadie, a los pilares fundamentales sobre los que se ha sustentado mi tesis. Sé que siempre se dice aquello de "sin vosotros no habría sido posible" pero vosotros más que nadie sabéis que en nuestro caso ha sido real al cien por cien, mil por mil. Chusa, estoy inmensamente agradecida por todo lo que has hecho por mi durante este tiempo, tanto a nivel profesional como personal. Gracias por mezclar entre algún que otro grito y amenaza tantos conocimientos y consejos. Gracias por que nunca haya hecho falta que te pidiese ayuda porque antes de decirlo ya estabas manejando la situación, ya sea poniendo en marcha un experimento, levantando el teléfono, yendo de compras, siendo la voz de la justicia, llevándome al médico o cualquiera de las otras cien mil cosas en las que me has ayudado. Lola, no he tenido la oportunidad de compartir mucho tiempo contigo, pero estas últimas semanas sentadas juntas he podido disfrutar mucho. Gracias por tener siempre una sonrisa en la cara, unas palabras para serenarnos a todos y por tener siempre un "qué asqueroso" que añadir. Marian, se está poniendo muy de moda un término que te define perfectamente: "persona vitamina". Tú eres exactamente eso, una persona empática, optimista, con sentido del humor y con una energía envidiable. Eres capaz de recargar las pilas a cualquiera, hasta el punto de hacer que sea capaz de soportar una hora de boxeo de Borja y de incluso hacerlo entre risas. Quiero darte las gracias por haber estado a mi lado todo este tiempo, gracias por escucharme siempre aunque te contase lo mismo una y otra vez. Nacho grande, no hay mucha gente que defienda sus ideas y convicciones con tanto ahínco como tú. Desde el otro lado del charco te van a quedar un poco lejos estos agradecimientos pero quiero que sepas que he disfrutado mucho de los años que hemos compartido. Muchas gracias por las risas, los consejos, los capotes, por amenizar el cuarto de cultivos con música y por muchas otras cosas. Nacho pequeño, a ti quiero agradecerte que hayas sido mi mentor desde el segundo mes que entré a este laboratorio y no hayas pedido que te sustituyese nadie, soy consciente de que no es fácil aguantarme durante tanto tiempo. Muchas gracias por haberme enseñado tanto sobre virus, miRNAs, dendrímeros y alguna otra cosa que no tiene nada que ver con el laboratorio. Una mención especial para tu tranquilidad y calma, a veces pueden rozar la pachorra, pero nos han sido tremendamente útiles en más de una ocasión. Vane, siempre recordaré tú primer día en el laboratorio, apenas dos semanas después del mío, esperando en la puerta del pasillo mientras te estirabas la manga del jersey escondiéndote las manos. A pesar de ese aspecto, a primera vista, nervioso y vergonzoso eres increíblemente fuerte, madura, responsable, paciente y generosa. Sobre todo esto último, siempre estás dispuesta a echar una mano a quien lo necesite y, en numerosas ocasiones, esa persona he sido yo. Muchas gracias por haber estado siempre ahí, por todas esas tardes que te has quedado conmigo, por todas las veces que te has ofrecido a ayudar tanto en asuntos profesionales como, sobre todo, personales. No solo eres generosa con tu tiempo, un día incluso me

regalaste tu montadito de bacón y queso, te estaré eternamente agradecida por eso especialmente. Gracias también a Elena y al resto de Inmuno I, he aprendido lecciones muy valiosas durante mi etapa allí. Al resto de miembros de Biobanco, Cristina, Jorge, Coral, Elba y Roxana, muchas gracias por haber estado dispuestos siempre a ayudar en cuanto os he pedido algo, espero no haber sido demasiado pesada en todas mis visitas allí.

Por otro lado, quería agradecer a otros miembros del Instituto la ayuda continuada que me han brindado durante estos cuatro años. Gracias a Miguel, Laura, Rafa, Marjorie y a sus chicos y chicas por haberme ayudado cada vez que lo he necesitado y haber lidiado con mis errores y mis nervios siempre con mucha paciencia y una sonrisa. Gracias por vuestros consejos y lecciones, me habéis guiado en muchos pasos a lo largo de este tiempo. También quería agradecer al grupo de la UAH, especialmente a Rafa, Paula, Tania y Sánchez-Nieves su paciencia y su buena disposición ante cualquier petición con la que les sorprendiésemos.

Mi siguientes agradecimientos van para esa familia que dicen que se elige, a mis amigos de toda y para toda la vida. Beatriz, Jesús, Diego e Irene vosotros no os merecéis un agradecimiento sino un premio por casi 28 años de amistad conmigo. Estoy tremendamente agradecida de que, aunque cada uno llevemos vidas en un sitio diferente, cuando nos juntemos parezca que no ha cambiado nada. Alba, la nostra amistat no té tants anys, però ho pareix; gràcies per tots els riures. Gràcies per confiar en mi més que jo mateixa. A todos vosotros y a los que no he nombrado, muchas gracias por tener siempre unas palabras de aliento.

Jesús, a ti podría agradecerte que me hayas acompañado durate todo este tiempo. Podría agradecerle a la suerte que nos pusiese en la misma clase de inglés en una academia cualquiera de una ciudad cualquiera de Inglaterra hace cinco años y de que me mostrase tan claramente que eres la persona con la que deseo pasar lo que me quede de vida (o a ti, según se tercie). Podría agradecerte tu cariño, respeto, confianza, alegría, humor y hasta tu paciencia en contadas ocasiones; podría agradecerte incluso que me hayas demostrado que eres la mano a la que siempre me voy a poder agarrar, pase lo que pase. Pero como no quieres que te ponga en los agradecimientos, pues nada. Así que aprovecho tu espacio para agradecerle a una de las familias que no se elige sino que te toca, la política, lo bien que me han acogido desde el primer día. Gracias Juana, Almudena y a todos los demás, incluidos vecinos de la Ossa de Montiel, por estar siempre pendientes de mi trabajo, aunque no tuvieseis claro del todo en qué consiste.

Por supuesto, muchísimas gracias a toda mi familia por todo su apoyo durante estos años, sé que a más de uno se os han hecho largos. Papà, Mamà i Héctor, a vosaltres us he deixat per al final perquè es la part que més em costa d'escriure sense emocionar-me. Moltes gràcies pel suport incondicional que m'heu donat durant tota meua vida. Gràcies per haver confiat en mi i haver estat sempre al meu costat inclús quan em vaig tornar l'adolescent més insuportable del planeta. Gràcies per tots els sacrificis que heu hagut de fer per a assegurar-vos que podia aconseguir cadascun dels meus propòsits. Heu sigut el millor referent i guia de com ha de ser una persona, intente paréixer-me a vosaltres cada dia. Espere que estigueu orgullosos d'aquest treball, és el meu objectiu principal en cada pas que done. No ens ho diem mai, però vos estime moltíssim.

SUMMARY

Despite being the cause of epidemics for thousands of years, the study of viruses is relatively young. However, the appearance of previously unknown viruses and the spread of already known viruses in new areas have led to a massive increase in virology research. Refined approaches in the study of viruses have allowed for an in depth understanding of the molecular, evolutionary, and epidemiological aspects of viruses, which has reduced the mortality and morbidity of these infectious diseases. Nevertheless, viral infections remain one of the major global health problems, mostly in vulnerable populations such as immunocompromised patients and people from developing countries.

To illustrate, the global population living with Human Immunodeficiency Virus-1 (HIV-1) exceeds 37 million people and each year there are more than 1,5 million new infections. Another sexually transmitted viral pathogen is Herpes Simplex Virus-2 (HSV-2), the causative agent of more than 490 million infections around the world. However, sexual transmission is not the only way by which viral pathogens are widely disseminated, for example Human Cytomegalovirus (HCMV), which affects more than 50% of the global population and reaches values of more than 90% in some regions, is mostly acquired during childhood or through organ transplant or blood transfusion. There are currently different therapies for diseases produced by these three viruses, but there is no definitive cure and treatments face diverse challenges such as timely diagnosis, access and adherence to treatment or appearance of resistances.

In this scenario, nanotechnology presents itself as a promising tool for the development of new antiviral therapies. In this work, novel PEGylated cationic carbosilane dendrimers (PCCDs) have demonstrated to be efficient for viral inhibition in two different approaches: their use as delivery vehicles and their antiviral activity per se. In the first approach, the use as delivery systems, these dendrimers have proven to be biocompatible and effectively delivered into target cells. In addition, they have proved to form stable complexes with miRNAs that present anti-HIV-1 activity, which significantly and specifically improved the inhibition capacity of these RNA molecules by themselves. In the second approach, the antiviral activity per se, PCCDs have shown to effectively inhibit the attachment of viral glycoproteins from HSV-2 and HCMV to heparan sulphate proteoglycans, thus preventing the infection of target cells. Both therapeutic strategies have demonstrated that G2-SN15-PEG and G3-SN31-PEG dendrimers are promising candidates to be used against *Retroviridae* and *Herpesviridae* infections.

Last part of this work consisted in the study of the application of micellar carbosilane dendrons in the development of a dendritic cell (DC)-based therapeutic vaccine for HIV-1. Dendrimicelles were shown to be valid carriers of HIV-1-derived peptides into moDCs, which induced them to a slight maturation. Experiments with T and B cell activation and release of inflammatory cytokines confirmed a slight stimulation of HIV-specific immune response. Collectively, these experiments confirmed that EG3SO_3Na, ChG3SO_3Na, EG3NMe_3I, and ChG3NMe_3I dendrimicelles are valid candidates to be used in the development of a therapeutic vaccine against HIV-1.

RESUMEN

A pesar de ser agentes causantes de epidemias desde hace miles de años, el estudio de los virus es relativamente reciente. Sin embargo, la aparición de virus antes desconocidos y la expansión de los ya conocidos a nuevas áreas ha provocado un aumento masivo de la investigación en virología. La mejora en los enfoques para el estudio de los virus ha permitido una comprensión más profunda de los aspectos moleculares, evolutivos y epidemiológicos de los virus, lo que ha reducido la mortalidad y la morbilidad de este tipo de enfermedades infecciosas. Sin embargo, las infecciones virales siguen siendo uno de los principales problemas de salud a nivel mundial, principalmente en poblaciones vulnerables como los pacientes inmunocomprometidos y las personas en países en desarrollo.

A modo ilustrativo, la población mundial infectada por el Virus de la Inmunodeficiencia Humana-1 (VIH-1) supera los 37 millones de personas y cada año hay más de 1,5 millones de nuevas infecciones. Otro patógeno viral de transmisión sexual es el Virus del Herpes Simple-2 (VHS-2), agente causal de más de 490 millones de infecciones en todo el mundo. Sin embargo, la transmisión sexual no es la única vía por la que los patógenos virales se diseminan ampliamente, por ejemplo, el Citomegalovirus Humano (CMVH), que afecta a más del 50% de la población mundial y alcanza valores superiores al 90% en algunas regiones, se adquiere mayoritariamente durante la infancia o mediante trasplante de órganos o transfusión de sangre. Actualmente existen diferentes terapias para las enfermedades producidas por estos tres virus, pero no existe una cura definitiva y los tratamientos se enfrentan a diversos desafíos como el diagnóstico temprano, el acceso y adherencia al tratamiento o la aparición de resistencias.

En este escenario, la nanotecnología se presenta como una herramienta prometedora para desarrollar nuevas terapias antivirales. En este trabajo, nuevos dendrímeros catiónicos carbosilanos PEGilados (DCCPs) han demostrado ser eficientes para la inhibición viral de dos formas: como vehículos de administración y por sí mismos. En el primer enfoque los DCCPs han demostrado ser biocompatibles y entregados eficientemente en células diana. Además, han demostrado formar complejos estables con miRNAs con actividad anti-VIH-1, mejorando significativa y específicamente la capacidad de inhibición de estas moléculas de RNA por sí mismas. En el segundo enfoque los DCCPs han demostrado impedir eficazmente la unión de glicoproteínas virales de VHS-2 y CMVH a receptores de membrana, evitando así la infección. Ambas estrategias terapéuticas han demostrado que los dendrímeros G2-SN15-PEG y G3-SN31-PEG son candidatos válidos para ser utilizados contra infecciones por Retrovirus y Herpesvirus.

La última parte de este trabajo consistió en el estudio del uso de dendrones carbosilanos micelares para el desarrollo de una vacuna terapéutica frente al VIH-1 basada en células dendríticas (CD). Las dendrimicelas demostraron ser válidas portadoras de péptidos derivados del VIH-1 en CD derivadass de monocitos (CDmo), lo que les indujo a una leve maduración. Experimentos de activación de células T y B y liberación de citocinas inflamatorias demostraron una leve estimulación de la respuesta inmunitaria. En conjunto, estos experimentos confirmaron que las dendrimicelas EG3SO_3Na, ChG3SO_3Na, EG3NMe_3I y ChG3NMe_3I son válidas candidatas para ser utilizadas en el desarrollo de una vacuna terapéutica frente al VIH.

TABLE OF CONTENTS

TABLE OF CONTENTS

ABBREVIATIONS

1. LIST OF ABBREVIATIONS

3-OST HS	3-O-sulphonated heparan sulphate
ACV	Acyclovir
AIDS	Acquired Immune Deficiency Syndrome
APC	Antigen presenting cell
ATCC	American Type Culture Collection
BdrU	5-bromo-2'-deoxyuridine
BI	Binding inhibition
BSA	Bovine serum albumin
cART	Combined antiretroviral therapy
CCR	Chemokine (C-C motif) receptor. It can be extended to the rest of abbreviations: CCR2, CCR3 and CCR5
CD	Cluster of differentiation. It can be extended to the rest of abbreviations: CD3, CD4, CD8…
CID	Cytomegalic inclusion disease
CNS	Central nervous system
CXCR4	Chemokine (C-X-C motif) receptor 4
Cy5	Sulfo-Cyanine5
DAPI	4',6-diamidino-2-phenylindole dihydrochloride
DC	Dendritic cell
DE	*Herpesviridae* delayed early or β genes
DLS	Dynamic light scattering
DMEM	Dulbecco's modified Eagle's medium
DMSO	Dimethyl sulfoxide
DNA	Deoxyribonucleic Acid
dsDNA	Double-stranded DNA
E	*Herpesviridae* early or β genes
ELISA	Enzyme-linked immunosorbent assay
EMEM	Eagle's minimum essential medium
Env	Gene encoding the structural Env polyprotein
FAIDS	Feline AIDS
FBS	Fetal bovine serum
FITC	Fluorescein isothiocyanate
FPG	Fluorescence plus Giemsa
G	Dendrimer generation

Gag	Group-associated antigen. Gene encoding the structural Gag polyprotein
GAG	Glycosaminoglycan
GCV	Ganciclovir
gB	Glycoprotein exposed in the surface of HSV-2 membrane. It can be extended to the rest of abbreviations: gB, gC, gD, etc.
gp	Glycoprotein
HCMV	Human Cytomegalovirus
HHV-5	Human Herpesvirus-5 (HHV-5)
HIV	Human Immunodeficiency Virus
HS	Heparan sulphate
HSPGs	Heparan sulphate proteoglycans
HSV	Herpes Simplex Virus
HVEM	Herpes virus entry mediator
IC	Infection control
iDC	Immature dendritic cells
IE	*Herpesviridae* immediate early or α genes
IgG	Immunoglobulin G
IL-2	Interleukin 2. It can be extended to the rest of interleukins
IN	Integrase
INM	Inner nuclear membrane
kb	Kilobase
kd	Dissociation constant
L	*Herpesviridae* late or γ genes
LDH	Lactate dehydrogenase
LPS	Lipopolysaccharide
LTR	Long terminal repeat
mDC	Mature dendritic cells
MFI	Mean fluorescence intensity
miRNA/miR	MicroRNA
MLR	Mixed lymphocyte reaction
MoDC	monocyte-derived dendritic cell
MOI	Multiplicity of infection
mRNA	Messenger RNA
MTT	3-(4,5-dimethylthiazol-2-yl)-2,5-diphenyl tetrazolium bromide
Nef	Negative regulating factor. Gene encoding the accessory Nef protein of HIV-1
NIH	National Institute of Health

nm	Nanometres
NNI	National Nanotechnology Initiative
NP	Nanoparticle
NT	Non-treated
ONM	Outer nuclear membrane
OR14I1	Olfactory receptor family 14 subfamily I-1
PAMAM	Polyamidoamine dendrimer
PBMC	Peripheral blood mononuclear cell
PBS	Phosphate buffered saline
PCCD	PEGylated cationic carbosilane dendrimer
PEG	Polyethylene glycol
PFA	Paraformaldehyde
PFU	Plaque forming unit
PHA	Phytohaemagglutinin
Pol	Gene encoding the structural Pol polyprotein
PPI	Poly (propylene imine) dendrimer
PR	Protease
Pro	Gene encoding the structural Pro protein
Rev	RNA splicing regulator. Gene encoding the accessory Rev protein of HIV-1
RNA	Ribonucleic acid
rpm	Revolutions per minute
RPMI	Roswell Park Memorial Institute
RT	Reverse transcriptase
RT	Room temperature
RU	Resonance units
SAIDS	Simian AIDS
SCE	Sister chromatids exchange
SD	Standard deviation
SEM	Standard error of the mean
SES	Socioeconomic status
SPR	Surface plasmon resonance
STI	Sexually transmitted infection
TAE	Tris–acetate-EDTA buffer
TAMRA	Tetramethylrhodamine
Tat	Transactivator protein. Gene encoding the accessory Tat protein of HIV-1
UL	Unique long segment

US	Unique short segment
Vhs	Virion Host Shutoff protein
VI	Viral inactivation
Vif	Viral infectivity factor. Gene encoding the accessory Vif protein of HIV-1
Vpr	Viral Protein R. Gene encoding the accessory Vpr protein of HIV-1
Vpu	Viral Protein Unique. Gene encoding the accessory Vpu protein of HIV-1
WHO	World Health Organization
ZP	Zeta potential

INTRODUCTION

2. INTRODUCTION

2.1 *RETROVIRIDAE*

Retroviridae is a family of enveloped, single-stranded, positive-sense RNA viruses characterised by their unusual replication in which the viral RNA genome is converted into a double-stranded DNA (dsDNA) copy by a reverse transcriptase to be finally integrated into the host genome (MacLachlan and Dubovi, 2016b).

This family of viruses was first discovered in 1908 by Vilhelm Ellermann and Oluf Bang, who were investigating neoplastic diseases in chickens. With time, the study of this family of viruses was extended to mammals and now it is known that retroviruses infect a wide range of animal species, including others such as reptiles or fish (Schelhaas, 2017). The retrovirus family is divided into two subfamilies: *Orthoretrovirinae*, which is subdivided into six genera (*Alpharetrovirus*, *Betaretrovirus*, *Gammaretrovirus*, *Deltaretrovirus*, *Epsilonretrovirus,* and *Lentivirus*) and *Spumaretrovirinae*, which is divided into five genera (*Bovispumavirus*, *Equispumavirus*, *Felispumavirus*, *Prosimiispumavirus,* and *Simiispumavirus*) (ICTV, 2022).

The characteristic biological aspects of this family of viruses, including the ability to undergo mutation and to alter and integrate into the host genome, relies on the unique properties of the genome. Virions from the *Retroviridae* family share common genomic organization and four essential genes in their genome: *gag, pro, pol,* and *env*. *Gag* (group-associated antigen) encodes the major structural proteins required for virion formation; *pro* encodes a viral protease required for viral protein maturation; *pol* encodes multifunctional proteins (including RT and integrase enzymes); and *env* encodes the transmembrane envelope proteins (Painter and Collins, 2019).

The retroviral cycle begins with the attachment of viral particles to specific surface receptors on their target cells. Once the binding has occurred these particles cross the plasma membrane through interactions with viral glycoproteins of the envelope. This fusion leads to the uncoating of the viral particle, where the viral RNA is dissembled and released to the cytoplasm. Here, as previously mentioned, the viral RNA is reverse transcribed into a dsDNA molecule. Afterwards, this molecule enters the nucleus where it will be integrated into the host cell genome, becoming part of the cellular genome (Hizi and Herzig, 2015, Albritton, 2018). This so-called provirus can replicate with the host genome and be transcribed into viral mRNA, which will be then translated by the host's ribosomal machinery to produce different viral proteins. Then, on the cell membrane, these proteins will be assembled into immature viral particles inducing the formation of a curvature that will constitute a membrane-coated spherical viral particle. Finally, these immature progeny virions will be released from the host cell in a process called budding and will undergo a reorganization of the components that will generate mature infectious virus (Perilla and Gronenborn, 2016, Wang-Shick, 2017).

Diseases produced by virus belonging to the *Retroviridae* family are very diverse and include: (i) different types of neoplasia, such as lymphoma, sarcoma, or leukaemia (Nair et al., 2020); (ii) various neurodegenerative diseases as spongiform encephalopathy, encephalomyelitis, or astrocyte degeneration (Soung and Klein, 2018); (iii) immunodeficiencies such as Acquired Immune Deficiency Syndrome (AIDS), Feline AIDS (FAIDS) or Simian AIDS (SAIDS) (Sahay and Yamamoto, 2018); and (iv) other diseases like

anaemia, osteoporosis or inflammatory diseases such as arthritis or mastitis (Brotto Rebuli et al., 2021, Nishiura et al., 2020, Wang et al., 2018).

2.1.1 Human Immunodeficiency Virus-1

One of the main causes of morbidity and mortality worldwide is human immunodeficiency virus-1 (HIV-1) infection: since the start of the pandemic in the 1980s, more than 79 million people have been infected. This virus, which belongs to the genus *Lentivirus*, causes progressive $CD4^{+}$T cell loss leading to different immunological abnormalities which conduce to infectious and oncological complications and other morbidities such as renal, cardiovascular, and hepatic dysfunction. Currently, the combined antiretroviral therapy (cART) can inhibit HIV-1 replication achieving durable suppression of viral replication preventing the development of AIDS. However, access and adherence to these treatments are not within everyone's reach and there are still undiagnosed and late diagnosed individuals; in addition, prevailing therapy is not curative and stopping of the treatment or the appearance of resistances lead to viral rebounds of viral reservoirs (Deeks et al., 2015).

2.1.1.1 Epidemiology

According to the latest available data (2020), the number of people living with HIV-1 currently exceeds 37 million, of whom 53% are women and girls. In the same year, more than 1,5 million people became newly infected, which represents a 11% decrease since 2010, and around 7.000 people died from an AIDS-related cause, which is a 47% reduction since 2010. It is interesting how key populations differ depending on local HIV-1 prevalence: in countries with high-prevalence (East and Southern Africa) young woman face the highest risk of infection, however, in countries with lower-prevalence (e.g. Eastern Europe and Central Asia) the highest risk of infection is faced by gay men, prostituted persons, transgender people and intravenous drug users (UNAIDS, 2022).

Although 84% of infected people know their HIV-1 status, only 87% of them are being treated, and, in total, one quarter of the population living with HIV is not on treatment, and one third presents unsuppressed viral loads. Policies implemented by each country have led to an increase of resources to improve preventing measures and access to cART, improving the situation of the pandemic in regions such as sub-Saharan Africa, Latin America, Oceania, Western and Central Europe and North America. However, other regions, such as the Middle East, North Africa, Central Asia, and Eastern Europe, have experienced an aggravation of the situation (UNAIDS, 2021).

Regardless of the progress achieved with the global commitment to fight against HIV-1, it is still one of the deadliest pandemics of our times and major efforts still must be made to end up with this unbearable situation.

2.1.1.2 Morphology and structure

As other viruses belonging to the *Lentivirus* genus, HIV-1 virions are spherical in shape and have a diameter of roughly 100 nm. HIV-1 genome is composed of two copies of positive-sense, single stranded RNA of approximately 9.8 kb which contains long terminal repeats (LTRs) at the 5’ and 3’ ends, enabling its

circularisation fundamental for its integration into the host genome. The genetic material is encapsulated by a capsid which, in turn, is protected by a lipidic membrane that proceeds from the host (Figure 1A) (German Advisory Committee Blood (Arbeitskreis Blut), 2016).

The HIV-1 genome contains three of the previously mentioned essential genes: *gag*, *pol,* and *env*. *Gag* encodes different proteins such as p24, p17 or p6, which are structural proteins that compose the nucleocapsid, build the matrix and are involved in viral encapsulation, respectively (van Domselaar et al., 2019). On the other hand, *pol* encodes protease (PT, viral maturation), reverse transcriptase (RT, synthesis of DNA from RNA), and integrase (IN, integration into host genome (Adamson and Freed, 2007)). Lastly, *env* gene encodes the glycoprotein (gp) gp160, which is the precursor of gp120, the exterior envelope gp that interacts with cellular receptors, and gp41, the transmembrane gp that mediates fusion between viral and host membranes (Wyatt and Sodroski, 1998). Furthermore, the HIV-1 genome encodes several regulatory proteins including Tat (activator of viral gene transcription), Rev (regulator of mRNA processing and transport), Nef (negative regulator of CD4 and HLA-I), Vif (increase of viral production), Vpr (induction of apoptosis) or Vpu (increase of virion release (Langer and Sauter, 2016)) (Figure 1B).

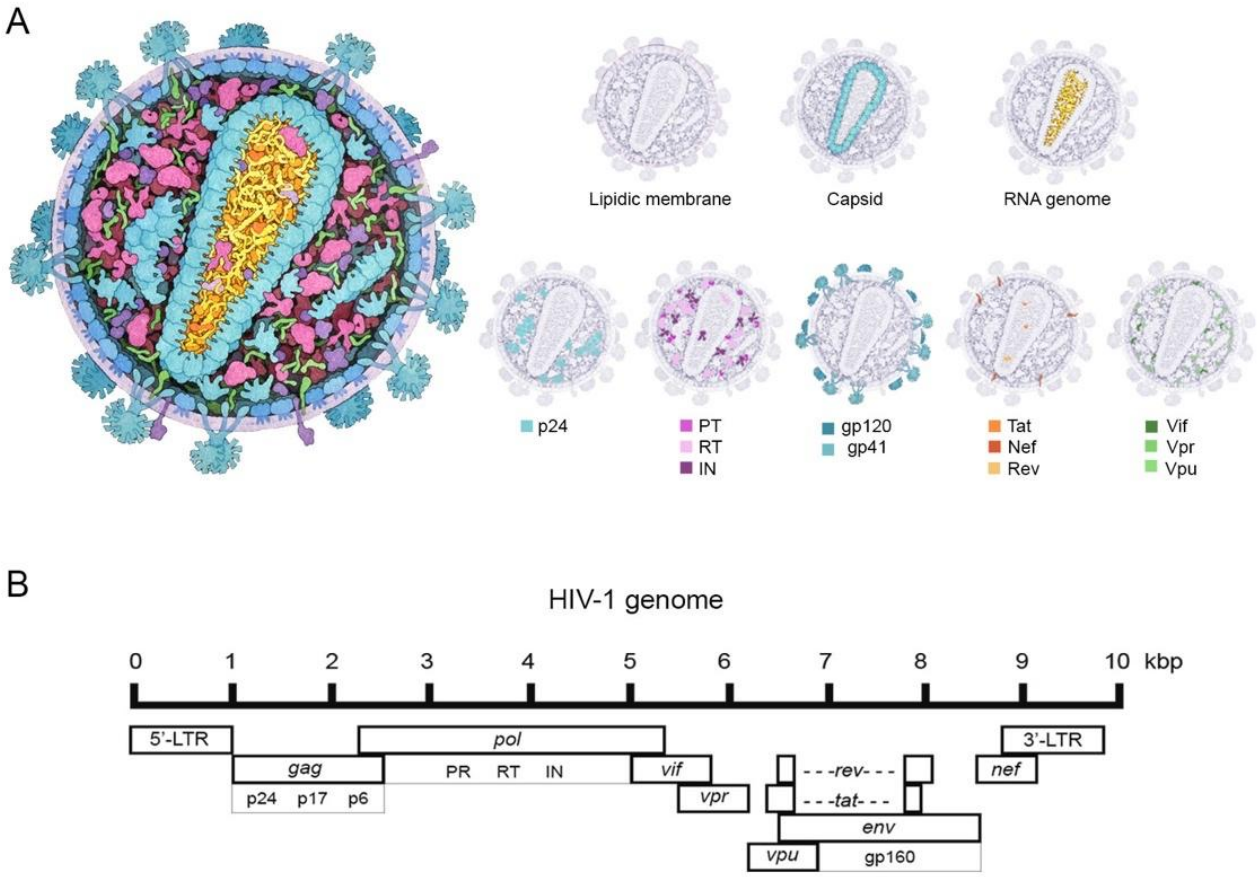

Figure 1: Structure of the HIV-1 virion. **(A)** Representation of the HIV-1 virion structure with its principal proteins. Blue refers to structural proteins, purple to viral enzymes and green and orange to accessory proteins **(B)** Representation of the HIV-1 genome. HIV-1 virion image modified from: Research Collaboratory for Structural Bioinformatics Protein database (RCSB PDB).

2.1.1.3 Viral cycle

The viral cycle of HIV-1 is identical to the cycle of other viruses belonging to the *Retroviridae* family. It can be divided into two phases: early and late phase. The early phase begins with the binding of virus receptors to the target cell, the primary receptor that mediates HIV-1 attachment is the cell surface glycoprotein CD4. The interaction of gp120 and gp 41 with CD4 induces a conformational change that brings closer the virus to the coreceptors CCR5 or CXCR4 (Mukherjee et al., 2021). This process is followed by the fusion of viral and cellular membranes and the release of the viral core into the cytoplasm. Then, as previously mentioned, viral RT transcribes the viral RNA genome into DNA which will enters the nucleus where it will get integrated by IN into the cellular genome. This step constitutes the beginning of the late phase, where the viral genome is transcribed and further transported to the cytoplasm where the viral mRNA will be translated to produce the aforementioned proteins. Eventually, the different proteins and two copies of genomic RNA will get assembled into the matrix forming a complex that will accumulate at the plasma membrane leading to the formation of membrane-coated particles. Lastly, new virions bud off the host cell and suffer different reorganizations that generate mature infectious particles (Figure 2) (Kirchhoff, 2021).

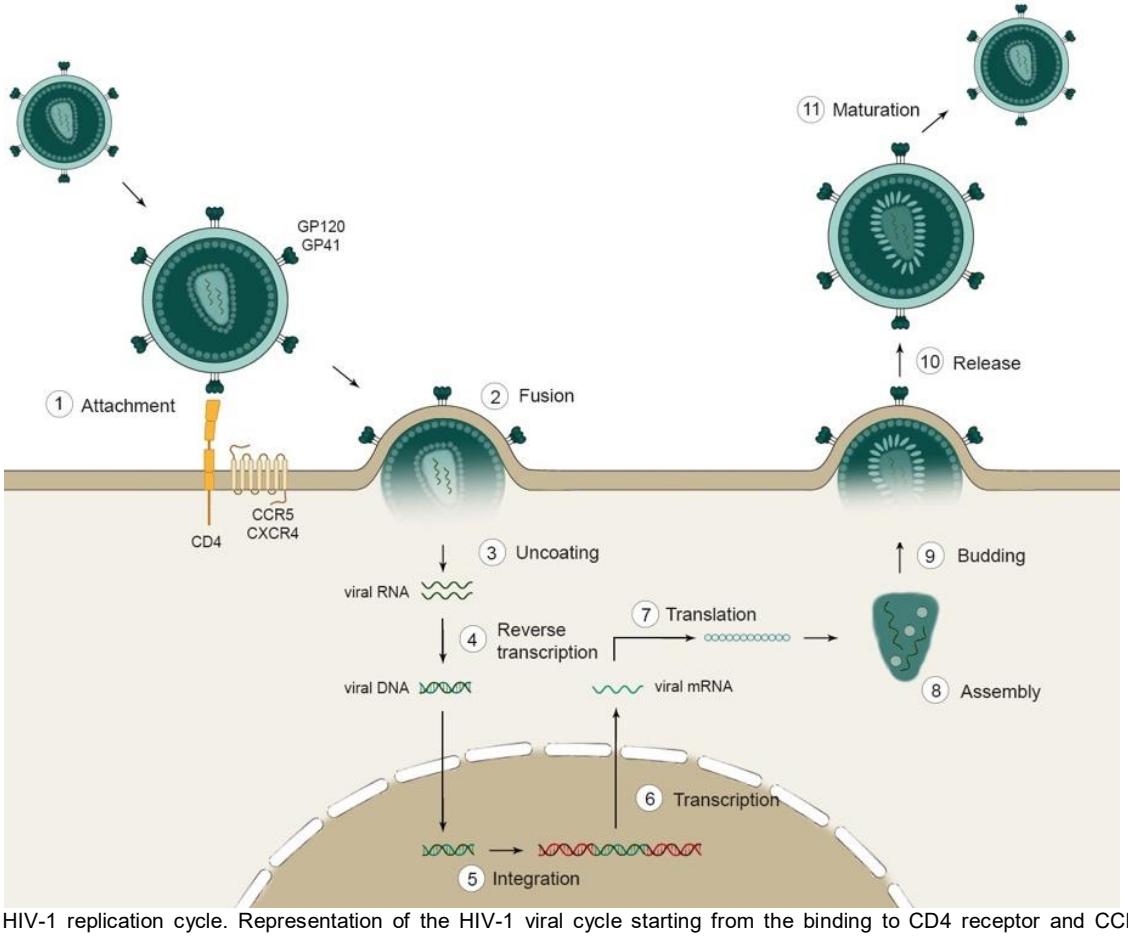

Figure 2: HIV-1 replication cycle. Representation of the HIV-1 viral cycle starting from the binding to CD4 receptor and CCR5 and CXCR4 co-receptors, followed by the fusion with the host membrane and the uncoating and release of the viral RNA into the cytoplasm. Subsequently, it gets reversely transcribed into viral DNA which translocates to the nucleus to be integrated into the host DNA and ubsequently transcribed and translated into new viral RNA and proteins, which assembly into new virions that bud off and are released to be finally maturated outside the cell. Image modified from Scholarly Community Encyclopaedia.

A key step of the HIV-1 viral cycle is the establishment of latency in infected cells. This occurs when the integrated DNA fails to express viral RNA and proteins due to the transition of infected $CD4^+$T cells to a quiescent cell stage in which the transcription machinery stops. This process makes infected cells undetectable and unclearable for the immune system until fortuitous reactivation, which remains the main challenge to a permanent cure (Romani and Allahbakhshi, 2017).

2.1.1.4 Transmission mechanisms and clinical course

In 1981, different physicians noticed severe immunosuppression, opportunistic infections, and unusual cancers among a group of young gay men; these were the first reports of what would later be termed AIDS (CDC, 1981). Several years later, Dr. Robert Gallo, Dr. Luc Montagnier, and Dr. Jay Levy proved that the viral agent causing this disease was HIV-1 and claimed that it was transmitted by intimate contact or blood products (Barre-Sinoussi et al., 1983, Gallo et al., 1983, Popovic et al., 1984). Nowadays, it is known that the epidemic is mainly driven by sexual transmission, but there are other transmission routes such as maternal-infant infections (either intrauterine, intrapartum or breastmilk) and injection drug use (Shaw and Hunter, 2012).

The clinical course of HIV-1 is characterised by an initial acute phase which lasts up to 6 weeks, during this phase the virus gets rapidly replicated in infected cells, the viral load in plasma increases and there is an abrupt decline in $CD4^+$ T lymphocytes. Infected people in this phase exhibit variable clinical symptoms including fever, fatigue, lymph node enlargement, diarrhoea and neuropathy (German Advisory Committee Blood (Arbeitskreis Blut), 2016). This phase is followed by an asymptomatic period that can last a decade in which immunodeficiency progresses through continuous depletion of $CD4^+$ T cells, leaving the patient susceptible to opportunistic infections (usually by *Toxoplasma gondii, Cryptosporidium parvum, Pneumocystis jirovecii,* or *Mycobacterium tuberculosis*) and development of neoplasms (Deeks et al., 2015).

Different antiretroviral drugs, and the combination of them, have been approved for the treatment of infection, each targeting a different step in the life cycle of the virus: nucleoside and nucleotide analogues (Abacavir and Tenofovir, respectively), non-nucleoside reverse transcriptase inhibitors (Efavirenz), protease inhibitors (Lopinavi) and fusion inhibitors (Enfuvirtide). Adherence to the treatments reduces the level of viremia and allows recovery of the functionality of the immune system to some extent, usually preventing AIDS. However, the fact that cART must be administered for life involves developing drug toxicity with symptoms among which fat redistribution, renal and hepatic dysfunction, osteopenia, and depression stand out. Additionally, other conditions such as poor mental health, social isolation, and stigma appear due to chronic lifelong infection. Furthermore, despite treatment, some patients do not restore proper immune function and others develop resistance to cART, which complicates efforts to control viral replication (Clavel and Hance, 2004).

2.2 *HERPESVIRIDAE*

Herpesviridae is a large and diverse family of linear dsDNA viruses characterised by a unique morphology in which the genome is encapsulated in an icosahedral capsid that is, in turn, surrounded by a layer of globular material called the tegument and a lipoprotein envelope with abundant glycoproteins spikes (Davison et al., 2009).

The herpesvirus family is divided into three tenuously related subfamilies: *Alphaherpesvirinae*, which is subdivided into five genera (*Iltovirus*, *Mardivirus*, *Scutavirus*, *Simplexvirus* and *Varicellovirus*), *Betaherpesvirinae,* which is further divided into five more genera (*Cytomegalovirus, Muromegalovirus, Proboscivirus, Quwivirus* and *Roseolovirus*) and *Gammaherpesvirinae* which is separated into seven genera (*Bossavirus*, *Lymphocryptovirus, Macavirus, Manticavirus, Patagivirus, Percavirus* and *Rhadinovirus*) (ICTV, 2022). Infections by this family of viruses occur in both invertebrates and cold- and warm-blooded vertebrates, including molluscs, fish, reptiles, amphibians, and all species of mammals and birds investigated (MacLachlan and Dubovi, 2016a).

One of the most characteristic biological aspects of herpesviruses is that, following host infection, they can establish a latent lifelong infection alternative to lytic infection, leading to unlimited production of virions. Reactivation of virus replication is restricted but recurrent with expression of viral proteins, production of progeny virus and transmission to other hosts (Gatherer et al., 2021).

Despite the high genetic diversity of members within this family, they all share common features in their replicative cycle. As with other viruses, the cycle starts with the adsorption of the viral envelope to the plasma membrane through different receptors, followed by the fusion of these membranes and the penetration of the capsid into the cytoplasm. The viral genome is then translocated to the nucleus where immediate early (IE or α), early (E or β) and late (L or γ) genes are replicated and transcribed (Roizman, 2013). This newly generated DNA is packaged into immature capsids that bud to the cytoplasm in a primary envelope through the inner nuclear membrane. There is a de-envelopment at the outer nuclear membrane that allows the release to the cytoplasm, where a secondary envelopment and the assembly of the tegument proteins lead to the maturation of the virion, which is required to produce infectious virions (Roller and Johnson, 2021).

Diseases caused by the infection of *Herpesviridae* viruses are very diverse and depend on the subfamily of the infecting agent and the infected species. Clinical manifestations include fully asymptomatic, fever, pain, gingivostomatitis, laryngotracheitis, hepatomegaly, located lymphadenopathy, necrosis in fetal organs, encephalitis, and ulcerative and vesicular lesions on the skin and mucosae of the genital and respiratory tracts (MacLachlan and Dubovi, 2016a).

2.2.1 Herpes Simplex Virus-2

The first descriptions of genital lesions such as those caused by Herpes Simplex Virus (HSV) were found in the Ebers papyrus (circa 1500 BC). Later, in ancient Greece, Hippocrates documented the cutaneous spread of these lesions and defined them with the word *herpes* derived from *herpein* which means “to creep or crawl”

for their spreading nature. John Astruc in the 17th century published a book describing genital herpes, and Fournier, in 1896, wrote about the diagnosis and treatment of herpes in infants. Active research of HSV started in 1919, after Lowenstein confirmed that herpes was an infectious disease (Rechenchoski et al., 2017).

Herpes Simplex Virus-2 belongs to the genus *Simplexvirus* in the subfamily *Alphaherpesvirinae* and is generally associated with infection of genital mucosal surfaces. Infections with this virus represent an enormous global health problem since a huge amount of the population is infected. Invasion of the cornea or the central nervous system (CNS) and infection of new-borns or immunocompromised individuals can lead to live threatening conditions. There are currently several drugs approved for primary and recurrent disease, which prevent and shorten rebounds of the virus and reduce risk of transmission. However, asymptomatic and unrecognised individuals remain untreated and there is no effective vaccine or definitive cure, which leads to the emergence of resistant strains entailing viral reactivations (Brady and Bernstein, 2004).

2.2.1.1 Epidemiology

Infections produced by HSV-2 are among the most common sexually transmitted diseases in humans. It is important to mention that estimations are based on reported cases; this implies an underestimation of the prevalence since a considerable amount of HSV-2 infected people are unaware of their situation (Wald and Ashley-Morrow, 2002).

According to the latest available data, there are around 491 million people between 15 and 49 years infected with HSV-2 worldwide (W.H.O, 2022). Highest seroprevalence is found in the World Health Organization (WHO) African Region, where it reaches 37% of the population, followed by the Western Pacific, South-East Asia and Americas Regions (Harfouche et al., 2021). There are also differences in sex: prevalence in women (313 million) is almost twice as often as in men (178 million). As with other sexually transmitted infections (STI), risk populations exposed to sexual risk behaviour, such as prostituted people, present much higher seroprevalence (James et al., 2020).

There has been an increase in global HSV-2 prevalence, latest accessible data estimates that 23,9 million people under 50 became infected in 2016, which implies a 13,7% increase from previous years. This increase has followed the same pattern; almost twice as many women as men were infected, and the WHO African Region had the highest prevalence (James et al., 2020).

There is enough evidence for a biological association between HSV-2 and HIV infections: HSV-2 enhances five times the risk of acquisition of HIV. As mentioned above, both infections are associated with similar risk factors (such as age, sex, or sexual behaviour) (Kaushic et al., 2011, Matoga et al., 2021, Omori and Abu-Raddad, 2017). In addition, incident HSV-2 infection involves inflammation with concentration of $CD4^+$ T lymphocytes in the genital area and genital ulceration, through which HIV can enter and infect (Looker et al., 2017a).

These observations demonstrate the critical need to perform interventions that target HSV-2, mainly the development of protecting vaccines and treatments which will potentially benefit against this and other infections especially in regions with high incidence of co-infections of these viruses.

2.2.1.2 Morphology and structure

Being a virus of the *Simplexvirus* genus, HSV-2 virions are composed of four main layers, giving rise to a spherical particle with spikes of 225 nm in diameter (Figure 3A) (Widener and Whitley, 2014):

i) a core formed by the single linear dsDNA molecule.
ii) an icosahedral capsid formed by 100nm capsomeres that surround the core. There are three types of capsids: A-capsids that lack scaffold proteins and viral DNA, B-capsids that only lack viral DNA and C-capsids that contain the viral genome.
iii) an amorphous tegument wrapping the capsid formed by viral enzymes needed to subvert control of chemical processes of the host cell and to defend from immediate host responses.
iv) an outer lipoprotein envelope made up of host membrane proteins and viral glycoproteins.

The HSV-2 genome has 155 kbp and consists of two segments (unique long, U_L, and unique short, U_S) which are flanked by inverted repeats (TR_L and IR_L, TR_S and IR_S). The presence of these repeats allows the inversion of U_L and U_S regions leading to the formation of four different linear genomes (Figure 3B) (Knipe and Whitley, 2021).

The U_L region contains 56 viral genes, while the U_S region contains only 12, which encode essential (to regulate transcription and virion construction) and dispensable (to enhance viral production and spread) genes. Some important proteins encoded by these genes are those that conform the tegument, including virion host shutoff (Vhs) protein (which facilitates host mRNA degradation after infection), UL36 (which facilitates viral DNA entry into the nucleus) or the VP16 transactivating protein (which enhances replication of immediate-early genes (Kukhanova et al., 2014, Taylor et al., 2002)). Other important proteins are those glycoproteins mentioned to form the lipid envelope (gB, gC, gD, gE, gG, gH, gI, gJ, gK, gL, and gM) that are responsible for the attachment and internalisation of the virion into the host cell (Mettenleiter et al., 2009).

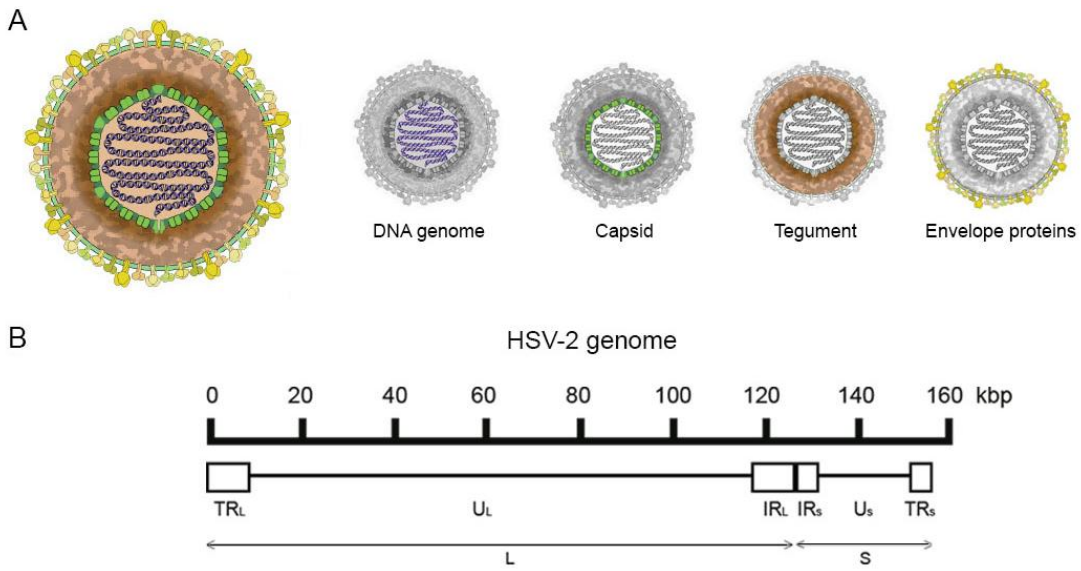

Figure 3: Structure of the HSV-2 virion. **(A)** Representation of the HSV-2 virion structure with its four main layers. **(B)** Representation of the HSV-2 genome.

2.2.1.3 Viral cycle

Despite the variety of cell types that can be infected by virus from the *Herpesviridae* family, the mechanisms used to entry into host cells is highly conserved. In the case of HSV-2, attachment to host cell starts with the association of gB and/or gC with heparan sulphate (HS) proteoglycans (HSPGs) present on the cell surface (Sathiyamoorthy et al., 2017). After this first contact, gD binds to three classes of receptors, including nectin1 and 2, herpes virus entry mediator (HVEM), and 3-O-sulphonated HS (3-OST HS) (Connolly et al., 2021). This interaction produces conformational changes in gD that allow its interaction with gB and gH-gL to trigger fusogenic activity between the viral outer envelope and the cell plasma membrane (Agelidis and Shukla, 2015).

After entering, the viral particle is transported through microtubules to the nuclear membrane, where the capsid interacts with the nuclear pore complex, leading to the release of the viral genome to the nucleus (Madavaraju et al., 2020). Here, the viral genome will be replicated and transcribed by the cell RNA polymerase II, which will synthetize viral mRNA in a sequential transcriptional cascade of expression of immediate early (IE or α), delayed early (DE or β), and late (L or γ) genes (Kukhanova et al., 2014). The viral genome is then cleaved and packaged into capsids, which will egress from the nucleus by budding at the inner nuclear membrane (INM) acquiring a first envelope. Subsequently, capsids fuse with the outer nuclear membrane (ONM), resulting in the loss of the primary envelope. The capsid is then transported to the cytoplasm where virion maturation occurs by tegumentation and secondary envelopment of capsids. Virions are then transported to the cell surface, where they fuse with plasma membranes, releasing enveloped mature virions (Figure 4) (Mettenleiter et al., 2009).

Upon primary infection, HSV-2 can infect neuronal dendrites of sensory ganglia and, by axonal transport, move to cell bodies of peripheral neurons where it can continue with the previous explained lytic replication or

undergo latent infection. In latency, viral genome is retained within sensory neurons were lytic genes get repressed. Upon certain stimuli, virus replication reactivates, producing infectious virions that travel through anterograde axonal spread through peripheral sensory nerves back to other mucosal surfaces (Singh and Tscharke, 2020).

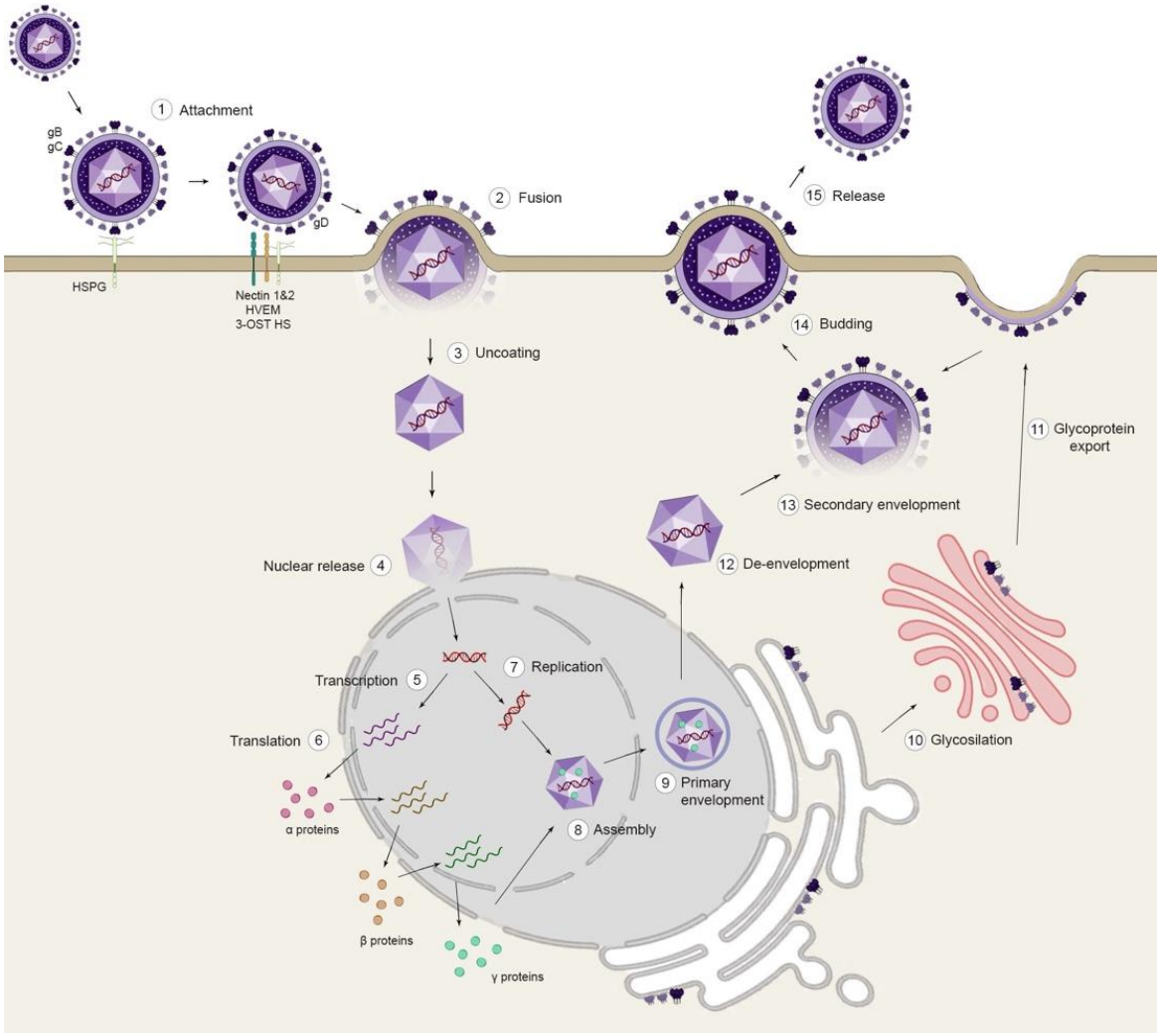

Figure 4: HSV-2 replication cycle. Representation of the HSV-2 viral cycle starting from the binding to different cell receptors, followed by the fusion with the host membrane and the uncoating and the nuclear release of the viral DNA into the cytoplasm. Afterwards, it gets transcribed and translated into new viral DNA and α, β AND γ proteins, which assembly into new virions that are enveloped and de-enveloped to be subsequently enveloped again before budding off to be released.

2.2.1.4 Transmission mechanisms and clinical course

Acquisition of HSV-2 usually occurs by inoculation of the virus through breaks in the mucosa via direct intimate contact and establishes acute infections in epithelial cells and fibroblasts in the genital regions and in the accessing nerves that innervate the site of infection. After an incubation period of 4 to 6 days in which HSV-2 replicates, cell lysis and inflammation result in characteristic vesicular or ulcerative lesions in the vulva, vagina, and cervix in women and glans penis, prepuce, and penile shaft in men. Primary disease frequently

entails fever, malaise, dysuria, and bilateral inguinal lymphadenopathy (Johnston and Corey, 2016). Less commonly, HSV-2 causes mucocutaneous infections such as gingivostomatitis producing sore throat, erythema, pharyngeal edema and painful ulcerative lesions on the oral mucosa. Less commonly, HSV-2 can produce encephalitis which is characterised by haemorrhagic necrosis of the temporal lobe causing headache and alterations in consciousness, speech, and behaviour (Gnann and Whitley, 2017, Whitley and Baines, 2018). Despite being uncommon, it is lethal in more than 15% of cases even with appropriate antiviral therapy. In immunocompromised individuals, infection can progress to extensive perineal ulcerations, multiforme erythema, pneumonitis, hepatitis, and disseminated cutaneous disease (Knipe and Whitley, 2021).

HSV-2 transmission from mother to child happens mainly through peripartum neonatal transmission by viral shedding from vaginal secretions but can also happen through *in utero* transmission via placental or amniotic involvement and postnatal infection by contact with cutaneous lesions (Looker et al., 2017b). Although rare, neonatal infection has a high mortality and disability rate and manifests itself with ophthalmologic symptoms such as epithelial keratitis, chorioretinitis, and optic atrophy, and neurological symptoms such as hydranencephaly, intracranial calcifications, microcephaly, and meningoencephalitis (Bhatta et al., 2018, Hammad and Konje, 2021).

Symptoms caused by HSV-2 infections can be treated; the gold standard drugs used in the treatment of these infections are Acyclovir (ACV) and Famciclovir (Birkmann and Zimmermann, 2016). Both are synthetic nucleoside analogue that cause chain termination inhibiting the synthesis of viral DNA. Recurrent orolabial and genital infections can be treated with any of them in adult and paediatric patients; however, patients with encephalitis must only be treated with ACV (Harris and Holmes, 2017, Taylor and Gerriets, 2022). The treatment of choice for ophthalmologic symptoms is Trifluridine, another nucleoside analogue, which is not specific to HSV-2 (Roozbahani and Hammersmith, 2018).

The fact that these molecules share the mode of action entails sharing the same deficiencies: incomplete suppressive treatment, minimal effect upon acute episodes and emergence of resistances. This highlights the urgent need to develop new therapies to combat HSV-2 infection.

2.2.2 Human Cytomegalovirus

First observations of cytomegalic cells were done by Hugo Ribbert in 1881, who described large cells with an eccentrically placed nucleus containing a central nuclear body that was surrounded by a clear halo (Ribbert, 1904). It was not until 1925 that Von Glahn and Pappenheimer claimed that these cells were produced by viral infections and related them to herpesviruses, describing the infection as generalised cytomegalic inclusion disease (CID) (Vonglahn and Pappenheimer, 1925). In 1956, Dr. Margaret Smith isolated for the first time the virus causing CID and in 1960 this virus was named Human Cytomegalovirus (HCMV) by Thomas Weller (Smith, 1956, Weller et al., 1960).

HCMV, also known as human herpesvirus-5 (HHV-5), is one of the largest viruses known to cause clinical disease and to harbour the most genes dedicated to altering innate and adaptive host immunity. *Cytomegalovirus* is a genus belonging to the subfamily *Betaherpesvirinae* that is mainly asymptomatic but can

lead to life-threatening complications for fetal development, transplant recipients, and other immunocompromised individuals (Dioverti and Razonable, 2016). This virus establishes a life-long persistent infection that reactivates intermittently throughout life casing conditions such as sepsis, allograft rejection, cardiovascular disease and other systemic inflammatory conditions (Forte et al., 2020). Antiviral treatment controls direct effects of HCVM infection, but there is not curative treatment, and the existing therapies are not accessible worldwide allowing the appearance of resistances that involve viral reactivations.

2.2.2.1 Epidemiology

Epidemiological studies of HCMV have been performed since the development of a test for complement-fixing antibodies by Dr. Rowe in 1956 (Rowe et al., 1956). However, it is difficult to generalise prevalence estimates across regions since the number of reporting countries is low and the measurement and detection protocols are inconsistent. However, HCMV infection has been shown to be endemic throughout the world despite exhibiting significant geographic variability: prevalence rates in developing countries tend to be 20-30% higher than in developed countries, and therefore race and ethnicity are evaluated as risk factors. Specifically, seropositivity in some regions of Africa and Asia reaches 100%, in Russia 95% and in America 80% whereas in some regions of Europe (e.g. France and the Netherlands) it barely approaches 50% (Vilibic-Cavlek et al., 2017).

It has also been observed that prevalence generally increases with age, as seropositivity in children younger than 5 years old is 30% whereas it reaches 50% in adults older than 50 years (CDC, 2020). Organ transplantation and blood transfusions are also high-risk factors, HCMV infection has been shown to occur in up to 70% of recipients in some regions (Al Mana et al., 2019).

Another risk factor is socioeconomic status (SES). Diverse studies show that people with a lower SES have between 10 and 30% higher prevalence than people with a high SES. However, sex studies have not shown an association with seropositive HCMV, as the differences shown are inconsistent between reports (Cannon et al., 2010).

The extensive prevalence of HCMV worldwide and the morbidity and mortality associated with it make it necessary to develop mitigation plans, especially for vulnerable populations, including preventive measures and novel treatments to combat this infection.

2.2.2.2 Morphology and structure

The virion of HCMV shares many features with other viruses belonging to the *Betaherpesvirinae* subfamily; firstly it consists of the same layers previously explained: an icosahedral nucleocapsid densely packing the linear dsDNA genome, surrounded by the proteinaceous tegument, which is, in turn, enclosed by a lipid bilayer containing numerous glycoproteins. This conforms a mature virion particle measuring 150 to 200 nm in diameter (Figure 5A) (Gugliesi et al., 2020).

Another shared feature is its genome, of 230 kbp, which is the largest of all human herpesviruses and is structured in the characteristic division of U_L, U_S and flanking inverted repeats that allow the production of four

linear genomes in viral progeny (Figure 5B) (Sijmons et al., 2015). This genome encodes for over 200 proteins, whose expression, divided into three temporal classes, regulates different aspects of the viral cycle: immediate early, delayed early and late (Jean Beltran and Cristea, 2014). The main proteins are the four proteins that make up the capsid (pUL46, pUL48.5, UL85 and UL86) and the glycoproteins of the lipidic envelope (gB, gN, gO, gH, gM, gL, UL128, UL130 and UL131), involved in viral entry, maturation, and spread. Other proteins involved in viral maturation and regulation of viral and cellular promoters are ppUL32, ppUL65, ppUL69, and ppUL82 found in the tegument (Landolfo et al., 2003).

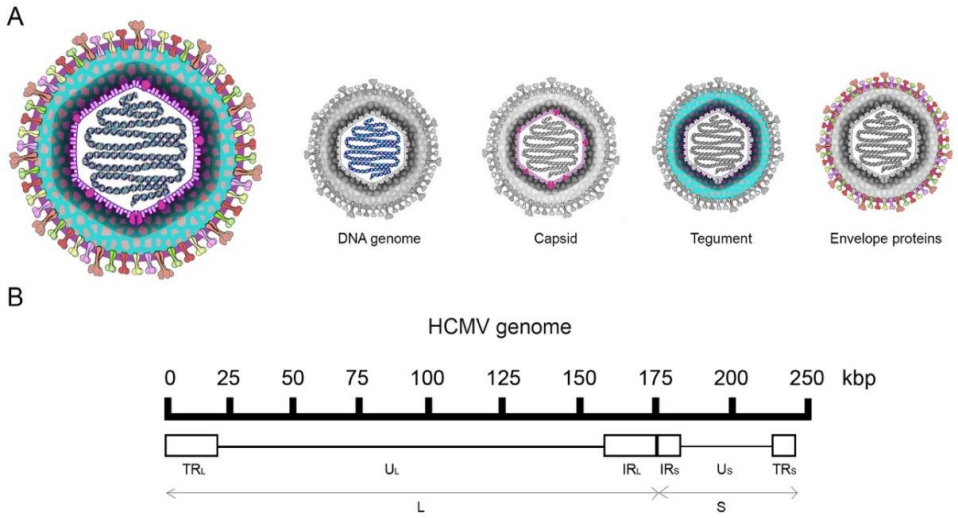

Figure 5: Structure of the HCMV virion. **(A)** Representation of the HCMV virion structure with its four main layers. **(B)** Representation of the HCMV genome.

2.2.2.3 Viral cycle

Human cytomegalovirus presents a wide cell tropism, including epithelial, endothelial, smooth muscle, neuronal, and dendritic cells, as well as fibroblasts, hepatocytes, trophoblasts, and monocytes/macrophages (Gerna et al., 2019), however, viral infection and cycle are conserved among these cell types. It starts with the interaction of infectious virions with host receptors, including platelet-derived growth factor receptor- α (PDGFRα), neuropilin 2 and olfactory receptor family 14 subfamily I-1 (OR14I1) (Connolly et al., 2021).This interaction takes place either through a trimeric complex formed by gO and gH-gL or through a pentameric complex formed by gH-gL and UL128, UL130 and UL131, depending on the cell type (Zhou et al., 2015). Membrane anchoring of gH-gL triggers gB refolding leading to the fusion of viral and cell membranes, creating a pore through which the virus enters the cell (Sathiyamoorthy et al., 2017).

Once inside the host cell, viral tegument proteins interact with the cell microtubule machinery to be transported to the nucleus. After replication takes place, capsid assembly occurs and it egresses from the nucleus to the cytoplasm through a process of envelopment at INM and de-envelopment at ONM (Sanchez and Britt, 2021). Here, hijacked cellular secretory machinery contributes to the assembly of virions, which acquire the tegument layer and the viral envelope (Close et al., 2018). Following successful maturation of the virions, they are released from the host cell, most probably through a secretory vesicle-like pathway (Figure 6).

HCMV can stablish latency by robustly supressing expression of almost all E and L genes through processes such as histone methylation. In addition, latency requires the induction of expression of small RNAs (e.g. miR-UL148D) that, being non-immunogenic, can modulate host cell environment by regulating expression of targets involved in immune e evasion, survival, and proliferation. A combination of viral and cellular factors, including inflammation, trigger the reactivation of latently infected cells (Lau et al., 2016).

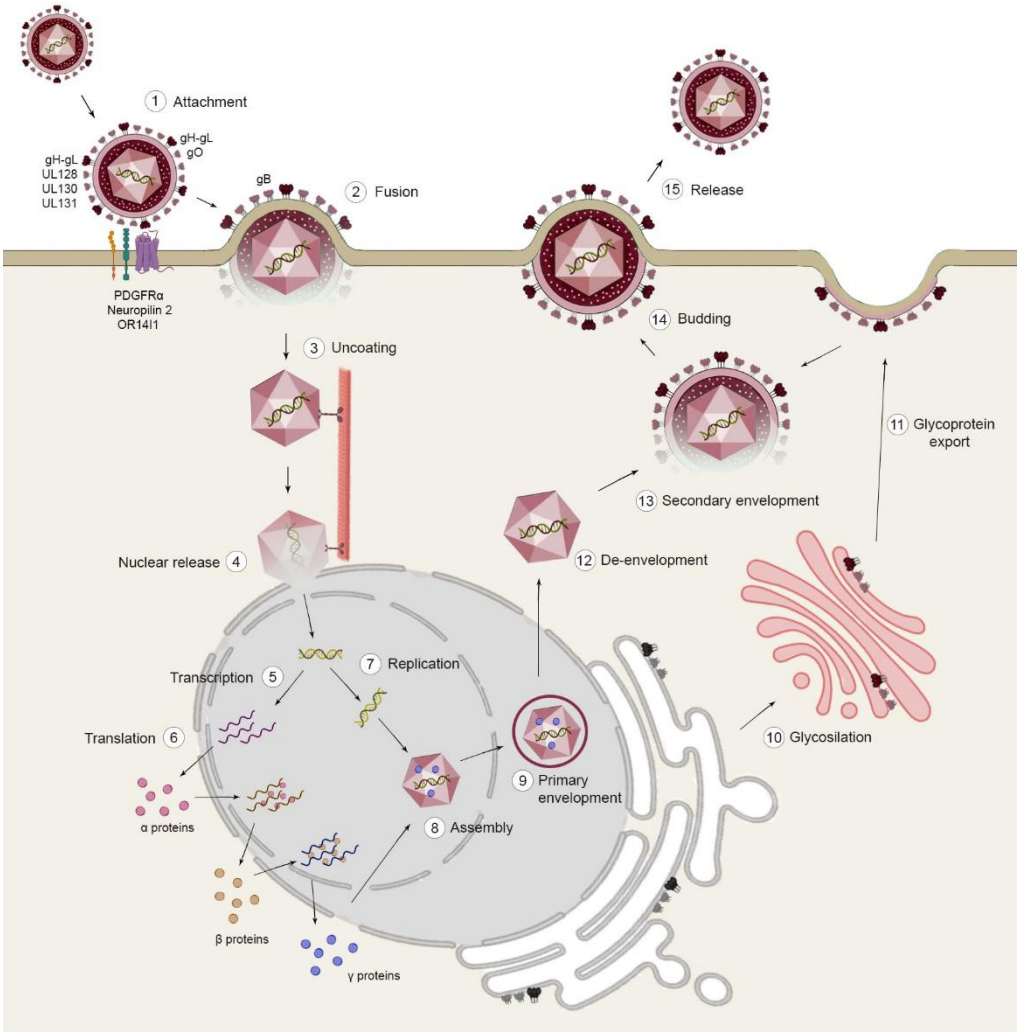

Figure 6: HCMV replication cycle. Representation of the HCMV viral cycle starting from the binding to different cell receptors, followed by the fusion with the host membrane and the uncoating the and nuclear release of the viral DNA into the cytoplasm. Afterwards, it gets transcribed and translated into new viral DNA and α, β and γ proteins, which assembly into new virions that are enveloped and de-enveloped to be subsequently enveloped again before budding off to be released.

2.2.2.4 Transmission mechanisms and clinical course

Acquisition of HCMV occurs most frequently during childhood and early adulthood; however, transmission can occur vertically (through placenta, during birth, or through breast feeding) and horizontally (via contact with contaminated saliva, urine, semen, or other bodily secretions, and organ transplant or blood transfusion) (Dioverti and Razonable, 2016).

In healthy immunocompetent individuals, primary infection is usually asymptomatic; however, it may present as a mononucleosis-like syndrome with fever, malaise, lymphadenopathy, and lymphocytosis. However, sever infection produces alterations in the gastrointestinal tract (colitis) and in the CNS (meningitis or encephalitis), cardiovascular abnormalities (haemolytic anaemia or thrombosis) and impairment in other organs such as eyes (retinitis), liver (hepatitis) or lungs (pneumonitis) (Rafailidis et al., 2008).

Congenital HCMV infection is the most frequent intrauterine infection, occurring in 40% of the cases where mothers develop primary infection during pregnancy (Akpan and Pillarisetty, 2021). It manifests as clinical disease only in 10 to 15% of cases, at birth or later, with mild to severe conditions such as petechial rash, hepatosplenomegaly, optic nerve atrophy, hearing loss, developmental and motor delay, prematurity, microcephaly, and death of the unborn baby (Fowler and Boppana, 2018).

One of the most frequent opportunistic infections in transplant patients is HCMV, it can occur both by reactivation in seropositive patients due to immunosuppressive treatments or by a primary infection in seronegative patients after transplantation (Azevedo et al., 2015). The clinical manifestations are very diverse and depend on the pro-inflammatory cytokine cocktail derived from transplantation, the duration of HCMV replication, and the status of the immune response. Milder manifestations include gastrointestinal symptoms such as diarrhoea, esophagitis, or gastroenteritis. Most severe disease exhibits symptoms such as hepatitis, pneumonia, myocarditis, pancreatitis, and meningoencephalitis, which may lead to patient death despite treatment (Razonable and Humar, 2019). Other immunosuppressed individuals, such as elderly patients or those with AIDS, leukaemia, lymphoma, or other malignancies, have similar manifestations, with ulcerative colitis being the most common (Griffiths et al., 2015, Griffiths and Reeves, 2021).

The approved drugs for the treatment and prophylaxis of HCMV are ganciclovir (GCV), its prodrug valganciclovir, cidofovir, foscarnet, and, more recently, letermovir. The front-line of action is GCV, nucleoside analogue of guanine which, similarly to cidofovir and foscarnet, inhibits the synthesis of HCVM DNA. On the other hand, letermovir blocks the packaging of DNA in the viral capsid (Poole and James, 2018). However, there are no effective vaccines or treatments that protect from reactivations, and prolonged therapies lead to appearance of resistances and toxicity. The high incidence and nature of the clinical manifestations of infection highlight the need for new effective therapies to protect high-risk populations exposed to HCVM.

2.3 NANOTECHNOLOGY AND NANOMEDICINE

Humanity has been exposed to nanoparticles (NPs) throughout its history, but it was not until 1925 that Richard Zsigmondy proposed the word *nanometre* to refer to particles size. Later, in 1960, another Nobel Prize Laureate, Richard Feynman, introduced in his speech ‘‘There’s Plenty of Room at the Bottom’’ the idea of manipulating matter at the atomic level (Feynman, 1960). Fifteen years later, Norio Taniguchi defined this technology as the one consisting of the processing, consolidation, separation, and deformation of materials by one atom or one molecule (Bhushan, 2017). In ‘‘Engines of Creation: The Coming Era of Nanotechnology’’ Eric Drexler proposed the idea of *molecular nanotechnology* in 1986 (Drexler, 1986). Nanotechnology has experimented its golden age in the 21st century when many different fields of nanoscience have emerged,

becoming a national priority in the legislation of the United States with the creation of the National Nanotechnology Initiative (NNI) in 2000 (Interagency Working Group on Nanoscience, 2000). This initiative describes nanotechnology as the understanding and control of matter at dimensions between 1 and 100 nanometres, enabling them with novel properties and functions because of their size (NNI).

This technology integrates different scientific fields, including physics, chemistry, and engineering among others (Huang et al., 2021, Riley et al., 2019, Wang et al., 2021). These integrations have provided original solutions to current medical, industrial, and environmental issues related to materials, manufacturing, energy, water, security, biotechnology, and more. In terms of nanomedicine, its main applications lie in the ability to control the size of the particles, making them of the same size as biological entities. Furthermore, the freedom to design and modify materials and their surfaces is the key to their impact in clinical applications such as medical diagnostics or drug development (Ramsden, 2016).

Some characteristics of these nanomolecules are their ability to transit through blood vessel walls and vascular epithelium (Tee et al., 2019), to penetrate the blood-brain barrier and the stomach epithelium (Ball et al., 2018, Rodriguez-Izquierdo et al., 2020b), to extravasate through splenic and liver fenestrae avoiding rapid filtration (Alphandery, 2019), to act as delivery vehicles (Mitchell et al., 2021), to interact with cell surface biomolecules (Salatin et al., 2015), to image biomolecular processes (Han et al., 2019) and to target specific molecules (Huang et al., 2017).

2.3.1 Dendritic structures

Nanoparticles are very diverse and can have multiple chemical compositions and shapes, but the most commonly used in nanomedicine are liposomes, gold NPs, quantum dots, carbon nanotubes and dendrimers (Figure 7) (Bozzuto and Molinari, 2015, Deng et al., 2020, Dias et al., 2020, Giljohann et al., 2010, Zhang et al., 2015). The later, dendrimers, are one of the nanoparticles that have experienced the greatest evolution in recent years since they have high significance in the field of medicine for being promising candidates for a wide range of applications.

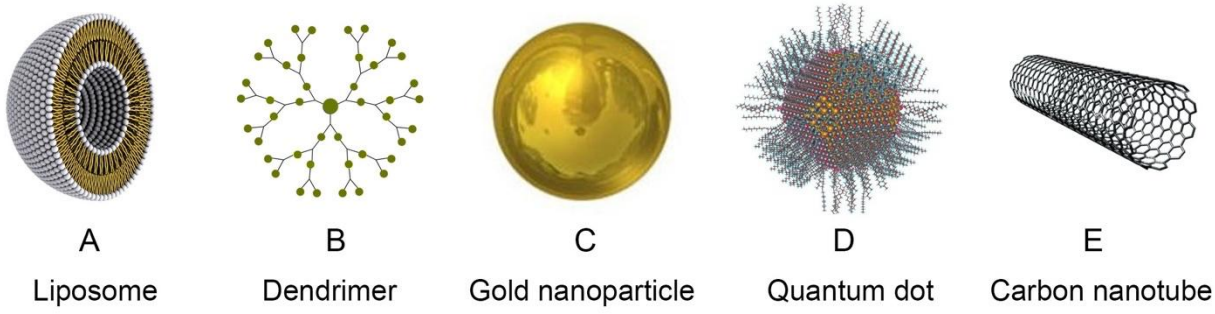

Figure 7: . Most common types of nanocompounds used in nanomedicine. **(A)** liposomes, **(B)** dendrimers, **(C)** gold nanoparticles, **(D)** quantum dots and **(E)** carbon nanotubes.

Vogtle created the first dendritic structure in 1978, but it was not until 1981, 1983, and 1985 that Denkewalter, Tomalia, and Newkome, respectively, confirmed the discovery of this type of nanoparticles (Baig et al., 2015). Since then, a lot of research has been carried out to determine the properties and applications of this molecules. Dendrimers can be used both as targeted delivery vehicles and as single treatments, such as those directed against viral and bacterial infections (Shaunak, 2015), inflammatory diseases (Fruchon and Poupot, 2018), cardiovascular diseases (Yu et al., 2015), and cancer (Kim et al., 2018).

2.3.1.1 Characterisation and properties

Dendrimers are well-defined, radially symmetric, homogeneous and monodisperse three-dimensional structures that consist of tree-like branches, which explains the use of this term to describe them: from Greek words ‘‘δένδρονand’’ and ‘‘μέροσ’’, which are translated to tree and parts, respectively (Fradet et al., 2019). They are formed by a functional core where hydrocarbon scaffolds (known as dendrons) are attached forming branching layers that surround the core, named generations (G), which can have specific functional groups at the periphery conforming a flexible multivalent structure (Figure 8) (Chis et al., 2020).

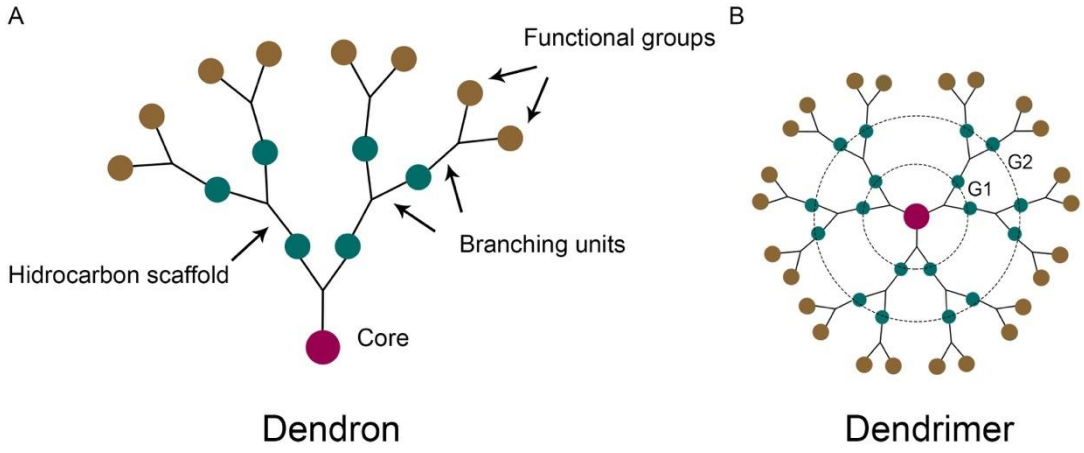

Figure 8: . Schematic representation of **(A)** dendrons and **(B)** dendrimers. The figure shows the repetitive layers from the central core with their branching units, the hydrocarbon scaffold structure, and the functional groups on the periphery.

Some of the dendrimers properties include their pharmacokinetic features (including rapid absorption, distribution, metabolism, and elimination), their polyvalency to produce various interactions with biological receptors, and the ability to establish electrostatic interactions useful for molecular recognition. The physicochemical properties of dendrons and the number of generations can be adjusted to control size, shape, folding, solubility, and multivalence to conjugate diverse drug molecules and specific targets (Abbasi et al., 2014).

These molecules feature both polymer (because they are made up of repetitive monomers) and molecular chemistry (because they are synthesised in a controlled manner step by step), and these features grant their physical nature, giving rise to different classifications of dendrimers based on either properties or structure. According to property classification, there are six types of dendrimers: (i) biodegradable, (ii) amino acid-based, (iii) hydrophilic, (iv) hydrophobic, (v) glycosylated, and (vi) asymmetric dendrimers. According to

structural classification, there are ten types of dendrimers: (i) simple, (ii) crystalline, (iii) chiral, (iv) micellar, (v) hybrid, vi) amphiphilic, (vii) metallic, (viii) multilingual, (ix) tectodendrimers, and (x) multiple antigen peptides (Mittal et al., 2021).

2.3.1.2 Synthesis

There are two different methods by which dendrimers can be synthesised (Figure 9) (Sherje et al., 2018, Wu et al., 2015)

i) Divergent methodology. This strategy is based on building the dendrimer from the core outward, through the reaction of the core molecule with monomers forming a first-generation dendrimer (G0). Then, the periphery of this G0 might react with more monomers to increase to G1 and repeat the process for several generations building the dendrimer layer after layer. This method usually forms dendrimers with imperfect structures and asymmetric shape that stop growing further because of steric constraints of the increasing branch density.

ii) Convergent methodology. In this approach, dendrons are grown separately and attached to the multifunctional core in the final step. This methodology overcomes limitations associated with the previous strategy such an easier purification of the end-product and the occurrence of fewer structural defects during build-up. However, steric impediments at the reactions of dendrons with the core do not allow the assembly of high-generation dendrimers.

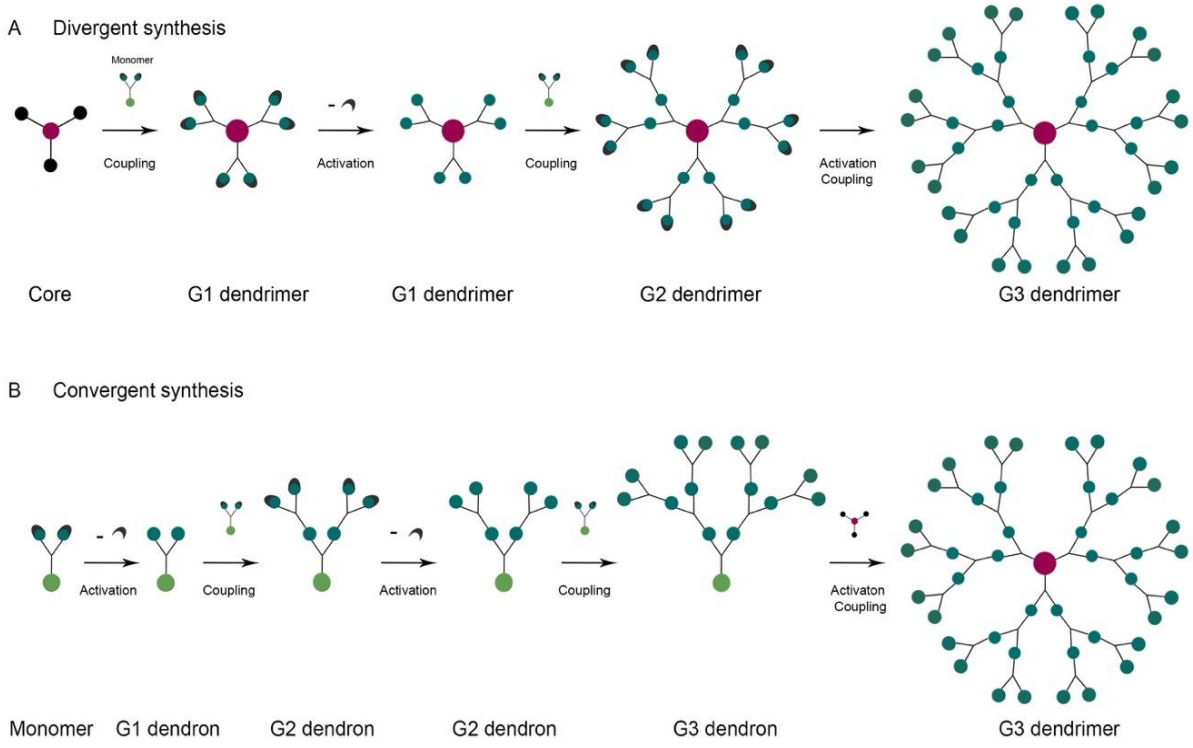

Figure 9: Schematic representation of dendrimer synthesis. **(A)** Divergent growth synthesis from the inside to the outside. **(B)** Convergent growth synthesis from the outside to the inside.

In the field of biomedicine and, more precisely, in virology, the mentioned nature of dendrimers makes them great candidates to be used against viral infections. Some antiviral strategies that can be developed, depending on the characteristics of each dendrimer, include their use as nanocarriers for different cargos (such as peptides, miRNAs or different drugs) and their use *per se* as direct antivirals for prophylactic or therapeutic treatments (Figure 10). The first dendrimer to be synthesised and commercialised was the poly (propylene imine) (PPI) dendrimer, consisting of a core of tertiary propylene amines and primary amines as terminal groups (Singh et al., 2021). The second oldest dendrimer to be synthetised was polyamidoamine (PAMAM) dendrimer, thus it is the most well-characterised class of dendrimer and has been enhanced to be used as drug delivery vehicle (Araujo et al., 2018). Other widely studied dendrimers are poly(L-Lysine) dendrimer, phosphorous dendrimers or carbosilane dendrimers.

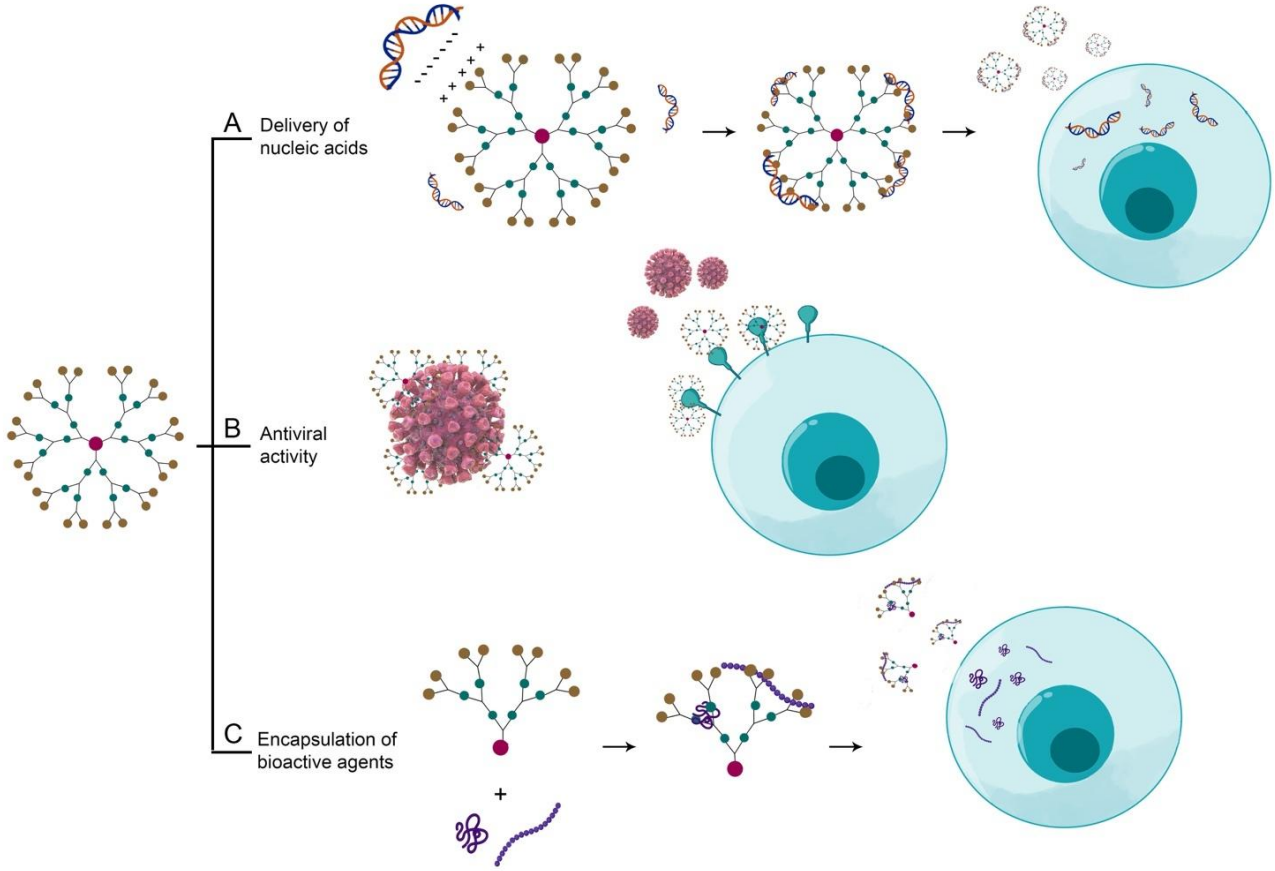

Figure 10: Nanomedical applications of nanoparticles. **(A)** Use as delivery vehicles for nucleic acids, **(B)** as antiviral agents per se and **(C)** as encapsulators of bioactive agents.

2.3.1.3 Cationic carbosilane dendrimers and micellar carbosilane dendrons

Among the different dendritic structures with promising nanomedical applications, one can find carbosilane dendrimers dendrons. Carbosilanes are compounds formed by silica and carbon in the molecular skeleton, leading to highly energetic and hydrophobic scaffolds. Surface functionalisation with specific moieties increases their usability in biomedical fields and gives rise to different types of dendrimers: anionic and cationic carbosilane dendrimers (Rabiee et al., 2020).

The following sections are dedicated to the description of the different nanoparticles used in this doctoral thesis.

2.3.1.3.1 Cationic carbosilane dendrimers

Cationic carbosilane dendrimers have proven to be powerful platforms for the formation of complexes with nucleic acids or drugs, termed dendriplexes, through the attachment of these molecules by electrostatic interactions (Palmerston Mendes et al., 2017). In addition, cationic groups of the periphery render them soluble in water, increasing the bioavailability of attached molecules, thus enabling them as non-viral vehicles (Bravo-Osuna et al., 2016). They also exhibit higher cytotoxicity than anionic carbosilane dendrimers, as a result of the favourable electrostatic interactions that can occur with negatively charged plasma membranes that compromise membrane integrity (Sepulveda-Crespo et al., 2017). However, the nature and number of functional surface groups will determine the extent of this toxicity. Binding of polyethylene glycol (PEG) residues has been shown to reduce toxicity and improve biocompatibility, biodistribution, and resistance to biodegradation of PEGylated dendrimers (Pedziwiatr-Werbicka et al., 2019).

2.3.1.3.2 Micellar carbosilane dendrons

Initial studies of the use of dendritic structures as delivery vehicles of drugs were focused on finding the mechanism by which drug molecules could be loaded to form dendriplexes. Research led to the development of dendritic micelles, termed dendrimicelles, in which dendrons arrange themselves in a spherical form, thus leading to the encapsulation of functional cargos of opposite charge (Mignani et al., 2021, Wang et al., 2020).

Different strategies are being exploited to facilitate optimal micellisation and overcome the main caveats of the design of these structures, namely control over their structure, size, aggregation number and stability, and controlled release of cargo (Kaup et al., 2021, Wang et al., 2014). Dendrimicelles are among the most versatile nanoparticles and have been successfully used for the controlled release and delivery of different cargoes, including nucleic acids and different drugs (Korkmaz et al., 2015, Sumer Bolu et al., 2016, Wei et al., 2015, Dong et al., 2018). These studies have shown that the use of dendrimicelles improved drug internalisation, potency, biocompatibility biodistribution, biodegradability, and reduced the appearance of drug resistances (Bolu et al., 2018).

OBJECTIVES

3. OBJECTIVES

Given the current state of the HIV-1, HSV-2, and HCMV epidemics, there is an urgent need to develop new therapeutic strategies. Based on previous results obtained from the investigation group, the hypothesis of this thesis is that dendritic nanostructures could be used to develop innovative therapeutic approaches to face the previously mentioned viral infections. Consistent with this, the objectives of this work are:

Objective 1:

To study the use of a new family of PEGylated cationic carbosilane dendrimers as microRNA (miRNA) delivery systems with anti-HIV-1 activity.

Objective 2:

To develop a new promising therapy against HSV-2 and HCMV infections based on the use of PEGylated cationic carbosilane dendrimers as inhibitors of the interaction between viral glycoproteins and cell HSPGs.

Objective 3:

To design a dendritic cell-based therapeutic vaccine against HIV-1 relying on the use of micellar carbosilane dendrons as delivery vehicles of HIV-1 immunogenic peptides.

MATERIALS AND METHODS

4. MATERIALS

4.1 NANOPARTICLES

Water-soluble and stable dendrimers and dendrons were synthesised according to the methods reported by the Dendrimers for Biomedical Applications Group (BioInDen) of the University of Alcalá (UAH, Alcalá de Henares, Madrid, Spain). Stock solutions of dendrimers and dendrons (1 or 5 mM) and their subsequent dilutions were prepared in nuclease-free water (Promega, Madrid, Spain).

4.1.1 PEGylated cationic carbosilane dendrimers

In this doctoral thesis, four PEGylated cationic carbosilane dendrimers (PCCDs) have been used: (i) second generation G2-SN15-PEG dendrimer, (ii) third generation G3-SN31-PEG dendrimer and their fluorescein isothiocyanate (FITC) labelled analogous, (iii) second generation G2-SN15-PEG FITC dendrimer and (iv) third generation G3-SN31-PEG FITC dendrimer. This nomenclature is based on the number of generations (G2 and G3 for second and third generation, respectively) and the number and nature of the functional groups (S for silica dendrimer and N for trimethylamine at the periphery). Figure 11 represents the schematic structure of these dendrimers and Table 1 includes a brief description of them.

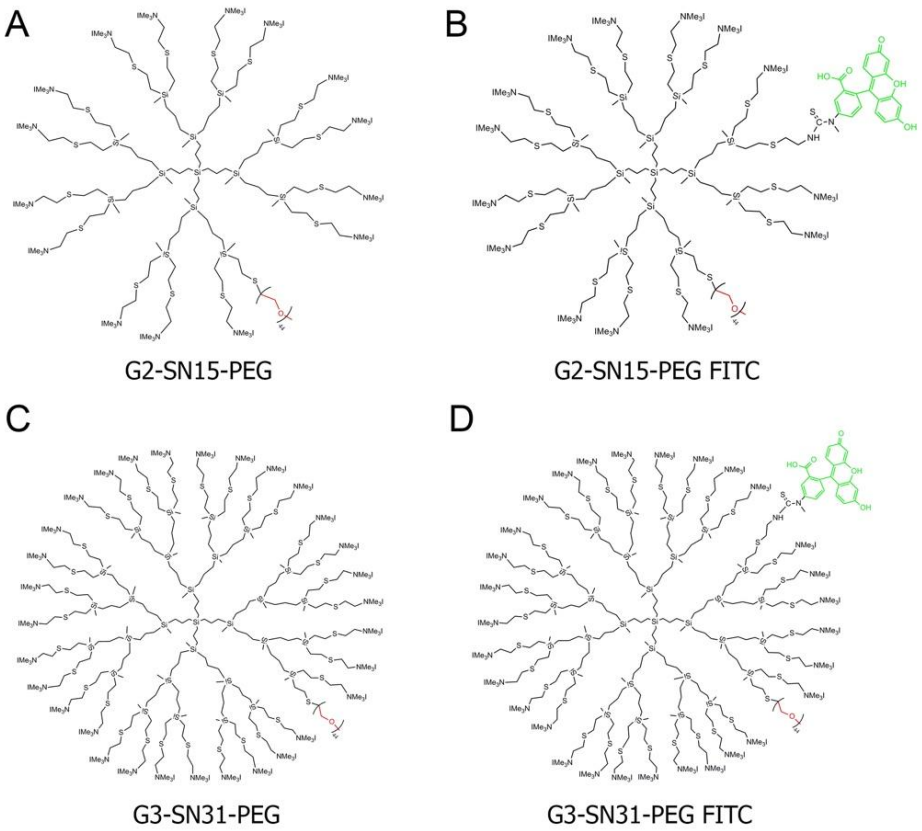

Figure 11: Schematic representation of PEGylated cationic dendrimers. **(A)** G2-SN15-PEG, **(B)** G2-SN15-PEG FITC, **(C)** G3-SN15-PEG and **(D)** G3-SN31-PEG FITC. Green molecule refers to FITC, and red molecule refers to PEG chains. **FITC:** fluorescein isothiocyanate. **PEG:** polyethylene glycol.

Table 1. Chemical and structural characteristics of PEGylated cationic carbosilane dendrimers.

Nomenclature	Molecular Formula	Functional Groups	Molecular Weight (g/mol)	Number of charges
G2-SN15-PEG	$C_{190}H_{438}I_{15}N_{14}O_{17}S_{16}Si_{13}$	NMe_3 and PEG	5987,31	15
G3-SN31-PEG	$C_{420}H_{969}I_{31}N_{31}O_{44}S_{32}Si_{29}$	NMe_3 and PEG	12926,92	31
G2-SN15-PEG FITC	$C_{209}H_{445}I_{14}N_{16}O_{22}S_{17}Si_{13}$	NMe_3, PEG and FITC	6221,74	14
G3-SN31-PEG FITC	$C_{439}H_{969}I_{30}N_{32}O_{49}S_{33}Si_{29}$	NMe_3, PEG and FITC	13161,34	30

4.1.2 Micellar anionic and cationic carbosilane dendrons

In this doctoral thesis, third generation anionic and cationic carbosilane micellar dendrons with cholesterol and d-α-tocopherol (vitamin E) at the focal point, namely (i) $EG3SO_3Na$, (ii) $ChG3SO_3Na$, (iii) $EG3NMe_3I$, and (iv) $ChG3NMe_3I$ have been used. This nomenclature is also based on the number of generations (G3 for the third generation) and the nature of the functional groups (E for d-α-tocopherol and Ch for cholesterol). Figure 12 represents a schematic representation of the structure of these dendrimers and Table 2 includes a molecular description of them.

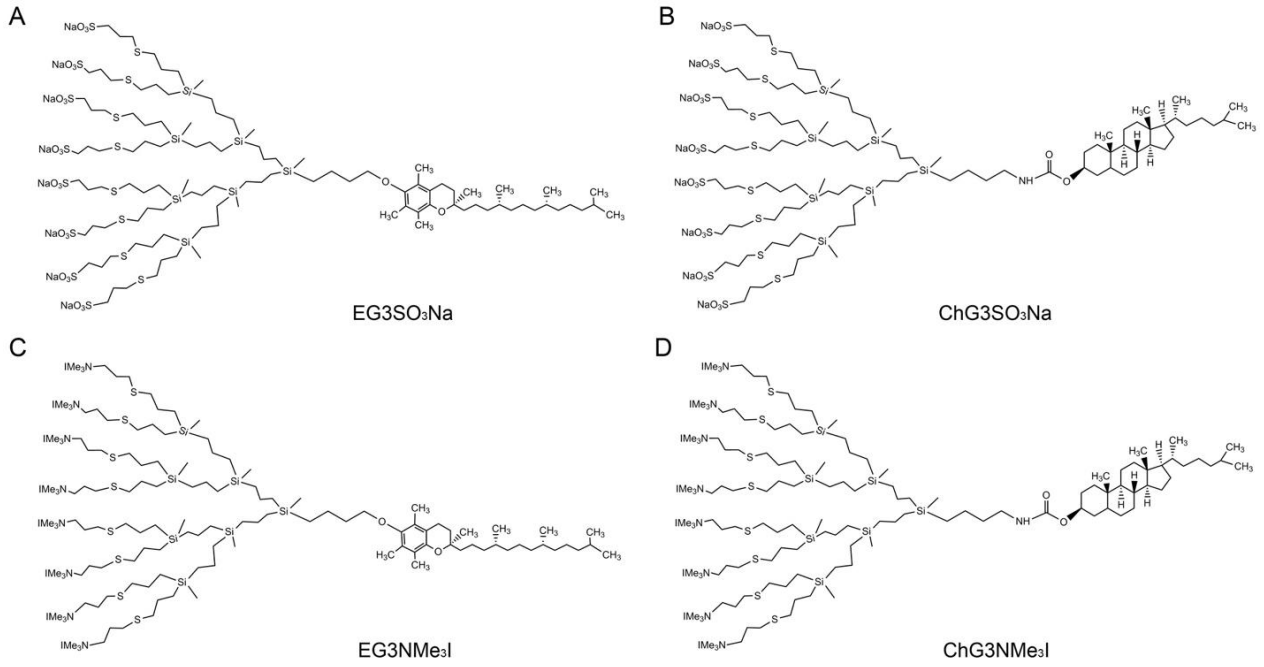

Figure 12: Schematic representation of micellar carbosilane dendrons. **(A)** $EG3SO_3Na$, **(B)** $ChG3SO_3Na$, **(C)** $EG3NMe_3I$ and **(D)** $ChG3NMe_3I$. **E:** d-α-tocopherol (vitamin E); **Ch:** cholesterol.

Table 2. Chemical and structural characteristics of micellar carbosilane dendrons.

Nomenclature	Molecular Formula	Functional Groups	Molecular Weight (g/mol)	Number of charges
EG3SO_3Na	$C_{106}H_{210}Na_8O_{26}S_{16}Si_7$	SO_3 and d-α-tocopherol	2794,34	8
ChG3SO_3Na	$C_{105}H_{209}Na_8O_{26}S_{16}Si_7$	SO_3 and cholesterol	2795,33	8
EG3NMe_3I	$C_{122}H_{266}I_8N_8O_2S_8Si_7$	NMe_3 and d-α-tocopherol	3345,82	8
ChG3NMe_3I	$C_{121}H_{265}I_8N_9O_2S_8Si_7$	NMe_3 and cholesterol	3346,81	8

4.2 REAGENTS

The approved antiviral compounds used as inhibition controls throughout this report include:

- ACV 50 mg (Selleckchem, Houston, TX, USA): $C_8H_{11}N_5O_3$, MW: 225,21 g/mol. It is a nucleoside analogue that inhibits the synthesis of HSV-2 DNA. It was purchased as a lyophilised product and reconstituted into a 10 mM dilution with dimethyl sulfoxide (DMSO, Honeywell, Charlotte, NC, USA).
- GCV 500 mg (Hoffmann-La Roche, Basel, Switzerland): $C_9H_{13}N_5O_4$, 255,23 g/mol. Another nucleoside analogue that inhibits the synthesis of HCVM DNA. It was purchased as a lyophilised product and reconstituted into a 5.4 mg/mL dilution with nuclease-free water (Promega, Madrid, Spain).

Other reagents include heparin (13.6 kDa, Laboratori Derivati Organici Spa, Milan, Italy), an analogue of HSPGs; heparinase II from *Flavobacterium heparinum* (Merck KGaA, Darmstadt, Germany), an enzyme that cleaves glycosidic bonds and phytohemagglutinin (PHA; Remel, Dartford, Kent, UK) used as a positive control of cell proliferation and as an activator of peripheral blood mononuclear cells (PBMCs).

4.3 miRNAS

Different cellular miRNAs reported to have activity against HIV-1 were selected based on their homology with its genome: (i) hsa-miR-29a-3p, (ii) hsa-miR-29b-3p, (iii) hsa-miR-92a-3p, (iv) hsa-miR-133b and (v) hsa-miR-149-5p (Ahluwalia et al., 2008, Houzet et al., 2012). One random miRNA (hsa-miR-Random) with no activity against HIV-1 but similar length was selected as a negative control (QUIAGEN, Hilden, Germany). Table 3 shows the sequence, HIV-1 genome target and effect on HIV-1 replication. Stock solutions (66,7 μM) and working concentrations (6670 nM) were prepared in nuclease-free water (Promega, Madrid Spain) and stored at – 20 ºC until use.

Table 3. Characterisation of selected miRNAs with anti-HIV-1 activity and control miRNA.

Nomenclature	Sequence	HIV-1 genome target	Effect on HIV-1 replication
hss-miR-29a-3p	UAGCACCAUCUGAAAUCGGUUA	*Nef*/3'UTR	Negative
hsa-miR-29b-3p	UAGCACCAUUUGAAAUCAGUGUU	*Nef*/3'UTR	Negative
hsa-miR-92a-3p	UAUUGCACUUGUCCCGGCCUGU	*Pol*	Negative
hsa-miR-133b	UUUGGUCCCCUUCAACCAGCUA	*Env*	Negative
hsa-miR-149-5p	UCUGGCUCCGUGUCUUCACUCCC	*Gag*	Negative
hsa-miR-Random	UCACCGGGUGUAAAUCAGCUUG	-	None

4.4 HIV-1-DERIVED PEPTIDES

Immunogenic HIV-1-derived peptides from different locations were synthesised by Genscript Biotech (Piscataway, NJ, USA). Peptides were designed to belong to different protein regions; thus, the nomenclature used refers to the name of the complete protein to which they belong, namely Rev, Vif, Gag-Pol, or Env. This work has been carried out with six different peptides (ranging from 18 to 20 amino acids) and their sulfo-Cyanine5- (Cy5), tetramethylrhodamine- (TAMRA) or FITC-labelled forms; Table 4 shows their amino acid sequence, the protein they belong to, their net charge, the label used and the approximate molecular weight of each peptide. Peptides were purchased as a lyophilised product and reconstituted into a 5 mM solution with nuclease-free water (Promega, Madrid, Spain) or 20% DMSO (Honeywell, Charlotte, NC, USA) depending on their solubility.

Table 4. Characterisation of designed peptides belonging to different HIV-1 proteins.

Nomenclature	Sequence	Protein	Net charge	Label	Molecular Weight (g/mol)
Pep-Rev	EGTRQARRNRRRRWRERQRQ	Rev	+8	-	2752,05
Pep-Rev-L				Cy5	3216,64
Pep-Vif	ALAALITPKKIKPPLPSVRK	Vif	+5	-	2141,70
Pep-Vif-L				Cy5	2895,44
Pep-GagPol-1	KIRLRPGGKKKYKLKHIVWA	Gag-Pol	+8	-	2420,01
Pep-GagPol-1-L				Cy5	2884,60
Pep-GagPol-2	TEVIPLTEEAELELAENREI	Gag-Pol	-6	-	2298,51
Pep-GagPol-2-L				TAMRA	2710,95
Pep-GagPol-3	ETWETWWTEYWQATWIPEWE	Gag-Pol	-5	-	2757,93
Pep-GagPol-3-L				FITC	3260,47
Pep-Env	GPDRPEGIEEEGGERDRD	Env	-5	-	2013,01
Pep-Env-L				TAMRA	2425,45

4.5 CELL LINES

TZM.bl cell line (National Institute of Health, NIH, AIDS Research and Reference Reagent Program, Germantown, MD, USA) is a human cervical epithelial carcinoma cell line (HeLa cell line), which expresses CD4 receptor and CCR5 co-receptor and contains β-galactosidase and luciferase genes under the control of LTR regions of the HIV-1 promoter (Polonis et al., 2008). This cell line was maintained in Dulbecco's Modified Eagle's Medium (DMEM) (Biochrom GmbH, Berlin, Germany) supplemented with 5% heat-inactivated fetal bovine serum (FBS) (Biochrom GmbH), 2 mM L-glutamine (Lonza, Base, Switzerland) and a cocktail of antibiotics (125 mg/ml ampicillin, 125 mg/ml cloxacillin and 40 mg/ml gentamicin) (Normon, Madrid, Spain).

U87MG-$CD4^+CCR5^+$ (NIH AIDS Research and Reference Reagent Program) is a human glioblastoma cell line derived from U87MG that expresses the CD4 receptor and the CCR5 and CXCR4 coreceptors. This cell line was cultured in DMEM supplemented with 10% heat-inactivated FBS, 2 mM L-glutamine and the aforementioned antibiotic cocktail.

Vero cell line is a fibroblast-like kidney cell line from *Chlorocebus aethiops*, it was obtained from the American Type Culture Collection (ATCC) (CCL-81TM, ATCC, Manassas, VA, USA). This cell line was maintained in DMEM supplemented with 5% FBS, 2 mM L-glutamine, and the same cocktail of antibiotics.

MRC-5 cell line, a human fibroblast lung cell, was obtained from ATCC (CCL-171TM). This cell line was cultured in Eagle's minimum essential medium (EMEM) (ATCC) supplemented with 10% FBS, 2 mM L-glutamine, and the previously mentioned cocktail of antibiotics.

All cell lines were cultured in an environment at 37 ºC with 5% CO_2 and seeded in 6, 12, 24 or 96-well plates at specific concentrations, depending on the cell line and the experiment to be performed.

4.6 PRIMARY CELL CULTURES

4.6.1 Human peripheral blood mononuclear cells

Human PBMCs were obtained from buffy coats acquired from healthy anonymous donors from the Madrid Transfusion Center (Madrid, Spain) following current legislation. PBMCs were isolated by Ficoll-Hypaque density gradient (Rafer, Madrid, Spain) according to the standard procedures of the Spanish HIV HGM BioBank (Garcia-Merino et al., 2009).

After isolation, PBMCs ($5x10^6$ cells/mL) were cultured in RPMI-1640 (Biochrom GmbH, Berlin, Germany) supplemented with 10% FBS, 2 mM L-glutamine and the aforementioned cocktail of antibiotics. Survival of T cells was ensured by adding 60 IU/mL of interleukin-2 (IL-2, Bachem, Budendorf, Switzerland). Activation of T cells was achieved by stimulation with 2 µg/mL of PHA (Remel, Dartford, Kent, UK) for 48 h.

4.6.2 Monocyte-derived dendritic cells

Human monocytes were purified from PBMCs isolated from buffy coats of healthy donors using immune-magnetic anti-CD14 microbeads (Miltenyi Biotec, Madrid, Spain) according to the manufacturer's instructions.

Purified monocytes were seeded in 6-well plates at 10^6 cells/mL in RPMI-1640 (Biochrom GmbH, Berlin, Germany) supplemented with 10% FBS, 2 mM L-glutamine and the previous cocktail of antibiotics.

Differentiation of monocytes into monocyte-derived dendritic cells (moDCs) was achieved by adding of 20 ng/mL of recombinant human IL-4 (rhIL-4, ImmunoTools GmbH, Friesoythe, Germany), 50 ng/mL of recombinant human granulocyte macrophage colony-stimulating factor (rhGM-CSF, ImmunoTools GmbH) and 50 µM of 2-mercaptoethanol (Merck KGaA, Darmstadt, Germany). Three days after culture, the medium was renewed and cells were maintained for two more days. To obtain mature DCs (mDCs) cells were stimulated with 20 ng/mL of lipopolysaccharide (LPS, Sigma-Aldrich, San Luis, MO, USA) for 48 h.

4.7 VIRAL ISOLATES

The viral isolate CCR5-tropic R5-HIV-$1_{NL(AD8)}$ was obtained by calcium chloride transfection with pNL(AD8) plasmid (NIH AIDS Research and Reference Reagent Program, Germantown, MD, USA) into the HEK- 293 T cell line (ATCC, Manassas, VA, USA). Viral production was collected and clarified by centrifugation of culture supernatants after 48 h. Viral titter was evaluated using an HIV-1 p24gag enzyme-linked immunosorbent assay (ELISA) kit (INNOTEST HIV, Antigen mAb, Innogenetics, Ghent, Belgium), as previously reported (Garcia-Broncano et al., 2017). Stock aliquots were stored at -80 ºC.

Viral strain HSV-2_{333} (GenBank accession number LS480640, NIH, Bethesda, MD, USA) and HCMVAD-169 (ATCC VR-538TM, ATCC) were grown and propagated in Vero and MRC-5 cells, respectively, and titrated by plaque assay as previously described (Guerrero-Beltran et al., 2020, Relano-Rodriguez et al., 2021a). Briefly, cells were seeded in 12-well plates and infected with different dilutions of viral stocks when growth reached a confluent monolayer. After incubation, cells were stained with Methylene Blue (Sigma-Aldrich, San Luis, MO, USA) and viral plaques were counted; the viral stock was titrated in plaque-forming units (PFU). Stock aliquots were also stored at -80 ºC.

5. METHODS

5.1 CELL VIABILITY ASSAYS

The determination of the toxicity produced by the diverse experiments carried out was done through five different methods: (i) MTT assay, (ii) lactate dehydrogenase (LDH) assay, (iii) genotoxicity assay, (iv) flow cytometry and (v) haemolytic assay.

5.1.1 MTT assay

Nanoparticle or peptide-induced mitochondrial toxicity was evaluated by the MTT assay (Sigma, St Louis, MO, USA) following manufacturer's instructions. Briefly, $2x10^5$ PBMCs, $7{,}5x10^3$ U87MG-$CD4^+CCR5^+$, $1{,}5x10^4$ Vero and MRC-5 and $1x10^5$ iDCs cells/well were seeded into 96-well plates. After incubating adherent cells for 24 h at 37 ºC, cells were treated with different concentrations of PCCDs, dendrimicelles or peptides for different times depending on the cell line (48 or 72 h or 6 days). After incubation, plates were centrifuged at 1500 rpm

for 10 min and culture medium was replaced by 200 µL of a solution formed by MTT (5 mg/mL) and Opti-MEMTM (Thermo Fisher Scientific, Waltham, MA, USA) (1:11). Three hours later, the reaction was stopped by removing this solution and dissolving the formazan crystals in DMSO (Honeywell, Charlotte, NC, USA). Formazan concentration was determined by spectrophotometry using a Synergy 4 plate reader (BioTek, Winooski, VT, USA) recording the absorbance at 490 nm. Culture medium was used as non-treated (NT) control and 10% DMSO as death control. Experiments were made three times in triplicate.

5.1.2 LDH assay

The determination of the membrane integrity of cells treated with PCCDs was performed using the LDH CytoTox 96® Non-Radioactive Cytotoxicity assay (Promega, Spain, Madrid) according to the manufacturer's instructions. Shortly, Vero and MRC-5 cell lines were seeded at $1{,}5x10^4$ cells/well into 96-well plates. Then, 24 h after incubation at 37 ºC, cells were treated with increasing concentrations of PCCDs for 48 h (Vero cells) and 6 days (MRC-5 cells). Afterwards, supernatants were discarded and cells were lysed for 45 min at 37 ºC with 0.9% Triton X-100 (Promega). Then 50 µL of LDH reagent (Promega) was added to the lysate and incubated for 30 min at room temperature (RT) in the dark. The concentration of LDH concentration was determined by spectrophotometry using a Synergy 4 plate reader (BioTek, Winooski, VT, USA) measuring the absorbance at 490 nm. Culture medium was used as non-treated (NT) control. Experiments were made three times in triplicate.

5.1.3 Genotoxicity assay

The genotoxicity of PCCDs in PBMCs was measured by performing the sister chromatids exchange (SCE) assay. To carry out this assay, PBMCs from five healthy donors were treated with 10 µM of G2-SN15-PEG or 5 µM of G3-SN31- PEG dendrimers for 72 h. NT cells were used as genetic viability control and radiation at 1 Gy was used as the genotoxic control. The cultures were then treated with 25 µM of 5-bromo-2'-deoxyuridine (BdrU) (Thermo Fisher Scientific, Waltham, MA, USA) to monitor second divisions. After 70 h, 0,1 µM/mL of colcemid (Thermo Fisher Scientific), a mitosis inhibitor, was added and, 2 h after, metaphases were extended and analysed by fluorescence plus Giemsa (FPG). Shortly, cells were centrifuged 10 min at 600 g, supernatant was discarded, and 10 mL of 5,6 µg/mL potassium chloride (Merck KGaA, Darmstadt, Germany) was added. Cells were then centrifuged 10 min at 600 g, supernatant was discarded, and the pellet was fixed with methanol/glacial acetic acid (3:1) (PanReac AppliChem, Madrid, Spain). This procedure was repeated 3 times and the resulting metaphases were dropped onto slides (Thermo Fisher Scientific). After 48 h maturing at 56 ºC, slides were immersed in Hoechst solution (Sigma, St Louis, MO, USA) for 30 min, rinsed with water, and immersed in McIlvaine buffer (0,55 mL citric acid and 19,45 mL di-Sodium hydrogen phosphate) (Merck KGaA), for 40 min in a thermostatic plate at 56 ºC 5 cm away from UV light. Afterwards, slides were washed and stained with Giemsa (Merck KGaA) for 7 min. Images were obtained with a Leica DM 5000 B Microscope and analysed with Cytovision® software (Leica, Wetzlar, Germany).

5.1.4 Flow cytometry viability determination

Viability of cells after being treated with dendrimers, dendrimicelles or peptides was complementarily studied by flow cytometry using LIVE/DEAD™ Fixable Aqua Dead Cell Stain (Thermo Fisher Scientific, Waltham, MA, USA). This amine-reactive dye binds to intracellular and extracellular amines in cells with compromised membranes, exhibiting a great difference in fluorescence intensity with viable cells, in which it binds only to extracellular amines, allowing easy discrimination between them (ThermoFisher).

Briefly, after the desired treatment, cell lines or primary cell cultures were washed with 3% bovine serum albumin (BSA, Sigma, St Louis, MO, USA) phosphate buffered saline (PBS, Lonza, Base, Switzerland) and resuspended to a density of 10^6 cells/mL. Then, cells were stained with 1 μL/mL of the reconstituted fluorescent reactive dye for 30 min at RT in the dark. Subsequently, cells were washed with 3% BSA PBS and fixed with 2% paraformaldehyde (PFA, Sigma). Flow cytometry was performed on a Gallios or CytoFLEX flow cytometer and measurements were analysed using Kaluza 2.1 software (Beckman Coulter, Brea, CA, USA).

5.1.5 Haemolitic assay

The haemolytic potential of PCCDs was studied by performing a haemolytic test, in which the capacity of dendrimers to cause erythrocyte haemolysis was tested. To do so, $1x10^6$ PBMCs were incubated with PCCDs at the maximum non-toxic concentration and half this value for 1 h at 37 ºC. Afterwards, samples were centrifuged at 1500 rpm for 10 min, and supernatants were collected. Cell-free haemoglobin concentration in each sample was evaluated by measuring absorbance at 540 nm with a Synergy 4 plate reader (BioTek, Winooski, VT, USA). PBS was used as negative control, distilled water was used as positive control, and 0,2% Triton X-100 was used as a haemolytic agent. Experiments were performed twice.

5.2 DENDRIPLEXES FORMATION

Two types of dendriplexes have been used throughout this work: (i) dendrimer-miRNA complexes and (ii) dendrimicelles-peptide complexes. Both types have been constructed by mixing 100 nM of the desired miRNAs or 1 μM of the selected peptides and the maximum non-toxic concentration of PCCDs or dendrimicelles. Dendriplexes were formed in nuclease-free water (Promega, Madrid, Spain) within 2 h of incubation at 37 ºC.

5.2.1 Agarose gel electrophoresis

Formation and stability of the dendriplexes was studied by agarose gel electrophoresis. To do so, complexes were built as previously mentioned. After formation, they were treated with Blue/Orange Loading Dye 6X (Promega, Madrid, Spain) and loaded on a 2 or 6% agarose (Sigma, St Louis, MO, USA) gel in Tris–acetate-EDTA (TAE) buffer (PanReac AppliChem, Darmstadt, Germany). For dendrimer-miRNA complexes, 0,01%

GelRed® (Biotium, Fremont, CA, USA) was added to gels. Gels were run at 120 mV for 30 or 50 min on a PowerPac Universal power supply (Bio-Rad Laboratories, Hercules, CA, USA).

5.2.2 Zeta potential and dynamic light scattering

The formation, surface charge, and stability of dendriplexes were also evaluated by measuring the electrical potential (by zeta potential, ZP) and the hydrodynamic size (by dynamic light scattering, DLS). These measurements were also useful to evaluate how miRNAs affect to the properties of PCCDs. Measurements were performed at 25 ºC with a Zetasizer Nano ZS spectrometer (Malvern Instrument, Malvern, UK). For ZP measurements, dendriplexes were prepared as previously detailed and loaded into folded capillary cells and measured using a voltage of 100 V. For DLS, samples were loaded into quartz cuvettes with a path length of 10 mm. Three measurements with an average of fourteen cycles were made for each sample.

5.2.3 Heparin competition and RNase protection assays

To test the capacity of miRNAs to disengage from complexes and to test whether the formation of dendriplexes confers protection against RNases, heparin exclusion and RNase protection assays were performed, respectively. Dendriplexes were formed as earlier described and were treated with 0.2 UI/µL of heparin (Lab Ramón Sala, Barcelona, Spain) for 5 min at RT and/or 1 µg/µL of RNase (Promega, Madrid, Spain) for 10 min at RT. Samples were analysed by agarose gel electrophoresis as mentioned in section 5.2.1 Agarose gel electrophoresis.

5.3 NANOPARTICLE AND PEPTIDE INTERNALISATION ASSAYS

Internalisation of fluorescent labelled PCCDs and peptides into cells was analysed both by confocal microscopy and flow cytometry.

5.3.1 Confocal microscopy

Internalisation studies were performed by confocal microscopy with a Leica TSC SPE Confocal Microscope (Leica, Wetzalar, Germany) on different cell lines and primary cell cultures. PBMCs and DCs were seeded in 24-well plates at a density of $1x10^6$ and $5x10^5$ cell/well, respectively. On the other hand, U87MG-$CD4^+CCR5^+$, Vero, and MRC-5 cell lines were seeded at $7,5x10^3$, $1,75x10^5$, and $8x10^4$ cells in 12 mm circle cover slips (Thermo Fisher Scientific, Waltham, MA, USA) pre-treated for 24 h with poly-L-lysine (Sigma, St Louis, MO, USA). Cells were treated with the maximum non-toxic concentrations of FITC-labelled PCCDs (G2-SN15-PEG FITC and G3-SN31-PEG FITC) or with the various labelled dendrimicelles-peptide complexes for different times (1, 2, 6, or 24 h) at 37ºC. After incubation, handling PBMCs and DCs as suspension cells and the rest as adherents, cells were rinsed twice with 3% BSA (Sigma) PBS (Lonza, Base, Switzerland). Then, cells were treated with 0,2 M glycine (Sigma) pH 3 for 30 sec at RT and immediately washed twice with 3% BSA PBS. Cells were fixed with 2% PFA (PanReac AppliChem, Madrid, Spain) for 15 min and permeabilised with 0.1% Triton 100X (Sigma) for 15 min. Actin labelling was carried out by incubation with Alexa Fluor™ 555 or 488

Phalloidin (Thermo Fisher Scientific) for 1 h at RT. Following two rinses with 3% BSA PBS, cells were incubated for 15 min with 4',6-diamidino-2-phenylindole dihydrochloride (DAPI, Sigma) for nuclear visualisation. Finally, cells were mounted on microscope slides with fluorescent mounting media (Dako, Carpinteria, CA, USA). Image analysis was performed with ImageJ (NIH, Bethesda, MD, USA).

5.3.2 Flow cytometry

Internalisation of PCCDs and peptides was confirmed by flow cytometry using a Gallios or CytoFLEX flow cytometer (Beckman Coulter, Brea, CA, USA), respectively. In-brief, $1x10^6$ PBMCs, $5x10^5$ DCs, $1{,}5x10^4$ U87MG-$CD4^+CCR5^+$, $1{,}75x10^5$ Vero, and $8x10^4$ MRC-5 cells/well were seeded in 24-well plates and treated with the corresponding maximum nontoxic concentrations of FITC-labelled PCCDs (G2-SN15-PEG FITC and G3-SN31-PEG FITC) or with the various labelled dendrimicelles-peptide complexes for different times (1, 2, 6, 24 or 48 h) at 37ºC. After incubation, handling PBMCs and DCs as suspension cells and the rest as adherents, cells were rinsed twice with 3% BSA (Sigma, St Louis, MO, USA) PBS (Lonza, Base, Switzerland). Afterwards, cells were treated with 0,2 M glycine (Sigma) pH 3 for 30 sec at RT and immediately washed twice with 3% BSA PBS. PBMCs were then incubated with anti-human-CD3-PC5 (Beckman Coulter, Brea, CA, USA) and DCs were incubated with anti-human-CD11c-PC7 (BioLegend, San Diego, CA, USA) for 30 min at RT and then rinsed twice with 3% BSA PBS. Viable cells were identified using LIVE/DEAD™ Fixable Aqua Dead Cell Stain (Thermo Fisher Scientific, Waltham, MA, USA) as previously described. Finally, cells were fixed with 2% PFA. Measurements were analysed using Kaluza software 2.1 (Beckman Coulter). Experiments were performed three times.

5.4 HIV-1 INHIBITION EXPERIMENTS

Anti-R5-HIV-1 activity of dendrimer-miRNA complexes was evaluated by HIV-1 inhibition experiments. Shortly, PBMCs were seeded at a density of $1x10^6$ cells/well in 24-well plates and U87MG-$CD4^+CCR5^+$ at $7{,}5x10^3$ cells/well in 96-well plates. Then, 24 h after seeding, cells were infected with R5-HIV-$1_{NL(AD8)}$ strain at a concentration of 15 ng of p24 per10^6 cells and treated with the desired dendriplexes formed as described in section 5.2. This is 100 nM of the desired miRNAs and 10 and 5 μM of G2-SN15-PEG and G3-SN31-PEG dendrimers for PBMCs and 5 and 1 μM of G2-SN15-PEG and G3-SN31-PEG dendrimers for U87MG-$CD4^+CCR5^+$ cells. Supernatants were collected 72 h after the infection and were titrated by TZM.bl or frozen at -80 ºC. Experiments were carried out three times in triplicate.

5.4.1 Supernatant titration

Luciferase activity measurements were performed to infer viral infectivity. To do so, the supernatants collected from HIV-1 inhibition experiments were titrated on TZM.bl cells. Briefly, TZM.bl cells were seeded at a density of $1x10^4$ cells/well in 96-well plates. After 24 h of incubation at 37 ºC, culture medium was replaced with 100 μL of fresh medium and 100 μL of supernatants from PBMCs or U87MG-$CD4^+CCR5^+$ infected and treated. Then 48 h after titration, medium was removed, and cells were lysed with 50 μL of Cell Culture Lysis 5X

Reagent (Promega, Madrid, Spain) for 30 min at 4 ºC. Finally, 25 µL of cell lysates were transferred to white clear bottom plates and 25 µL of Luciferase Assay Reagent (Promega) were added just before reading the luciferase activity in a Synergy 4 plate reader at 135/200 nm.

5.5 HSV-2 AND HCMV INHIBITION EXPERIMENTS

Antiviral activity of PCCDs was evaluated through inhibition experiments by plaque reduction assay. In-brief, Vero and MRC-5 cells were seeded at a density of $1{,}75x10^5$ and $6x10^4$ cells/well in 24-well plates, respectively, and incubated at 37 ºC for 24 h. Then, both cell lines were treated with increasing concentrations (from 0.2 µM to the maximum non-toxic) of G2-SN15-PEG and G3-SN31-PEG dendrimers for 1 h. In addition, increasing concentrations (from 0.2 µM to 10 µM) of reference treatments ACV or GCV were used for comparison with current treatments.

Afterwards, pre-treated Vero and MRC-5 cells were infected with HSV- 2_{333} and $HCMV_{AD\text{-}169}$ strains, respectively, at a multiplicity of infection (MOI) of 0,001. Three hours after infection, cells were washed with PBS (Lonza, Base, Switzerland) to remove unabsorbed viruses. HSV-2 infection remained in DMEM (Biochrom GmbH, Berlin, Germany) supplemented with 2% FBS (Biochrom GmbH) and 0.4% Immunoglobulin G (IgG, Berigloblin P, CSL Behring GmbH, Marburg, Germany) for 48 h. HCMV infection remained in EMEM (ATCC, Manassas, VA, USA) supplemented with 2% FBS for 6 days. Then the medium was discarded and both cell lines were stained with 300 mg/L Methylene Blue (Sigma, St Louis, MO, USA) for 30 min (Vero) and 3 h (MRC-5). Inhibition was determined as the reduction of the plaques formed with treatments regarding the infection control. Noninfected samples were used as untreated samples and NT samples as infection controls (IC). Experiments were carried out three times in triplicate.

5.5.1 HSV-2 and HCMV viral inactivation assay

To determine whether PCCDs interact directly with HSV-2 or HCMV, the viral inactivation assay was performed. Briefly, Vero and MRC- 5 cells were seeded at a density of $1{,}75x10^5$ and $6x10^4$ cells/well in 24-well plates, respectively, and incubated at 37 ºC for 24 h. Subsequently, 1 µM of G2-SN15-PEG or 1 µM of G3-SN31-PEG dendrimers were incubated for 2 h at 37 ºC with 175 pfu/mL or 60 pfu/mL of cell-free HSV-2_{333} and $HCMV_{AD\text{-}169}$, respectively. After incubation, the mixture was centrifuged at 12000 rpm for 1 h at 4 ºC and the supernatant was discarded. The obtained pellet was rinsed with PBS (Lonza, Base, Switzerland) and centrifuged again at 12,000 rpm for 1 h at 4 ºC. Subsequently, the supernatant was discarded and replaced with fresh DMEM (Biochrom GmbH, Berlin, Germany) supplemented with 2% FBS (Biochrom GmbH) to be added to Vero cells or fresh EMEM (ATCC, Manassas, VA, USA) supplemented with 2% FBS to be added to MRC-5 cells. Infections were revealed as described in the previous section. Triton X-100 at 0.1% was used as positive control of viral disruption and a culture medium was used as a negative control. Experiments were carried out three times in triplicate.

5.5.2 HSV-2 and HCMV binding inhibition assay

To resolve if PCCDs are capable of blocking viral receptors at cell membranes a binding inhibition study by plaque reduction assay was performed. In-brief, Vero and MRC-5 cells were seeded at a density of $1{,}75x10^5$ and $6x10^4$ cells/well in 24-well plates, respectively, and incubated at 37 ºC for 24 h. Then, cells were cooled at 4 ºC for 15 min and then treated with 1 µM of G2-SN15-PEG or G3-SN31-PEG dendrimers for 1 h at 4 ºC. Subsequently, cells were infected with 175 pfu/mL or 60 pfu/mL of HSV-2_{333} and $HCMV_{AD\text{-}169}$, respectively, at 4 ºC for 2 h. Afterwards, inoculum was discarded and replaced either with fresh DMEM (Biochrom GmbH, Berlin, Germany) supplemented with 2% FBS (Biochrom GmbH) and 0.4% IgG (Berigloblin P, CSL Behring GmbH, Marburg, Germany) in Vero cells, or fresh EMEM (ATCC, Manassas, VA, USA) supplemented with 2% FBS in MRC-5 cells. Infections were revealed as previously described. Culture medium was used as a negative control. Experiments were carried out three times in triplicate.

5.5.3 Dendrimer interaction with HSPGs

To determine if the studied dendrimers act through an interaction with HSPGs two types of assays were performed: (i) binding assay, including heparin competition, NaCl wash and heparinase treatment, and (ii) surface plasmon resonance (SPR).

5.5.3.1 HSPGs binding assay

The capacity of PCCDs to bind to HSPGs was first studied by a heparin competition assay, to study whether there was any type of binding competition with a structural analogue of HSPGs. To do so, cells were seeded in 24-well plates and incubated at 4 ºC for 2 h in PBS (Lonza, Base, Switzerland) with 1 µM of G2-SN15-PEG or 0.5 µM of G3-SN31-PEG dendrimers in the presence or absence of 10 µg/mL of heparin. In additional experiments, to disrupt the bound of dendrimers to HSPGs, cells were incubated at 37 ºC for 1 h with dendrimers at the same concentration and washed with PBS containing 2 M NaCl (Sigma, St Louis, MO, USA). Along with these experiments, inhibition of HSPG-dependent binding was studied through an enzymatical cleavage of HSPGs by pre-treating cells for 2 h at 37 ºC with 200 mU/mL of heparinase II (Merck KGaA, Darmstadt, Germany), before incubating for 1 h at 37 ºC with PCCDs at this same concentration. Assessment of cell-associated dendrimers after these assays was done by evaluating the dendrimer internalisation in the form of mean fluorescence intensity (MFI) of dendrimers in cells by flow cytometry, as described in section 5.3.2. Experiments were performed three times in triplicate.

5.5.3.2 Surface plasmon resonance

The capacity of dendrimers to bind to heparin/HSPGs was studied by conducting SPR. To do so, measurements were made on a BIAcore X100 instrument (Cytiva, Marlborough, MA, USA) using a research grade sensor chip SA (Cytiva, Marlborough, MA, USA) whose surface consists of a carboxymethylated dextran matrix preimmobilised with streptavidin. One cell of the sensor chip was conditioned with three consecutives 1 min injections of 1 M NaCl in 50 mM NaOH; Afterwards, heparin biotinylated at its reducing

end diluted in 10 mM HEPES buffer was injected for 8 min, allowing the immobilisation of 134,1 resonance units (RU) of glycosaminoglycans (GAGs). Then, the heparin-containing flow cell was over-coated by injecting biotinylated BSA re-suspended in HBS-EP for 8 min, allowing immobilisation of 104 RU (equal to 1,6 fmol/mm^2) of the protein, to help masking the residual unspecific negatively charged binding sites. The remaining flow cell of the sensor chip was coated only with biotinylated BSA protein as described above, allowing the immobilisation of 569,2 RU of protein, used to evaluate nonspecific binding and blank subtraction. To study their interaction with heparin, G2-SN15-PEG and G3-SN31-PEG dendrimers were resuspended in HBS-EP and injected at increasing concentrations over heparin and control BSA flow cells for 3 min (to allow association with immobilised molecules). The dissociation constant (Kd) was calculated by fitting the Scatchard equation for the RU plot measured at equilibrium as a function of the ligand concentration in solution. To evaluate the specificity of the binding of dendrimers to surface-immobilised heparin, they were injected onto the biosensor in the presence of a molar excess (5 mg/mL) of free heparin.

5.6 PEPTIDE TRANSFECTION INTO DCS

Dendrimicelles-peptide complexes were formed as described in Section 5.2, with 1 µM of the selected peptides and the maximum non-toxic concentration of dendrimicelles (1 µM $EG3SO_3Na$, 1 µM $ChG3SO_3Na$, 2,5 µM $EG3NMe_3I$ and 5 µM $ChG3NMe_3I$) within 2 h of incubation and were added to moDCs.

5.6.1 Detection of maturation markers on moDC

To determine whether transfected dendriplexes induced moDC maturation, flow cytometry analysis of maturation markers was performed. Briefly, moDCs were seeded at a density of $1x10^6$ cells/mL in 12-well plates and treated with dendriplexes for 48 h. Maturation control was obtained treating cells with 20 ng/mL of LPS (Sigma-Aldrich, San Luis, MO, USA) for 48 h. Afterwards, cells were rinsed twice with 3% BSA (Sigma) PBS (Lonza, Base, Switzerland), blocked for 5 min with 10% heat-inactivated human AB serum (Sigma) and incubated with specific surface markers for 30 min at RT in the dark. The following markers were used: anti-human-CD11c-PC7 (BioLegend, San Diego, CA, USA), anti-human-CD80- BV421 (BD Biosciences, East Rutherford, NY, USA), anti-human-CD83-AF488 (R&D Systems, Minneapolis, MN, USA), anti-human-CD86-APC/R700 (BD Biosciences), anti-human-HLA-DR-ECD (Beckman Coulter, Brea, CA, USA) and anti-human-CD179-APC/Cy7 (BioLegend). Then, cells were rinsed twice with 3% BSA PBS. Viable cells were identified using LIVE/DEAD™ Fixable Aqua Dead Cell Stain (Thermo Fisher Scientific, Waltham, MA, USA) as previously described. Finally, cells were fixed with 2% PFA. Measurements were done with by flow cytometry using a CytoFLEX flow cytometer and analysed using Kaluza software 2.1 (Beckman Coulter). Experiments were performed with samples from three different healthy donors.

5.6.2 Autologous mixed lymphocyte reaction

To study the effect of peptide-transfected mDC on lymphocytes from the same patient an autologous mixed lymphocyte reaction (MLR) was performed. For that, PBMCs and $CD14^+$ cells were separated from buffy

coats acquired from healthy anonymous donors. PBMCs were kept frozen at -80 ºC until use. On the other hand, moDCs were seeded at $1x10^6$ cells/mL in 12-well plates and matured with 20 ng/mL of LPS (Sigma-Aldrich, San Luis, MO, USA) for 24 h. At the time of maturation, mDCs were transfected with dendriplexes and, 24 h later, PBMCs were added to mDC in a 1:10 ratio. Cells were maintained for six days in RPMI-1640 (Biochrom GmbH, Berlin, Germany) supplemented with 10% FBS, 2 mM L-glutamine, the cocktail of antibiotics and 60 IU/mL of interleukin-2 (IL-2, Bachem, Budendorf, Switzerland). PHA 2 µg/mL was used as activation control. Experiments were carried out with samples from three different healthy donors.

5.6.2.1 Bright-field microscopy

To determine if the co-culture of peptide-transfected mDCs and autologous PBMCs had any visible effect on PBMCs bright-field microscopy images were taken at day 1, 3 and 6 after MLR. To do so, images were taken using a Zeiss Axiovert 40C (Carl Zeiss, Jena, Germany) inverted microscope with a 10x0,25 objective.

5.6.2.2 Detection of activation markers on B and T cells

To determine whether the effect of the co-culture of peptide-transfected mDCs and autologous PBMCs on the activation of B and T lymphocytes was visible, flow cytometry analysis of activation markers were performed. Briefly, on days 1, 3, and 6 after MLR, cells were rinsed twice with 3% BSA (Sigma, St Louis, MO, USA) PBS (Lonza, Base, Switzerland), blocked for 5 min with 10% heat-inactivated human AB serum (Sigma) and incubated with specific surface markers for 30 min at RT in the dark. The following human antibodies for B cells were used: anti-CD45-FITC (Beckman Coulter, Brea, CA, USA), anti-CD19-PE (BioLegend, San Diego, CA, USA), anti-HLA-DR-ECD (Beckman Coulter), anti-CD25-APC (BioLegend), anti-CD27-PC7 (BioLegend), anti-CD71-AF700 (Beckman Coulter). For T cells, the following human antibodies were used: anti-CD4-FITC (Miltenyi Biotec, Madrid, Spain), anti-CD3-PE (Beckman Coulter), anti-CD8-PC7 (Beckman Coulter), anti-HLA-DR-ECD (Beckman Coulter) and anti-CD69-PC5-ECD (Beckman Coulter). Then, cells were rinsed twice with 3% BSA PBS. Viable cells were labelled using LIVE/DEAD™ Fixable Aqua Dead Cell Stain (Thermo Fisher Scientific, Waltham, MA, USA) as previously described. Finally, cells were fixed with 2% PFA. Measurements were done with by flow cytometry using a CytoFLEX flow cytometer and analysed using Kaluza software 2.1 (Beckman Coulter).

5.6.2.3 Quantification of inflammatory cytokines

To study if the co-culture of peptide-transfected mDCs and autologous PBMCs triggered an inflammatory response different inflammatory cytokines/chemokines were measured, including IL-1β, IFN-α2, IFN-γ, TNF-α, MCP-1 (CCL2), IL-6, IL-8 (CXCL8), IL-10, IL-12p70, IL-17A, IL-18, IL-23, and IL-33. Briefly, 200 µL of supernatants from cell cultures were collected 1, 3 and 6 days after MLR and stored at -80 ºC until analysis. To measure the cytokines, the LEGENDplex™ Human Inflammation Panel 1 was used (BioLegend, San Diego, CA, USA) following manufacturer's instructions. The results obtained were analysed using the LEGENDplex™ Data Analysis Software (BioLegend).

5.7 STATISTICAL ANALYSIS

The different statistical analyses were performed using GraphPad software Prism v.5.0 (GraphPad Software, San Diego, CA, USA). Data were obtained from two or three independent experiments performed in duplicate or in triplicate. Data with two or three replicates are displayed as bars ±SD or SEM. A p-value of $\leq 0,05$ was considered statistically significant (* $p < 0,05$; ** $p < 0,01$, *** $p < 0,001$, **** $p < 0,0001$.).

RESULTS

6. RESULTS

6.1 DENDRIPLEXES AS DELIVERY VEHICLES OF ANTI-HIV-1 miRNAs

The current status of the HIV-1 pandemic, still a major problem in both developed and developing countries, faces two main drawbacks: (i) the appearance of resistance against new treatments and (ii) the development of reservoirs in different cell types. HIV-1 treatments based on cART can inhibit HIV-1 replication achieving long-lasting suppression of viral replication, but it is not curative. In addition, cART is not accessible for everyone, and some patients fail to adhere to it. Altogether, these factors lead to the appearance of resistances, which may confer adaptive advantages to new virions, allowing higher infectivity and rebounds of viral reservoirs. This makes it necessary to develop new therapeutic approaches to face HIV-1 infection.

A well-known mechanism of gene silencing is mediated by miRNAs, which bind to target cellular mRNAs by sequence homology, causing their silencing by deadenylation or degradation, depending on whether the sequences are partially or completely complementary, respectively (Bajan and Hutvagner, 2020). Certain cellular miRNAs have been proved to interfere with HIV-1 genome, silencing several viral proteins affecting viral replication (Swaminathan et al., 2012, Ruelas et al., 2015, Wang et al., 2015, Adoro et al., 2015). However, naked miRNAs are subjected to phagocytosis, enzymatic degradation, and protein aggregation at the circulatory system, thus their effective delivery is a limiting factor for their utilisation (Whitehead et al., 2009). A useful strategy to overcome this problem is the delivery of miRNAs with carrying vehicles, and here nanotechnology presents itself as one of the most promising tools to carry out this task.

Therefore, the objective of this section was to study the usability of PCCDs as effective delivery vehicles for synthetic anti-HIV-1 miRNAs to be delivered into host cells and reservoirs to truncate HIV-1 replication (Figure 13).

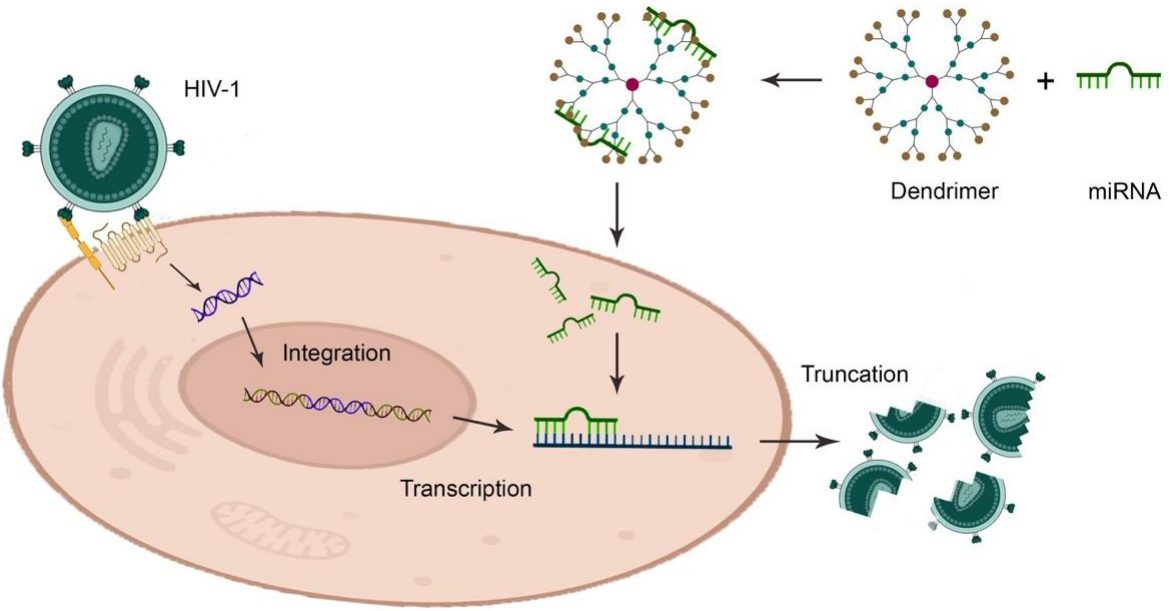

Figure 13: Graphical abstract of the study of PCCDs as miRNA delivery vehicles as possible therapy against HIV-1 infection. **miRNA:** microRNA.

6.1.1 Biocompatibility of PCCDs in PBMCs and U87MG-CD4$^+$CCR5$^+$ cell line

6.1.1.1 Determination of the mitochondrial toxicity

Mitochondrial toxicity induced by G2-SN15-PEG, G3-SN31-PEG, G2-SN15-PEG FITC, and G3-SN31-PEG FITC dendrimers was evaluated by the MTT assay following manufacturer's instructions. This colorimetric assay, indicator of the cellular mitochondrial metabolism, is based on the reduction of the 3-(4-5-dimethylthiazol-2-yl)-2,5-diphenyltetrazolium bromide (MTT) into purple formazan crystals (Merck).

PBMCs and U87MG-CD4$^+$CCR5$^+$ cells were treated for 72 h with increasing concentrations of PCCDs, from 0,01 to 30 µM. Culture medium was used as NT control and 10% DMSO as death control. Concentrations were considered nontoxic when the survival rate was above 80%. The results indicated that the maximum non-toxic working concentrations of the G2-SN15-PEG, G3-SN31-PEG, G2-SN15- PEG FITC and G3-SN31-PEG FITC dendrimers were 10, 5, 5 and 1 µM, respectively, in PBMCs (Figure 14A) and 5, 1, 1 and 0.5 µM, respectively, in U87MG-CD4$^+$CCR5$^+$ cells (Figure 14B).

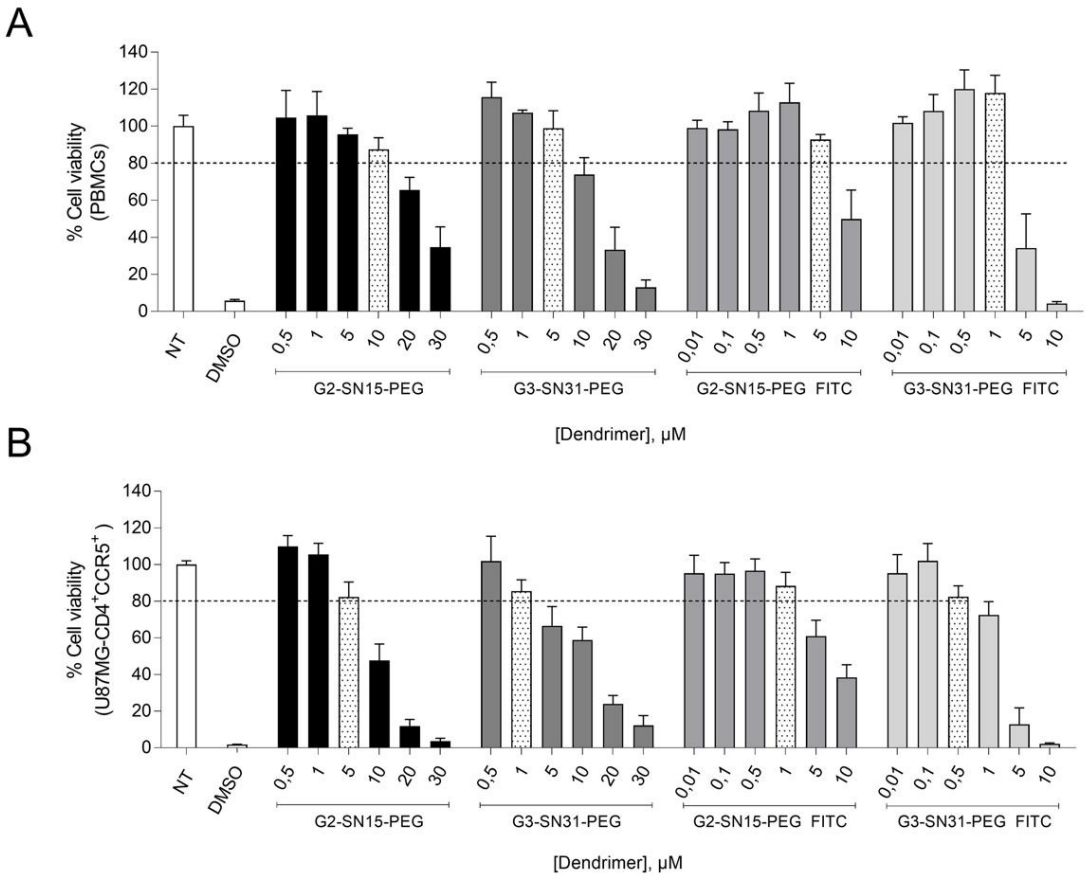

Figure 14: Cytotoxicity of PCCDs in PBMCs and U87MG-CD4$^+$CCR5$^+$ cell line determined by MTT assay. PBMCs **(A)** and U87MG-CD4$^+$CCR5$^+$ cells **(B)** were treated with G2-SN15-PEG, G3-SN31-PEG, G2-SN15-PEG FITC and G3-SN31-PEG FITC dendrimers in a rage of concentrations from 0,01 to 30 µM. Cell viability ≥ 80 % was established as non-toxic working concentrations. Culture medium was used as NT control and 10% DMSO as death control. Data are represented as mean ± SD of three individual experiments performed in triplicate. **NT:** non-treated; **DMSO:** dimethyl sulfoxide.

6.1.1.2 Evaluation of the genotoxicity

Genotoxicity of PCCDs in PBMCs was measured by the sister chromatids exchange (SCE) assay, which detects DNA exchange between two identical chromatids in the chromosome due to persistent genetic damage after DNA duplication (González-Beltrán and Morales-Ramírez, 2003). This assay was carried out to eliminate the possibility that PCCDs mistakenly interfered with the host genome because of their positively charged functional groups.

PBMCs from five healthy donors were treated with G2-SN15-PEG 10 µM or G3-SN31-PEG 5 µM carbosilane cationic dendrimers for 72 h in presence of BdrU following FPG stain (Figure 15A). NT samples and a dose of 1 Gy of radiation were used as untreated and genotoxicity control, respectively. Results indicate that PCCDs do not generate genetic toxicity in PBMCs, since there were no significant differences among NT and treated control samples, contrarily to what happens in genotoxicity control, which shows a statistical difference of $p <$ 0,001 regarding NT (Figure 15B).

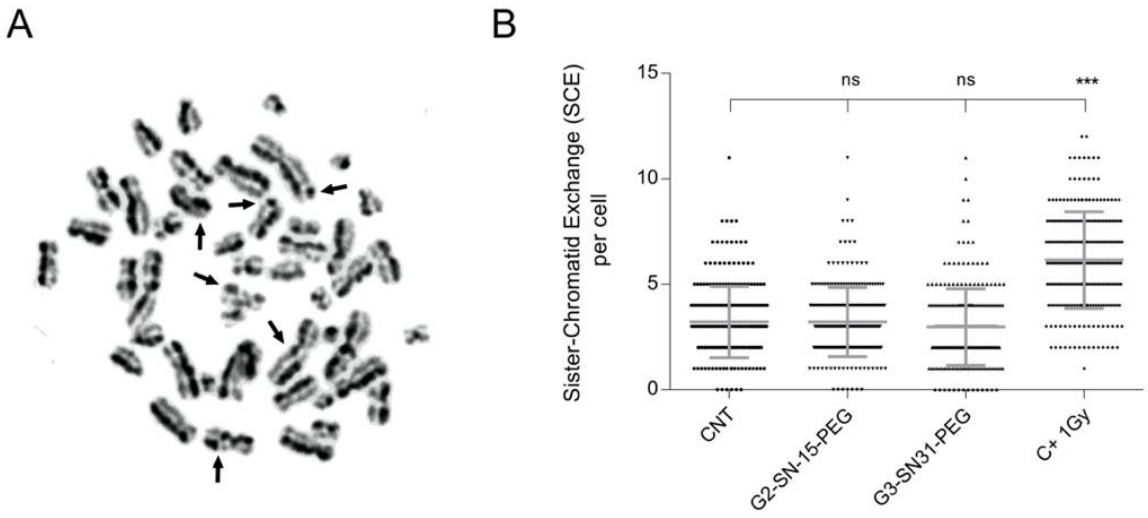

Figure 15: Genotoxicity of PCCDs measured by SCE. Quantification of the number of SCE per cell in PBMCs untreated and treated with G2-SN15-PEG 10 µM, G3-SN31-PEG 5 µM or 1 Gy radiation for 72 h. **(A)** Images of random field obtained from the SCE assay after FPG staining. Arrows indicate SCEs. **(B)** Statistical analysis of the assay. Data are represented as dot plots of five individual experiments (50 mitosis analysed per healthy donor). **C+ 1Gy**: 1 Gy radiation genotoxicity control; **CNT**: nontreated; **ns:** non-significant. ***p < 0,001.

6.1.1.3 Assessment of the haemolytic potential

The capacity of dendrimers to cause erythrocyte haemolysis was evaluated by a haemolytic test. Briefly, PBMCs were incubated with PCCDs at different concentrations, and, after centrifugation, the absorbance of supernatants was measured to determine the concentration of cell-free haemoglobin, which is interpreted as erythrocyte haemolysis. PBS was used as negative control, distilled water was used as positive control, and 2% Triton X-100 was used as a haemolytic agent.

Results obtained from the measurements clearly indicate that exposure to tested PCCDs does not produce erythrocyte haemolysis at any concentration tested (Figures 16A and 16B).

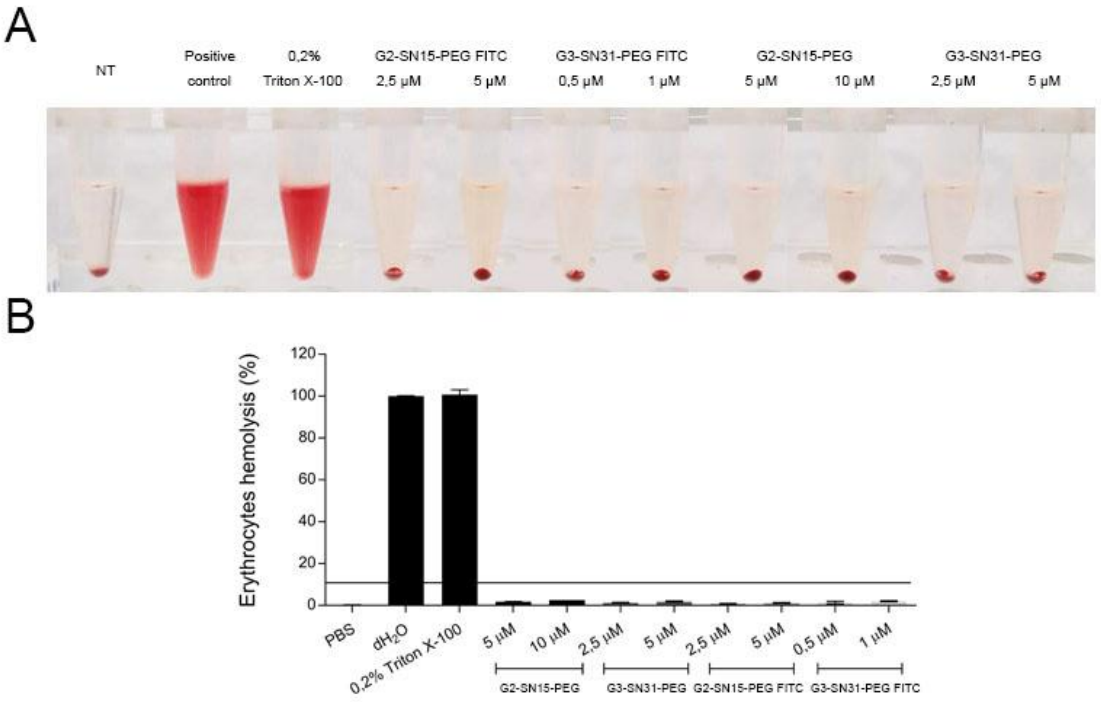

Figure 16: Haemolytic potential of PCCDs determined by haemolytic test. **(A)** Images taken from PBMCs treated with 5 and 10 µM of G2-SN15-PEG, 2,5 and 5µM of G3-SN31-PEG, 2,5 and 5µM of G2-SN15-PEG FITC and 0,5 and 1µM of G3-SN31-PEG FITC dendrimers. **(B)** Analysis of absorbance measurements. PBS was used as negative control, dH_2O was used as positive control and 2% Triton X-100 as the haemolytic agent. Data are represented as mean ± SD of two individual experiments. **dH_2O:** distilled water.

6.1.2 Internalisation of PCCDs into PBMCs and U87MG-$CD4^+CCR5^+$ cell line

Internalisation of FITC labelled PCCDs in PBMCs and U87MG-CD4+CCR5+ cell line was evaluated by confocal microscopy and flow cytometry. For both experiments, cells were treated with 5 and 1 µM (PBMCs) or 1 and 0,5 µM (U87MG-CD4+CCR5+ cells) of G2-SN15-PEG FITC and G3-SN31-PEG FITC dendrimers, respectively, for 1 , 2 or 6 h.

Results indicate a notable difference in the uptake of both dendrimers in $CD3^+$ cells. For G2-SN15-PEG FITC dendrimer, there were no differences in uptake among the studied time points: 1 h after incubation nearly 90% of PBMCs were positive for its presence inside cells and there were no significant differences with this percentage of entry at 2 or 6 h. Similarly, when PBMCs were treated with G3-SN31-PET FITC there were no significant differences in the uptake at the studied time points. However, percentage of positivity of G3-SN31-PEG FITC dendrimer was much lower than G2-SN15-PEG FITC dendrimer, with only around 16% of positive cells (Figure 17A and 17B).

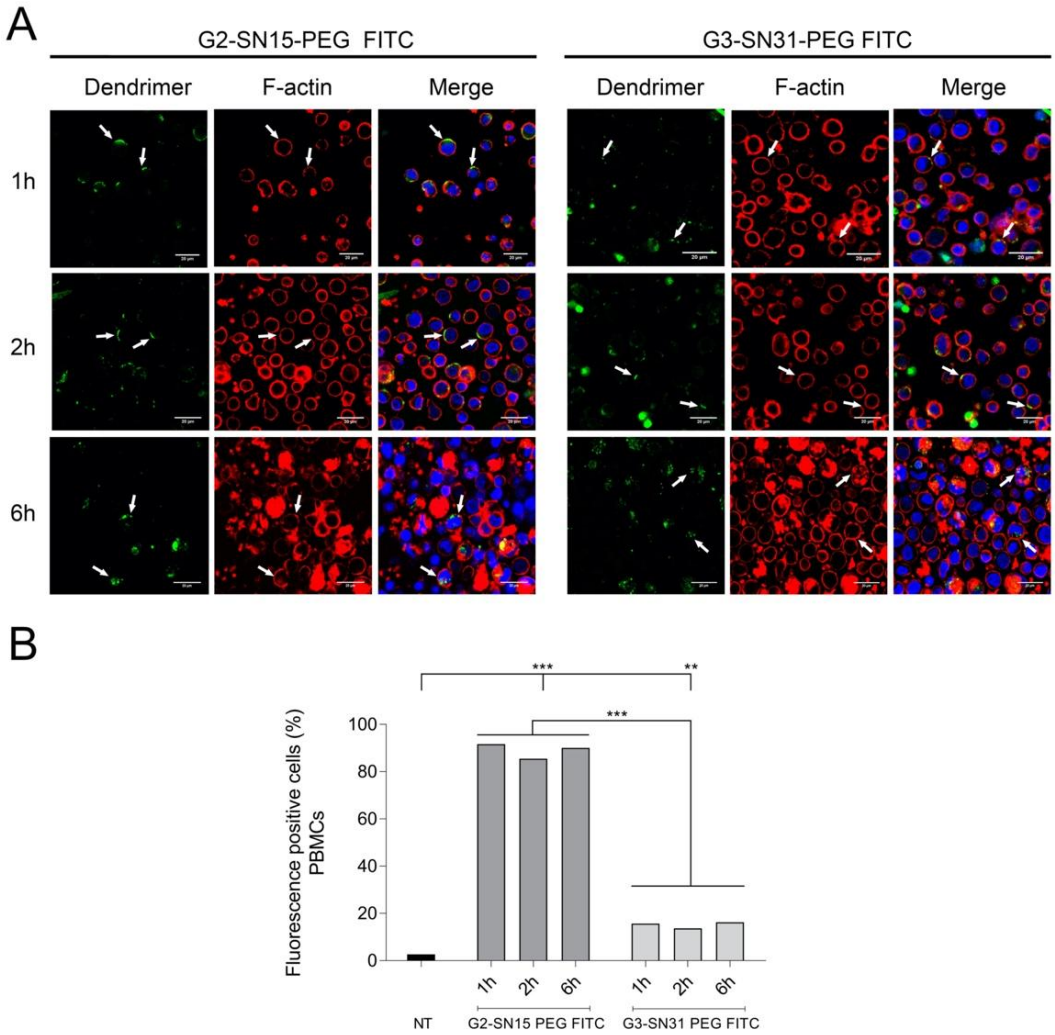

Figure 17: Internalisation of PCCDs in PBMCs. Confocal microscopy images of PBMCs treated for 1, 2 or 6 h with 5 μM G2-SN15-PEG FITC or 1 μM G3-SN31-PEG FITC dendrimers. **(A)** Representative images of cells treated with dendrimers (green) and stained with Phalloidin (red, actin filaments) and DAPI (blue, nucleus). **(B)** Entry of FITC-labelled dendrimers into cells observed by flow cytometry 1, 2 and 6 h after treatment. **DAPI**: 4′,6-Diamidino-2-phenylindole dihydrochloride. ** $p < 0{,}005$; *** $p < 0{,}001$.

Likewise, a large difference in internalisation between G2-SN15-PEG FITC and G3-SN31-PEG FITC dendrimers in U87MG-CD4^{+}CCR5^{+} cell line was noted, however, in these cells a notable increase in the number of positive cells was observed at the chosen time points. After 1 h of incubation, both dendrimers were located at the outer part of the cell membrane, since both dendrimers co-localised with F-actin. At this time point, flow cytometry indicated that 40% of cells were positive for G2-SN15- PEG FITC dendrimer whereas only 20% where positive for G3-SN31-PEG FITC dendrimer. After 2 h of incubation, a notable increase was detected, reaching values of 50 and 45% for G2-SN15- PEG FITC and G3-SN31-PEG FITC dendrimers, respectively. Thus suggesting that both dendrimers take at least 2 h to internalise into this cell line (Figure 18A and 18B). These results indicate that both G2-SN15-PEG FITC and G3-SN31-PEG FITC dendrimers can enter PBMCs and U87MG-CD4^{+}CCR5^{+} cell line in 2 h or less, indicating that both dendrimers could be used as delivery systems.

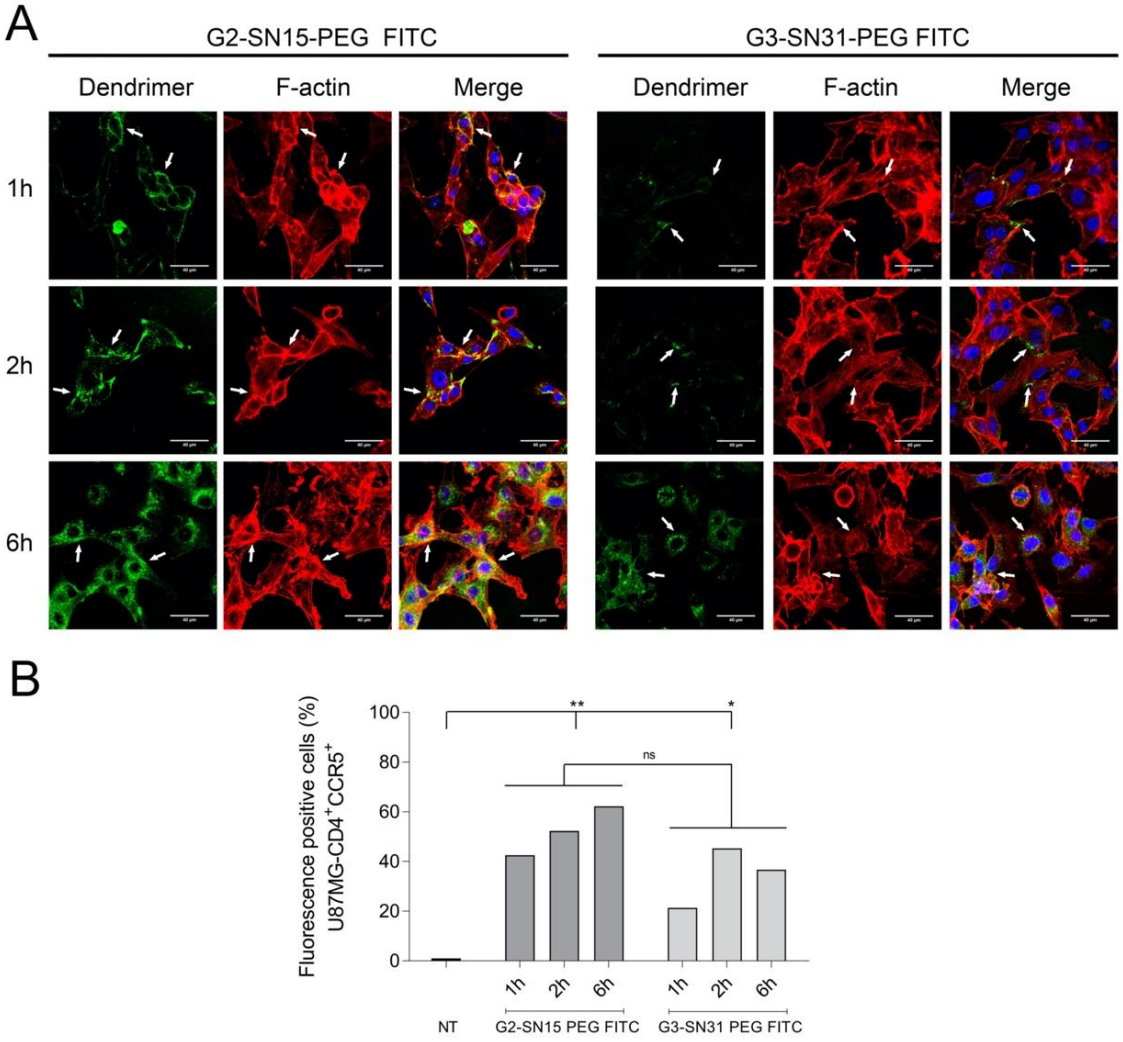

Figure 18: Internalisation of PCCDs in U87MG-CD4$^+$CCR5$^+$ cell line. Confocal microscopy images of U87MG-CD4$^+$CCR5$^+$ cell line treated for 1, 2 or 6 h with 1 µM G2-SN15-PEG FITC or 0,5 µM G3-SN31-PEG FITC dendrimers. **(A)** Representative images of cells treated with dendrimers (green) and stained with Phalloidin (red, actin filaments) and DAPI (blue, nucleus). **(B)** Entry of FITC-labelled dendrimers into cells observed by flow cytometry 1, 2 and 6 h after treatment. **DAPI**: 4′,6-Diamidino-2-phenylindole dihydrochloride; **ns:** non-significant. * $p < 0,05$; ** $p < 0,005$.

6.1.3 miRNA-PCCDs dendriplexes formation and characterisation

Determination of the ability of PCCDs to form dendriplexes with miRNAs was tested by 2% agarose gel electrophoresis. Complexes were formed mixing 100 nM of the desired miRNAs with the maximum non-toxic concentration of PCCDs for each cell type: 10 µM G2-SN15-PEG and 5 µM G3-SN31-PEG for PBMCs and 5 µM G2-SN15-PEG and 1 µM G3-SN31-PEG for U87MG-CD4$^+$CCR5$^+$ cell line, within 2 h of incubation.

Results shown in Figures 19A and 19B illustrate that, using working concentrations for PBMCs, G2-SN15-PEG and G3-SN31-PEG dendrimers can bind more than 90% of the tested miRNAs after 2 h of incubation. When dendrimer concentrations were decreased to match maximum non-toxic concentrations for U87MG-CD4$^+$CCR5$^+$ cell line, similar results were found. G2-SN15-PEG and G3-SN31-PEG dendrimers bind around 90% and 70% of the miRNAs tested, respectively (Figures 19C and 19D). These results confirm that both dendrimers can perform efficient and stable bonds with chosen miRNAs.

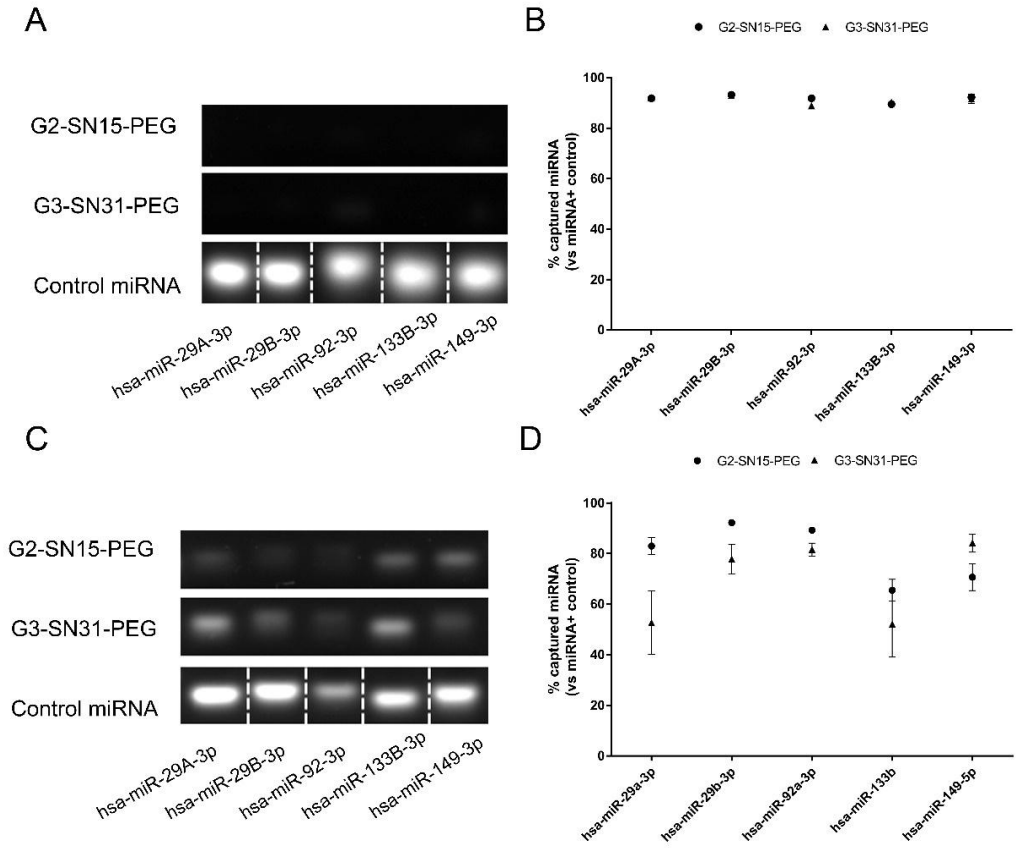

Figure 19: miRNA-PCCDs dendriplexes formation and characterisation. **(A)** Two percent agarose gel electrophoresis showing formation of dendriplexes with anti-HIV-1 miRNAs (hsa-miR-29a-3p, hsa-miR-29b-3p, hsa-miR-92a-3p, hsa-miR-133b and hsa-miR-149-5p) and G2-SN15-PEG (10 μM) and G3-SN31-PEG (5 μM) dendrimers after 2 h of incubation. **(B)** Percentage of miRNA captured vs. miRNA control. **(C)** Formation of dendriplexes with anti-HIV-1 microRNAs and G2-SN15-PEG (5 μM) and G3-SN31-PEG (1 μM) dendrimers after 2 h of incubation. **(D)** Percentage of miRNA captured vs. miRNA control. **miRNA**: microRNA.

6.1.3.1 Stability and distribution of dendriplexes

The evaluation of the formation and stability of dendriplexes and of the effects of miRNAs on dendrimers was done measuring the electrical potential (by ZP) and the hydrodynamic size (by DLS). As shown in Table 5, the surface charge values obtained from the ZP measurements confirmed the cationic density of the periphery of the nanoparticles. Specifically, G2-SN15-PEG dendrimer has the highest potential value (52,5 mV), followed by G3-SN31-PEG dendrimer, which has a moderate value (30,24 mV), resulting in high electrical stability, respectively. The formation of dendriplexes with an example miRNA (hsa-miR-29a-3p) produced a change in the ZP values of both dendrimers. More precisely, the potential value decreased when complexing the G2-SN15-PEG dendrimer with the miRNA, while it increased when forming the dendriplex with the G3-SN31-PEG dendrimer, suggesting that the formation of dendriplexes occurred.

Results obtained from the study of the particle size distribution by DLS (Table 5) suggest aggregation or self-assembly of G2-SN15-PEG (302,95 nm). On the contrary, values obtained for G3-SN31- PEG dendrimer (4,93 nm) were much lower indicating that it could be described as a single molecule. As for hsa-miR-29a-3p, its degree of aggregation is low (14 nm). In terms of dendriplexes, both presented moderate aggregation values: around 30 and 40 nm, for G2-SN15-PEG and G3-SN31-PEG dendrimers, respectively. All of these

values, supported by data obtained in electrophoresis assays, confirm the correct formation and stability of complexes.

Table 5. Measurement of ZP values (mV) and hydrodynamic size (nm) of dendrimers, miRNAs and dendriplexes formed with G2-SN15-PEG or G3-SN31-PEG dendrimers and hsa-miR-29a-3p. Invalid measurements are indicated with dashes (-).

Compound	Zeta potential (mV)	Hydrodynamic size (diameter, nm)
G2-SN15-PEG	52,50 ± 0,42	302,95 ± 14,78
G2-SN15-PEG + hsa-miR-29a-3p	49,45 ± 1,62	30,19 ± 2,88
G3-SN31-PEG	30,60 ± 0,00	4,93 ± 0,26
G3-SN31-PEG + hsa-miR-29a-3p	32,24 ± 2,37	41,10 ± 2,88
hsa-miR-29a-3p	-	14,42 ± 4,16

6.1.3.2 Releasability and protectiveness of dendriplexes

To test if miRNAs can be released from dendriplexes heparin competition assays were performed. Dendriplexes were formed as previously detailed and treated with 0.2 UI/µL of heparin for 5 min at RT. Results shown in Figure 20 indicate that after heparin treatment miRNA signal was recovered, demonstrating that, at any concentration tested, miRNAs can be released form the complex when exposed to molecules of this nature. In addition, the protection conferred by dendriplexes against RNase-mediated degradation was tested. Here, dendriplexes were treated with 1 µg/µL of RNase for 10 min at RT. After RNase treatment, miRNAs were fully recovered, demonstrating that dendriplex formation protects this type of cargo.

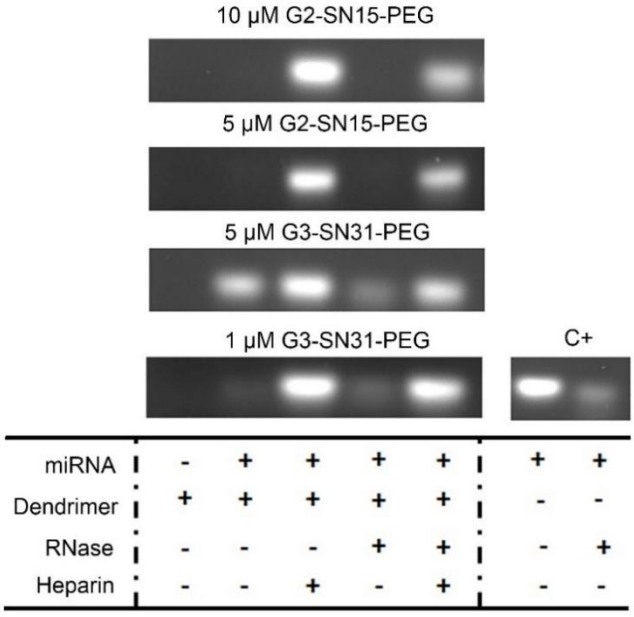

Figure 20: Releasability and protectiveness of miRNA-PCCDs dendriplexes. Heparin competition assays (0.2 UI/µL of heparin for 5 min at RT) and RNase protection assays (1 µg/µL of RNase for 10 min at RT) performed on dendriplexes. Dendriplexes were formed with 10 µM or 5 µM of G2-SN15-PEG and 5 µM or 1 µM of G3-SN31-PEG dendrimers.

6.1.4 HIV- 1 inhibition activity of dendriplexes

To determine whether dendriplexes have anti-HIV-1 activity, inhibition experiments were performed. PBMCs or U87MG-CD4^{+}CCR5^{+} cell line were infected with R5-HIV-$1_{NL(AD8)}$ and treated with dendriplexes formed as previously described. Then, 72 h after infection, PBMCs or U87MG-CD4^{+}CCR5^{+} cells supernatants were collected and titrated on TZM.bl cells to quantify infection by measurements of luciferase activity. Nontreated samples were used as an uninfected control.

Treatment of PBMCs with only G2-SN15-PEG and G3-SN31-PEG dendrimers achieved around 80 and 45% of HIV-1 inhibition, respectively, regarding the infection control. Inhibition was even greater when treated with dendriplexes formed with anti-HIV-1 miRNAs and both G2-SN15-PEG or G3-SN31-PEG dendrimer showing a significant increase of inhibition reaching values of 96 and 73% reduction of HIV-1 infection, respectively (Figure 21A).

Treatment of U87MG-CD4^{+}CCR5^{+} cells (Figure 21B) with G2-SN15-PEG FITC or G3-SN31-PEG dendrimer achieved around 40% inhibition of HIV-1 infection. Likewise, treatment with some of dendriplexes, for example the ones formed with hsa-miR-29A-3p and G2-SN15-PEG or G3-SN31-PEG dendrimer, induced even higher inhibition. However, this increase was not significant compared to the inhibition resulting from treatment with only G2-SN15-PEG or G3-SN31-PEG dendrimers, suggesting that dendriplexes cause a significant inhibition of R5-HIV-1 infection only in specific cell lines such as PBMCs.

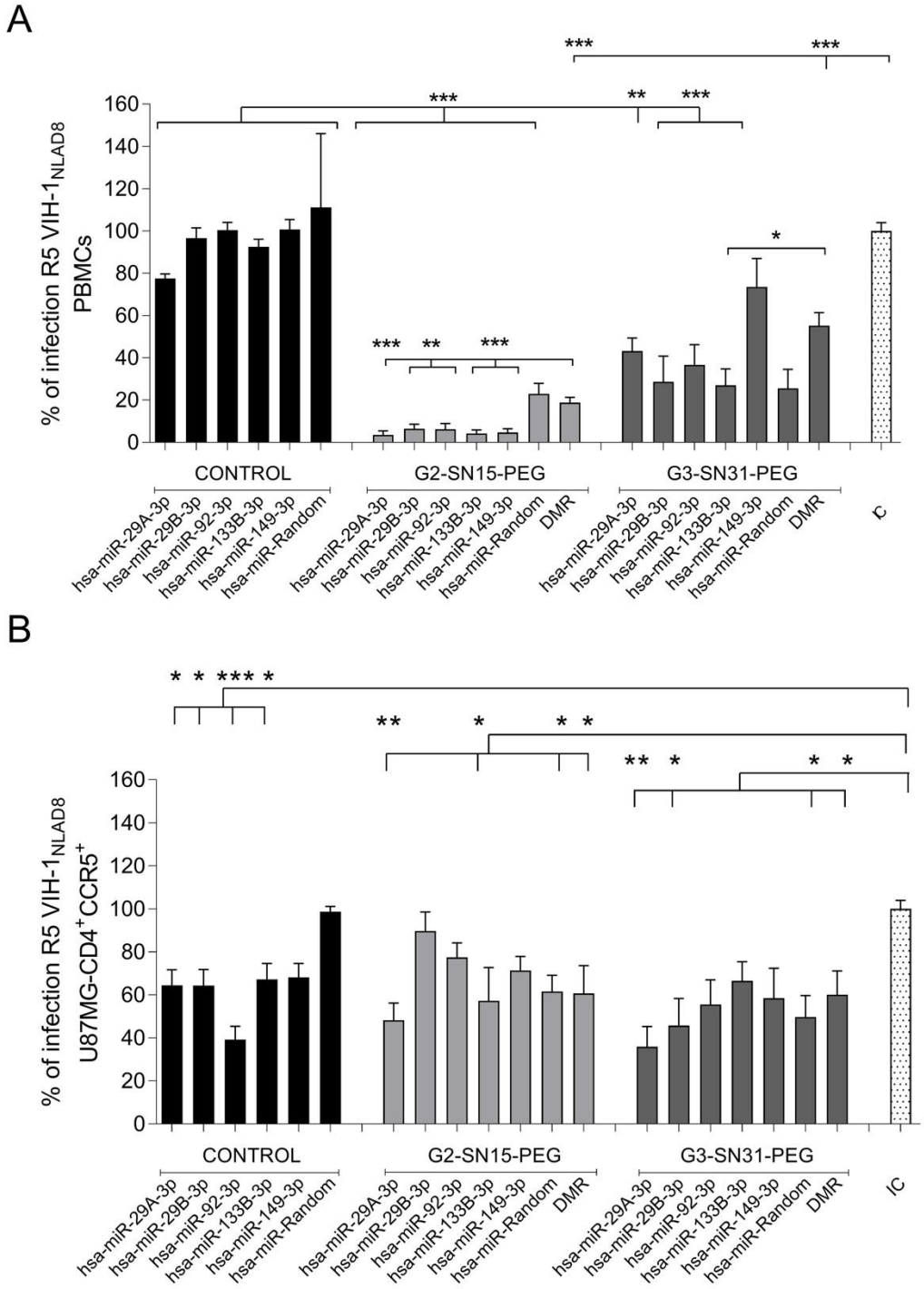

Figure 21: HIV-1 antiviral efficacy of miRNA-PCCDs dendriplexes. Quantification of R5-HIV-1 infection measured by titration of supernatants on TZM.bl cell line. Infection was inferred from the measurement of luciferase activity 48 h after titration and is represented as percentage with respect to infection control. Dendriplexes were formed with nonlabelled PCCDs and control or anti-HIV-1 miRNAs (hsa-miR-29a-3p, hsa-miR-29b-3p, hsa-miR-92a-3p, hsa-miR-133b, and hsa-miR-149-5p). **(A)** PBMCs, dendriplexes were formed with 10 µM G2-SN15-PEG and 5 µM G3-SN31-PEG dendrimers. **(B)** U87MG-CD4$^+$CCR5$^+$ cell line, dendriplexes formed with 5 µM G2-SN15-PEG and 1 µM G3-SN31-PEG dendrimers. Data are represented as mean ±SD of three individual experiments performed in triplicate. **DMR**: dendrimer; **IC:** infection control; **HIV-1:** Human Immunodeficiency Virus-1. * $p < 0,05$; ** $p < 0,005$; *** $p < 0,001$.

6.2 EFFECT OF PEGylated CATIONIC CARBOSILANE DENDRIMERS AGAINST HSV-2 AND HCMV

Virus belonging to the *Herpesviridae* family, including HSV-2 and HCMV, produce some of the most prevalent transmitted diseases in the world. This family of viruses is characterised by being highly successful in the establishment of latent long-lasting infections after infection of the host, which leads to unlimited production of virions. Different stressors can induce reactivation of herpesviruses, being the most frequents local trauma, fever, exposure to UV light, hormones and emotional or physical stress (Roizman and Whitley, 2013).

Lifelong infections entail the need for prolonged therapies, leading to exposure to drug toxicity and appearance of resistances. The lack of a definitive suppressive treatment for *Herpesviridae* infections opens the ways to the emergence of resistant strains that lead viral reactivations. The high incidence of infections caused by HSV-2 and HCMV and the nature of their clinical manifestations highlight the need for novel effective therapies to protect high-risk populations exposed to them.

In this sense, nanotechnology is also a promising alternative to current treatments as previously demonstrated (Relano-Rodriguez et al., 2021b, Rodriguez-Izquierdo et al., 2020a, Guerrero-Beltran et al., 2019, Sepulveda-Crespo et al., 2015a). This work proposes the use of novel PCCDs as inhibitors of the interaction between viral glycoproteins and cell HSPGs to develop a promising therapy against HSV-2 and HCMV infections (Figure 22).

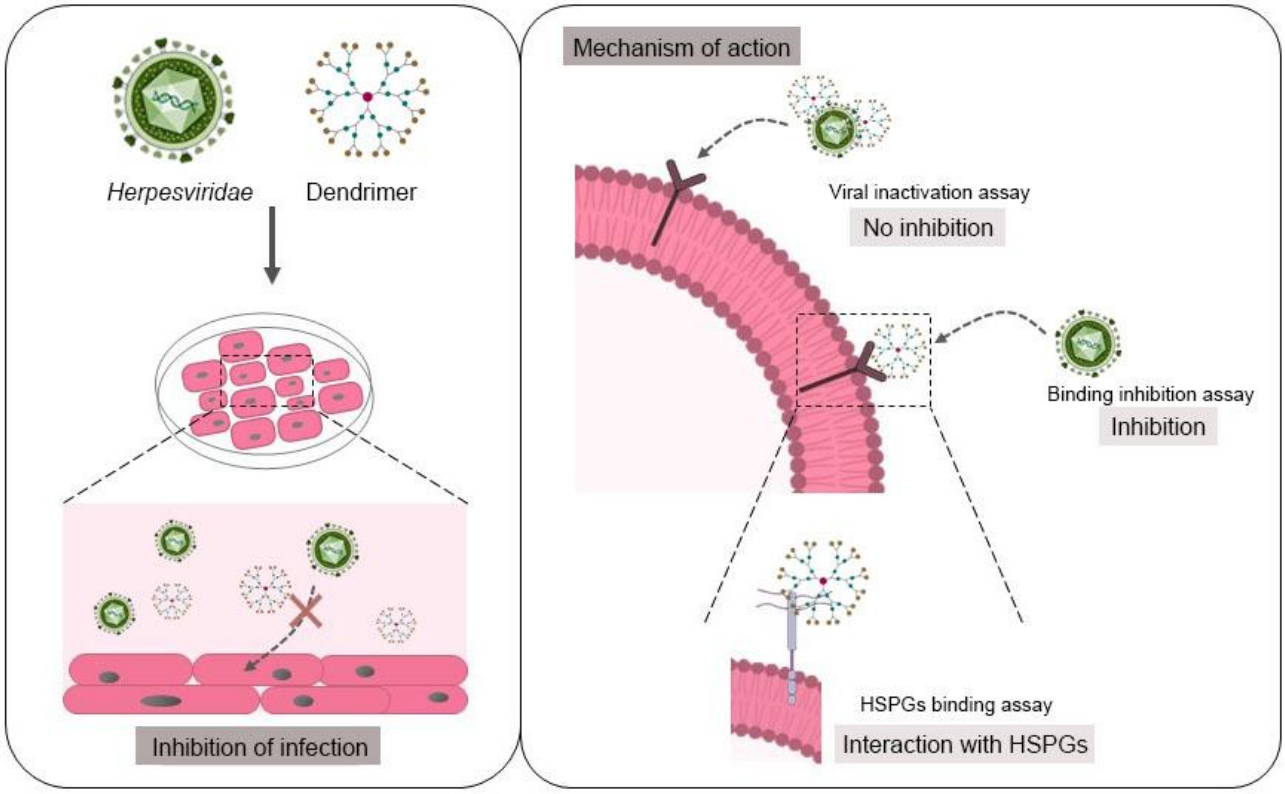

Figure 22: Graphical abstract of the study of PCCDs as a possible therapy to fight *Herpesviridae* infections. **HSPGs:** Heparan sulphate proteoglycans.

6.2.1 Viability of PCCDs on Vero and MRC-5 cell lines

6.2.1.1 Assessment of mitochondrial toxicity

Mitochondrial toxicity induced by G2-SN15-PEG, G3-SN31-PEG, G2-SN15-PEG FITC and G3-SN31-PEG FITC dendrimers was assessed by MTT assay following manufacturer's instructions. In this experiment, Vero and MRC-5 cell lines were treated for 48 h and 6 days, respectively, with increasing concentrations of PCCDs, from 0,01 to 30 µM. Culture medium was used as NT control and 10% DMSO as death control. Concentrations were considered toxic when the survival rate was less than 80%. Results indicated that the maximum nontoxic concentrations of G2-SN15-PEG, G3-SN31-PEG, G2-SN15- PEG FITC and G3-SN31-PEG FITC dendrimers were 1 µM, 1 µM, 1 µM and 0,5 µM, respectively, in Vero (Figure 23A) and MRC-5 cells (Figure 23B).

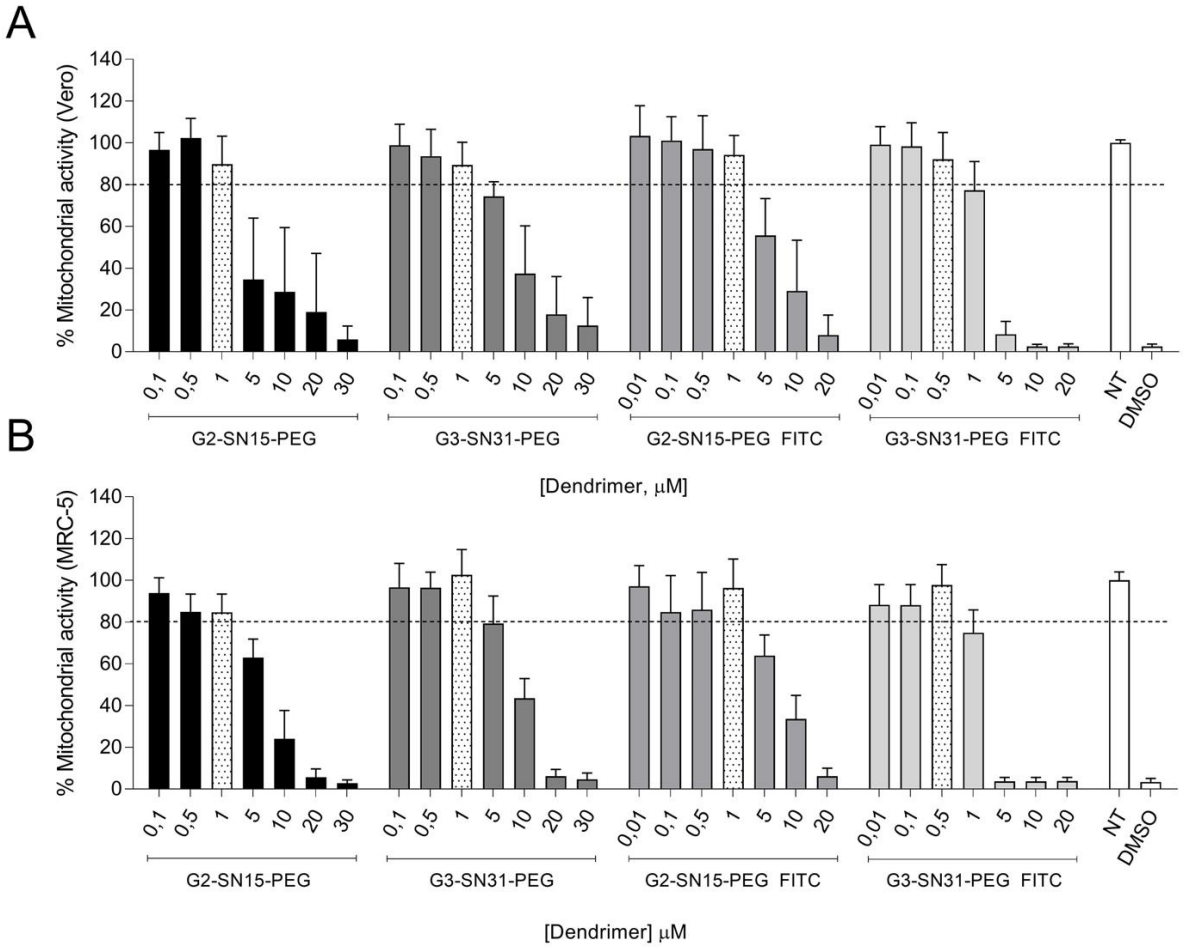

Figure 23: Cytotoxicity of PCCDs in Vero and MRC-5 cell lines determined by MTT assay. Vero **(A)** and MRC-5 **(B)** cells were treated with increasing concentrations of G2-SN15-PEG, G3-SN31-PEG, G2-SN15-PEG FITC and G3-SN31-PEG FITC dendrimers from 0,01 to 30 µM. Cell viability ≥ 80 % was established as non-toxic working concentrations. Culture medium was used as NT control and 10% DMSO as death control. Data are represented as mean ± SD of three individual experiments performed in triplicate. **NT:** non-treated; **DMSO:** dimethyl sulfoxide.

6.2.1.2 Evaluation of membrane disruption ability

Determination of membrane integrity of cells treated with PCCDs was tested using the LDH CytoTox 96® nonradioactive cytotoxicity assay following manufacturer's instructions. Similarly to the MTT assay, it is a colorimetric coupled enzymatic assay based on the conversion of a tetrazolium salt into a red formazan product. The intensity of the color obtained is proportional to the amount of LDH released during cell lysis resulting from the loss in membrane integrity (Promega). Here, Vero and MRC-5 cells were treated with increasing concentrations of G2-SN15-PEG, G3-SN31-PEG, G2-SN15-PEG FITC and G3-SN31-PEG FITC dendrimers from 0,01 to 30 µM for 48 h (Vero) and 6 days (MRC-5). Culture medium was used as NT control. Concentrations were considered nontoxic when the survival rate was above 80%. The results indicate that membrane integrity loss occurs when treating with concentrations above 1 µM, 10 µM, 1 µM and 1 µM (in Vero, Figure 24A) and 10 µM, 10 µM, 10 µM and 1 µM (in MRC-5, Figure 24B) of G2-SN15-PEG, G3-SN31-PEG, G2-SN15-PEG FITC and G3-SN31-PEG FITC dendrimers, respectively. This suggests that membrane integrity is not as affected as mitochondrial activity after PCCDs treatment. Therefore, to ensure complete cell viability, the results of the MTT assay were used to define working concentrations.

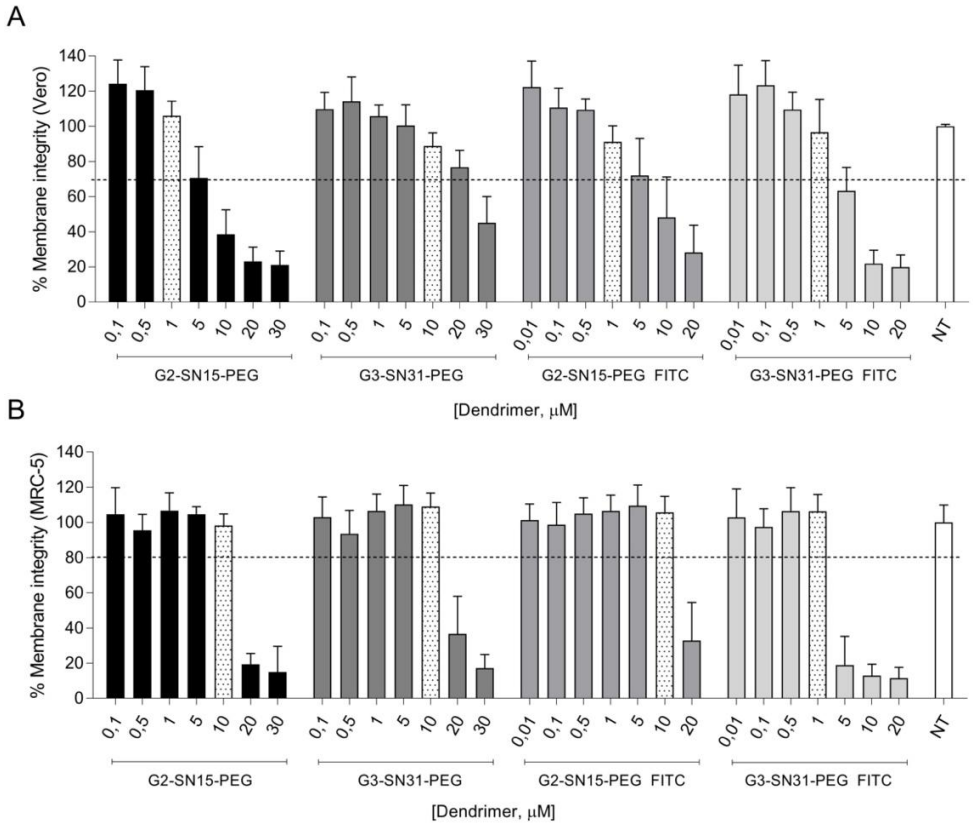

Figure 24: Cytotoxicity of PCCDs in Vero and MRC-5 cell lines determined by LDH assay. Vero **(A)** and MRC-5 **(B)** cells were treated with increasing concentrations of G2-SN15-PEG, G3-SN31-PEG, G2-SN15-PEG FITC and G3-SN31-PEG FITC dendrimers from 0,01 to 30 µM. Cell viability ≥ 80 % was established as non-toxic concentrations. Culture medium was used as NT control. Data are represented as mean ± SD of three individual experiments performed in triplicate. **NT:** nontreated.

6.2.1 Internalisation of PCCDs into Vero and MRC-5 cell lines

Capacity of FITC-labelled dendrimers to internalise into Vero and MRC-5 cell lines was determined by flow cytometry and confocal microscopy. The internalisation process was studied by incubating both cell lines with 1 μM G2-SN15-PEG FITC or 0,5 μM G3-SN31-PEG FITC dendrimers at different times (1, 2, 6, or 24 h). To assess their distribution, actin filaments and nucleus were labelled with phalloidin and DAPI, respectively, in confocal microscopy studies.

The entry studies showed a significant increase in fluorescent positive cells in both cell lines (14% in Vero and 26% in MRC-5, with respect to the control) after the first hour of incubation; demonstrating that G2-SN15-PEG FITC dendrimer has faster uptake dynamics than G3-SN31-PEG FITC dendrimer (Figures 25A and 26A). Furthermore, an important increase in the number of positive fluorescent marks from both dendrimers was observed at all-time points. More precisely, in Vero cells, an evident increase of G2-SN15-PEG FITC dendrimer signal (45%) was noted from 1 to 24 h, whilst for G3-SN31-PEG FITC dendrimer it was not so remarkable (20%). On the other hand, in MRC-5 cells, both dendrimers showed a 30% increase in the number of positive cells from 1 to 24 h.

Confocal microscopy allowed for a more detailed study of PCCDs distribution in cells, which suggested that both G2-SN15-PEG FITC and G3-SN31-PEG FITC dendrimers have a distribution pattern that depends on the incubation time: short times showed peripheral distribution of dendrimers (co-localising with F-actin), while longer times showed that treatments reach more internal regions with a punctate intracellular distribution (Figures 25B and 26B). In summary, both dendrimers can rapidly interact with the surface of both Vero and MRC-5 cell lines and be easily internalised and remain concentrated in a granular manner.

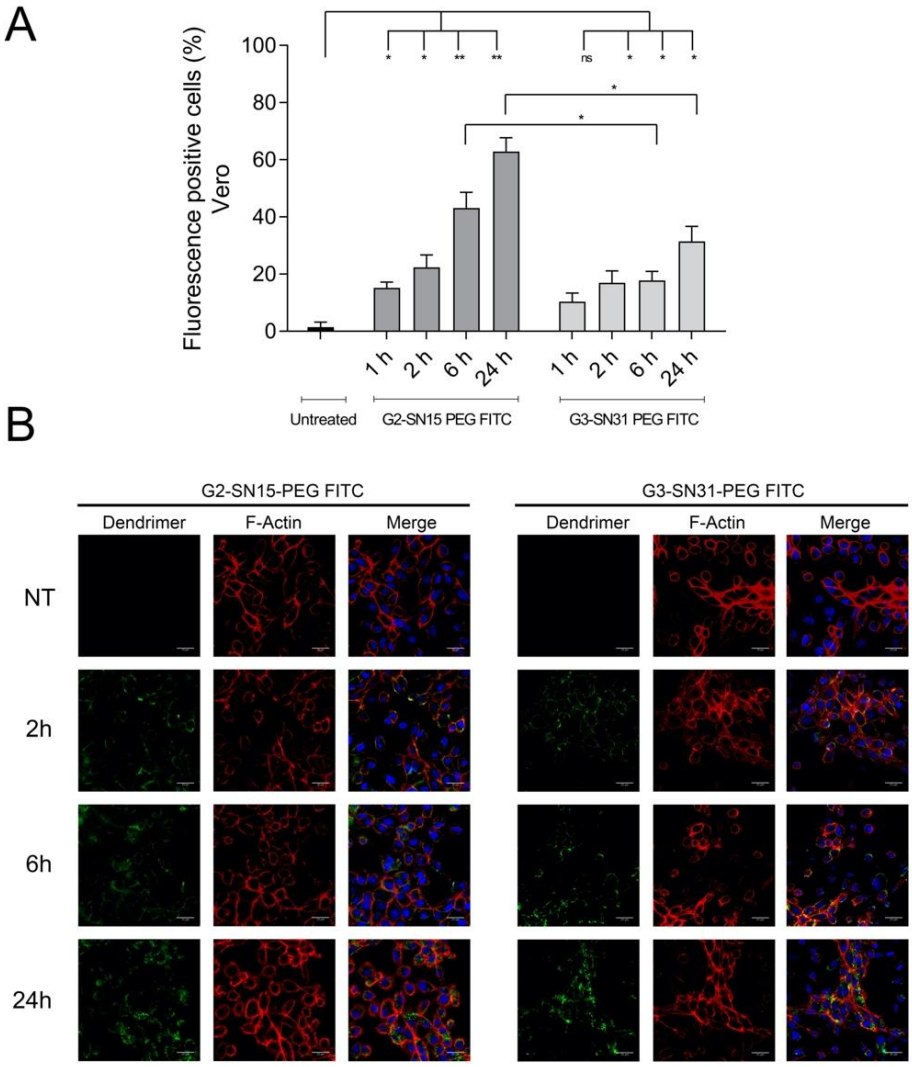

Figure 25: Internalisation study of PCCDs into Vero cell line. **(A)** Percentage of FITC-positive cells analysed by flow cytometry 1, 2, 6 and 24 h post-treatment. Data are represented as mean ± SD of two individual experiments. **(B)** Confocal images of cells treated with 1 µM G2-SN15-PEG FITC or 0,5 µM G3-SN31-PEG FITC dendrimers (green) for 2 h, 6 h, or 24 h. Actin filaments were labelled with phalloidin (red) and nucleus with DAPI (blue). Scale bars indicate 25 µm. **DAPI:** 40,6-diamidino-2-phenylindole dihydrochloride; **ns:** non-significant. * $p < 0,05$; ** $p < 0,01$.

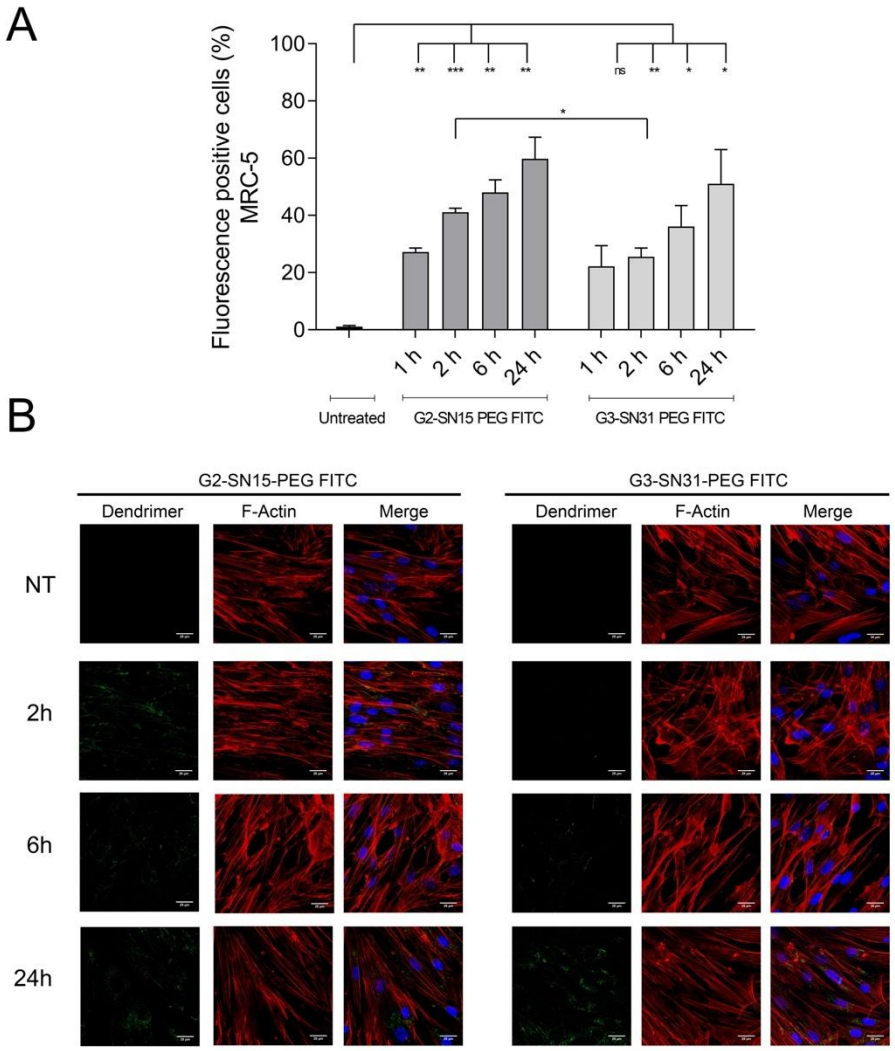

Figure 26: Internalisation study of PCCDs into MRC-5 cell line. **(A)** Percentage of FITC-positive cells analysed by flow cytometry 1, 2, 6 and 24 h post-treatment. Data are represented as mean ± SD of two individual experiments. **(B)** Confocal images of cells treated with 1 µM G2-SN15-PEG FITC or 0,5 µM G3-SN31-PEG FITC dendrimers (green) for 2 h, 6 h, or 24 h. Actin filaments were labelled with phalloidin (red) and nucleus with DAPI (blue). Scale bars indicate 25 µm. **DAPI:** 40,6-diamidino-2-phenylindole dihydrochloride; **ns:** non-significant. * $p < 0,05$; ** $p < 0,01$, *** $p < 0,001$.

6.2.2 HSV-2 and HCMV antiviral efficacy of PCCDs

The antiviral activity of PCCDs against HSV-2 and HCMV infections was determined by inhibition experiments through a plaque reduction assay. In brief, Vero and MRC-5 cell lines were treated with increasing concentrations of G2-SN15-PEG or G3-SN31-PEG dendrimers, from 0,2 µM to the maximum non-toxic concentration one-hour prior infection with 0,001 MOI of HSV-2_{333} and $HCMV_{AD-169}$. After 48 h (in Vero cells) or 6 days (in MRC-5 cells), lysis plaques were revealed by methylene blue staining and counted.

Figures 27A and 27B show that both G2-SN15-PEG and G3-SN31-PEG dendrimers can inhibit HSV-2 and HCMV infections at maximum nontoxic concentrations. Against both viruses, the G3-SN31-PEG dendrimer presented better inhibition values at all tested concentrations, reaching 99 and 86% inhibition of HSV-2 and HCMV, respectively, at the maximum concentration. It is important to note that, at all tested concentrations, both dendrimers have higher inhibition activity than ACV and GCV, which are the actual reference treatments.

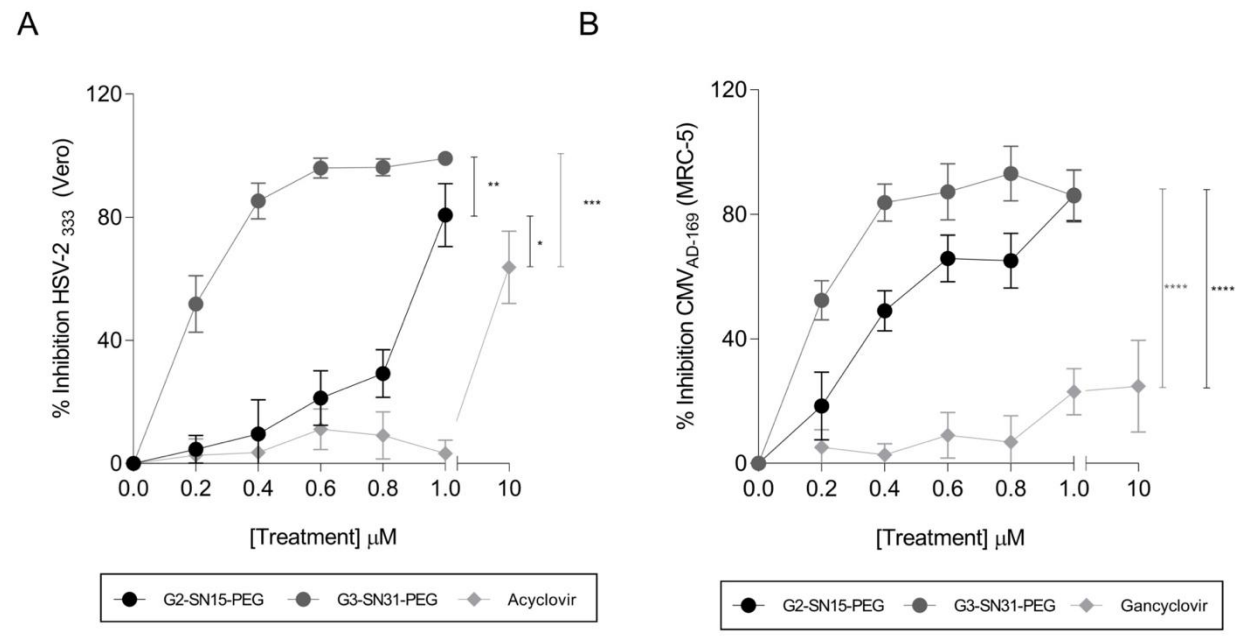

Figure 27: Antiviral activity of PCCDs against HSV-2 and HCMV. Inhibition of HSV-2_{333} in Vero **(A)** and of $HCMV_{AD-169}$ in MRC-5 **(B)** cell lines pre-treated with increasing concentrations of G2-SN15-PEG and G3-SN31-PEG dendrimers from 0,2 µM to the maximum non-toxic concentration. ACV and GCV were used as reference treatments for comparison. Infection was measured by plaque reduction assay. Data are represented as mean ± SD of three individual experiments performed in triplicate. **ACV:** acyclovir; **GCV:** ganciclovir; **HSV-2:** Herpes Simplex Virus-2; **HCMV:** Human Cytomegalovirus. * $p < 0,05$; ** $p < 0,01$, *** $p < 0,001$, **** $p < 0,0001$.

6.2.2.1 Mechanism of action of PCCDs

To study the mechanism by which PCCDs can inhibit HSV-2 and HCMV infections, two different approaches were used: viral inactivation (VI) and binding inhibition (BI). For VI, 1µM G2-SN15-PEG or G3-SN31-PEG dendrimers were incubated with cell-free HSV-2_{333} or $HCMV_{AD-169}$ at 37 ºC for 2 h. The pellet obtained after two rounds of ultracentrifugation was resuspended and added to cells. For BI, cells were precooled at 4 ºC for 15 min, treated with dendrimers and infected with HSV-2_{333} or $HCMV_{AD-169}$ at the same temperature to make the membrane less permeable to both virus and dendrimers and force their interaction there. After 48 h (Vero cells) or 6 days (MRC-5 cells) of incubation, lysis plaques were revealed by methylene blue staining and counted.

Results shown in Figures 28A and 28B exhibit similar inhibition values as those obtained in the antiviral efficacy study when performing BI assay, indicating that both dendrimers can significantly inhibit viral attachment to both cell lines. However, G2-SN15-PEG and G3-SN31-PEG dendrimers can only inactivate $HCMV_{ad169}$ and with lower inhibition values suggesting null and low virucidal activity against HSV-2 and HCMV infections, respectively. These results imply that inhibition is achieved in the first stages of infection, most probably by impeding viral attachment to the cell membrane, thus preventing infection.

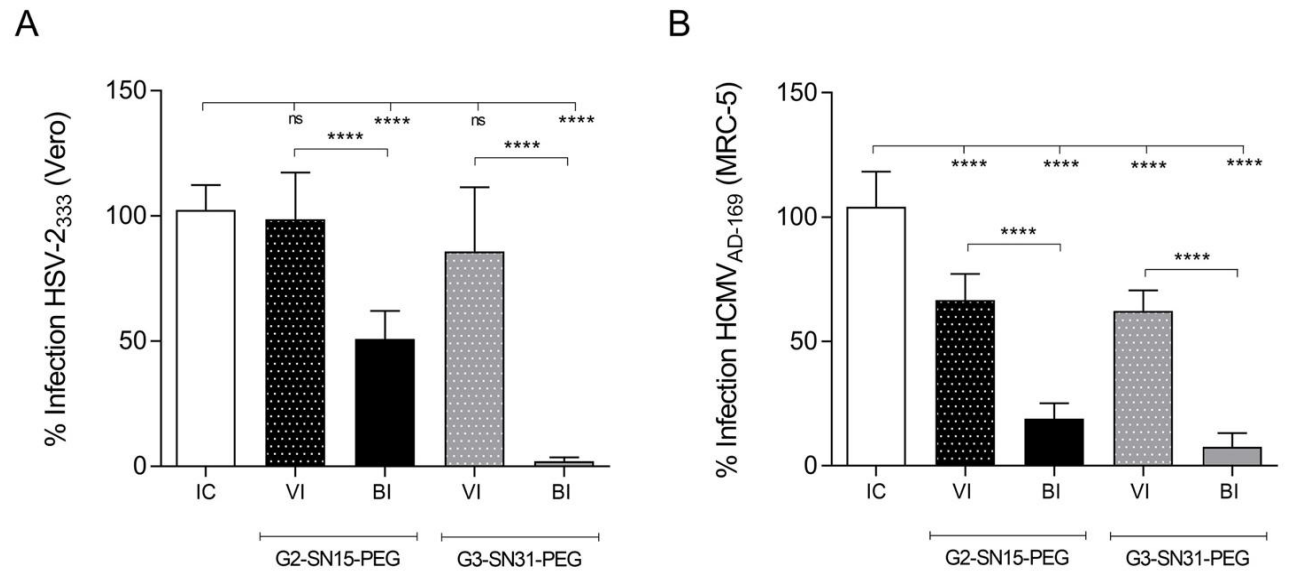

Figure 28: Antiviral mechanism of action of PCCDs. Effect of 1 µM G2-SN15-PEG and 1 µM G3-SN31-PEG dendrimers on the infectivity and binding of HSV-2_{333} **(A)** and $HCMV_{AD-169}$ **(B).** VI and BI assays were performed and measured using a plaque reduction assay. Data are represented as mean ± SD of three individual experiments performed in triplicate. **HSV-2:** Herpes Simplex Virus-2; **HCMV:** Human Cytomegalovirus; **VI:** viral inactivation; **BI:** binding inhibition; **ns:** non-significant. **** $p < 0{,}0001$.

6.2.2.2 Interaction with cell surface receptors

To study in depth the mechanism through which PCCDs inhibit HSV-2 and HCMV infections, their capacity to bind to anionic HSPGs thus preventing attachment of viruses to these receptors was examined. To do so, different binding assays were carried out, including (i) heparin competition assay, to study competition with a structural analogue of HSPGs, (ii) 2 M NaCl wash, to detach molecules bound to heparin/HSPG, and (iii) heparinase II treatment, to enzymatically cleave HSPGs. For the first experiment, cells were treated with 1 µM G2-SN15-PEG FITC or 0,5 µM G3-SN31-PEG FITC dendrimers in the absence or presence of heparin. For the second, cells were treated and washed with 2 M NaCl. In the third experiment, cells were pre-treated with 200 mU/mL of heparinase II before incubating with dendrimers. Flow cytometry was used to quantify the remaining amounts of cell-associated dendrimers after performing these assays.

As observed in Figures 29A and 29B, there is a notable decrease in the number of cell-associated G2-SN15-PEG FITC and G3-SN31-PEG FITC dendrimers in both cell lines after treatment with heparin. HSPGs interactions were also partially disrupted when rinsed with 2 M NaCl, due to a reduction of the number of cell-associated dendrimers in all samples, however differences were only statistically significant for the G2-SN15-PEG FITC dendrimer in Vero cell line and for the G3-SN31-PEG FITC dendrimer in MRC-5 cell line. Figures 29C and 29D show a notable decrease in dendrimer binding capacity to cells after treatment with heparinase II, observed in the important decrease in MFI in every sample; however, this decrease was only significant for G2-SN15-PEG FITC dendrimer in Vero cell line. All these results suggest that HSPGs play a prominent role in the interaction of the studied PCCDs with the cell surface.

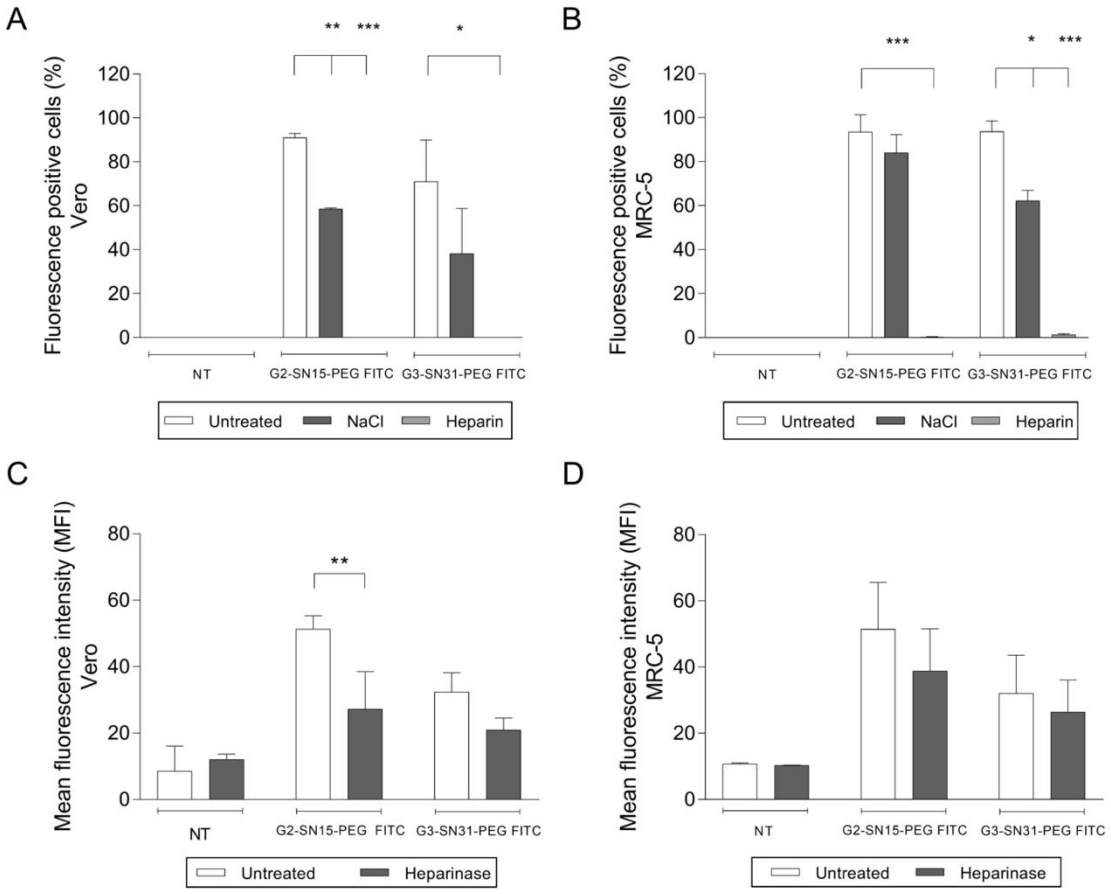

Figure 29: Interaction of PCCDs with cell surface HSPGs. Fluorescent positive cells and mean fluorescence intensity of 1 µM G2-SN15-PEG FITC or 0,5 µM G3-SN31-PEG FITC dendrimers measured by flow cytometry in Vero **(A, C)** and MRC-5 **(B, D)** cell lines. Heparin competition, 2 M NaCl wash, and heparinase II treatment assays were performed to study the interaction of PCCDs with HSPGs on the cell surface. Data are represented as mean ± SD of two individual experiments. **NT:** nontreated. * $p < 0,05$; ** $p < 0,01$, *** $p < 0,001$.

The capacity of PCCDs to bind to heparin/HSPGs was evaluated by SPR in collaboration with Prof. Marco Rusnati from the Department of Molecular and Translational Medicine of the University of Brescia. Considering the strong structural analogy that exists between heparin and HSPGs, a SPR biosensor containing immobilised heparin was used as a simplified “cell-free” model to study the interaction of various compounds to HSPGs.

As presented in Figures 30A and 30B, both dendrimers show significant and specific binding to surface-immobilised heparin. Injection of dendrimers at increasing concentrations onto the sensor chip indicated a dose-response binding. Furthermore, the fact that dendrimers do not spontaneously detach from heparin at the end of the injection phase and can only be removed by high salt washing indicates that the binding of dendrimers to heparin is very stable (Figures 30C and 30D). On the other hand, values of dendrimer binding at equilibrium were used to calculate Kd values and to obtain the dose-response curves shown in Figures 30E and 30F. Values shown in Table 6 suggest that both G2-SN15-PEG and G3-SN31-PEG dendrimers bind surface-immobilised heparin in a saturable manner with relatively high affinity. The specificity of this binding is confirmed by the fact that a molar excess of heparin completely abolished binding of dendrimers to surface-immobilised heparin (Figures 30E and 30F).

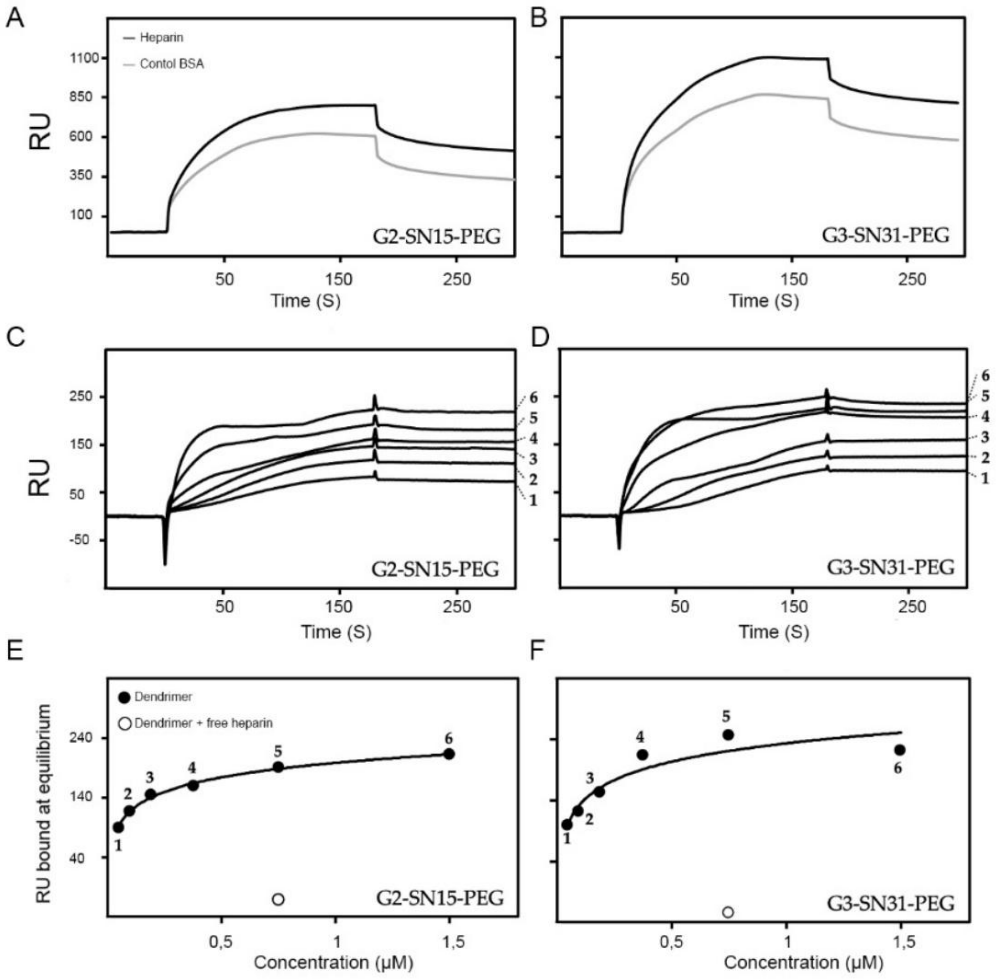

Figure 30: SPR analysis of the interaction of PCCDs with heparin. **(A, B)** Sensorgrams showing binding of G2-SN15-PEG and G3-SN31-PEG dendrimers to flow cells coated with heparin or BSA. **(C, D)** Blank-subtracted sensorgram overlays showing specific binding of increasing concentrations of dendrimers (1: 0,047 µM; 2: 0,094 µM; 3: 0,188 µM; 4: 0,375 µM; 5: 0,75 µM; 6: 1,5 µM) to surface-immobilised heparin. Response (in RU) was recorded as a function of time. **(E, F)** Saturation curves obtained using the values of RU bound at equilibrium from panels (C, D). Result of the competition assay with free heparin is also reported. **BSA:** bovine serum albumin; **S:** seconds; **RU:** resonance units.

Table 6. Kd values of the interactions of G2-SN15-PEG and G3-SN31-PEG dendrimers with heparin. Data correspond to mean ± SEM of three individual experiments.

Dendrimer	Kd (nM) at Equilibrium
G2-SN15-PEG	368,3 ± 108,1
G3-SN31-PEG	186,7 ± 82,6

6.3 DESIGN OF A DENDRITIC CELL-BASED THERAPEUTIC VACCINE AGAINST HIV-1 INFECTION

Despite different policies have been implemented to improve access to cART, still more than 25% of the 37 million of people living with HIV-1 are not receiving any type of treatment. In addition to access to treatment, adherence to it is another risk factor, as interruption of treatment leads to a rapid increase in viral load and lymphocyte death. These give rise to one of the biggest challenges of the biomedical community nowadays: finding a more accessible and lasting therapeutic approach against HIV-1.

It is widely agreed that a complete cure for HIV-1 infection is the main objective to achieve; however, a functional cure would reduce the burden of the disease associated with the infection: It would help reach a higher percentage of the population, improve their quality of life, and reduce the costs of lifelong treatments (Davenport et al., 2019). An example of functional cures are therapeutic vaccines, which face infection by keeping it latent under a specific immune response and reducing the number of cells susceptible to infection and replication. DC-based vaccines, designed to contain specific antigens, such as antigenic peptides, are becoming promising strategies (Skwarczynski and Toth, 2016, Martin-Moreno and Munoz-Fernandez, 2019). These antigen-presenting cells (APCs) can induce primary and secondary immune responses through the major histocompatibility complex (MHC)-class II pathway to helper $CD4^+$ T lymphocytes and through the MHC-class I to cytotoxic $CD8^+$ T (Nakayama, 2014).

However, peptides might not be highly immunogenic because such a small portion of the pathogen fails to trigger the natural activation of the immune system. To overcome this drawback, delivery systems may act as adjuvant stimulators enhancing vaccine efficiency and prolonging their half-life (Yang et al., 2019). In this sense, different studies have been carried out on the use of nanoparticles to improve peptide delivery and ensure good activation of the immune system by potentiating antigenic presentation and immune activation (Martin-Moreno et al., 2020, Vacas-Cordoba et al., 2014a, Vacas-Cordoba et al., 2014b).

The objective of this work was to study whether $EG3SO_3Na$, $ChG3SO_3Na$, $EG3NMe_3I$ and $ChG3NMe_3I$ micellar carbosilane dendrons could be used in the development of a DC-based therapeutic vaccine when associated with HIV-1-derived peptides (Figure 31). To do so, moDCs obtained from healthy patients were matured in the presence of HIV-1-derived peptides and co-cultured with autologous PBMCs to study the effect on lymphocyte activation and cytokine release.

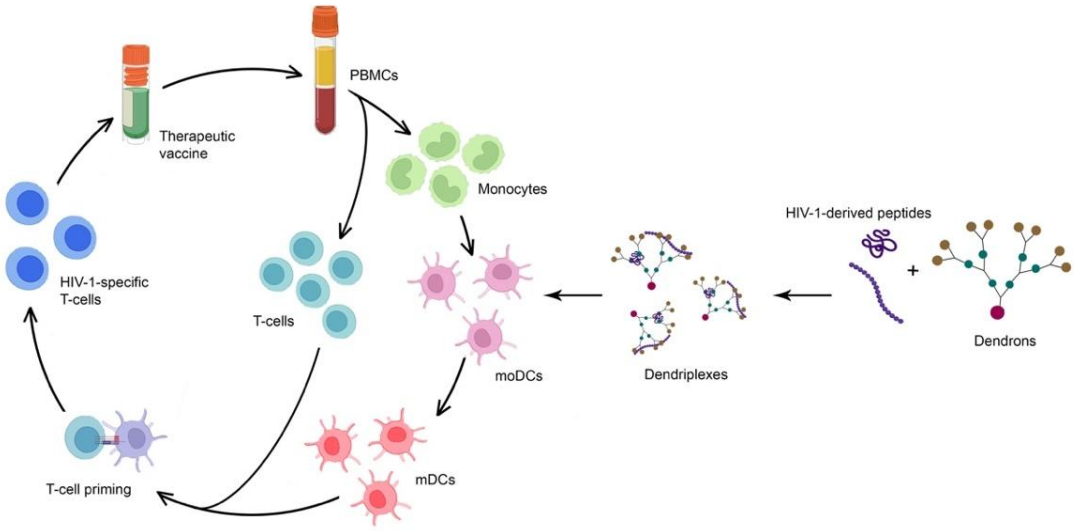

Figure 31: Graphical abstract of the development of a DC-based therapeutic vaccine based on the use of micellar carbosilane dendrons as delivery vehicles of HIV-1-derived peptides. **PBMCs:** peripheral mononuclear cells; **moDCs:** monocyte-derived dendritic cells; **HIV-1:** Human Immunodeficiency Virus-1; **DCs:** dendritic cells.

6.3.1 Biocompatibility of dendrimicelles and HIV-1 peptides in moDCs

6.3.1.1 Assessment of the mitochondrial toxicity of dendrimicelles

Evaluation of the mitochondrial toxicity induced by dendrimicelles was done by the MTT assay following manufacturer's instructions. MoDCs were treated for 6 days with increasing concentrations of dendrimicelles, from 0,25 to 50 μM. Culture medium was used as untreated control and 10% DMSO as death control. Concentrations were considered non-toxic when the survival rate was greater than 80%. Results shown in Figure 32 indicate that the maximum non-toxic concentrations of the $EG3SO_3Na$, $ChG3SO_3Na$, $EG3NMe_3I$ and $ChG3NMe_3I$ dendrimicelles are 1 μM, 1 μM, 2,5 μM and 5 μM, respectively.

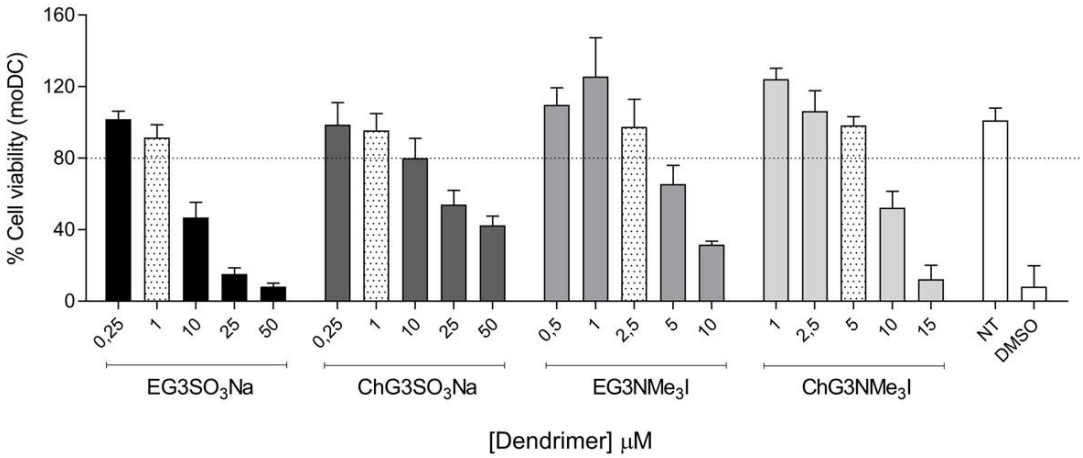

Figure 32: Cytotoxicity of dendrimicelles in moDCs determined by MTT assay. MoDCs were treated for 6 days with $EG3SO_3Na$, $ChG3SO_3Na$, $EG3NMe_3I$ and $ChG3NMe_3I$ dendrimicelles at concentrations ranging from 0,25 to 50 μM. Cell viability ≥ 80 % was established as non-toxic working concentrations. Culture medium was used as NT control and 10% DMSO as death control. Data are represented as mean ± SD of three individual experiments performed in triplicate. **MoDC:** monocyte-derived dendritic cell; **NT:** non-treated; **DMSO:** dimethyl sulfoxide.

6.3.1.2 Determination of the viability of HIV-1-derived peptides

Assessment of the mitochondrial toxicity induced by HIV-1-derived peptides and dendrimicelles-peptide dendriplexes was also done by the MTT assay following manufacturer's instructions. MoDCs were treated for 6 days with 0,5, 1 and 5 µM of labelled and non-labelled HIV-1-derived peptides. In addition, MoDCs were treated for 6 days with dendriplexes formed with these peptides (1 µM) and $EG3SO_3Na$, $ChG3SO_3Na$, $EG3NMe_3I$ or $ChG3NMe_3I$ dendrimicelles (at maximum non-toxic concentration). Culture medium was used as untreated control and 10% DMSO as death control. Concentrations were considered nontoxic when the survival rate was above 80%. Results shown in Figure 33A indicate that all cationic peptides (Pep-Rev, Pep-Vif and Pep-GagPol-1) and their labelled forms are viable at the desired working concentration (1 µM). Figure 33B shows that all anionic peptides (Pep-GagPol-2, Pep-GagPol-3, and Pep-Env) and their labelled forms are also viable at 1 µM. Additionally, both figures determine that the dendriplexes formed present viability rates greater than 80% after 6 days of treatment.

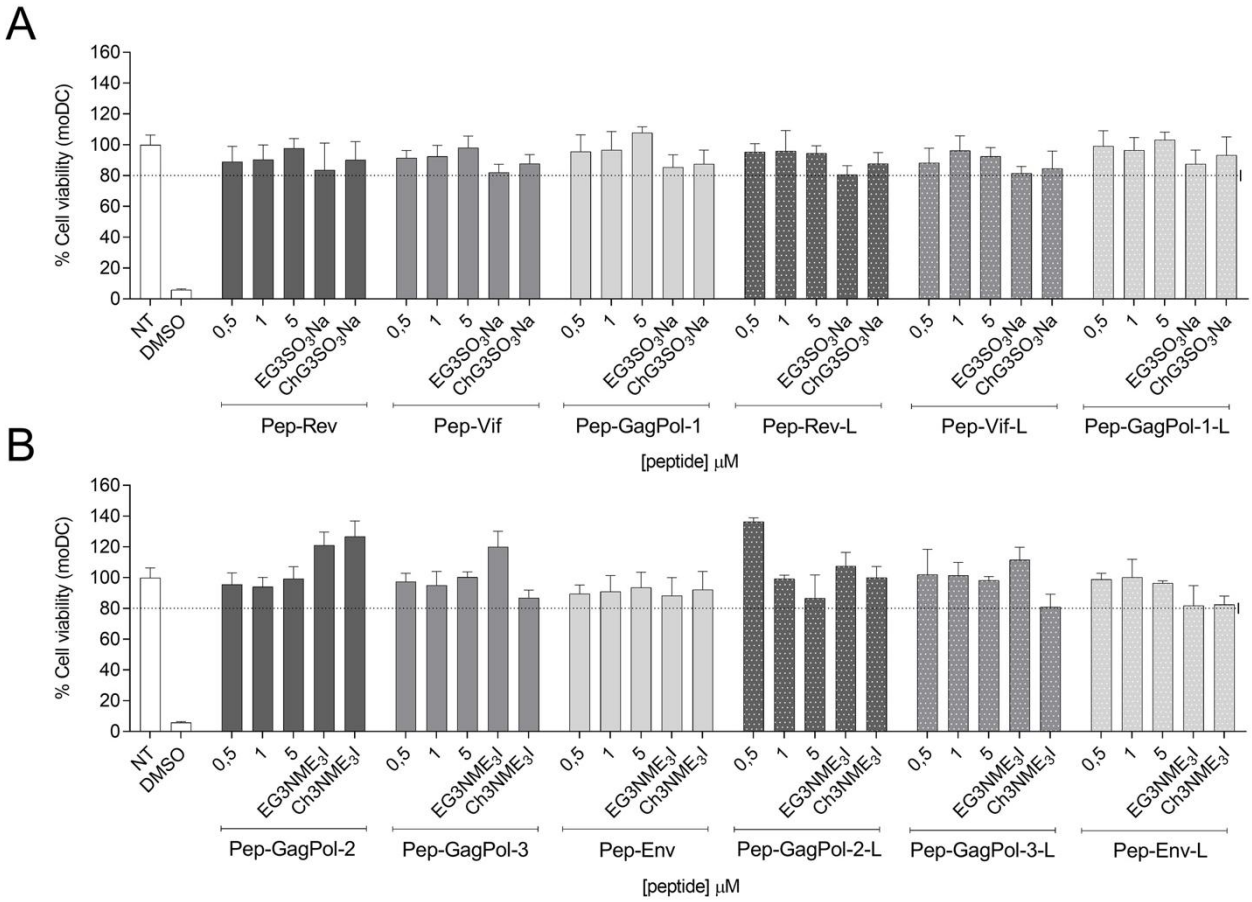

Figure 33: Cytotoxicity of HIV-1-derived peptides and dendrimicelles-peptide dendriplexes in moDCs determined by the MTT assay. **(A)** MoDCs were treated for six days with Pep-Rev, Pep-Vif and Pep-GagPol-1 cationic peptides at 0,5, 1 and 5 µM and dendriplexes formed with 1 µM $EG3SO_3Na$ or 1 µM $ChG3SO_3Na$ dendrimicelles and 1 µM of peptides. **(B)** MoDCs were treated for six days with Pep-GagPol-2, Pep-GagPol-3 and Pep-Env anionic peptides at 0,5, 1 and 5 µM and dendriplexes formed with 2,5 µM $EG3NMe_3I$ or 5 µM $ChG3NMe_3I$ dendrimicelles and 1 µM of peptides. Cell viability ≥ 80 % was established as non-toxic working concentrations. Culture medium was used as NT control and 10% DMSO as death control. Data are represented as mean ± SD of three individual experiments performed in triplicate. **DC:** dendritic cell; **NT:** non-treated; **DMSO:** dimethyl sulfoxide; **L:** labelled.

6.3.2 Dendrimicelles-peptide dendriplexes formation and characterisation

Determination of the capacity of the cationic dendrimicelles to form dendriplexes with Pep-GagPol-2-L, Pep-GagPol-3-L and Pep-Env-L anionic peptides was tested by 6% agarose gel electrophoresis. Complexes were formed mixing 1 µM of the desired peptide and 2,5 µM of $EG3NMe_3I$ or 5 µM of $ChG3NMe_3I$, within 2 h of incubation at 37 ºC.

Results shown in Figures 34A and 34B illustrate that the maximum working concentrations of $EG3NMe_3I$ or $ChG3NMe_3I$ dendrimicelles can bind peptides with different efficiency: $EG3NMe_3I$ can encapsulate 18 and 30% of Pep-GagPol-3 and Pep-Env peptides, while $ChG3NMe_3I$ can encapsulate 24 and 23% of Pep-GagPol-3 and Pep-Env peptides. However, these dendrimicelles cannot form complexes with Pep-GagPol-2 peptide.

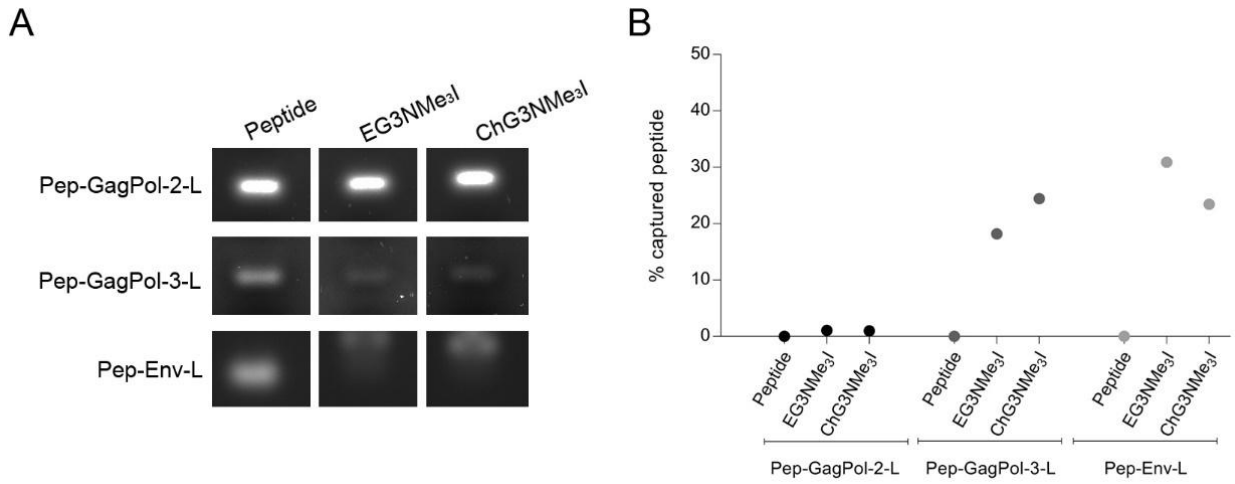

Figure 34: Dendrimicelle-peptide dendriplexes formation and characterisation. **(A)** Six percent agarose gel electrophoresis showing formation of dendriplexes with anionic HIV-1-derived peptides (Pep-GagPol-2, Pep-GagPol-3 and Pep-Env, 1 µM) and $EG3NMe_3I$ (2,5 µM) or $ChG3NMe_3I$ (5 µM) dendrimicelles after 2 h of incubation at 37 ºC. **(B)** Percentage of peptide captured relative to the control.

The inability to visualise the Cy5 label of Pep-Rev-L, Pep-Vif-L, and Pep-GagPol-1-L cationic peptides by agarose gel electrophoresis involved the measurement of the electrical potential (by ZP) and the hydrodynamic size (by DLS) to evaluate the capacity of anionic dendrimicelles to form dendriplexes.

As shown in Table 7, surface charge values obtained from ZP measurements confirmed the anionic density of the periphery of the studied dendrimicelles; more precisely, the potential values obtained (-17,5 mV for $EG3SO_3Na$ and -9,36 for $ChG3SO_3Na$ dendrimicelles) indicate low electrical stability, thus inclination of these molecules towards agglomeration. In all the cases studied, the formation of the dendriplexes involved a change in the surface charge, which in some cases tended to more stable electrical molecules (higher than ±25 mV) but in others to molecules with a tendency to rapid agglomerate (close to ±5 mV).

Formation of dendriplexes was also studied by measuring the particle size distribution by DLS; a five-fold increase with respect to the dendrimicelles or peptide control was considered to be proof of the encapsulation of peptides. Following this rule, $EG3SO_3Na$ and $ChG3SO_3Na$ dendrimicelles were able to encapsulate Pep-Rev and Pep-Vif peptides at tested concentrations, but were unable to form complexes with Pep-GagPol-1 peptide (Table 7).

Table 7. Measurement of ZP values (mV) and hydrodynamic size (nm) of $EG3SO_3Na$ and $ChG3SO_3Na$ dendrimicelles, Pep-Rev, Pep-Vif, and Pep-GagPol-1 peptides and dendriplexes formed with these cationic HIV-1-derived peptides (1 μM) and $EG3SO_3Na$ or $ChG3SO_3Na$ (1 μM) dendrimicelles after 2 h of incubation at 37 ºC. Invalid measurements are indicated with dashes (-).

Compound	Zeta potential (mV)	Hydrodynamic size (diameter, nm)
$EG3SO_3Na$	-17,50 ± 7,23	0,68 ± 0,02
$ChG3SO_3Na$	-9,36 ± 2,91	1,12 ± 0,11
Pep-Rev	-	-
$EG3SO_3Na$ + Pep-Rev	-3,90 ± 0,43	141,10 ± 6,50
$ChG3SO_3Na$ + Pep-Rev	-4,08 ± 0,92	190,20 ± 17,11
Pep-Vif	11,43 ± 1,89	0,87 ± 0,29
$EG3SO_3Na$ + Pep-Vif	-8,13 ± 0,38	116,99 ± 18,48
$ChG3SO_3Na$ + Pep-Vif	-30,40 ± 1,08	97,53 ± 12,55
Pep-GagPol-1	-	22,33 ± 6,21
$EG3SO_3Na$ + Pep-GagPol-1	-28,27 ± 0,58	-
$ChG3SO_3Na$ + Pep-GagPol-1	-35,47 ± 1,46	105,7 ± 10,61

6.3.3 Delivery of HIV-1-derived peptides into moDCs

The next step after confirmation of the ability of the dendrimicelles to encapsulate the different peptides consisted of assessing if these complexes facilitated the entry of the peptides into moDCs. To do so, moDCs were treated for 2 and 24 h with peptides, dendrimicelles, or complexes formed as previously described and, afterwards, internalisation was determined by measuring the fluorescent signal of the labelled peptides by confocal microscopy and flow cytometry. It is important to mention that these studies were only performed for three peptides: Pep-Rev-L, Pep-Vif-L and Pep-GagPol-3-L. Peptides Pep-GalPol-1 and Pep-GalPol-2 were discarded because they were unable to encapsulate any dendrimicelle and Pep-Env was discarded because its label was poorly detected by both techniques.

Images obtained from confocal microscopy suggest a similar internalisation pattern for the studied peptides: encapsulation of peptides with $EG3SO_3Na$, $ChG3SO_3Na$, $EG3NMe_3I$ and $ChG3NMe_3I$ dendrimicelles enhances cellular uptake of the peptides. This was easily observed due to the increase in the fluorescent signal inside cells that have been treated with the complexes in comparison with those treated only with the peptides (Figures 35A, 36A, and 37A). Furthermore, the images show that the fluorescent signal is greater after 2 h of treatment rather than after 24 h, suggesting that after this time moDCs have processed the peptide.

Flow cytometry internalisation studies, which are more sensitive than confocal microscopy, confirmed these observations. Figure 35B shows a significant increase in Pep-Rev-L signal in cells treated with complexes formed with $EG3SO_3Na$ and $ChG3SO_3Na$ dendrimicelles, which increases from 22% to 67 and 82%, respectively, after 2 h of treatment. This increase, although still statistically significant, was much lower after

24 h of treatment, when it increased from 6 to around 40% in both cases. Similar observation was done for Pep-Vif-L peptide in Figure 36B, in this case the increase from naked peptide to encapsulated peptide only raised from 63% to 71 and 78% for complexes formed with $EG3SO_3Na$ and $ChG3SO_3Na$, respectively. On the other hand, the internalisation of this peptide after 24 h of treatment was also much lower, with values that increased from 28% of the naked peptide to 51 and 70% of $EG3SO_3Na$ and $ChG3SO_3Na$ complexed peptide, respectively. The anionic Pep-GagPol-3-L peptide also confirmed better internalisation when forming complexes, with values that increased from 50 and 60% of the naked peptide, after 2 and 24 h of treatment, to values greater than 92% when forming complexes with $EG3NMe_3I$ and $ChG3NMe_3I$ dendrimicelles at the same incubation times (Figure 37B). In this case, there were no significant differences in entry between the studied treatment times.

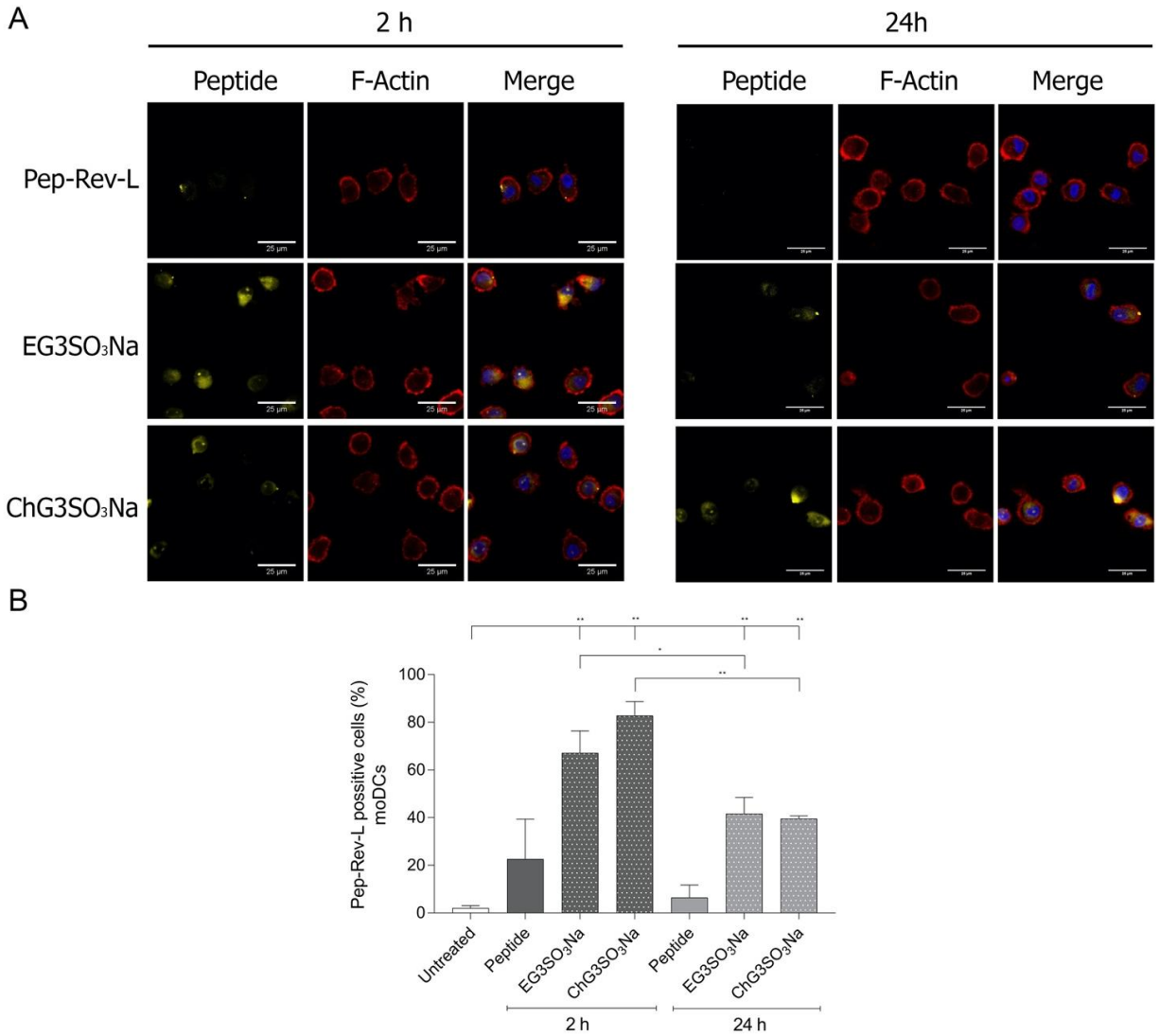

Figure 35: Internalisation of Pep-Rev-L peptide in moDCs. Cells were treated for 2 and 24 h with 1 μM of Pep-Rev-L or complexes formed with it and 1 μM of $EG3SO_3Na$ or $ChG3SO_3Na$ dendrimicelles within 2 h of incubation. **(A)** Representative confocal microscopy images of moDCs treated with this peptide or complexes (in green) and stained with Phalloidin for actin filaments (red) and DAPI for the nucleus (blue). **(B)** Entry of this peptide into moDCs determined by flow cytometry. **DAPI**: 4′,6-Diamidino-2-phenylindole dihydrochloride. * $p < 0,05$; ** $p < 0,01$.

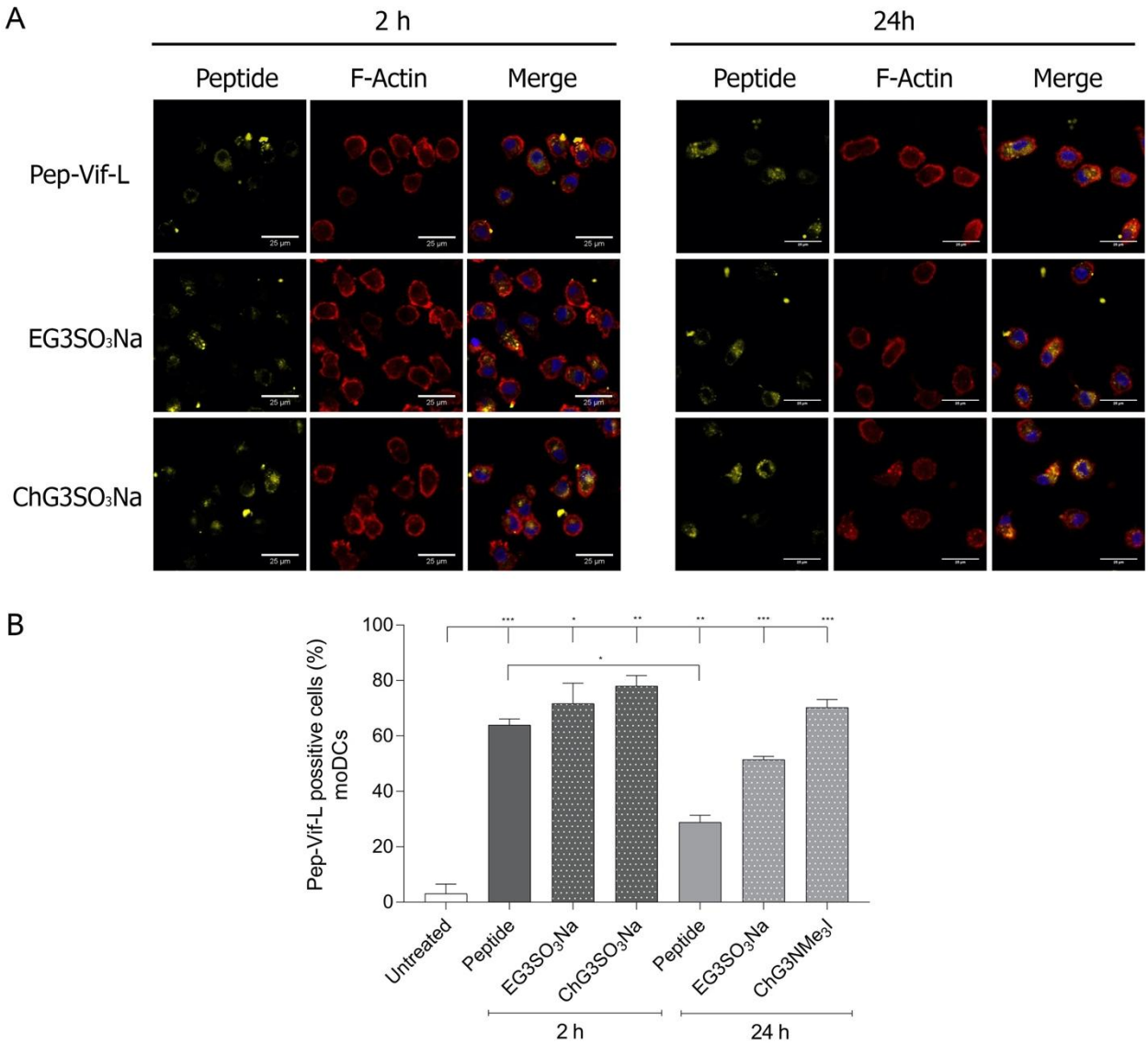

Figure 36: Internalisation of Pep-Vif-L peptide in moDCs. Cells were treated for 2 and 24 h with 1 µM of Pep-Vif-L or complexes formed with it and 1 µM of $EG3SO_3Na$ or $ChG3SO_3Na$ dendrimicelles within 2 h of incubation. **(A)** Representative confocal microscopy images of moDCs treated with this peptide or complexes (in green) and stained with Phalloidin for actin filaments (red) and DAPI for the nucleus (blue). **(B)** Entry of this peptide into moDCs determined by flow cytometry. **DAPI**: 4′,6-Diamidino-2-phenylindole dihydrochloride. * $p < 0,05$; ** $p < 0,01$, *** $p < 0,001$.

Both studies confirmed that $EG3SO_3Na$, $ChG3SO_3Na$, $EG3NMe_3I$ and $ChG3NMe_3I$ dendrimicelles are effective delivery vehicles for Pep-Rev-L, Pep-Vif-L and Pep-GagPol-3-L peptides. Since improvement of the uptake was greater in complexes formed with cationic Pep-Rev-L and anionic Pep-GagPol-3-L peptides, following studies will only be done in those two peptides.

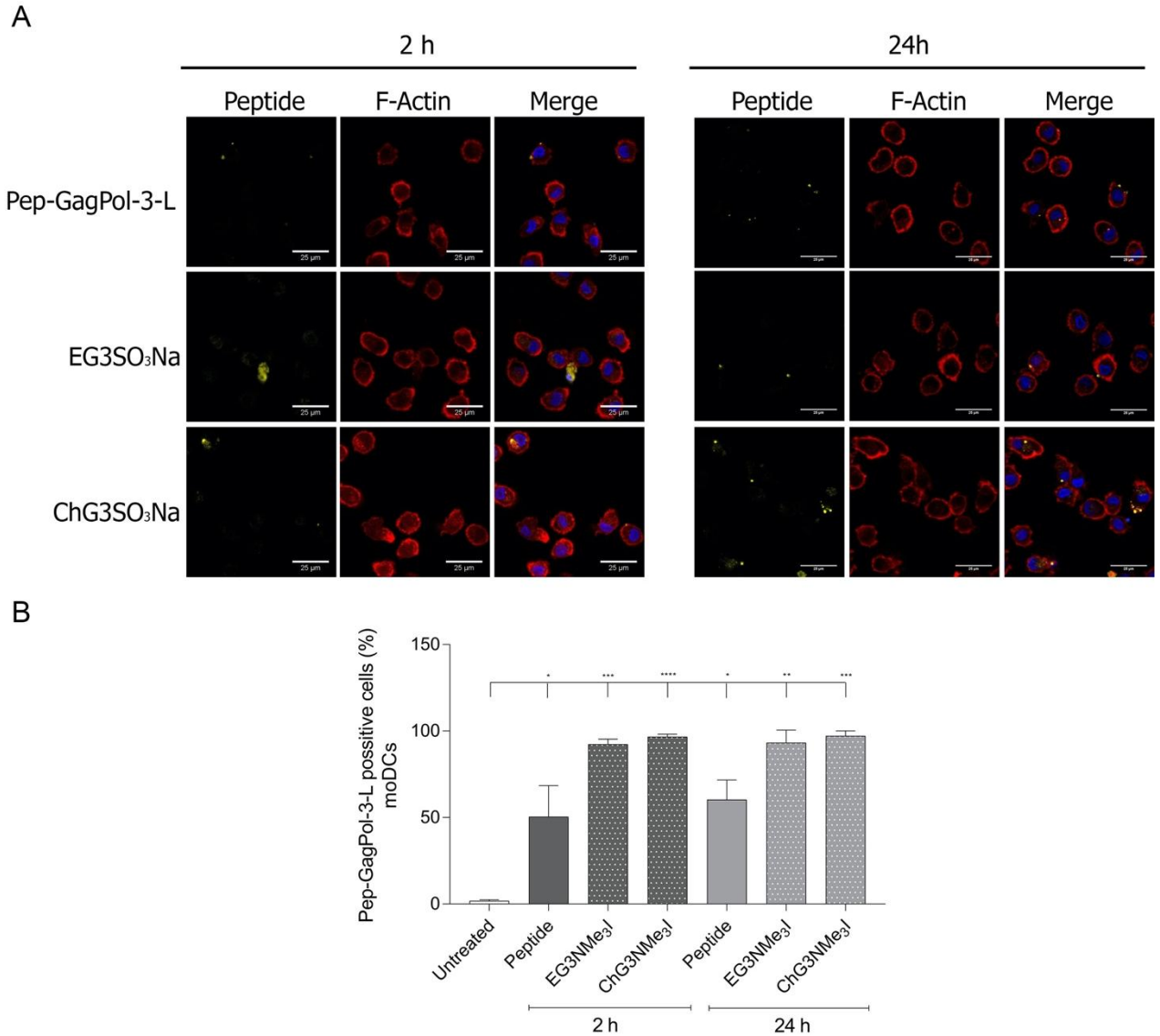

Figure 37: Internalisation of Pep-GagPol-3-L peptide in moDCs. Cells were treated for 2 and 24 h with 1 µM of Pep-GagPol-3-L or complexes formed with it and 2,5 µM of $EG3SO_3Na$ or 5 µM $ChG3SO_3Na$ dendrimicelles within 2 h of incubation. **(A)** Representative confocal microscopy images of moDCs treated with this peptide or complexes (in green) and stained with Phalloidin for actin filaments (red) and DAPI for the nucleus (blue). **(B)** Entry of this peptide into moDCs determined by flow cytometry. **DAPI**: 4′,6-Diamidino-2-phenylindole dihydrochloride. * $p < 0,05$; ** $p < 0,01$, *** $p < 0,001$, **** $p < 0,0001$.

6.3.4 Effect of dendriplexes on moDCs maturation

In order to determine if the uptake of the peptides induced maturation of the moDCs, the expression of different maturation markers was studied by flow cytometry. To do so, Pep-Rev and $EG3SO_3Na$ or $ChG3SO_3Na$ and Pep-GagPol-3 and $EG3NMe_3I$ or $ChG3NMe_3I$ complexes were formed as previously described and added to moDCs. After 48 h, cells were stained with CD11c to stablish the moDCs population and with the following maturation markers: CD80, CD83, CD86, CD179 and HLA-DR.

Figure 38 shows the changes in the expression of these maturation markers in moDCs treated with Pep-Rev or complexes formed with it and $EG3SO_3Na$ or $ChG3SO_3Na$ dendrimicelles. No significant changes were observed for CD83, CD179 or HLA-DR, however, a significant increase in the percentage of CD80 expressing

cells when treating with $EG3SO_3Na$ dendrimicelles was detected. Furthermore, treatment with complexes produced a significant increase in CD86-expressing cells.

On the other hand, Figure 39 shows changes in the expression of the maturation markers in moDCs treated with Pep-GagPol-3 or complexes formed with it and $EG3NMe_3I$ or $ChG3NMe_3I$ dendrimicelles. In this case, there were no significant changes in the percentage of CD80, CD86, CD179 and HLA-DR markers, but a significant increase in the expression of CD83 when treating with complexes was observed. The increase in the expression of these markers suggests that upon uptake, moDCs recognise peptides or dendrimicelles as antigens, thus slightly promoting their maturation.

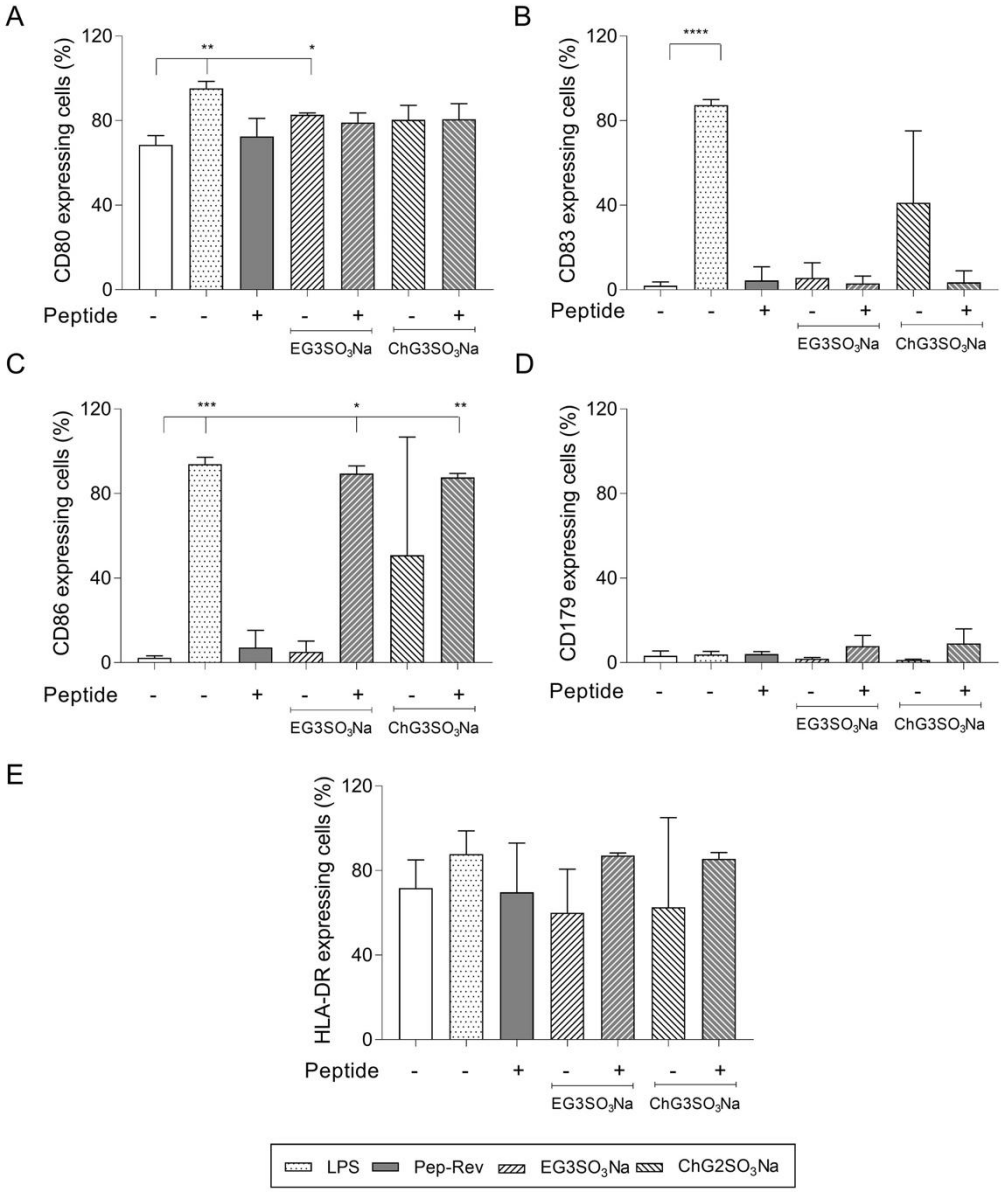

Figure 38: Maturation of moDCs upon uptake of Pep-Rev peptide. Flow cytometry measurements of cells treated for 48 h with 1 μM of Pep-Rev or complexes formed with it and 1 μM of $EG3SO_3Na$ or $ChG3SO_3Na$ dendrimicelles within 2 h of incubation. Percentage of **(A)** CD80, **(B)** CD83, **(C)** CD86, **(D)** CD179, and **(E)** HLA-DR expressing moDCs. **LPS:** lipopolysaccharide. * $p < 0,05$; ** $p < 0,01$, *** $p < 0,001$, **** $p < 0,0001$.

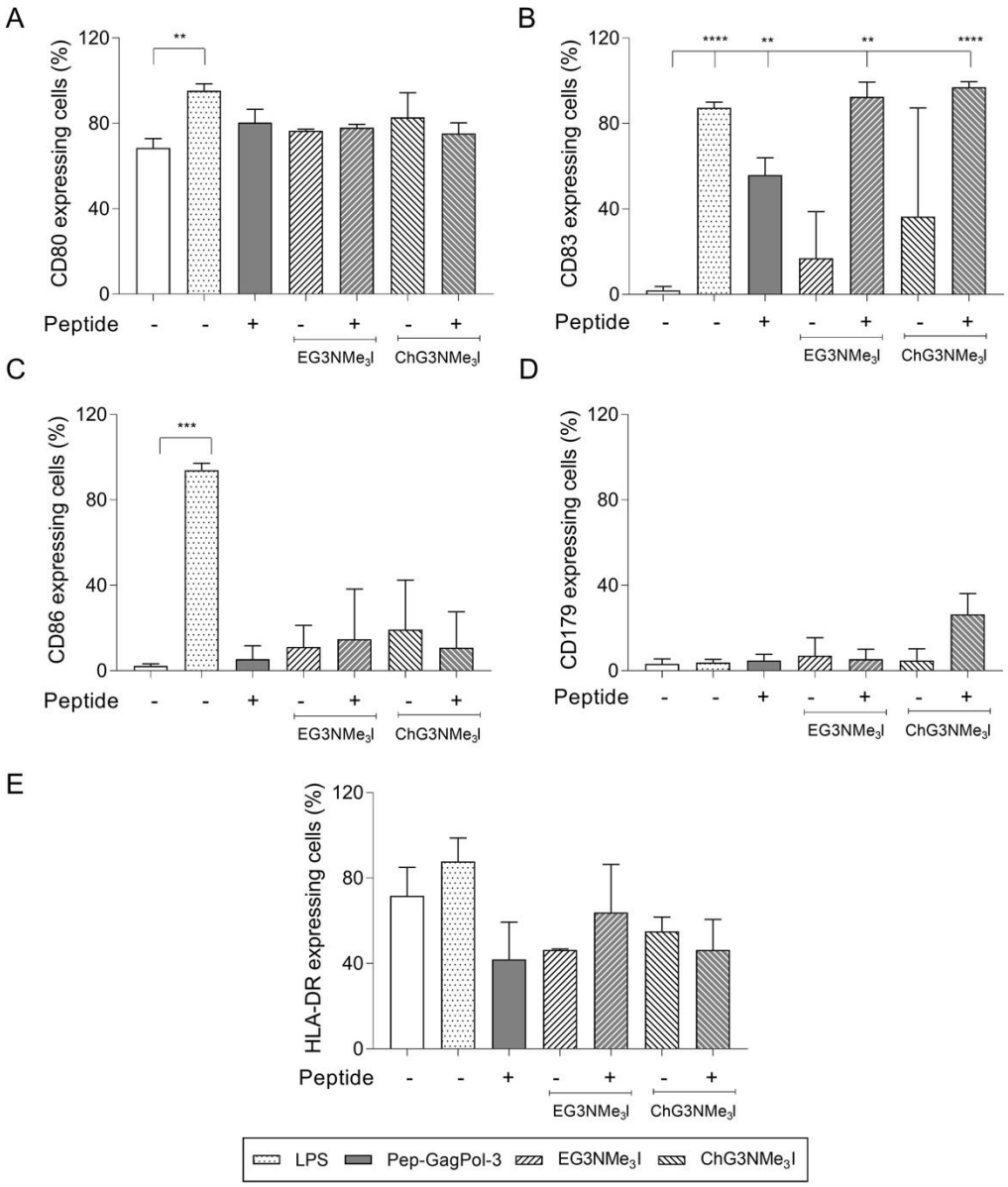

Figure 39: Maturation of moDCs upon uptake of Pep-GagPol-3 peptide. Flow cytometry measurements of cells treated for 48 h with 1 µM of Pep-GagPol-3 or complexes formed with it and 2,5 µM of $EG3NMe_3I$ or 5 µM $ChG3NMe_3I$ dendrimicelles within 2 h of incubation. Percentage of **(A)** CD80, **(B)** CD83, **(C)** CD86, **(D)** CD179, and **(E)** HLA-DR expressing moDCs. **LPS:** lipopolysaccharide. ** $p < 0,01$, *** $p < 0,001$, **** $p < 0,0001$.

6.3.5 Effect of dendriplexes on autologous PBMCs

The effect of mature moDCs transfected with Pep-Rev, Pep-GagPol-3 or the different complexes on lymphocytes was assessed by an autologous MLR. Since uptake of peptides only slightly produced maturation of moDCs, these cells were treated for 24 h with LPS to ensure induction of maturation prior to co-culture with PBMCs. At time of maturation, moDCs were transfected and, after 24 h, PBMCs resultant form the separation of $CD14^+$ cells were added to the culture in a 1:10 ratio.

Cells were observed by microscopy on days 1, 3 and 6 of the MLR to determine changes in proliferation and clumping of cells, which are indicators of PBMCs activation. Controls shown in Figure 40C illustrate that proper activation of PBMCs, despite treating with PHA, does not occur without the presence of mDCs.

Figure 40A indicates that aggregation of PBMCs increases along the time points studied, showing the highest activation at day 6 in all studied cases. It is visible that treatment with $EG3SO_3Na$ or $ChG3SO_3Na$ dendrimicelles alone produces less activation than Pep-Rev alone or encapsulated. Furthermore, it is observable that the complex formed with Pep-Rev and $EG3SO_3Na$ requires more time for activation than peptide alone or encapsulated with $ChG3SO_3Na$. However, at day 6 all three treatments presented resembling aggregation.

Different results were obtained from the study of the effects of treatment with Pep-GagPol-3 (Figure 40B). In this case, higher aggregation is obtained at day 3, afterwards there is an observable decline of the activation. At this time point, it is visible that Pep-GagPol-3 peptide and $EG3NMe_3I$ alone produce less activation than complexes. However, $ChG3NMe_3I$ dendrimicelle alone produces more activation than in complex with the peptide.

It is important to mention that activation observed in activation controls (PHA treated cells) is greater than the observed in the different treatments. Therefore, this confirms that co-culture of peptide-transfected mDCs with autologous PBMCs produces a microscopically observable slight activation of lymphocytes after 3 or 6 days of the MLR.

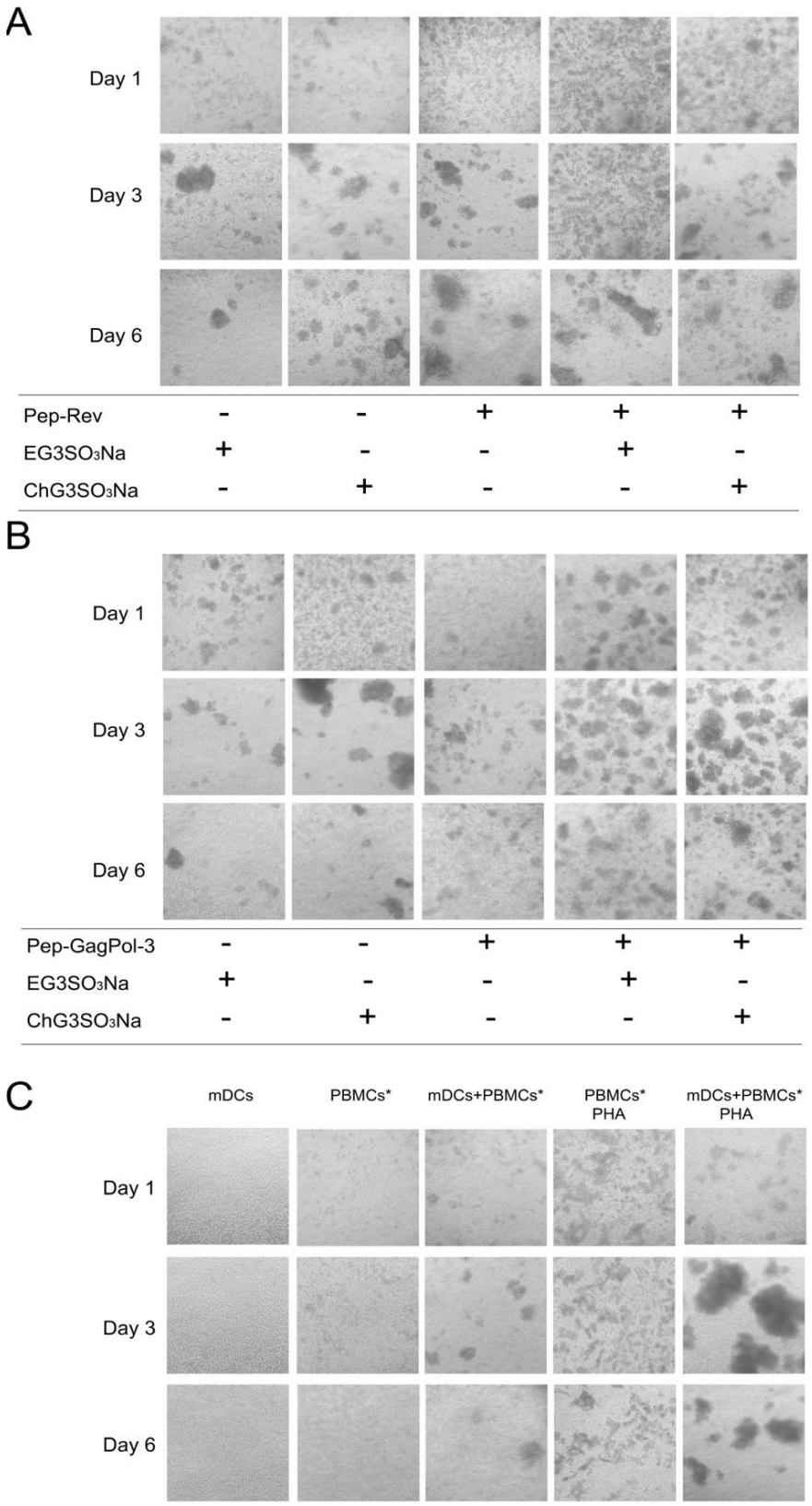

Figure 40: Activation of lymphocytes as a result of the MLR of moDCs with autologous PBMCs after 1, 3 and 6 days of co-culture. Bright-field microscopy images of random field of the co-culture of mDCs transfected with **(A)** Pep-Rev or complexes formed with $EG3SO_3Na$ or $ChG3SO_3Na$ dendrimicelles or **(B)** Pep-GagPol-3 or complexes formed with $EG3SO_3Na$ or $ChG3SO_3Na$ dendrimicelles. **(C)** Control of unproliferation and PHA activated PBMCs. **PBMCs*:** autologous PBMCs without $CD14^+$ cells; **PHA:** phytohaemagglutinin.

6.3.5.1 Expression of activation markers

Next step consisted of determining if the activation of lymphocytes after MLR observed by bright-field microscopy corresponded with the expression of activation markers on T and B cells. To check the expression of activation markers on T cells, cells were collected from the previous experiment on days 1, 3 and 6 and were labelled with CD3, CD4, and CD8 to stablish T cell populations and with CD69 and HLA-DR to study early and late activation, respectively. To assess the expression of activation markers on B cells, cells were labelled with CD45, CD19 and CD27 markers to stablish B cell populations and with CD25 to study activation.

Results obtained from the analysis of the expression of T and B cell population and maturation markers by flow cytometry showed no significant differences among the treatments at any studied time points (Figures 41, 42, 43 and 44). The only significant increase was observed in CD69 and C25 activation markers of T and B cells, respectively, between the unstimulated control and the PHA activation control. These measurements did not correspond with the level of proliferation and activation observed on microscopic images of the same conditions, which could be explained because the level of expression needed to be detected by flow cytometry is higher than the obtained from the treatments, as in the case of the PHA activation control.

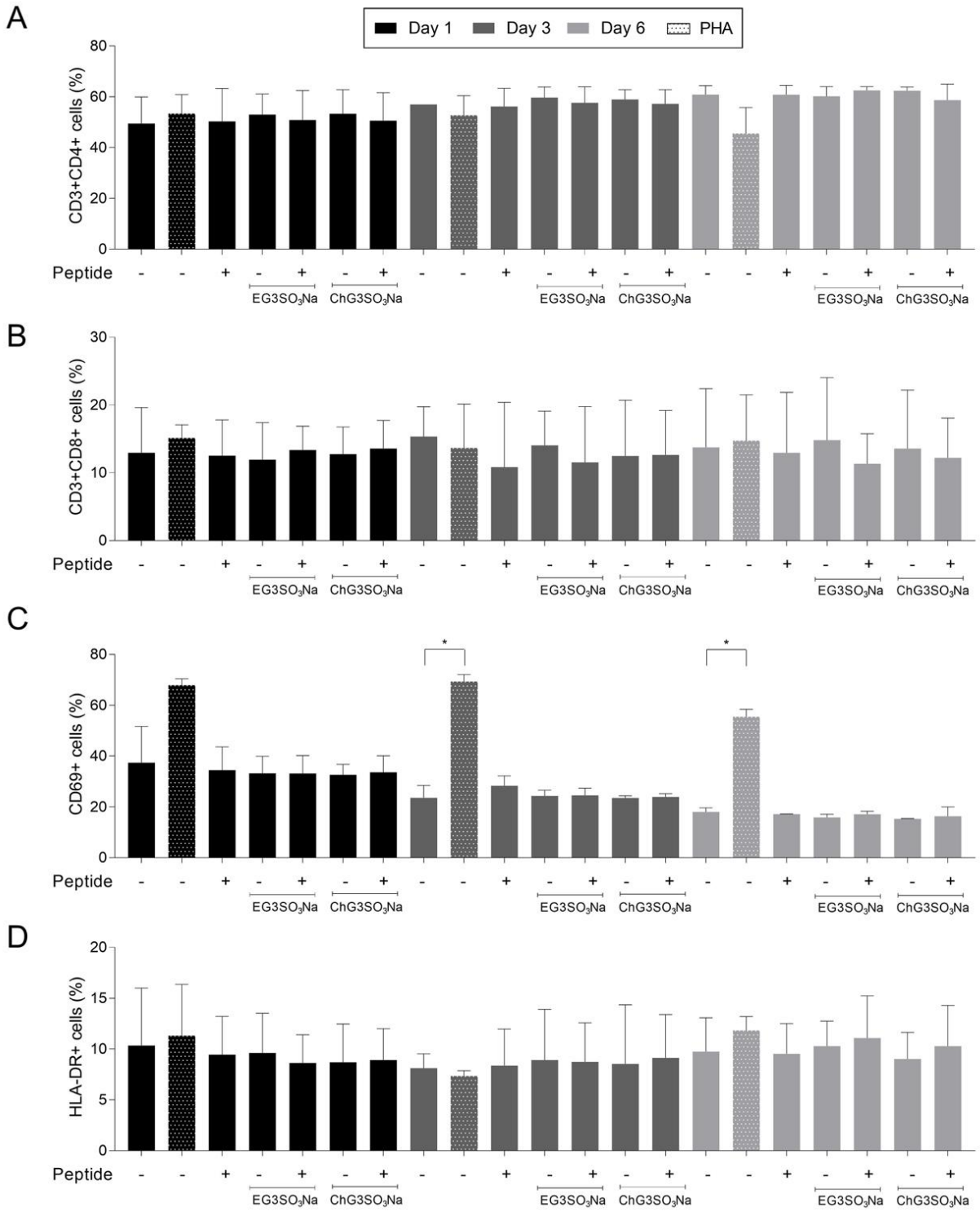

Figure 41: Analysis of T cell surface maturation markers after 1, 3 and 6 days of co-culture of mDCs transfected with Pep-Rev peptide. Flow cytometry measurements of cell population markers (A) CD3CD4 and (B) CD3CD8 and (C) CD69, and (D) HLA-DR early and late activation markers. PHA: phytohaemagglutinin. * $p < 0,05$.

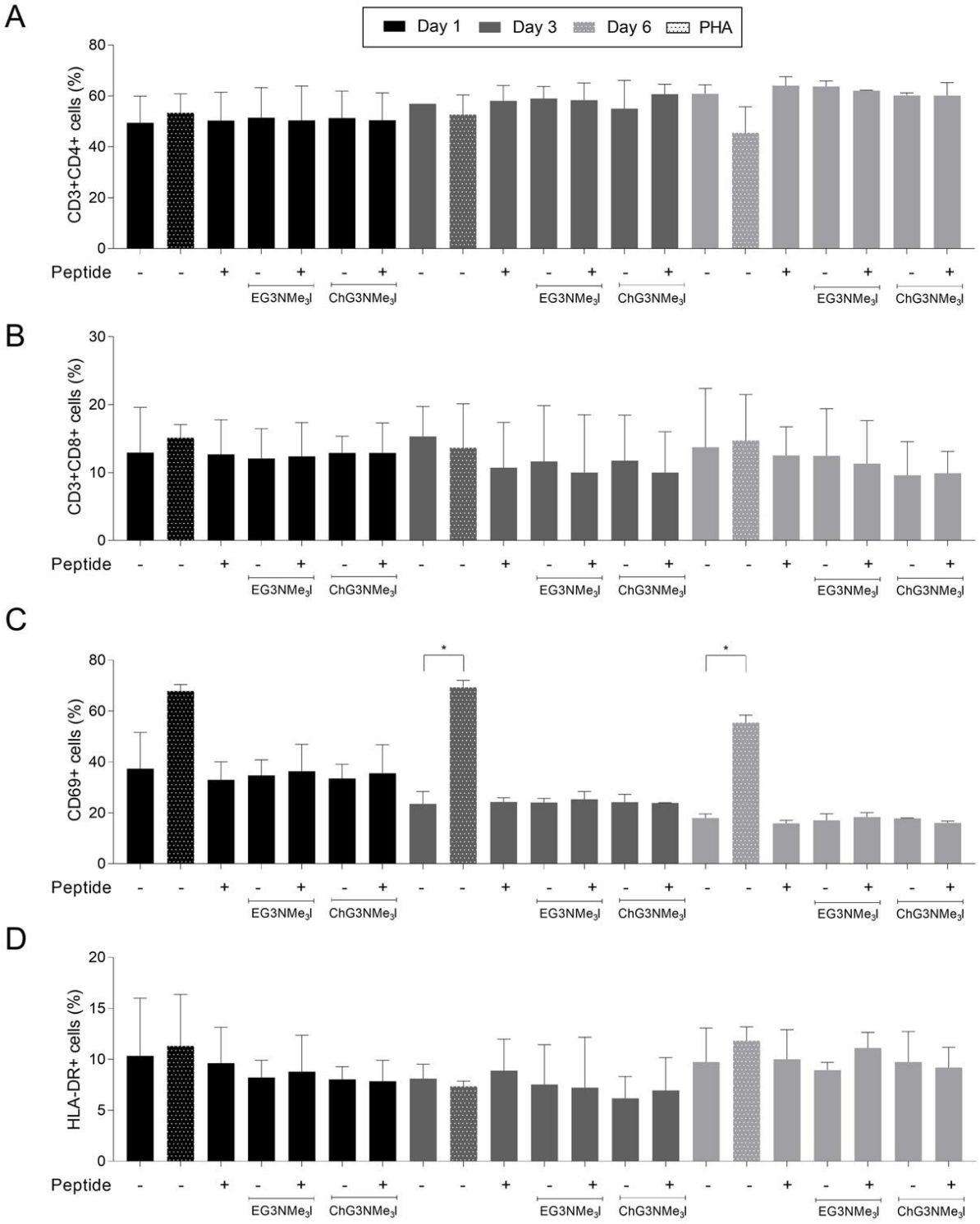

Figure 42: Analysis of T cell surface maturation markers after 1, 3 and 6 days of co-culture of mDCs transfected with Pep-GagPol-3 peptide. Flow cytometry measurements of cell population markers **(A)** CD3CD4 and **(B)** CD3CD8 and **(C)** CD69, and **(D)** HLA-DR early and late activation markers. **PHA:** phytohaemagglutinin. * $p < 0,05$.

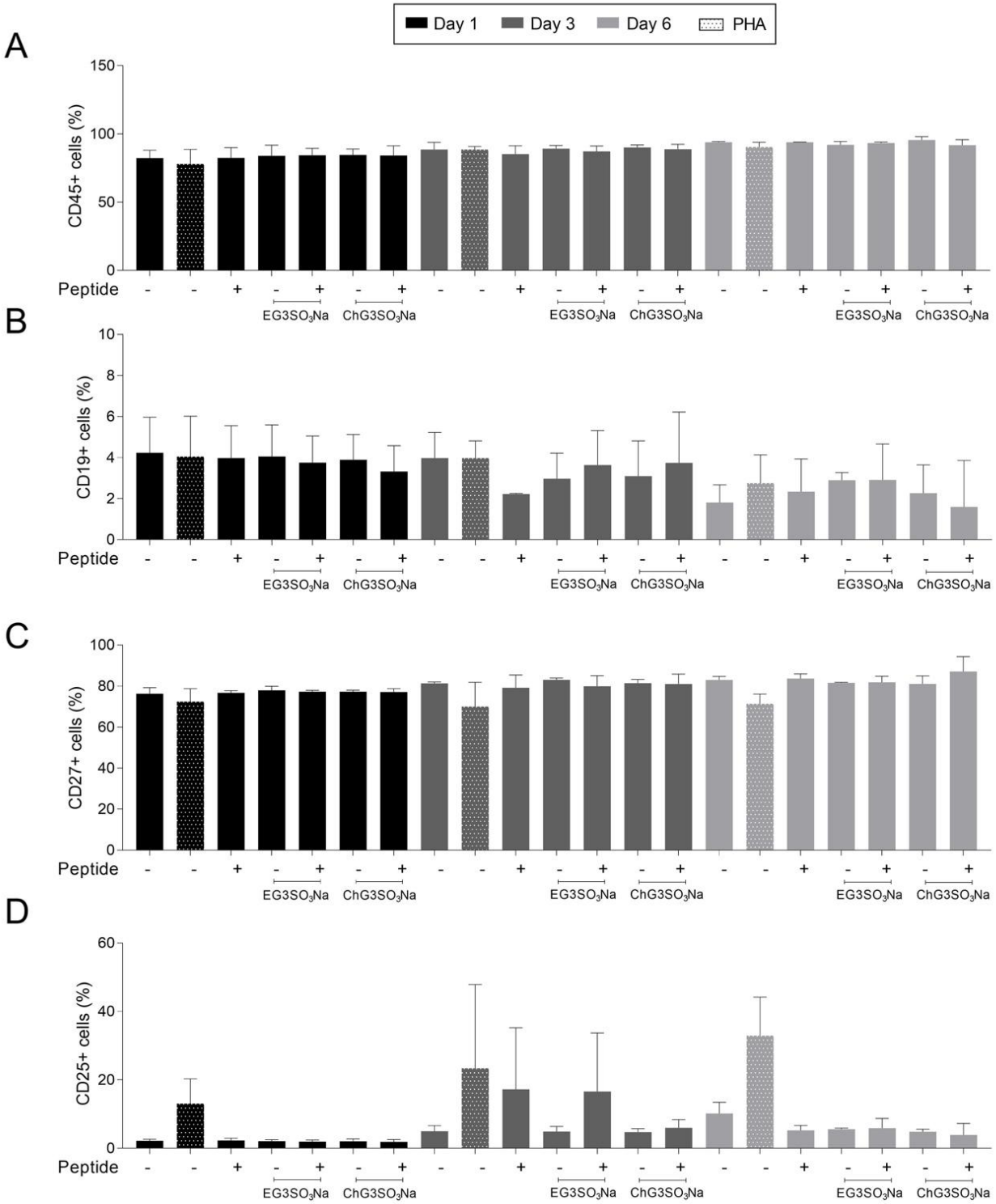

Figure 43: Analysis of B cell surface maturation markers after 1, 3 and 6 days of co-culture of mDCs transfected with Pep-Rev peptide. Flow cytometry measurements of cell population markers **(A)** CD45, **(B)** CD19 and **(C)** CD27, and **(D)** CD25 maturation markers. **PHA:** phytohaemagglutinin.

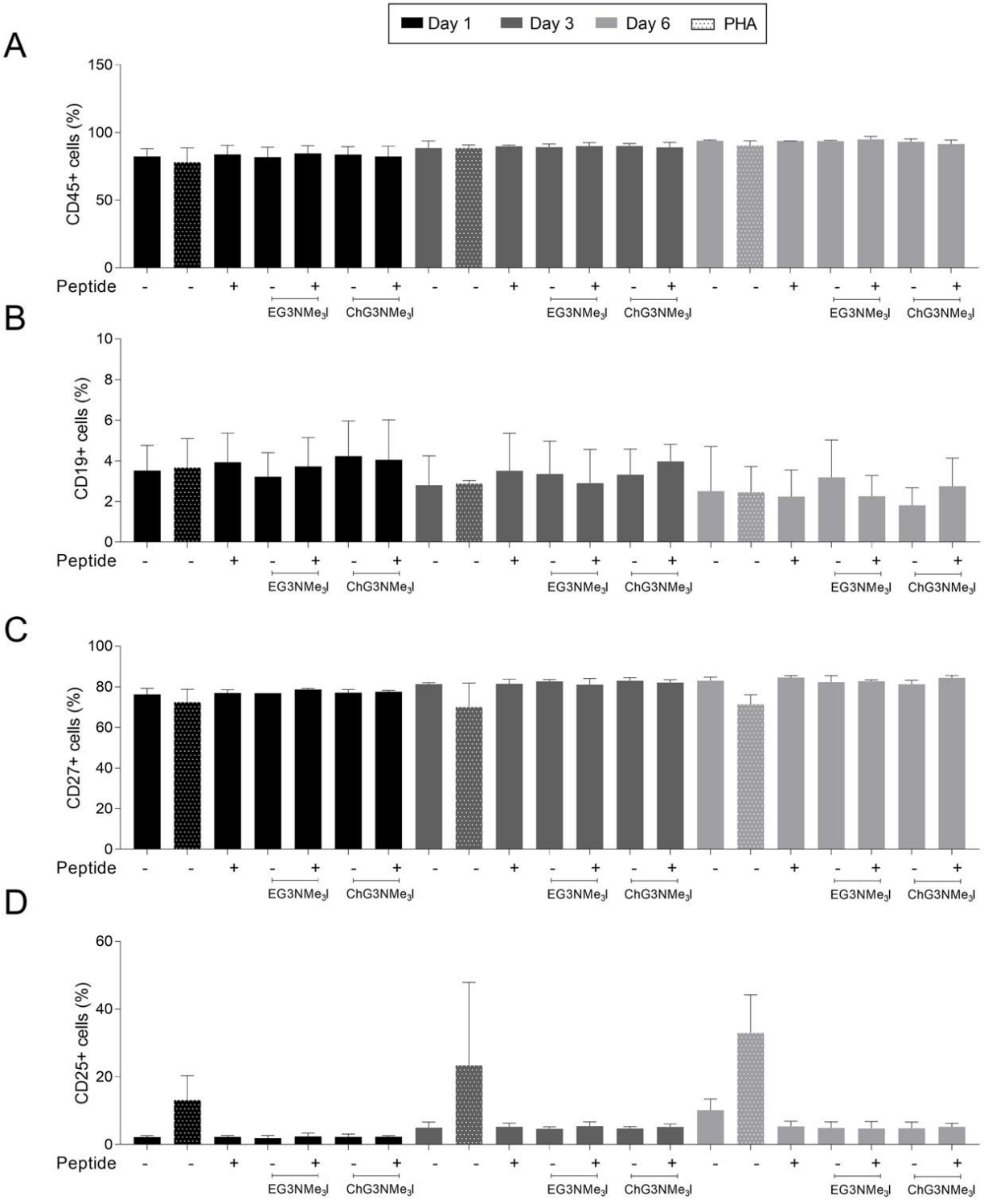

Figure 44: Analysis of B cell surface maturation markers after 1, 3 and 6 days of co-culture of mDCs transfected with Pep-GagPol-3 peptide. Flow cytometry measurements of cell population markers **(A)** CD45, **(B)** CD19 and **(C)** CD27, and **(D)** CD25 maturation markers. **PHA:** phytohaemagglutinin.

6.3.5.2 Release of inflammatory cytokines

The last step to determine the immune response produced after MLR consisted of studying the release of inflammatory cytokines. To do so, supernatants were collected from the previous experiment on days 1, 3 and 6 and a panel of pro-inflammatory and anti-inflammatory cytokines/chemokines (IL-1β, INF-α2, IFN-γ, TNF-α, IL-10, IL-12p70, IL-18 and IL-23) was quantified by flow cytometry.

Results from this study revealed a moderate increase of the amount of IL-1β regarding the unstimulated control after 1 day in all studied treatments with Pep-Rev and Pep-GagPol-3 peptides, the different dendrimicelles or complexes. This increase was lower after 3 and even lower after 6 days, when the complexes formed with $EG3SO_3Na$, $ChG3SO_3Na$, $EG3NMe_3I$ and $ChG3NMe_3I$ did not show a significant increase (Figure 45A and 46A).

On the other hand, a moderate increase of IFN-γ release after 1 day was only observed in Pep-Rev and Pep-GagPol-3 peptides, $EG3SO_3Na$ and $ChG3SO_3Na$ dendrimicelles, and the complex formed with $EG3SO_3Na$ and $EG3NMe_3I$ dendrimicelles. After 3 and 6 days, only $EG3SO_3Na$ and the complex formed with this dendrimicelle were significantly higher regarding the control (Figure 45B and 46B).

Regarding TNF-α, results from day 1 showed a moderate increase in all treatments except for the complex formed with Pep-Rev peptide and $EG3SO_3Na$ dendrimicelle (Figure 45C), whereas only Pep-GagPol-3 peptide and the complex formed with $EG3NMe_3I$ dendrimicelle showed a significant increase (Figure 46C). At day 3 the only significant increase was observed in the complex formed with $EG3SO_3Na$.

Lastly, the results of the release of IL-10 suggest a moderate increase in all the treatments tested (Figure 45D) but only in the treatment with Pep-GagPol-3 peptide and the complex formed with $EG3NMe_3I$ dendrimicelle (Figure 46D). On day 3, only Pep-Rev and $EG3SO_3Na$ dendrimicelle showed a significant increase. In all four mentioned cytokines, the observed increase was higher than the unstimulated control but much more lower than the PHA-stimulated control.

Regarding the measurement of the release of INF-α2, IL-12p70, IL-18 and IL-23 cytokines, no significant increase between any of the treatments studied with respect to the unstimulated control was noted, they were all found in similar amounts (data not shown). These results resemble the activation observed on microscopic images of the same conditions, where a slight activation of lymphocytes was observed. However, quantification in treatments was much lower than in the stimulated control, suggesting that the level of cytokines released to the media would not be detrimental.

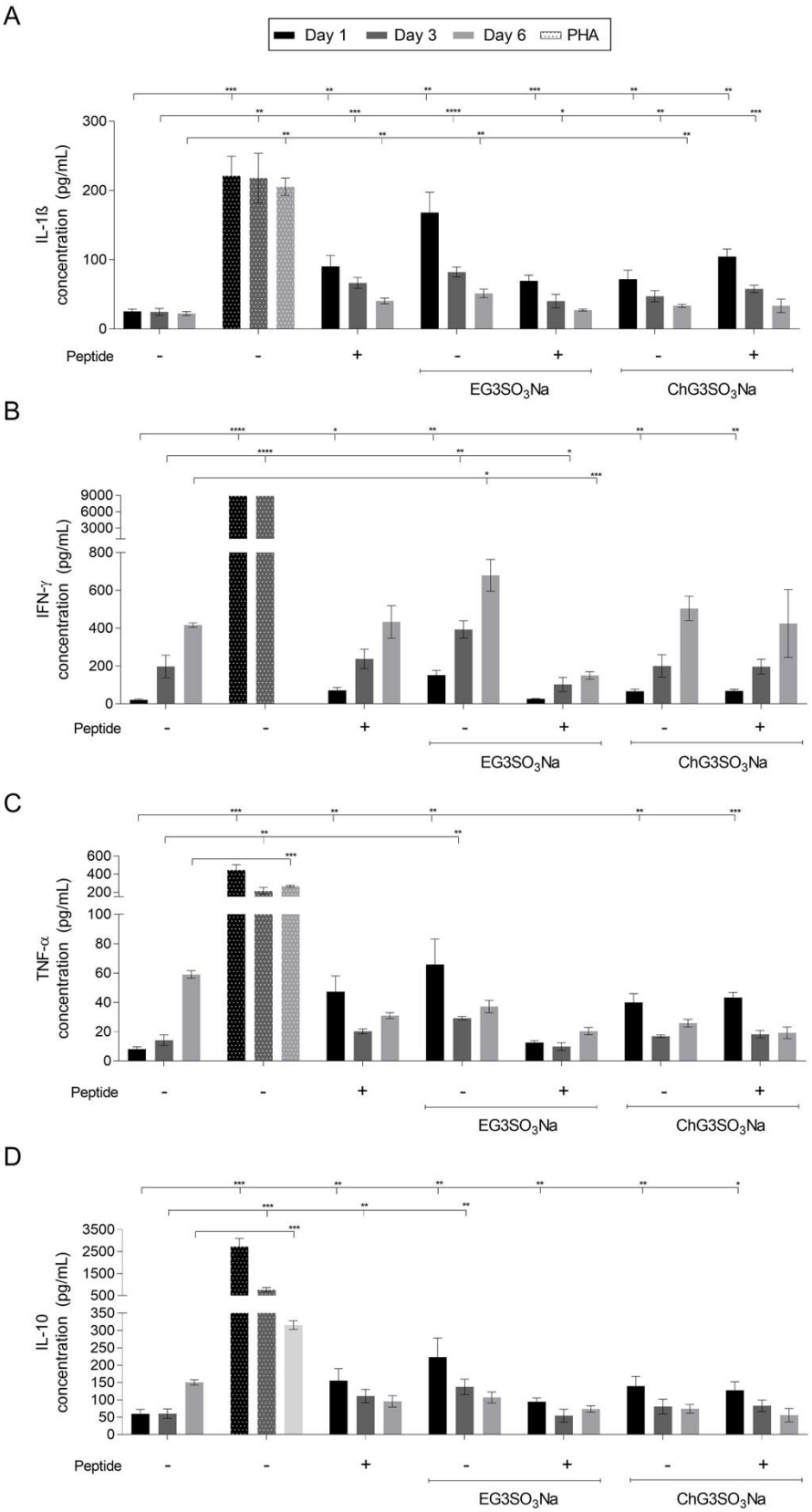

Figure 45: Release of cytokines/chemokines to the media after 1, 3 and 6 days of co-culture of mDCs transfected with Pep-Rev peptide. **(A)** IL-1β, **(B)** IFN-γ, **(C)** TNF-α, **(D)** IL-10. **PHA:** phytohaemagglutinin. * $p < 0,05$; ** $p < 0,01$, *** $p < 0,001$, **** $p < 0,0001$.

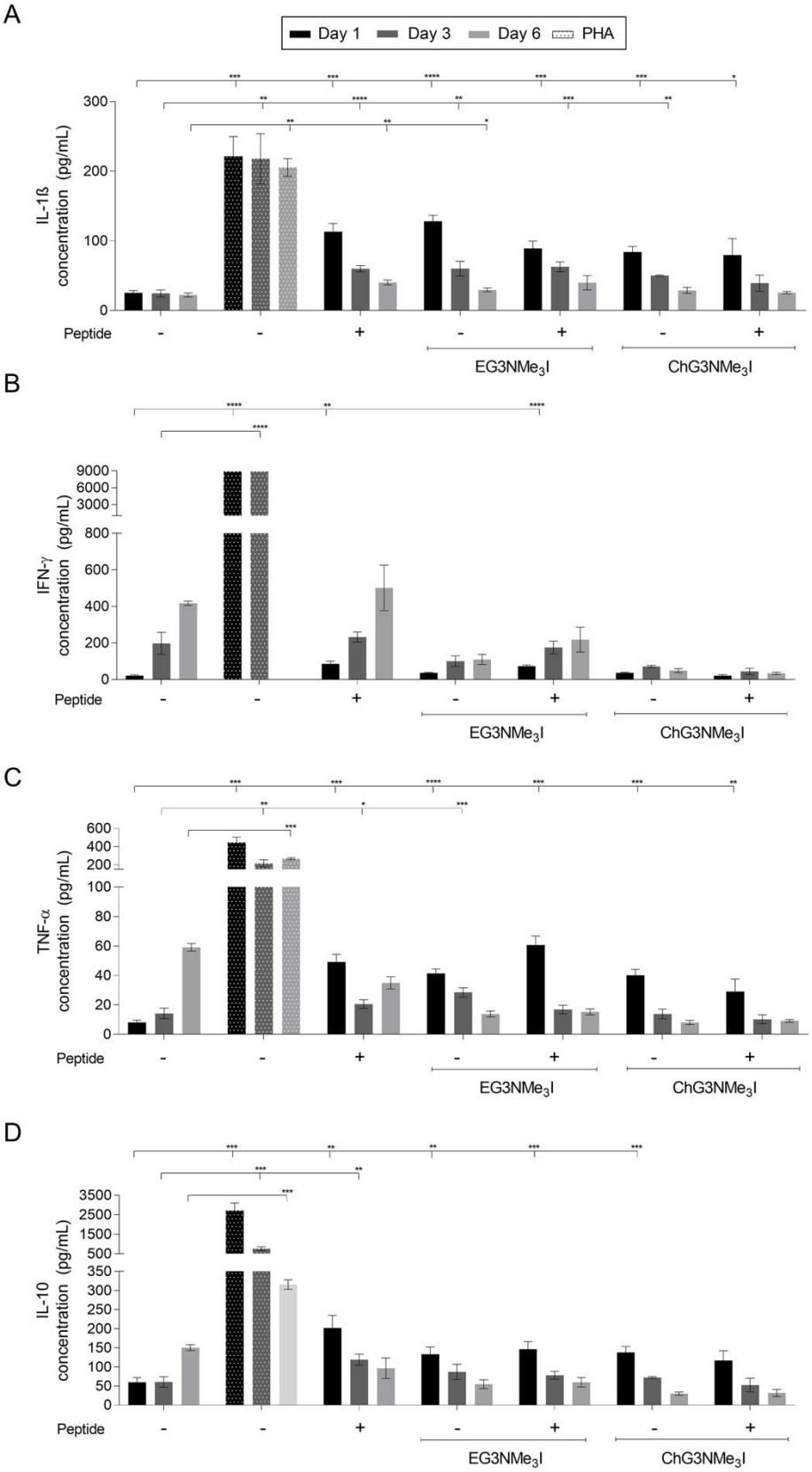

Figure 46: Release of cytokines/chemokines to the media after 1, 3 and 6 days of co-culture of mDCs transfected with Pep-GagPol-3 peptide. **(A)** IL-1β, **(B)** IFN-γ, **(C)** TNF-α, **(D)** IL-10. **PHA:** phytohaemagglutinin. * $p < 0,05$; ** $p < 0,01$, *** $p < 0,001$, **** $p < 0,0001$.

DISCUSSION

7. DISCUSSION

7.1 DENDRIPLEXES AS DELIVERY VEHICLES OF ANTI-HIV-1 miRNAs

The introduction of cART, which suppresses the viral load to undetectable levels, thus controlling HIV-1 infection, has achieved a reduction in HIV-1 mortality and morbidity (Laskey and Siliciano, 2014, Saylor et al., 2016). However, there are two main drawbacks that current treatments are unable to overcome: (i) the appearance of resistant strains and (ii) the existence of viral reservoirs susceptible to reactivation (Clutter et al., 2016, Taylor and Hammer, 2008). Additionally, there is no curative therapy which involves other problems, such as the toxicity of lifelong treatments and the failure to adhere to treatments.

Together, these problems illustrate the urgent need to develop new therapeutic approaches to deal with HIV-1 infection. A powerful approach is the use of small RNAs which, through binding to cellular mRNAs, cause their silencing or degradation (Bajan and Hutvagner, 2020). Various cellular miRNAs have shown the ability to interfere with the HIV-1 genome, affecting viral replication (Swaminathan et al., 2012, Ruelas et al., 2015, Wang et al., 2015, Adoro et al., 2015). Nevertheless, their naked delivery to target cells is a limiting factor for their application, what implies the need to encapsulate them into useful delivery vehicles (Whitehead et al., 2009).

Nanotechnology is a valid strategy to address this problem, as it has previously been demonstrated to efficiently deliver miRNAs (Dahlman et al., 2014, Ratajczak et al., 2018). Our group has carried out wide research about this topic, specially related to the use of dendrimers in the context of delivery of small RNA molecules HIV-1 infection (Sepulveda-Crespo et al., 2015b, Rodriguez-Izquierdo et al., 2019, Perise-Barrios et al., 2014, Guerrero-Beltran et al., 2018). Dendrimers are three-dimensional nanostructures which are characterised by their multiple branches with modifiable edges. When functionalised with positively charged molecules, dendrimers can form, through electrostatic interactions, complexes with the negatively charged backbone of nucleic acids. In this work, the potential application of novel PCCDs as delivery vehicles for miRNAs with anti-HIV-1 activity was studied to control HIV-1 progression in PBMCs and U87MG-CD4^{+}CCR5^{+} cells.

Determining the biocompatibility of G2-SN15-PEG and G3-SN31-PEG dendrimers and their FITC-labelled forms was the initial phase of this study. It has been proven that cationic dendrimers interact with the extracellular membrane of cells, which is negatively charged, causing nanoscale pores on the cell surface that affect its integrity. The extent of the damage produced depends on features of dendrimers such as the presence of fluorescent markers or the molecular size and composition (Jain et al., 2010). For this, PCCDs were conjugated with PEG residues to improve their biocompatibility, solubility, biodistribution, and drug loading and delivery (Pedziwiatr-Werbicka et al., 2019, Suk et al., 2016). Cell viability assays, performed by the MTT assay, confirmed that G2-SN15-PEG dendrimer had the lowest toxicity rates, followed by G3-SN31-PEG, G2-SN15-PEG FITC and G3-SN31-PEG FITC dendrimers. These results are in agreement with previous works, confirming that larger molecules and the introduction of fluorescent marks increase cytotoxicity. It was also important to ensure that dendrimers do not affect the genome of cells by producing

genetic modifications; this was proved in PBMCs by the SCE assay. Finally, the assessment of the haemolytic potential confirmed that that exposure to these dendrimers does not produce erythrocyte haemolysis at maximum working concentrations.

Molecule size and composition, together with the chemical composition of cell membranes, determine the effectiveness with which dendrimers interact with the cell surface: higher amounts of positive charges lead to stronger interactions, entailing longer resident times on the membrane and, thus, slower internalisation (Albertazzi et al., 2010, Heyder et al., 2017, Salatin et al., 2015). Results from internalisation studies by confocal microscopy and flow cytometry reflected this fact since G2-SN15-PEG FITC dendrimer showed faster internalisation dynamics compared to G3-SN15-PEG FITC dendrimer in PBMCs and U87MG-$CD4^+CCR5^+$ cells, probably because G3-SN15-PEG FITC dendrimer, being a bigger molecule, presents more positive charges in the periphery thus it interacts with higher affinity with the cell surface. Nevertheless, both dendrimers are able to enter PBMCs and U87MG-$CD4^+CCR5^+$ cell line in a short period of time, confirming that they can be used as delivery vehicles.

The next step was to determine whether G2-SN15-PEG and G3-SN31-PEG dendrimers were able to form complexes with different miRNAs. As mentioned previously, the formation of dendriplexes occurs through electrostatic interactions between the negatively charged backbone of nucleic acids and the positively charged functional groups at the edges of dendrimers (Liu et al., 2012). Agarose gel electrophoresis confirmed dendriplexes formation with miRNAs and PCCDs at the maximum non-toxic concentrations after 2 h of incubation. The RNase protection assay showed that, after incubation with RNases, miRNAs could be completely recovered, demonstrating that dendriplexes protect miRNAs from this type of degradation. In addition, when dealing with a binding site competitor, such as heparin, dendriplexes were completely dissociated, proving that miRNAs would be released from the complex upon internalisation into the host cell, thus enabling further binding with the target mRNA.

Measurement of ZP and DLS allowed to determine particles surface charge and size distribution, to study how the addition of miRNAs affects intrinsic properties of PCCDs. Measurements indicated that G2-SN15-PEG and G3-SN31-PEG dendrimers are stable and their surface charges are positive in solution. In addition, they showed a decrease in the ZP value in G3-SN31-PEG dendrimer compared to G2-SN15-PEG dendrimer. This result can be explained by a more effective wrapping of the PEG moiety, which has been shown to reduce charge density (Somani et al., 2018). Measurements of dendriplexes confirmed a change in ZP values of the complexes compared to those of dendrimers, indicating the formation of dendrimer-miRNA complexes. PSD measurements showed that, while G3-SN31-PEG dendrimer can be described as a single molecule, G2-SN15-PEG dendrimer forms aggregates, probably due to a reorganisation over time resulting from interactions among different molecules when being in solution. As expected, the dendriplex formed with G3-SN31-PEG dendrimer presented a hydrodynamic size superior to the individual dendrimer. However, the dendriplex formed with G2-SN15-PEG dendrimer presented lower aggregation values, which could be explained because the introduction of miRNA leads to a more favourable electrostatic binding which

contributes to the formation of more stable systems in solution. Taken together, all these results confirm that G2-SN15-PEG and G3-SN31-PEG dendrimers can form stable and protective complexes with miRNAs.

The next step was to determine whether these complexes improved the anti-HIV-1 activity of naked miRNAs. Results from R5-HIV-1 inhibition experiments showed that both dendrimers can significantly inhibit HIV-1 infection in PBMCs and U87MG-CD4^{+}CCR5^{+} cell lines. However, this inhibition was only significantly improved by dendriplexes when PBMCs were treated, suggesting a specific behaviour that was dependent on the cell lineage. As expected, the selected miRNAs were unable to inhibit infection by themselves, confirming that they need to be complexed with dendrimers to carry out their activity.

Results from this work confirm that G2-SN15-PEG and G3-SN31-PEG PEGylated cationic dendrimers can be used as delivery vehicles of miRNAs to improve their anti-HIV-1 activity in specific cell lines. These findings suggest that this technology could replace current methods with a new and safer method with possible *in vivo* perspectives.

7.2 PEGylated CATIONIC CARBOSILANE DENDRIMERS AGAINST HSV-2 AND HCMV INFECTION

Infections caused by viruses belonging to the *Herpesviridae* family are a major global cause of acute diseases and morbidity, with serious physiological and psychological sequela for millions of men, women, and infants. These infections have been studied for years, paying special attention to the entry mechanism into host cells. Research has led to the conclusion that, despite the extensive cell tropism they exhibit, host cell infection occurs through a conserved mechanism (Sathiyamoorthy et al., 2017). This mechanism is based on the entry machinery, which is formed by a conserved set (composed of the heterodimer gH-gL and the fusion protein gB) and by divergent proteins such as gD for HSV-2 or gO for HCMV (Agelidis and Shukla, 2015, Nishimura and Mori, 2019). These proteins are key players in the first step of infection, acting as ligands that bind to different host cell receptors, highlighting different classes of HSPGs located on the exterior surface of target cells (Koganti et al., 2021). For this reason, HSPGs are a therapeutic target for the development of innovative inhibitors of HS-mediated binding to prevent the subsequent infection of herpesviruses.

The objective of this work was to evaluate the ability of PCCDs to prevent HSV-2 and HCMV infections, based on the characteristics of their structure. The presence of two main features at the periphery makes them relevant candidates: (i) PEGylated residues, which improve their biocompatibility, and (ii) positively charged functional groups, which compete for electrostatic binding with viral glycoproteins (Dogra et al., 2015, Suk et al., 2016).

Initial studies of this work focused on evaluating the cytotoxicity of G2-SN15-PEG, G3-SN31-PEG and their FITC-labelled forms in Vero and MRC-5 cell lines. As explained in the previous work, the positively charged groups in the periphery of dendrimers, which interact with the negatively charged cell surface, produce minuscule pores that affect cell membrane integrity to an extent that depends on different characteristics of the dendrimers, such as their molecular weight or the presence of fluorescent labels (Mignani et al., 2019). Previous work has demonstrated that masking these positively charged groups in the periphery by conjugation with PEG residues reduces immunogenicity and toxicity, therefore, these PCCDs were coupled

with PEG (Thakur et al., 2015). The results of the MTT and LDH assays indicated that certain concentrations had negative effects on mitochondrial activity despite not affecting membrane integrity; therefore, to ensure complete biocompatibility, the values selected as working concentrations were those that exhibited cell viability above 80% in the MTT assay. This assay revealed that G2-SN15-PEG, G3-SN31-PEG, and G2-SN15-PEG FITC dendrimers have similar viability profiles, while G3-SN31-PEG FITC presents greater toxicity, in accordance with previous affirmations that larger molecular sizes and the addition of these fluorescent labels enhances the dendrimers cytotoxicity.

The next step was to examine if FITC-labelled dendrimers were able to internalise into both cell lines at maximum working concentrations. As described in previous works, size and surface charge of dendrimers influence their effectiveness of crossing cell membranes (Heyder et al., 2017, Salatin et al., 2015). This fact was also observed in flow cytometry and confocal microscopy internalisation studies into Vero and MRC-5 cell lines: G2-SN15-PEG FITC dendrimer has faster uptake dynamics than G3-SN31-PEG FITC dendrimer. Therefore, being a larger molecule, G3-SN31-PEG FITC dendrimer presents more positive charges that lead to higher affinity and stronger interaction with the target cell surface, leading to longer resident times on its membrane, resulting in slower internalisation. Furthermore, the study of fluorescent traces showed an increase of the uptake of both dendrimers and a change in their distribution along the studied time points: short periods of incubation resulted in peripheral distribution, while longer times showed them to be in more internal regions, in a granular manner.

After confirming that G2-SN15-PEG FITC and G3-SN31-PEG FITC dendrimers are biocompatible and internalise in short periods of time into Vero and MRC-5 cell lines, it was crucial to study their ability to inhibit HSV-2 and HCMV infections. Antiviral activity studies proved that both dendrimers achieved higher inhibition values than Acyclovir and Ganciclovir, actual reference treatments for these infections. Furthermore, the mechanism through which inhibition is achieved was studied. The results demonstrated that both dendrimers act in the initial stages of infection by inhibiting viral attachment to Vero and MRC-5 cell lines. Regarding their virucidal activity, G2-SN15-PEG and G3-SN31-PEG dendrimers can only inactivate HCMV infection with low inhibition values but not HSV-2 infection, suggesting low and null virucidal activity. The fact that G3-SN31-PEG dendrimer, which presented longer resident times on the cell surface, has better inhibition outcomes supports the idea that this is achieved through impediment of viral binding to cell membrane, thereby preventing infection.

The mechanism through which viral attachment is impeded was determined by studying the interactions of G2-SN15-PEG and G3-SN31-PEG dendrimers with HS chains of HSPGs, which are the receptors involved in the first stages of viral infection of the *Herpesviridae* family. The first study was a cell culture-based heparin competition assay, which is based on the fact that heparin is a GAG with a structure very similar to HS, thus being able to behave as an antagonist of the HSPGs present of cell surface for the biding of PCCDs (Meneghetti et al., 2015). The second study, 2 M NaCl wash, was performed to force the disruption of the bound of cationic molecules with HSPGs (Donalisio et al., 2016). The third study, heparinase II treatment, was performed to enzymatically digest the GAG moiety of HSPGs, thus inhibiting HSPG-dependent binding

(Alekseeva et al., 2019). Quantification of the remaining amounts of cell-associated dendrimers after performing these assays confirmed a disruption of the interaction of G2-SN15-PEG and G3-SN31-PEG dendrimers with Vero and MRC-5 cell membranes. The last study, a cell-free SPR analysis, confirmed that these PCCDs are able to effectively, stably and specifically bind to surface immobilised heparin. However, residual amounts of cell-associated dendrimers suggest the existence of alternative binding sites.

Results obtained from this research confirmed that G2-SN15-PEG and G3-SN31-PEG dendrimers are effective inhibitors of the interaction between certain viral glycoproteins of HSV-2 and HCMV and HSPGs at the cell surface, which prevents further infection, proving that these PCCDs are valid candidates as antiviral agents against these *Herpesviridae* infections.

7.3 DESIGN OF A DENDRITIC CELL-BASED THERAPEUTIC VACCINE AGAINST HIV-1 INFECTION

Combined ART has proven to be highly effective to decrease morbidity and mortality of HIV-1 patients by increasing $CD4^+$T-cell count, thus preventing clinical progression. However, this therapy is not curative as it does not eradicate the infection and the incomplete control of viral replication in some patients limits de recovery of $CD4^+$T-cells (Battegay et al., 2006). For these reasons, treatment must be maintained throughout life, resulting in consequences such as appearance of resistances, adverse effects, high costs, and lack of adherence to therapy. Therefore, new therapeutic strategies must be developed to effectively control the epidemic.

In this sense, a functional cure that could reduce the burden of the disease associated with infection, improve the quality of life of patients, reach a greater number of patients, and reduce the costs of lifelong treatments would be a promising option. One of the best examples of these cures are therapeutic vaccines, which focus on inducing a strong and durable cellular response by increasing the magnitude of T-cell immunity, thus improving control of viral replication to the point of discontinuing lifelong treatments (Rinaldo, 2009). DC-based vaccines, designed to present and direct antigen-specific immune responses, are becoming promising strategies to target different diseases (Pizzurro and Barrio, 2015, Mody et al., 2015, Reardon and Mitchell, 2017, Griffiths et al., 2016). Regarding HIV-1 infection, these vaccines are designed to induce, with immunogens such as peptides, strong specific $CD4^+$T-cell responses to achieve an effective and sustained cytotoxic $CD8^+$T-cell response that would control HIV replication (Garcia et al., 2013).

There has been a great deal of research on the development of DC-therapeutic vaccination based on the use of HIV-1-derived peptides with more or less success (Coelho et al., 2016), but there are two main characteristics of these works that could be reviewed to improve their results, the design of immunogens and the adjuvants that could favour antigen presentation. Since peptides only represent a small proportion of the pathogen, they often do not trigger natural activation of the immune system. Different delivery systems, such as nanoparticles, have been used to improve peptide delivery and act as adjuvant stimulators to enhance antigenic presentation and enhance immune activation, thus improving vaccine efficiency and prolonging its half-life (Vacas-Cordoba et al., 2014a, Vacas-Cordoba et al., 2014b, Yang et al., 2019).

The aim of this work was to determine if different micellar carbosilane dendrons could be used in the development of an effective DC-based therapeutic vaccine when associated with HIV-1-derived peptides. The first step of this research consisted in the evaluation of the cytotoxicity of $EG3SO_3Na$, $ChG3SO_3Na$, $EG3NMe_3I$, and $ChG3NMe_3I$ dendrimicelles, HIV-1 derived peptides, and dendrimicelles-peptide dendriplexes. Results from the MTT assay performed on moDCs from healthy patients showed that cationic $EG3NMe_3I$ and $ChG3NMe_3I$ dendrimicelles were less toxic for the mitochondrial activity than anionic $EG3SO_3Na$ and $ChG3SO_3Na$ dendrimicelles. Furthermore, results indicated that cationic Pep-Rev, Pep-Vif and Pep-GagPol-1 peptides and anionic Pep-GagPol-2, Pep-GagPol-3 and Pep-Env peptides are viable at the desired working concentration (1 μM). Furthermore, the dendriplexes formed with both molecules also presented viability rates greater than 80% after 6 days of treatment, confirming that all three treatments could be used without affecting the integrity of the mitochondrial activity of moDCs.

The next challenge consisted of achieving the formation of dendrimicelles-peptide dendriplexes. $EG3SO_3Na$, $ChG3SO_3Na$, $EG3NMe_3I$ and $ChG3NMe_3I$ dendrimicelles have been rationally designed to exhibit cholesterol and d-α-tocopherol (vitamin E) at the focal point, as it has been widely demonstrated that these molecules allow the self-assembly of nanoparticles in micelles that can stably encapsulate different cargos such as nucleic acids or peptides (Lai et al., 2016, Wang et al., 2017, Zhang et al., 2019, Barnard et al., 2011, Ou et al., 2019). To determine whether they were able to encapsulate chosen peptides, 6% agarose gel electrophoresis was performed for anionic Pep-GagPol-2-L, Pep-GagPol-3-L, and Pep-Env-L peptides. Unfortunately, the wavelength emitted by the transilluminator did not match the absorbance spectrum of the Cy5 fluorescent dye with which Pep-Rev, Pep-Vif, and Pep-GagPol-1 peptides were labelled, therefore determination of the formation of such complexes was made by measurement of ZP and DLS. After 2 h of incubation at 37 ºC, working concentrations of $EG3NMe_3I$ and $ChG3NMe_3I$ dendrimicelles formed complexes with Pep-GagPol-3 and Pep-Env peptides but were unable to encapsulate Pep-GagPol-2 peptide. In addition, $EG3SO_3Na$ and $ChG3SO_3Na$ dendrimicelles formed complexes with Pep-Rev and Pep-Vif peptides at working concentrations, but were unable to encapsulate Pep-GagPol-1 peptide.

The internalisation of the peptides into moDCs by these complexes was studied by confocal microscopy and flow cytometry. Both techniques suggested a similar internalisation pattern for the studied peptides: formation of complexes enhanced cellular uptake after 2 h of treatment, however after 24 h of treatment moDCs seem to have processed the peptide. These studies showed that complexation with $EG3SO_3Na$, $ChG3SO_3Na$, $EG3NMe_3I$ and $ChG3NMe_3I$ dendrimicelles improves the delivery of Pep-Rev-L, Pep-Vif-L and Pep-GagPol-3-L peptides, confirming that they are effective delivery vehicles for these molecules.

Upon internalisation of an antigen, DCs process and transfer it to the MHC, where it gets exposed (Nakayama, 2014). At the same time, DCs undergo maturation and migrate to lymphoid organs to present the antigen; in order to achieve optimal activation of T-cells, moDCs must mature properly (Reis e Sousa, 2006, Schuurhuis et al., 2006). This activation can be determined by an enhanced expression of different maturation surface markers such as CD80, CD83, CD86, or HLA-DR assessed by flow cytometry. The results of these measurements suggested changes in CD80 and CD86 expression in moDCs treated with $EG3SO_3Na$

dendrimicelles and complexes formed with the Pep-Rev peptide and $EG3SO_3Na$ or $ChG3SO_3Na$ dendrimicelles, respectively. For Pep-GagPol-3 transfected moDCs, expression changes were only detected for CD83 when treated with complexes formed with $EG3NMe_3I$ or $ChG3NMe_3I$ dendrimicelles. The increase in the expression of these markers suggests a slight promotion of moDCs maturation after 48 h of incubation with dendrimicelles-peptide complexes.

The fact that proper maturation of DCs is key to activating T-cells made it necessary to further induce their maturation with LPS before proceeding to the stimulation of specific lymphocyte responses with peptide-pulsed DCs in an autologous MLR (Hu et al., 2009). This reaction was used to test if peptide-transfected moDCs were efficient in presenting this antigen to PBMCs from the same patient and stimulate the specific immune response of T and B cells. Bright-field microscopy images showed changes in aggregation and clumping of PBMCs after 3 and 6 days of co-culture, these changes depended on the treatment, but, in general, treatment with complexes led to greater clumping of PBMCs confirming that co-culture of peptide-transfected mDCs with autologous PBMCs produces an observable slight activation of lymphocytes. Unfortunately, analysis of the expression of T and B cell population and maturation markers by flow cytometry showed no significant differences among treatments at any studied time points. Expression of these markers was only increased in the PHA activation control, suggesting that the expression level that needs to be detected by this method must be higher than the obtained with the treatments, explaining the mismatch between the results of this assay and the microscopy images.

To deepen lymphocyte activation, the release of cytokines into the extracellular environment during MLR was analysed. Results indicated that release of IL-1β, TNF-α and IFN-γ was increased in almost all treatments after 1 day. These pro-inflammatory cytokines are essential for resistance to infections, as they are involved in stimulation of DC maturation, processing and migration and stimulation of phagocytic cells, oxidative bursts, and degradative enzymes against pathogens (Garcia et al., 2013, Roff et al., 2014). Furthermore, IL-10 release was also higher in almost all treatments after 1 day; this immunosuppressive cytokine plays a critical protective role in infectious diseases, as it suppresses the production of certain pro-inflammatory cytokines (Mosser and Zhang, 2008, Mittal et al., 2015). Release of these four cytokines was much lower than in the stimulated control and was reduced after 3 and, even more, 6 days, which is optimal since their long-term production can lead to detrimental effects such as inflammation, autoimmune disease and increase of viral replication and viral disease progression (Dinarello, 2000, Lopez-Castejon and Brough, 2011, Kumar et al., 2016, Brockman et al., 2009). These results are in accordance with the activation observed in microscopic images of the MLR: a moderate but not excessive increase of the release of pro- and anti-inflammatory cytokines, suggesting a slight activation of lymphocytes after being co-cultured with autologous peptide-pulsed DCs.

Results obtained from this investigation confirmed that $EG3SO_3Na$, $ChG3SO_3Na$, $EG3NMe_3I$ and $ChG3NMe_3I$ dendrimicelles are capable of transfecting HIV-1-derived peptides into DCs to induce their maturation and presentation of these antigens to autologous lymphocytes. This presentation induces an effective HIV-1-specific immune response observed in lymphocyte activation and cytokine production, demonstrating their

possible application in the development of a DC-based therapeutic vaccine. Further experiments with periodic peptide-pulsing and with samples from HIV-1 patients should be performed to confirm this.

CONCLUSIONS

8. CONCLUSIONS

8.1 CONCLUSIONS

i. PEGylated cationic carbosilane G2-SN15-PEG and G3-SN31-PEG dendrimers can effectively form dendrimer-miRNA complexes with miRNAs with anti-HIV-1 activity at maximum non-toxic concentrations.

ii. At these concentrations, G2-SN15-PEG and G3-SN31-PEG dendrimers do not produce cytotoxicity, genotoxicity, or erythrocyte haemolysis.

iii. Dendriplexes formation prevents the degradation of miRNAs by RNases and enables their delivery to different cell types in a short period of time.

iv. Upon release, these dendriplexes specifically and significantly improve the anti-R5-HIV-1 activity of miRNAs, which induces genetic silencing of HIV-1 mRNA thus impeding the generation of new virions, in HIV-1 infected PBMCs.

v. G2-SN15-PEG and G3-SN31-PEG dendrimers effectively compete with HSV-2 and HCMV for adsorption on the receptors involved in the first stages of infection of target cells.

vi. This competition leads to an impediment of viral attachment to susceptible cells, which produces inhibition of HSV-2 and HCMV viral infections.

vii. Anionic and cationic carbosilane micellar EG3SO_3Na, ChG3SO_3Na, EG3NMe3I and ChG3NMe_3I dendrons can effectively form dendrimicelles-peptide complexes at working concentrations.

viii. The formation of these dendriplexes improves HIV-1-derived peptide delivery to moDCs in a brief period of time. Upon uptake, moDCs recognise these dendriplexes as antigens, which slightly promotes their maturation.

ix. Co-culture of transfected and matured moDCs with autologous PBMCs induces slight activation of lymphocytes.

8.2 CONCLUSIONES

1. Los dendrímeros catiónicos carbosilanos PEGilados G2-SN15-PEG y G3-SN31-PEG forman eficientemente complejos dendrímero-miARN con miARNs con actividad anti-VIH-1 a las concentraciones máximas no tóxicas.

2. A estas concentraciones, los dendrímeros G2-SN15-PEG y G3-SN31-PEG no producen citotoxicidad, genotoxicidad ni hemólisis de eritrocitos.

3. La formación de dendriplejos previene la degradación de los miRNAs por parte de las RNasas y permite su internalización en diferentes tipos celulares en un corto periodo de tiempo.

4. Tras su liberación, estos dendriplejos mejoran específica y significativamente la actividad anti-R5-VIH de los miARNs, la cual induce el silenciamiento genético del ARNm del VIH-1 impidiendo así la generación de nuevos viriones, en CMSPs infectadas con VIH-1.

5. Los dendrímeros G2-SN15-PEG y G3-SN31-PEG compiten eficazmente con el VHS-2 y el CMVH por la adsorción en los receptores implicados en las primeras etapas de infección de las células diana.

6. Esta competición conduce al impedimento de la unión viral a las células susceptibles, produciendo así la inhibición de las infecciones virales por el VHS-2 y el CMVH.

7. Los dendrones micelares aniónicos y catiónicos de carbosilano EG3SO_3Na, ChG3SO_3Na, EG3NMe_3I y ChG3NMe_3I forman eficazmente complejos dendrimicelas-péptidos a las concentraciones de trabajo máximas.

8. La formación de estos dendriplejos mejora la internalización de péptidos derivados del VIH-1 a las CDmo en un breve período de tiempo. Tras la internalización, las CDmo reconocen estos dendriplejos como antígenos, lo que ligeramente promueve su maduración.

9. El cultivo conjunto de CDmo transfectadas y maduradas con PBMC autólogas induce una ligera activación de los linfocitos.

REFERENCES

9. LIST OF REFERENCES

ABBASI, E., AVAL, S. F., AKBARZADEH, A., MILANI, M., NASRABADI, H. T., JOO, S. W., HANIFEHPOUR, Y., NEJATI-KOSHKI, K. & PASHAEI-ASL, R. 2014. Dendrimers: synthesis, applications, and properties. *Nanoscale Res Lett,* 9**,** 247.

ADAMSON, C. S. & FREED, E. O. 2007. Human immunodeficiency virus type 1 assembly, release, and maturation. *Adv Pharmacol,* 55**,** 347-87.

ADORO, S., CUBILLOS-RUIZ, J. R., CHEN, X., DERUAZ, M., VRBANAC, V. D., SONG, M., PARK, S., MUROOKA, T. T., DUDEK, T. E., LUSTER, A. D., TAGER, A. M., STREECK, H., BOWMAN, B., WALKER, B. D., KWON, D. S., LAZAREVIC, V. & GLIMCHER, L. H. 2015. IL-21 induces antiviral microRNA-29 in CD4 T cells to limit HIV-1 infection. *Nat Commun,* 6**,** 7562.

AGELIDIS, A. M. & SHUKLA, D. 2015. Cell entry mechanisms of HSV: what we have learned in recent years. *Future Virol,* 10**,** 1145-1154.

AHLUWALIA, J. K., KHAN, S. Z., SONI, K., RAWAT, P., GUPTA, A., HARIHARAN, M., SCARIA, V., LALWANI, M., PILLAI, B., MITRA, D. & BRAHMACHARI, S. K. 2008. Human cellular microRNA hsa-miR-29a interferes with viral nef protein expression and HIV-1 replication. *Retrovirology,* 5**,** 117.

AKPAN, U. S. & PILLARISETTY, L. S. 2021. Congenital Cytomegalovirus Infection. 2019/05/15 ed.: StatPearls Publishing.

AL MANA, H., YASSINE, H. M., YOUNES, N. N., AL-MOHANNADI, A., AL-SADEQ, D. W., ALHABABI, D., NASSER, E. A. & NASRALLAH, G. K. 2019. The Current Status of Cytomegalovirus (CMV) Prevalence in the MENA Region: A Systematic Review. *Pathogens,* 8.

ALBERTAZZI, L., SERRESI, M., ALBANESE, A. & BELTRAM, F. 2010. Dendrimer internalization and intracellular trafficking in living cells. *Mol Pharm,* 7**,** 680-8.

ALBRITTON, L. M. 2018. Chapter 1 - Retrovirus Receptor Interactions and Entry. *Retrovirus-Cell Interactions*. 1 ed.: Academic Press.

ALEKSEEVA, A., URSO, E., MAZZINI, G. & NAGGI, A. 2019. Heparanase as an Additional Tool for Detecting Structural Peculiarities of Heparin Oligosaccharides. *Molecules,* 24.

ALPHANDERY, E. 2019. Biodistribution and targeting properties of iron oxide nanoparticles for treatments of cancer and iron anemia disease. *Nanotoxicology,* 13**,** 573-596.

ARAUJO, R. V., SANTOS, S. D. S., IGNE FERREIRA, E. & GIAROLLA, J. 2018. New Advances in General Biomedical Applications of PAMAM Dendrimers. *Molecules,* 23.

AZEVEDO, L. S., PIERROTTI, L. C., ABDALA, E., COSTA, S. F., STRABELLI, T. M., CAMPOS, S. V., RAMOS, J. F., LATIF, A. Z., LITVINOV, N., MALUF, N. Z., CAIAFFA FILHO, H. H., PANNUTI, C. S., LOPES, M. H., SANTOS, V. A., LINARDI CDA, C., YASUDA, M. A. & MARQUES, H. H. 2015. Cytomegalovirus infection in transplant recipients. *Clinics (Sao Paulo),* 70**,** 515-23.

BAIG, T., NAYAK, J., DWIVEDI, V., SINGH, A., SRIVASTAVA, A. & TRIPATHI, P. K. 2015. A review about dendrimers: synthesis, types, characterization and applications. *International Journal of Advances in Pharmacy, Biology and Chemistry,* 4**,** 44-59.

BAJAN, S. & HUTVAGNER, G. 2020. RNA-Based Therapeutics: From Antisense Oligonucleotides to miRNAs. *Cells,* 9.

BALL, R. L., BAJAJ, P. & WHITEHEAD, K. A. 2018. Oral delivery of siRNA lipid nanoparticles: Fate in the GI tract. *Sci Rep,* 8**,** 2178.

BARNARD, A., POSOCCO, P., PRICL, S., CALDERON, M., HAAG, R., HWANG, M. E., SHUM, V. W., PACK, D. W. & SMITH, D. K. 2011. Degradable self-assembling dendrons for gene delivery: experimental and theoretical insights into the barriers to cellular uptake. *J Am Chem Soc,* 133**,** 20288-300.

BARRE-SINOUSSI, F., CHERMANN, J. C., REY, F., NUGEYRE, M. T., CHAMARET, S., GRUEST, J., DAUGUET, C., AXLER-BLIN, C., VEZINET-BRUN, F., ROUZIOUX, C., ROZENBAUM, W. & MONTAGNIER, L. 1983. Isolation of a T-lymphotropic retrovirus from a patient at risk for acquired immune deficiency syndrome (AIDS). *Science,* 220**,** 868-71.

BATTEGAY, M., NUESCH, R., HIRSCHEL, B. & KAUFMANN, G. R. 2006. Immunological recovery and antiretroviral therapy in HIV-1 infection. *Lancet Infect Dis,* 6**,** 280-7.

BHATTA, A. K., KEYAL, U., LIU, Y. & GELLEN, E. 2018. Vertical transmission of herpes simplex virus: an update. *J Dtsch Dermatol Ges,* 16**,** 685-692.

BHUSHAN, B. 2017. Introduction to Nanotechnology. *In:* BHUSHAN, B. (ed.) *Springer Handbook of Nanotechnology.* Berlin, Heidelberg: Springer Berlin Heidelberg.

BIRKMANN, A. & ZIMMERMANN, H. 2016. HSV antivirals - current and future treatment options. *Curr Opin Virol,* 18**,** 9-13.

BOLU, B. S., SANYAL, R. & SANYAL, A. 2018. Drug Delivery Systems from Self-Assembly of Dendron-Polymer Conjugates (dagger). *Molecules,* 23.

BOZZUTO, G. & MOLINARI, A. 2015. Liposomes as nanomedical devices. *Int J Nanomedicine,* 10**,** 975-99.

BRADY, R. C. & BERNSTEIN, D. I. 2004. Treatment of herpes simplex virus infections. *Antiviral Res,* 61**,** 73-81.

BRAVO-OSUNA, I., VICARIO-DE-LA-TORRE, M., ANDRES-GUERRERO, V., SANCHEZ-NIEVES, J., GUZMAN-NAVARRO, M., DE LA MATA, F. J., GOMEZ, R., DE LAS HERAS, B., ARGUESO, P., PONCHEL, G., HERRERO-VANRELL, R. & MOLINA-MARTINEZ, I. T. 2016. Novel Water-Soluble Mucoadhesive Carbosilane Dendrimers for Ocular Administration. *Mol Pharm,* 13**,** 2966-76.

BROCKMAN, M. A., KWON, D. S., TIGHE, D. P., PAVLIK, D. F., ROSATO, P. C., SELA, J., PORICHIS, F., LE GALL, S., WARING, M. T., MOSS, K., JESSEN, H., PEREYRA, F., KAVANAGH, D. G., WALKER, B. D. & KAUFMANN, D. E. 2009. IL-10 is up-regulated in multiple cell types during viremic HIV infection and reversibly inhibits virus-specific T cells. *Blood,* 114**,** 346-56.

BROTTO REBULI, K., GIACOBINI, M. & BERTOLOTTI, L. 2021. Caprine Arthritis Encephalitis Virus Disease Modelling Review. *Animals (Basel),* 11.

CANNON, M. J., SCHMID, D. S. & HYDE, T. B. 2010. Review of cytomegalovirus seroprevalence and demographic characteristics associated with infection. *Rev Med Virol,* 20**,** 202-13.

CDC 1981. Pneumocystis pneumonia--Los Angeles. *MMWR Morb Mortal Wkly Rep,* 30**,** 250-2.

CDC. 2020. *About Cytomegalovirus (CMV)* [Online]. Available: https://www.cdc.gov/cmv/overview.html [Accessed 5 may 2022].

CLAVEL, F. & HANCE, A. J. 2004. HIV drug resistance. *N Engl J Med,* 350**,** 1023-35.

CLOSE, W. L., ANDERSON, A. N. & PELLETT, P. E. 2018. Betaherpesvirus Virion Assembly and Egress. *Adv Exp Med Biol,* 1045**,** 167-207.

CLUTTER, D. S., JORDAN, M. R., BERTAGNOLIO, S. & SHAFER, R. W. 2016. HIV-1 drug resistance and resistance testing. *Infect Genet Evol,* 46**,** 292-307.

COELHO, A. V., DE MOURA, R. R., KAMADA, A. J., DA SILVA, R. C., GUIMARAES, R. L., BRANDAO, L. A., DE ALENCAR, L. C. & CROVELLA, S. 2016. Dendritic Cell-Based Immunotherapies to Fight HIV: How Far from a Success Story? A Systematic Review and Meta-Analysis. *Int J Mol Sci,* 17.

CONNOLLY, S. A., JARDETZKY, T. S. & LONGNECKER, R. 2021. The structural basis of herpesvirus entry. *Nat Rev Microbiol,* 19**,** 110-121.

CHIS, A. A., DOBREA, C., MORGOVAN, C., ARSENIU, A. M., RUS, L. L., BUTUCA, A., JUNCAN, A. M., TOTAN, M., VONICA-TINCU, A. L., CORMOS, G., MUNTEAN, A. C., MURESAN, M. L., GLIGOR, F. G. & FRUM, A. 2020. Applications and Limitations of Dendrimers in Biomedicine. *Molecules,* 25.

DAHLMAN, J. E., BARNES, C., KHAN, O., THIRIOT, A., JHUNJUNWALA, S., SHAW, T. E., XING, Y., SAGER, H. B., SAHAY, G., SPECINER, L., BADER, A., BOGORAD, R. L., YIN, H., RACIE, T., DONG, Y., JIANG, S., SEEDORF, D., DAVE, A., SANDU, K. S., WEBBER, M. J., NOVOBRANTSEVA, T., RUDA, V. M., LYTTON-JEAN, A. K. R., LEVINS, C. G., KALISH, B., MUDGE, D. K., PEREZ, M., ABEZGAUZ, L., DUTTA, P., SMITH, L., CHARISSE, K., KIERAN, M. W., FITZGERALD, K., NAHRENDORF, M., DANINO, D., TUDER, R. M., VON ANDRIAN, U. H., AKINC, A., SCHROEDER, A., PANIGRAHY, D., KOTELIANSKI, V., LANGER, R. & ANDERSON, D. G. 2014. In vivo endothelial siRNA delivery using polymeric nanoparticles with low molecular weight. *Nat Nanotechnol,* 9**,** 648-655.

DAVENPORT, M. P., KHOURY, D. S., CROMER, D., LEWIN, S. R., KELLEHER, A. D. & KENT, S. J. 2019. Functional cure of HIV: the scale of the challenge. *Nat Rev Immunol,* 19**,** 45-54.

DAVISON, A. J., EBERLE, R., EHLERS, B., HAYWARD, G. S., MCGEOCH, D. J., MINSON, A. C., PELLETT, P. E., ROIZMAN, B., STUDDERT, M. J. & THIRY, E. 2009. The order Herpesvirales. *Arch Virol,* 154**,** 171-7.

DEEKS, S. G., OVERBAUGH, J., PHILLIPS, A. & BUCHBINDER, S. 2015. HIV infection. *Nat Rev Dis Primers,* 1**,** 15035.

DENG, S., GIGLIOBIANCO, M. R., CENSI, R. & DI MARTINO, P. 2020. Polymeric Nanocapsules as Nanotechnological Alternative for Drug Delivery System: Current Status, Challenges and Opportunities. *Nanomaterials (Basel),* 10.

DIAS, A. P., DA SILVA SANTOS, S., DA SILVA, J. V., PARISE-FILHO, R., IGNE FERREIRA, E., SEOUD, O. E. & GIAROLLA, J. 2020. Dendrimers in the context of nanomedicine. *Int J Pharm,* 573**,** 118814.

DINARELLO, C. A. 2000. Proinflammatory cytokines. *Chest,* 118**,** 503-8.

DIOVERTI, M. V. & RAZONABLE, R. R. 2016. Cytomegalovirus. *Microbiol Spectr,* 4.

DOGRA, P., MARTIN, E. B., WILLIAMS, A., RICHARDSON, R. L., FOSTER, J. S., HACKENBACK, N., KENNEL, S. J., SPARER, T. E. & WALL, J. S. 2015. Novel heparan sulfate-binding peptides for blocking herpesvirus entry. *PLoS One,* 10**,** e0126239.

DONALISIO, M., QUARANTA, P., CHIUPPESI, F., PISTELLO, M., CAGNO, V., CAVALLI, R., VOLANTE, M., BUGATTI, A., RUSNATI, M., RANUCCI, E., FERRUTI, P. & LEMBO, D. 2016. The AGMA1 poly(amidoamine) inhibits the infectivity of herpes simplex virus in cell lines, in human cervicovaginal histocultures, and in vaginally infected mice. *Biomaterials,* 85**,** 40-53.

DONG, Y., YU, T., DING, L., LAURINI, E., HUANG, Y., ZHANG, M., WENG, Y., LIN, S., CHEN, P., MARSON, D., JIANG, Y., GIORGIO, S., PRICL, S., LIU, X., ROCCHI, P. & PENG, L. 2018. A Dual Targeting Dendrimer-Mediated siRNA Delivery System for Effective Gene Silencing in Cancer Therapy. *J Am Chem Soc,* 140**,** 16264-16274.

DREXLER, E. 1986. Engines of creation: The coming era of nanotechnology. *In:* MINSKY, M. (ed.) 1 ed.: Anchor Press.

FEYNMAN, R. P. 1960. There's Plenty of Room at the Bottom. *Engineering and Science,* 23**,** 22-36.

FORTE, E., ZHANG, Z., THORP, E. B. & HUMMEL, M. 2020. Cytomegalovirus Latency and Reactivation: An Intricate Interplay With the Host Immune Response. *Front Cell Infect Microbiol,* 10**,** 130.

FOWLER, K. B. & BOPPANA, S. B. 2018. Congenital cytomegalovirus infection. *Semin Perinatol,* 42**,** 149-154.

FRADET, A., CHEN, J., HELLWICH, K.-H., HORIE, K., KAHOVEC, J., MORMANN, W., STEPTO, R. F. T., VOHLÍDAL, J. & WILKS, E. S. 2019. Nomenclature and terminology for dendrimers with regular dendrons and for hyperbranched polymers (IUPAC Recommendations 2017). *Pure and Applied Chemistry,* 91**,** 523-561.

FRUCHON, S. & POUPOT, R. 2018. The ABP Dendrimer, a Drug-Candidate against Inflammatory Diseases That Triggers the Activation of Interleukin-10 Producing Immune Cells. *Molecules,* 23.

GALLO, R. C., SLISKI, A. & WONG-STAAL, F. 1983. Origin of human T-cell leukaemia-lymphoma virus. *Lancet,* 2**,** 962-3.

GARCIA-BRONCANO, P., CENA-DIEZ, R., DE LA MATA, F. J., GOMEZ, R., RESINO, S. & MUNOZ-FERNANDEZ, M. A. 2017. Efficacy of carbosilane dendrimers with an antiretroviral combination against HIV-1 in the presence of semen-derived enhancer of viral infection. *Eur J Pharmacol,* 811**,** 155-163.

GARCIA-MERINO, I., DE LAS CUEVAS, N., JIMENEZ, J. L., GALLEGO, J., GOMEZ, C., PRIETO, C., SERRAMIA, M. J., LORENTE, R. & MUNOZ-FERNANDEZ, M. A. 2009. The Spanish HIV BioBank: a model of cooperative HIV research. *Retrovirology,* 6**,** 27.

GARCIA, F., PLANA, M., CLIMENT, N., LEON, A., GATELL, J. M. & GALLART, T. 2013. Dendritic cell based vaccines for HIV infection: the way ahead. *Hum Vaccin Immunother,* 9**,** 2445-52.

GATHERER, D., DEPLEDGE, D. P., HARTLEY, C. A., SZPARA, M. L., VAZ, P. K., BENKO, M., BRANDT, C. R., BRYANT, N. A., DASTJERDI, A., DOSZPOLY, A., GOMPELS, U. A., INOUE, N., JAROSINSKI, K. W., KAUL, R., LACOSTE, V., NORBERG, P., ORIGGI, F. C., ORTON, R. J., PELLETT, P. E., SCHMID, D. S., SPATZ, S. J., STEWART, J. P., TRIMPERT, J., WALTZEK, T. B. & DAVISON, A. J. 2021. ICTV Virus Taxonomy Profile: Herpesviridae 2021. *J Gen Virol,* 102.

GERMAN ADVISORY COMMITTEE BLOOD (ARBEITSKREIS BLUT), S. A. O. P. T. B. B. 2016. Human Immunodeficiency Virus (HIV). *Transfus Med Hemother,* 43**,** 203-22.

GERNA, G., KABANOVA, A. & LILLERI, D. 2019. Human Cytomegalovirus Cell Tropism and Host Cell Receptors. *Vaccines (Basel),* 7.

GILJOHANN, D. A., SEFEROS, D. S., DANIEL, W. L., MASSICH, M. D., PATEL, P. C. & MIRKIN, C. A. 2010. Gold nanoparticles for biology and medicine. *Angew Chem Int Ed Engl,* 49**,** 3280-94.

GNANN, J. W., JR. & WHITLEY, R. J. 2017. Herpes Simplex Encephalitis: an Update. *Curr Infect Dis Rep,* 19**,** 13.

GONZÁLEZ-BELTRÁN, F. & MORALES-RAMÍREZ, P. 2003. Repairability during G1 of lesions eliciting sister chromatid exchanges induced by methylmethanesulfonate or ethylmethanesulfonate in bromodeoxyuridine-substituted and unsubstituted DNA strands. *Mutagenesis,* 18**,** 13-17.

GRIFFITHS, K. L., AHMED, M., DAS, S., GOPAL, R., HORNE, W., CONNELL, T. D., MOYNIHAN, K. D., KOLLS, J. K., IRVINE, D. J., ARTYOMOV, M. N., RANGEL-MORENO, J. & KHADER, S. A. 2016. Targeting dendritic cells to accelerate T-cell activation overcomes a bottleneck in tuberculosis vaccine efficacy. *Nat Commun,* 7**,** 13894.

GRIFFITHS, P., BARANIAK, I. & REEVES, M. 2015. The pathogenesis of human cytomegalovirus. *J Pathol,* 235**,** 288-97.

GRIFFITHS, P. & REEVES, M. 2021. Pathogenesis of human cytomegalovirus in the immunocompromised host. *Nat Rev Microbiol,* 19**,** 759-773.

GUERRERO-BELTRAN, C., GARCIA-HEREDIA, I., CENA-DIEZ, R., RODRIGUEZ-IZQUIERDO, I., SERRAMIA, M. J., MARTINEZ-HERNANDEZ, F., LLUESMA-GOMEZ, M., MARTINEZ-GARCIA, M. &

MUNOZ-FERNANDEZ, M. A. 2020. Cationic Dendrimer G2-S16 Inhibits Herpes Simplex Type 2 Infection and Protects Mice Vaginal Microbiome. *Pharmaceutics,* 12.

GUERRERO-BELTRAN, C., PRIETO, A., LEAL, M., JIMENEZ, J. L. & MUNOZ-FERNANDEZ, M. A. 2019. Combination of G2-S16 dendrimer/dapivirine antiretroviral as a new HIV-1 microbicide. *Future Med Chem,* 11**,** 3005-3013.

GUERRERO-BELTRAN, C., RODRIGUEZ-IZQUIERDO, I., SERRAMIA, M. J., ARAYA-DURAN, I., MARQUEZ-MIRANDA, V., GOMEZ, R., DE LA MATA, F. J., LEAL, M., GONZALEZ-NILO, F. & MUNOZ-FERNANDEZ, M. A. 2018. Anionic Carbosilane Dendrimers Destabilize the GP120-CD4 Complex Blocking HIV-1 Entry and Cell to Cell Fusion. *Bioconjug Chem,* 29**,** 1584-1594.

GUGLIESI, F., COSCIA, A., GRIFFANTE, G., GALITSKA, G., PASQUERO, S., ALBANO, C. & BIOLATTI, M. 2020. Where do we Stand after Decades of Studying Human Cytomegalovirus? *Microorganisms,* 8.

HAMMAD, W. A. B. & KONJE, J. C. 2021. Herpes simplex virus infection in pregnancy - An update. *Eur J Obstet Gynecol Reprod Biol,* 259**,** 38-45.

HAN, X., XU, K., TARATULA, O. & FARSAD, K. 2019. Applications of nanoparticles in biomedical imaging. *Nanoscale,* 11**,** 799-819.

HARFOUCHE, M., ABU-HIJLEH, F. M., JAMES, C., LOOKER, K. J. & ABU-RADDAD, L. J. 2021. Epidemiology of herpes simplex virus type 2 in sub-Saharan Africa: Systematic review, meta-analyses, and meta-regressions. *EClinicalMedicine,* 35**,** 100876.

HARRIS, J. B. & HOLMES, A. P. 2017. Neonatal Herpes Simplex Viral Infections and Acyclovir: An Update. *J Pediatr Pharmacol Ther,* 22**,** 88-93.

HEYDER, R. S., ZHONG, Q., BAZITO, R. C. & DA ROCHA, S. R. P. 2017. Cellular internalization and transport of biodegradable polyester dendrimers on a model of the pulmonary epithelium and their formulation in pressurized metered-dose inhalers. *Int J Pharm,* 520**,** 181-194.

HIZI, A. & HERZIG, E. 2015. dUTPase: the frequently overlooked enzyme encoded by many retroviruses. *Retrovirology,* 12**,** 70.

HOUZET, L., KLASE, Z., YEUNG, M. L., WU, A., LE, S. Y., QUINONES, M. & JEANG, K. T. 2012. The extent of sequence complementarity correlates with the potency of cellular miRNA-mediated restriction of HIV-1. *Nucleic Acids Res,* 40**,** 11684-96.

HU, J., WINQVIST, O., FLORES-MORALES, A., WIKSTROM, A. C. & NORSTEDT, G. 2009. SOCS2 influences LPS induced human monocyte-derived dendritic cell maturation. *PLoS One,* 4**,** e7178.

HUANG, W., ZHOU, D., LEE, J., SUN, J., ZHANG, S., XU, H., LUO, J. & LIU, X. 2021. Ag-decorated GaN for high-efficiency photoreduction of carbon dioxide into tunable syngas under visible light. *Nanotechnology,* 32.

HUANG, Y., MAO, K., ZHANG, B. & ZHAO, Y. 2017. Superparamagnetic iron oxide nanoparticles conjugated with folic acid for dual target-specific drug delivery and MRI in cancer theranostics. *Mater Sci Eng C Mater Biol Appl,* 70**,** 763-771.

ICTV, I. C. O. T. O. V. 2022. *Virus Taxonomy: 2020 Release* [Online]. Available: https://talk.ictvonline.org/taxonomy/ [Accessed 15 April 2022].

INTERAGENCY WORKING GROUP ON NANOSCIENCE, E. A. T. 2000. National Nanotechnology Initiative: Leading to the Next Industrial Revolution.

JAIN, K., KESHARWANI, P., GUPTA, U. & JAIN, N. K. 2010. Dendrimer toxicity: Let's meet the challenge. *Int J Pharm,* 394**,** 122-42.

JAMES, C., HARFOUCHE, M., WELTON, N. J., TURNER, K. M., ABU-RADDAD, L. J., GOTTLIEB, S. L. & LOOKER, K. J. 2020. Herpes simplex virus: global infection prevalence and incidence estimates, 2016. *Bull World Health Organ,* 98**,** 315-329.

JEAN BELTRAN, P. M. & CRISTEA, I. M. 2014. The life cycle and pathogenesis of human cytomegalovirus infection: lessons from proteomics. *Expert Rev Proteomics,* 11**,** 697-711.

JOHNSTON, C. & COREY, L. 2016. Current Concepts for Genital Herpes Simplex Virus Infection: Diagnostics and Pathogenesis of Genital Tract Shedding. *Clin Microbiol Rev,* 29**,** 149-61.

KAUP, R., TEN HOVE, J. B., BUNSCHOTEN, A., VAN LEEUWEN, F. W. B. & VELDERS, A. H. 2021. Multicompartment dendrimicelles with binary, ternary and quaternary core composition. *Nanoscale,* 13**,** 15422-15430.

KAUSHIC, C., ROTH, K. L., ANIPINDI, V. & XIU, F. 2011. Increased prevalence of sexually transmitted viral infections in women: the role of female sex hormones in regulating susceptibility and immune responses. *J Reprod Immunol,* 88**,** 204-9.

KIM, Y., PARK, E. J. & NA, D. H. 2018. Recent progress in dendrimer-based nanomedicine development. *Arch Pharm Res,* 41**,** 571-582.

KIRCHHOFF, F. 2021. HIV Life Cycle: Overview. *In:* HOPE, T. J., STEVENSON, M. & RICHMAN, D. (eds.) *Encyclopedia of AIDS.* New York, NY: Springer New York.

KNIPE, D. M. & WHITLEY, R. 2021. Herpes Simplex Virus 1 and 2 (Herpesviridae). *Encyclopedia of Virology.* 4 ed.: Academic Press.

KOGANTI, R., MEMON, A. & SHUKLA, D. 2021. Emerging Roles of Heparan Sulfate Proteoglycans in Viral Pathogenesis. *Semin Thromb Hemost,* 47**,** 283-294.

KORKMAZ, H., TABUR, S., OZKAYA, M., AKSOY, N., YILDIZ, H. & AKARSU, E. 2015. Paraoxonase and arylesterase activities in patients with papillary thyroid cancer. *Scand J Clin Lab Invest,* 75**,** 259-64.

KUKHANOVA, M. K., KOROVINA, A. N. & KOCHETKOV, S. N. 2014. Human herpes simplex virus: life cycle and development of inhibitors. *Biochemistry (Mosc),* 79**,** 1635-52.

KUMAR, A., COQUARD, L. & HERBEIN, G. 2016. Targeting TNF-Alpha in HIV-1 Infection. *Curr Drug Targets,* 17**,** 15-22.

LAI, Y.-S., KAO, C.-L., CHEN, Y.-P., FANG, C.-C., HUA, C.-C. & CHU, C.-C. 2016. Photodegradable self-assembling PAMAM dendrons for gene delivery involving dendriplex formation and phototriggered circular DNA release. *New Journal of Chemistry,* 40**,** 2601-2608.

LANDOLFO, S., GARIGLIO, M., GRIBAUDO, G. & LEMBO, D. 2003. The human cytomegalovirus. *Pharmacol Ther,* 98**,** 269-97.

LANGER, S. & SAUTER, D. 2016. Unusual Fusion Proteins of HIV-1. *Front Microbiol,* 7**,** 2152.

LASKEY, S. B. & SILICIANO, R. F. 2014. A mechanistic theory to explain the efficacy of antiretroviral therapy. *Nat Rev Microbiol,* 12**,** 772-80.

LAU, B., POOLE, E., KRISHNA, B., SELLART, I., WILLS, M. R., MURPHY, E. & SINCLAIR, J. 2016. The Expression of Human Cytomegalovirus MicroRNA MiR-UL148D during Latent Infection in Primary Myeloid Cells Inhibits Activin A-triggered Secretion of IL-6. *Sci Rep,* 6**,** 31205.

LIU, X., ROCCHI, P. & PENG, L. 2012. Dendrimers as non-viral vectors for siRNA delivery. *New Journal of Chemistry,* 36**,** 256-263.

LOOKER, K. J., ELMES, J. A. R., GOTTLIEB, S. L., SCHIFFER, J. T., VICKERMAN, P., TURNER, K. M. E. & BOILY, M. C. 2017a. Effect of HSV-2 infection on subsequent HIV acquisition: an updated systematic review and meta-analysis. *Lancet Infect Dis,* 17**,** 1303-1316.

LOOKER, K. J., MAGARET, A. S., MAY, M. T., TURNER, K. M. E., VICKERMAN, P., NEWMAN, L. M. & GOTTLIEB, S. L. 2017b. First estimates of the global and regional incidence of neonatal herpes infection. *Lancet Glob Health,* 5**,** e300-e309.

LOPEZ-CASTEJON, G. & BROUGH, D. 2011. Understanding the mechanism of IL-1beta secretion. *Cytokine Growth Factor Rev,* 22**,** 189-95.

MACLACHLAN, N. J. & DUBOVI, E. J. 2016a. Chapter 9 - Herpesvirales. *Fenner's Veterinary Virology.* 5 ed.: Academic Press.

MACLACHLAN, N. J. & DUBOVI, E. J. 2016b. Chapter 14 - Retroviridae. *Fenner's Veterinary Virology.* 5 ed.: Academic Press.

MADAVARAJU, K., KOGANTI, R., VOLETY, I., YADAVALLI, T. & SHUKLA, D. 2020. Herpes Simplex Virus Cell Entry Mechanisms: An Update. *Front Cell Infect Microbiol,* 10**,** 617578.

MARTIN-MORENO, A., JIMENEZ BLANCO, J. L., MOSHER, J., SWANSON, D. R., GARCIA FERNANDEZ, J. M., SHARMA, A., CENA, V. & MUNOZ-FERNANDEZ, M. A. 2020. Nanoparticle-Delivered HIV Peptides to Dendritic Cells a Promising Approach to Generate a Therapeutic Vaccine. *Pharmaceutics,* 12.

MARTIN-MORENO, A. & MUNOZ-FERNANDEZ, M. A. 2019. Dendritic Cells, the Double Agent in the War Against HIV-1. *Front Immunol,* 10**,** 2485.

MATOGA, M., HOSSEINIPOUR, M. C., JEWETT, S., HOFFMAN, I. F. & CHASELA, C. 2021. Effects of HIV voluntary medical male circumcision programs on sexually transmitted infections. *Curr Opin Infect Dis,* 34**,** 50-55.

MENEGHETTI, M. C., HUGHES, A. J., RUDD, T. R., NADER, H. B., POWELL, A. K., YATES, E. A. & LIMA, M. A. 2015. Heparan sulfate and heparin interactions with proteins. *J R Soc Interface,* 12**,** 0589.

MERCK, K. *MTT Assay Protocol for Cell Viability and Proliferation* [Online]. Available: https://www.sigmaaldrich.com/ES/es/technical-documents/protocol/cell-culture-and-cell-culture-analysis/cell-counting-and-health-analysis/cell-proliferation-kit-i-mtt [Accessed 29 April 2022].

METTENLEITER, T. C., KLUPP, B. G. & GRANZOW, H. 2009. Herpesvirus assembly: an update. *Virus Res,* 143**,** 222-34.

MIGNANI, S., RODRIGUES, J., ROY, R., SHI, X., CENA, V., EL KAZZOULI, S. & MAJORAL, J. P. 2019. Exploration of biomedical dendrimer space based on in-vivo physicochemical parameters: Key factor analysis (Part 2). *Drug Discov Today,* 24**,** 1184-1192.

MIGNANI, S., SHI, X., ZABLOCKA, M. & MAJORAL, J. P. 2021. Dendritic Macromolecular Architectures: Dendrimer-Based Polyion Complex Micelles. *Biomacromolecules,* 22**,** 262-274.

MITCHELL, M. J., BILLINGSLEY, M. M., HALEY, R. M., WECHSLER, M. E., PEPPAS, N. A. & LANGER, R. 2021. Engineering precision nanoparticles for drug delivery. *Nat Rev Drug Discov,* 20**,** 101-124.

MITTAL, P., SAHARAN, A., VERMA, R., ALTALBAWY, F. M. A., ALFAIDI, M. A., BATIHA, G. E., AKTER, W., GAUTAM, R. K., UDDIN, M. S. & RAHMAN, M. S. 2021. Dendrimers: A New Race of Pharmaceutical Nanocarriers. *Biomed Res Int,* 2021**,** 8844030.

MITTAL, S. K., CHO, K. J., ISHIDO, S. & ROCHE, P. A. 2015. Interleukin 10 (IL-10)-mediated Immunosuppression: MARCH-I INDUCTION REGULATES ANTIGEN PRESENTATION BY MACROPHAGES BUT NOT DENDRITIC CELLS. *J Biol Chem,* 290**,** 27158-27167.

MODY, N., DUBEY, S., SHARMA, R., AGRAWAL, U. & VYAS, S. P. 2015. Dendritic cell-based vaccine research against cancer. *Expert Rev Clin Immunol,* 11**,** 213-32.

MOSSER, D. M. & ZHANG, X. 2008. Interleukin-10: new perspectives on an old cytokine. *Immunol Rev,* 226**,** 205-18.

MUKHERJEE, S., BOUTANT, E., REAL, E., MELY, Y. & ANTON, H. 2021. Imaging Viral Infection by Fluorescence Microscopy: Focus on HIV-1 Early Stage. *Viruses,* 13.

NAIR, V., GIMENO, I., DUNN, J., ZAVALA, G., WILLIAMS, S. M., REECE, R. L. & HAFNER, S. 2020. Neoplastic Diseases. *Diseases of Poultry.*

NAKAYAMA, M. 2014. Antigen Presentation by MHC-Dressed Cells. *Front Immunol,* 5**,** 672.

NISHIMURA, M. & MORI, Y. 2019. Entry of betaherpesviruses. *Adv Virus Res,* 104**,** 283-312.

NISHIURA, H., KUBOTA, I., KONDO, Y., KACHI, M., HATAI, H., SASAKI, J., GORYO, M. & OCHIAI, K. 2020. Neuropathogenicity of newly isolated avian leukosis viruses from chickens with osteopetrosis and mesenchymal neoplasms. *Avian Pathol,* 49**,** 440-447.

NNI. *About Nanotechnology* [Online]. Available: https://www.nano.gov/about-nanotechnology [Accessed 5 May 2022].

OMORI, R. & ABU-RADDAD, L. J. 2017. Sexual network drivers of HIV and herpes simplex virus type 2 transmission. *AIDS,* 31**,** 1721-1732.

OU, J. Y., SHIH, Y. C., WANG, B. Y. & CHU, C. C. 2019. Photodegradable coumarin-derived amphiphilic dendrons for DNA binding: Self-assembly and phototriggered disassembly in water and air-water interface. *Colloids Surf B Biointerfaces,* 175**,** 428-435.

PAINTER, M. M. & COLLINS, K. L. 2019. HIV and Retroviruses. *Encyclopedia of Microbiology.* 4 ed.: Academic Press.

PALMERSTON MENDES, L., PAN, J. & TORCHILIN, V. P. 2017. Dendrimers as Nanocarriers for Nucleic Acid and Drug Delivery in Cancer Therapy. *Molecules,* 22.

PEDZIWIATR-WERBICKA, E., MILOWSKA, K., DZMITRUK, V., IONOV, M., SHCHARBIN, D. & BRYSZEWSKA, M. 2019. Dendrimers and hyperbranched structures for biomedical applications. *European Polymer Journal,* 119**,** 61-73.

PERILLA, J. R. & GRONENBORN, A. M. 2016. Molecular Architecture of the Retroviral Capsid. *Trends Biochem Sci,* 41**,** 410-420.

PERISE-BARRIOS, A. J., JIMENEZ, J. L., DOMINGUEZ-SOTO, A., DE LA MATA, F. J., CORBI, A. L., GOMEZ, R. & MUNOZ-FERNANDEZ, M. A. 2014. Carbosilane dendrimers as gene delivery agents for the treatment of HIV infection. *J Control Release,* 184**,** 51-7.

PIZZURRO, G. A. & BARRIO, M. M. 2015. Dendritic cell-based vaccine efficacy: aiming for hot spots. *Front Immunol,* 6**,** 91.

POLONIS, V. R., BROWN, B. K., ROSA BORGES, A., ZOLLA-PAZNER, S., DIMITROV, D. S., ZHANG, M. Y., BARNETT, S. W., RUPRECHT, R. M., SCARLATTI, G., FENYO, E. M., MONTEFIORI, D. C., MCCUTCHAN, F. E. & MICHAEL, N. L. 2008. Recent advances in the characterization of HIV-1 neutralization assays for standardized evaluation of the antibody response to infection and vaccination. *Virology,* 375**,** 315-20.

POOLE, C. L. & JAMES, S. H. 2018. Antiviral Therapies for Herpesviruses: Current Agents and New Directions. *Clin Ther,* 40**,** 1282-1298.

POPOVIC, M., SARNGADHARAN, M. G., READ, E. & GALLO, R. C. 1984. Detection, isolation, and continuous production of cytopathic retroviruses (HTLV-III) from patients with AIDS and pre-AIDS. *Science,* 224**,** 497-500.

PROMEGA. *CytoTox 96 Non-Radioactive Cytotoxicity Assay* [Online]. Available: https://www.promega.es/products/cell-health-assays/cell-viability-and-cytotoxicity-assays/cytotox-96-non_radioactive-cytotoxicity-assay/?catNum=G1780 [Accessed 29 April 2022].

RABIEE, N., AHMADVAND, S., AHMADI, S., FATAHI, Y., DINARVAND, R., BAGHERZADEH, M. & HAMBLIN, M. R. 2020. Carbosilane dendrimers: Drug and gene delivery applications. *Journal of Drug Delivery Science and Technology,* 59.

RAFAILIDIS, P. I., MOURTZOUKOU, E. G., VARBOBITIS, I. C. & FALAGAS, M. E. 2008. Severe cytomegalovirus infection in apparently immunocompetent patients: a systematic review. *Virol J,* 5**,** 47.

RAMSDEN, J. 2016. Nanotechnology: An Introduction. 2 ed.: William Andrew PUB.

RATAJCZAK, K., KRAZINSKI, B. E., KOWALCZYK, A. E., DWORAKOWSKA, B., JAKIELA, S. & STOBIECKA, M. 2018. Optical Biosensing System for the Detection of Survivin mRNA in Colorectal Cancer Cells Using a Graphene Oxide Carrier-Bound Oligonucleotide Molecular Beacon. *Nanomaterials (Basel),* 8.

RAZONABLE, R. R. & HUMAR, A. 2019. Cytomegalovirus in solid organ transplant recipients-Guidelines of the American Society of Transplantation Infectious Diseases Community of Practice. *Clin Transplant,* 33**,** e13512.

REARDON, D. A. & MITCHELL, D. A. 2017. The development of dendritic cell vaccine-based immunotherapies for glioblastoma. *Semin Immunopathol,* 39**,** 225-239.

RECHENCHOSKI, D. Z., FACCIN-GALHARDI, L. C., LINHARES, R. E. C. & NOZAWA, C. 2017. Herpesvirus: an underestimated virus. *Folia Microbiol (Praha),* 62**,** 151-156.

REIS E SOUSA, C. 2006. Dendritic cells in a mature age. *Nat Rev Immunol,* 6**,** 476-83.

RELANO-RODRIGUEZ, I., ESPINAR-BUITRAGO, M. S., MARTIN-CANADILLA, V., GOMEZ-RAMIREZ, R., JIMENEZ, J. L. & MUNOZ-FERNANDEZ, M. A. 2021a. Nanotechnology against human cytomegalovirus in vitro: polyanionic carbosilane dendrimers as antiviral agents. *J Nanobiotechnology,* 19**,** 65.

RELANO-RODRIGUEZ, I., ESPINAR-BUITRAGO, M. S., MARTIN-CANADILLA, V., GOMEZ-RAMIREZ, R. & MUNOZ-FERNANDEZ, M. A. 2021b. G2-S16 Polyanionic Carbosilane Dendrimer Can Reduce HIV-1 Reservoir Formation by Inhibiting Macrophage Cell to Cell Transmission. *Int J Mol Sci,* 22.

RIBBERT, H. 1904. Ueber protozoenartige Zellen in der Niere eines syphilitischen Neugeborenen und in der Parotis von Kindern. *Zbl All Pathol,* 15**,** 945–948.

RILEY, R. S., JUNE, C. H., LANGER, R. & MITCHELL, M. J. 2019. Delivery technologies for cancer immunotherapy. *Nat Rev Drug Discov,* 18**,** 175-196.

RINALDO, C. R. 2009. Dendritic cell-based human immunodeficiency virus vaccine. *J Intern Med,* 265**,** 138-58.

RODRIGUEZ-IZQUIERDO, I., GASCO, S. & MUNOZ-FERNANDEZ, M. A. 2020a. High Preventive Effect of G2-S16 Anionic Carbosilane Dendrimer against Sexually Transmitted HSV-2 Infection. *Molecules,* 25.

RODRIGUEZ-IZQUIERDO, I., NATALIA, C., GARCIA, F. & LOS ANGELES MUNOZ-FERNANDEZ, M. 2019. G2-S16 sulfonate dendrimer as new therapy for treatment failure in HIV-1 entry inhibitors. *Nanomedicine (Lond),* 14**,** 1095-1107.

RODRIGUEZ-IZQUIERDO, I., SERRAMIA, M. J., GOMEZ, R., MATA, F. J. D. L., BULLIDO, M. J. & MUNOZ-FERNANDEZ, M. Á. 2020b. Gold Nanoparticles Crossing Blood-Brain Barrier Prevent HSV-1 Infection and Reduce Herpes Associated Amyloid-betasecretion. *J Clin Med,* 9.

ROFF, S. R., NOON-SONG, E. N. & YAMAMOTO, J. K. 2014. The Significance of Interferon-gamma in HIV-1 Pathogenesis, Therapy, and Prophylaxis. *Front Immunol,* 4**,** 498.

ROIZMAN, B. 2013. The Herpesviruses. *The Viruses.* 1 ed. Springer Science & Business Media: Springer, Boston, MA.

ROIZMAN, B. & WHITLEY, R. J. 2013. An inquiry into the molecular basis of HSV latency and reactivation. *Annu Rev Microbiol,* 67**,** 355-74.

ROLLER, R. J. & JOHNSON, D. C. 2021. Herpesvirus Nuclear Egress across the Outer Nuclear Membrane. *Viruses,* 13.

ROMANI, B. & ALLAHBAKHSHI, E. 2017. Underlying mechanisms of HIV-1 latency. *Virus Genes,* 53**,** 329-339.

ROOZBAHANI, M. & HAMMERSMITH, K. M. 2018. Management of herpes simplex virus epithelial keratitis. *Curr Opin Ophthalmol,* 29**,** 360-364.

ROWE, W. P., HARTLEY, J. W., WATERMAN, S., TURNER, H. C. & HUEBNER, R. J. 1956. Cytopathogenic agent resembling human salivary gland virus recovered from tissue cultures of human adenoids. *Proc Soc Exp Biol Med,* 92**,** 418-24.

RUELAS, D. S., CHAN, J. K., OH, E., HEIDERSBACH, A. J., HEBBELER, A. M., CHAVEZ, L., VERDIN, E., RAPE, M. & GREENE, W. C. 2015. MicroRNA-155 Reinforces HIV Latency. *J Biol Chem,* 290**,** 13736-48.

SAHAY, B. & YAMAMOTO, J. K. 2018. Lessons Learned in Developing a Commercial FIV Vaccine: The Immunity Required for an Effective HIV-1 Vaccine. *Viruses,* 10.

SALATIN, S., MALEKI DIZAJ, S. & YARI KHOSROUSHAHI, A. 2015. Effect of the surface modification, size, and shape on cellular uptake of nanoparticles. *Cell Biol Int,* 39**,** 881-90.

SANCHEZ, V. & BRITT, W. 2021. Human Cytomegalovirus Egress: Overcoming Barriers and Co-Opting Cellular Functions. *Viruses,* 14.

SATHIYAMOORTHY, K., CHEN, J., LONGNECKER, R. & JARDETZKY, T. S. 2017. The COMPLEXity in herpesvirus entry. *Curr Opin Virol,* 24**,** 97-104.

SAYLOR, D., DICKENS, A. M., SACKTOR, N., HAUGHEY, N., SLUSHER, B., PLETNIKOV, M., MANKOWSKI, J. L., BROWN, A., VOLSKY, D. J. & MCARTHUR, J. C. 2016. HIV-associated neurocognitive disorder--pathogenesis and prospects for treatment. *Nat Rev Neurol,* 12**,** 234-48.

SCHELHAAS, M. 2017. Viruses and cancer: molecular relations and perspectives. *Biol Chem,* 398**,** 815-816.

SCHUURHUIS, D. H., FU, N., OSSENDORP, F. & MELIEF, C. J. 2006. Ins and outs of dendritic cells. *Int Arch Allergy Immunol,* 140**,** 53-72.

SEPULVEDA-CRESPO, D., CENA-DIEZ, R., JIMENEZ, J. L. & ANGELES MUNOZ-FERNANDEZ, M. 2017. Mechanistic Studies of Viral Entry: An Overview of Dendrimer-Based Microbicides As Entry Inhibitors Against Both HIV and HSV-2 Overlapped Infections. *Med Res Rev,* 37**,** 149-179.

SEPULVEDA-CRESPO, D., GOMEZ, R., DE LA MATA, F. J., JIMENEZ, J. L. & MUNOZ-FERNANDEZ, M. A. 2015a. Polyanionic carbosilane dendrimer-conjugated antiviral drugs as efficient microbicides: Recent trends and developments in HIV treatment/therapy. *Nanomedicine,* 11**,** 1481-98.

SEPULVEDA-CRESPO, D., SERRAMIA, M. J., TAGER, A. M., VRBANAC, V., GOMEZ, R., DE LA MATA, F. J., JIMENEZ, J. L. & MUNOZ-FERNANDEZ, M. A. 2015b. Prevention vaginally of HIV-1 transmission in humanized BLT mice and mode of antiviral action of polyanionic carbosilane dendrimer G2-S16. *Nanomedicine,* 11**,** 1299-308.

SHAUNAK, S. 2015. Perspective: Dendrimer drugs for infection and inflammation. *Biochem Biophys Res Commun,* 468**,** 435-41.

SHAW, G. M. & HUNTER, E. 2012. HIV transmission. *Cold Spring Harb Perspect Med,* 2.

SHERJE, A. P., JADHAV, M., DRAVYAKAR, B. R. & KADAM, D. 2018. Dendrimers: A versatile nanocarrier for drug delivery and targeting. *Int J Pharm,* 548**,** 707-720.

SIJMONS, S., THYS, K., MBONG NGWESE, M., VAN DAMME, E., DVORAK, J., VAN LOOCK, M., LI, G., TACHEZY, R., BUSSON, L., AERSSENS, J., VAN RANST, M. & MAES, P. 2015. High-throughput

analysis of human cytomegalovirus genome diversity highlights the widespread occurrence of gene-disrupting mutations and pervasive recombination. *J Virol,* 89**,** 7673-7695.

SINGH, N. & TSCHARKE, D. C. 2020. Herpes Simplex Virus Latency Is Noisier the Closer We Look. *J Virol,* 94.

SINGH, V., SAHEBKAR, A. & KESHARWANI, P. 2021. Poly (propylene imine) dendrimer as an emerging polymeric nanocarrier for anticancer drug and gene delivery. *European Polymer Journal,* 158.

SKWARCZYNSKI, M. & TOTH, I. 2016. Peptide-based synthetic vaccines. *Chem Sci,* 7**,** 842-854.

SMITH, M. G. 1956. Propagation in tissue cultures of a cytopathogenic virus from human salivary gland virus (SGV) disease. *Proc Soc Exp Biol Med,* 92**,** 424-30.

SOMANI, S., LASKAR, P., ALTWAIJRY, N., KEWCHAROENVONG, P., IRVING, C., ROBB, G., PICKARD, B. S. & DUFES, C. 2018. PEGylation of polypropylenimine dendrimers: effects on cytotoxicity, DNA condensation, gene delivery and expression in cancer cells. *Sci Rep,* 8**,** 9410.

SOUNG, A. & KLEIN, R. S. 2018. Viral Encephalitis and Neurologic Diseases: Focus on Astrocytes. *Trends Mol Med,* 24**,** 950-962.

SUK, J. S., XU, Q., KIM, N., HANES, J. & ENSIGN, L. M. 2016. PEGylation as a strategy for improving nanoparticle-based drug and gene delivery. *Adv Drug Deliv Rev,* 99**,** 28-51.

SUMER BOLU, B., MANAVOGLU GECICI, E. & SANYAL, R. 2016. Combretastatin A-4 Conjugated Antiangiogenic Micellar Drug Delivery Systems Using Dendron-Polymer Conjugates. *Mol Pharm,* 13**,** 1482-90.

SWAMINATHAN, G., ROSSI, F., SIERRA, L. J., GUPTA, A., NAVAS-MARTIN, S. & MARTIN-GARCIA, J. 2012. A role for microRNA-155 modulation in the anti-HIV-1 effects of Toll-like receptor 3 stimulation in macrophages. *PLoS Pathog,* 8**,** e1002937.

TAYLOR, B. S. & HAMMER, S. M. 2008. The challenge of HIV-1 subtype diversity. *N Engl J Med,* 359**,** 1965-6.

TAYLOR, M. & GERRIETS, V. 2022. *Acyclovir.* 2019/06/14 ed.: Treasure Island (FL): StatPearls Publishing.

TAYLOR, T. J., BROCKMAN, M. A., MCNAMEE, E. E. & KNIPE, D. M. 2002. Herpes simplex virus. *Front Biosci,* 7**,** d752-64.

TEE, J. K., YIP, L. X., TAN, E. S., SANTITEWAGUN, S., PRASATH, A., KE, P. C., HO, H. K. & LEONG, D. T. 2019. Nanoparticles' interactions with vasculature in diseases. *Chem Soc Rev,* 48**,** 5381-5407.

THAKUR, S., KESHARWANI, P., TEKADE, R. K. & JAIN, N. K. 2015. Impact of pegylation on biopharmaceutical properties of dendrimers. *Polymer,* 59**,** 67-92.

THERMOFISHER, S. *LIVE/DEAD™ Fixable Aqua Dead Cell Stain Kit, for 405 nm excitation* [Online]. Available: https://www.thermofisher.com/order/catalog/product/L34957 [Accessed 29 April 2022].

UNAIDS. 2021. *Global AIDS Update 2021* [Online]. Available: https://www.unaids.org/en/resources/presscentre/pressreleaseandstatementarchive/2021/july/20210714_global-aids-update [Accessed 26 May 2022].

UNAIDS. 2022. *Global HIV & AIDS statistics — Fact sheet* [Online]. Available: https://www.unaids.org/en/resources/fact-sheet [Accessed 24 May 2022].

VACAS-CORDOBA, E., BASTIDA, H., PION, M., HAMEAU, A., IONOV, M., BRYSZEWSKA, M., CAMINADE, A. M., MAJORAL, J. P. & MUNOZ-FERNANDEZ, M. A. 2014a. HIV-antigens charged on phosphorus dendrimers as tools for tolerogenic dendritic cells-based immunotherapy. *Curr Med Chem,* 21**,** 1898-909.

VACAS-CORDOBA, E., CLIMENT, N., DE LA MATA, F. J., PLANA, M., GOMEZ, R., PION, M., GARCIA, F. & MUNOZ-FERNANDEZ, M. A. 2014b. Dendrimers as nonviral vectors in dendritic cell-based immunotherapies against human immunodeficiency virus: steps toward their clinical evaluation. *Nanomedicine (Lond),* 9**,** 2683-702.

VAN DOMSELAAR, R., NJENDA, D. T., RAO, R., SONNERBORG, A., SINGH, K. & NEOGI, U. 2019. HIV-1 Subtype C with PYxE Insertion Has Enhanced Binding of Gag-p6 to Host Cell Protein ALIX and Increased Replication Fitness. *J Virol,* 93.

VILIBIC-CAVLEK, T., KOLARIC, B., BEADER, N., VRTAR, I., TABAIN, I. & MLINARIC-GALINOVIC, G. 2017. Seroepidemiology of cytomegalovirus infections in Croatia. *Wien Klin Wochenschr,* 129**,** 129-135.

VONGLAHN, W. C. & PAPPENHEIMER, A. M. 1925. Intranuclear Inclusions in Visceral Disease. *Am J Pathol,* 1**,** 445-466 3.

W.H.O. 2022. *Herpes simplex virus* [Online]. Available: https://www.who.int/news-room/fact-sheets/detail/herpes-simplex-virus [Accessed 25 May 2022].

WALD, A. & ASHLEY-MORROW, R. 2002. Serological testing for herpes simplex virus (HSV)-1 and HSV-2 infection. *Clin Infect Dis,* 35**,** S173-82.

WANG-SHICK, R. 2017 Chapter 3 - Virus Life Cycle. *Molecular Virology of Human Pathogenic Viruses.* 1 ed.: Academic Press.

WANG, H. N., RAO, D., FU, X. Q., HU, M. M. & DONG, J. G. 2018. Equine infectious anemia virus in China. *Oncotarget,* 9**,** 1356-1364.

WANG, J., LEI, L., VOETS, I. K., COHEN STUART, M. A. & VELDERS, A. H. 2020. Dendrimicelles with pH-controlled aggregation number of core-dendrimers and stability. *Soft Matter,* 16**,** 7893-7897.

WANG, J., VOETS, I. K., FOKKINK, R., VAN DER GUCHT, J. & VELDERS, A. H. 2014. Controlling the number of dendrimers in dendrimicelle nanoconjugates from 1 to more than 100. *Soft Matter,* 10**,** 7337-45.

WANG, P., QU, X., ZHOU, X., SHEN, Y., JI, H., FU, Z., DENG, J., LU, P., YU, W., LU, H. & ZHU, H. 2015. Two cellular microRNAs, miR-196b and miR-1290, contribute to HIV-1 latency. *Virology,* 486**,** 228-38.

WANG, Q., ZHENG, Y., ZHOU, C., CHAN, M. & YANG, C. Y. 2021. Low-temperature grown vertically aligned carbon nanotube array for an optimal infrared bolometer. *Nanotechnology,* 32.

WANG, X., SHI, C., ZHANG, L., LIN, M. Y., GUO, D., WANG, L., YANG, Y., DUNCAN, T. M. & LUO, J. 2017. Structure-Based Nanocarrier Design for Protein Delivery. *ACS Macro Letters,* 6**,** 267-271.

WEI, T., CHEN, C., LIU, J., LIU, C., POSOCCO, P., LIU, X., CHENG, Q., HUO, S., LIANG, Z., FERMEGLIA, M., PRICL, S., LIANG, X. J., ROCCHI, P. & PENG, L. 2015. Anticancer drug nanomicelles formed by self-assembling amphiphilic dendrimer to combat cancer drug resistance. *Proc Natl Acad Sci U S A,* 112**,** 2978-83.

WELLER, T. H., HANSHAW, J. B. & SCOTT, D. E. 1960. Serologic differentiation of viruses responsible for cytomegalic inclusion disease. *Virology,* 12**,** 130-2.

WHITEHEAD, K. A., LANGER, R. & ANDERSON, D. G. 2009. Knocking down barriers: advances in siRNA delivery. *Nat Rev Drug Discov,* 8**,** 129-38.

WHITLEY, R. & BAINES, J. 2018. Clinical management of herpes simplex virus infections: past, present, and future. *F1000Res,* 7.

WIDENER, R. W. & WHITLEY, R. J. 2014. Chapter 11 - Herpes simplex virus. *Handbook of Clinical Neurology.* 1 ed.: Elsevier.

WU, L. P., FICKER, M., CHRISTENSEN, J. B., TROHOPOULOS, P. N. & MOGHIMI, S. M. 2015. Dendrimers in Medicine: Therapeutic Concepts and Pharmaceutical Challenges. *Bioconjug Chem,* 26**,** 1198-211.

WYATT, R. & SODROSKI, J. 1998. The HIV-1 envelope glycoproteins: fusogens, antigens, and immunogens. *Science,* 280**,** 1884-8.

YANG, J., LUO, Y., SHIBU, M. A., TOTH, I. & SKWARCZYNSKIA, M. 2019. Cell-penetrating Peptides: Efficient Vectors for Vaccine Delivery. *Curr Drug Deliv,* 16**,** 430-443.

YU, M., JIE, X., XU, L., CHEN, C., SHEN, W., CAO, Y., LIAN, G. & QI, R. 2015. Recent Advances in Dendrimer Research for Cardiovascular Diseases. *Biomacromolecules,* 16**,** 2588-98.

ZHANG, P., QIAO, Z. A. & DAI, S. 2015. Recent advances in carbon nanospheres: synthetic routes and applications. *Chem Commun (Camb),* 51**,** 9246-56.

ZHANG, X., LIANG, N., GONG, X., KAWASHIMA, Y., CUI, F. & SUN, S. 2019. Tumor-targeting micelles based on folic acid and alpha-tocopherol succinate conjugated hyaluronic acid for paclitaxel delivery. *Colloids Surf B Biointerfaces,* 177**,** 11-18.

ZHOU, M., LANCHY, J. M. & RYCKMAN, B. J. 2015. Human Cytomegalovirus gH/gL/gO Promotes the Fusion Step of Entry into All Cell Types, whereas gH/gL/UL128-131 Broadens Virus Tropism through a Distinct Mechanism. *J Virol,* 89**,** 8999-9009.

PUBLICATIONS

10. LIST OF PUBLICATIONS

1. Lozano-Cruz, T.; Rodríguez-Izquierdo, I.; Oliveros-Almendros, L.; **Royo-Rubio, E**.; Jimenez, J.L.; de la Mata, F.J.; Muñoz-Fernández, M.A.; Gómez, R. (Manuscript in preparation).

2. **Royo-Rubio, E.**; Martín-Cañadilla, V.; Rusnati, M.; Milanesi, M.; Lozano-Cruz, T.; Gómez, R.; Jiménez, J.L.; Muñoz-Fernández, M.Á. Prevention of *Herpesviridae* Infections by Cationic PEGylated Carbosilane Dendrimers. *Pharmaceutics* **2022**, *14*, 536. https://doi.org/10.3390/pharmaceutics14030536. **First authorship.** IF: 6.321 (Q1)

3. **Royo-Rubio, E.**; Rodríguez-Izquierdo, I.; Moreno-Domene, M.; Lozano-Cruz, T.; de la Mata, F.J.; Gómez, R.; Muñoz-Fernández, M.A.; Jiménez, J.L. Promising PEGylated cationic dendrimers for delivery of miRNAs as a possible therapy against HIV-1 infection. *J Nanobiotechnology* **2021**, 28;19(1):158. https://doi.org/10.1186/s12951-021-00899-0. **First authorship (Co-authors).** IF: 10.435 (D1)

Journal of Nanobiotechnology

RESEARCH Open Access

Promising PEGylated cationic dendrimers for delivery of miRNAs as a possible therapy against HIV-1 infection

E. Royo-Rubio[1,2†], I. Rodríguez-Izquierdo[1,2†], M. Moreno-Domene[3], T. Lozano-Cruz[4,5], F. J. de la Mata[4,5], R. Gómez[4,5], M. A. Muñoz-Fernández[1*] and J. L. Jiménez[2*]

Abstract

Background: The appearance of resistance against new treatments and the fact that HIV-1 can infect various cell types and develop reservoirs and sanctuaries makes it necessary to develop new therapeutic approaches to overcome those failures.

Results: Studies of cytotoxicity, genotoxicity, complexes formation, stability, resistance, release and particle size distribution confirmed that G2-SN15-PEG, G3-SN31-PEG, G2-SN15-PEG-FITC and G3-SN31-PEG-FITC dendrimers can form complexes with miRNAs being biocompatible, stable and conferring protection to these nucleic acids. Confocal microscopy and flow cytometry showed effective delivery of these four dendrimers into the target cells, confirming their applicability as delivery systems. Dendriplexes formed with the dendrimers and miRNAs significantly inhibited HIV-1 infection in PBMCs.

Conclusions: These dendrimers are efficient delivery systems for miRNAs and they specifically and significantly improved the anti-R5-HIV-1 activity of these RNA molecules.

Keyword: Carbosilane dendrimers, microRNAs, HIV-1 infection, Delivery, Inhibition

Background

Human Immunodeficiency Virus (HIV) infection mainly affects CD4+T lymphocytes, dendritic cells and macrophages [1]. Moreover, there is a wide range of cellular types susceptible to HIV-1 infection, such as central nervous system (CNS) cells including microglia or astrocytes [2]. Lymphocytes are mainly located in the circulatory system and lymphatic ganglions whereas dendritic cells and macrophages play a key role in the immune surveillance of mucosa and tissues. Current treatments against HIV-1 infection control viral replication and disease progression. These treatment combinations mainly include integrase inhibitors such as abacavir, lamivudine, tenofovir alafenamide or emtricitabine, or nucleoside reverse transcriptase inhibitors (NRTIs) such as bictegravir, dolutegravir or raltegravir [3, 4]. Combined therapy includes at least three of these drugs reducing the appearance of mutations and increasing the virological failure. However, the appearance of resistance against these new treatments, mainly in low- and middle-income countries [5–7] and the fact that HIV-1 can infect a wide range of cells and develop sanctuaries and reservoirs [8–11] bring to light the need of new possible therapeutic approaches to eliminate those failures.

*Correspondence: mmunoz.hgugm@salud.madrid.org; joseluis.jimenez@salud.madrid.org
†E. Royo-Rubio and I. Rodríguez-Izquierdo contributed equally to this work
[1] Laboratorio InmunoBiología Molecular, Hospital General Universitario Gregorio Marañón (HGUGM), Instituto Investigación Sanitaria Gregorio Marañón (IiSGM), Spanish HIV HGM BioBanco, Madrid, Spain
[2] Plataforma de Laboratorio (Inmunología), HGUGM, IiSGM, Spanish HIV HGM BioBank, Madrid, Spain
Full list of author information is available at the end of the article

Different delivery nanocarriers provide a scaffold through which different small RNA molecules have been successfully delivered in diverse studies [12–15]. We have carried out broad research about various dendrimers in the context of HIV-1 infection [16–20]. Previously, we reported amino-terminated carbosilane dendrimers that provide stability, protection and high transfection efficiency to oligodeoxynucleotides and siRNAs inhibiting HIV-1 replication in peripheral blood mononuclear cells (PBMCs) and CD4 T-cells [21–24]. Carbosilane dendrimers are three-dimensional hyperbranched molecules capable of forming complexes by electrostatic interactions between the positively charged functional terminal groups and negatively charged backbone of small RNAs, what confers protection and facilitates transfection of bound RNAs [25].

Novel therapeutic strategies are being developed from the study of HIV-host interactions, for example microRNAs able to target HIV-1 infection and replication [26]. These miRNAs are small non-coding RNAs, 19–25 long nucleotides, with capability to modulate gene expression at post-transcriptional level [27]. A wide range of different cellular miRNAs has been described to have a negative impact on HIV-1 replication through repressing its expression by targeting HIV-1 3'-UTR or enhancing HIV-1 mRNA interactions with RISC complex [28–30]. The effective delivery of these miRNAs is a limiting factor in their therapeutic applications since naked miRNAs face several difficulties when navigating the circulatory system such as phagocytosis, enzymatic degradation or protein aggregation [31]. Nanotechnology is a promising strategy for the delivery of small RNAs. In this work, G2-SN15-PEG, G3-SN31-PEG, G2-SN15-PEG FITC and G3-SN31-PEG FITC with PEG modifications, were selected. These four carbosilane dendrimers present different PEGylation residues to reduce toxicity and improve the biocompatibility of molecules [32]. Our objective was to form cationic dendrimers-miRNAs complexes that improved the therapeutic effect of current treatments against HIV-1 infection in different cells. We report the potential therapeutic effect of complexation of PEGylated G2-SN15-PEG, G3-SN31-PEG, G2-SN15-PEG-FITC and G3-SN31-PEG-FITC cationic dendrimers with hsa-miR-29a-3p, hsa-miR-29b-3p, hsa-miR-92a-3p, hsa-miR-133b and hsa-miR-149-5p miRNAs in peripheral blood mononuclear cells (PBMCs) and U87MG-CD4$^+$CCR5$^+$ cell line with anti-HIV-1 activity [33, 34]. First, the biosafety of four cationic dendrimers in PBMCs and l cell line were assessed by measuring cytotoxicity and genetic safety. We characterized several parameters of dendrimers-miRNAs (dendriplexes) formed to determine their stability, resistance to RNases and release capability. The internalization effectiveness of FITC-labelled dendrimers in PBMCs and U87MG-CD4$^+$CCR5$^+$ cell line was studied. Finally, HIV-1 inhibition capacity of dendriplexes in PBMCs and U87MG-CD4$^+$CCR5$^+$ cell was determined.

Results

Cytotoxicity of the dendrimers on PBMCs and U87MG-CD4$^+$CCR5$^+$ cell line

Cytotoxicity of G2-SN15-PEG, G3-SN31-PEG, G2-SN15-PEG FITC and G3-SN31-PEG FITC cationic dendrimers in PBMCs and U87MG-CD4$^+$CCR5$^+$ cells was evaluated analyzing the mitochondrial toxicity by the 3-(4–5-dimethylthiazol-2-yl)-2,5-diphenyltetrazolium bromide (MTT) assay. PBMCs and U87MG-CD4$^+$CCR5$^+$ cells were treated with increasing concentrations of dendrimers, ranging from 0.01 to 30 μM, for 72 h. Culture medium was used as non-treated control and DMSO 10% as death control. Non-toxic concentrations were considered when the survival rate was $\geq$ 80%. Our data indicated that G2-SN15-PEG, G3-SN31-PEG, G2-SN15-PEG FITC and G3-SN31-PEG FITC dendrimers were non-toxic in PBMCs at concentrations of 10, 5, 5 and 1 μM, respectively (Fig. 1a) and non-toxic in U87MG-CD4$^+$CCR5$^+$ cells up at concentrations of 5, 1, 1 and 0.5 μM, respectively (Fig. 1b).

Genotoxicity of cationic dendrimers

If dendrimers generated genotoxicity by interfering with the host genome by sister-chromatid exchange (SCE) assay was studied. It is important to note that dendrimers can bind to miRNAs as well as to host genome due to their positively charged functional groups. If these cationic dendrimers mistakenly targeted the host genome it could cause dangerous genetic changes to its stability. Therefore, it is recommended to perform genetic studies to rule out this event. The SCE assay detects the physical exchange of DNA that occurs between two identical chromatids in the chromosome, determining the genetic damage caused by treatments which persist after the DNA duplication [35–37]. Due to the fact that only fluorochrome unlabeled cationic dendrimers can be used in some studies, genotoxicity tests for G2-SN15-PEG and G3-SN31-PEG cationic dendrimers were performed. PBMCs from five healthy donors were treated with G2-SN15-PEG 10 μM or G3-SN31-PEG 5 μM carbosilane cationic dendrimers for 72 h in presence of 5-bromo-2'-deoxyuridine (BdrU) following fluorescent plus Giemsa stain (FPG) (Fig. 2a). Non-treated samples and a dose of 1 Gy of radiation were used as untreated and genotoxicity control, respectively. Carbosilane cationic dendrimers did not generate genetic toxicity in PBMCs, since there are no significant differences among the non-treated and treated control samples, contrarily

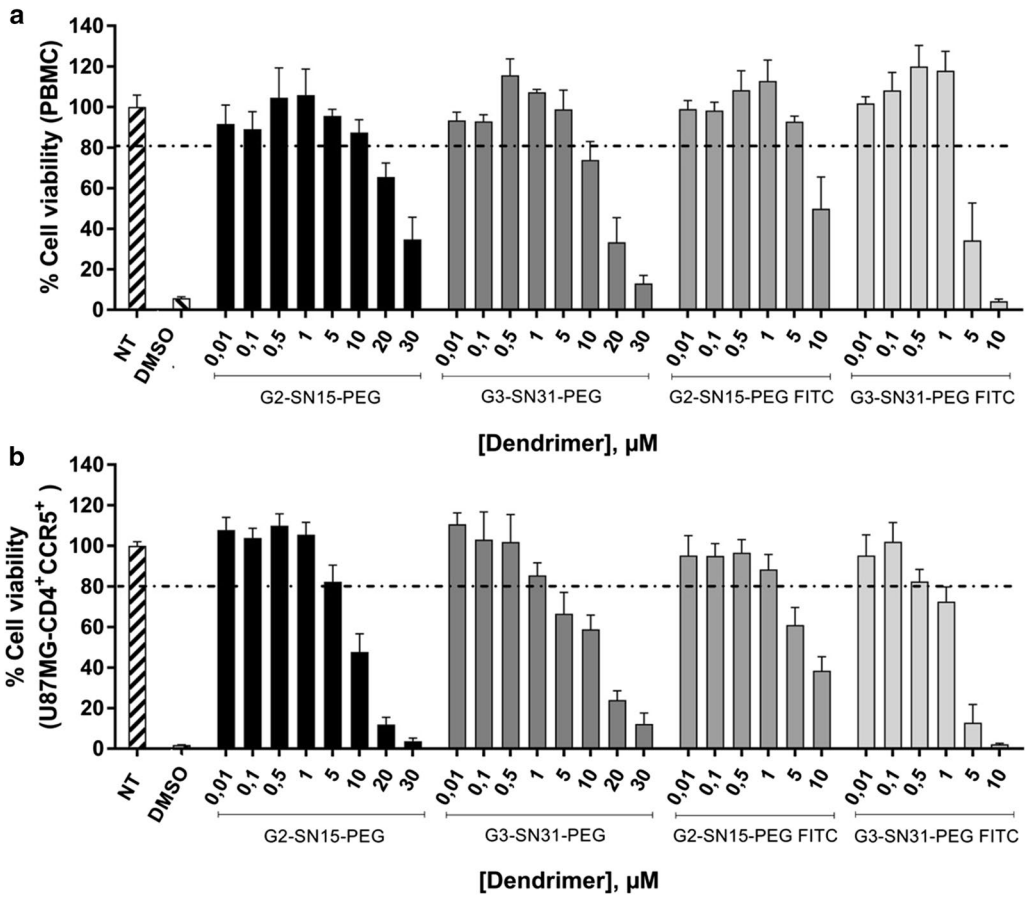

Fig. 1 Cytotoxicity of cationic carbosilane dendrimers by MTT assay. PBMCs (**a**) and U87MG-CD4$^+$CCR5$^+$ cells (**b**) were treated in a range of concentrations from 0.01 to 30 µM of each cationic dendrimer. Cell viability > 80% was established as non-toxic concentration. Culture medium samples were used as cell viability control and DMSO 10% was used as death control. Data represented as mean ± SD of three individual experiments performed in triplicate. *DMSO* dimethyl sulfoxide 10%, *NT* non-treated

to what happens in genotoxicity control studied (Fig. 2b; Table 1).

Dendriplexes formation and characterization

First of all, whether unlabeled or FITC-labelled dendrimers could form dendriplexes with the studied miRNAs, were explored. Dendrimers were used at the maximal non-toxic concentrations and dendrimers-miRNAs complexes were analyzed using 2% agarose gel. After 2 h of incubation, G2-SN15-PEG and G3-SN31-PEG dendrimers efficiently bound 99% of miRNA with stable binding up to 48 h (Fig. 3a, b). When dendrimer concentrations were lowered to match maximal non-toxic concentrations for U87MG-CD4$^+$CCR5$^+$ cells, similar results were found. G2-SN15-PEG and G3-SN31-PEG dendrimers bound around 90% and 80% of siRNAs, respectively, confirming that both dendrimers can perform and efficient and stable bond with these miRNAs (Fig. 3c–f).

Heparin competition and RNase protection assays

We first analyzed whether miRNAs were released by conducting heparin competition assays. miRNAs were released after heparin treatment, demonstrating that miRNAs could be released from the dendrimer. We also analyzed whether miRNA dendrimer binding protected miRNAs from RNase-mediated degradation, showing that dendrimers confer protection since miRNAs were completely recovered after treatment with RNases followed by heparin (Fig. 4a, b).

Dendriplexes were prepared with miRNA control 2 h before being treated with heparin and/or RNases. Dendrimers concentrations were (a) G2-SN15-PEG 10 µM and G3-SN31-PEG 5 µM, or (b) G2-SN15-PEG 5 µM and G3-SN31-PEG 1 µM.

Zeta potential and dynamic light scattering

To evaluate how miRNAs affects the properties of the dendrimer we studied the surface charge and stability by

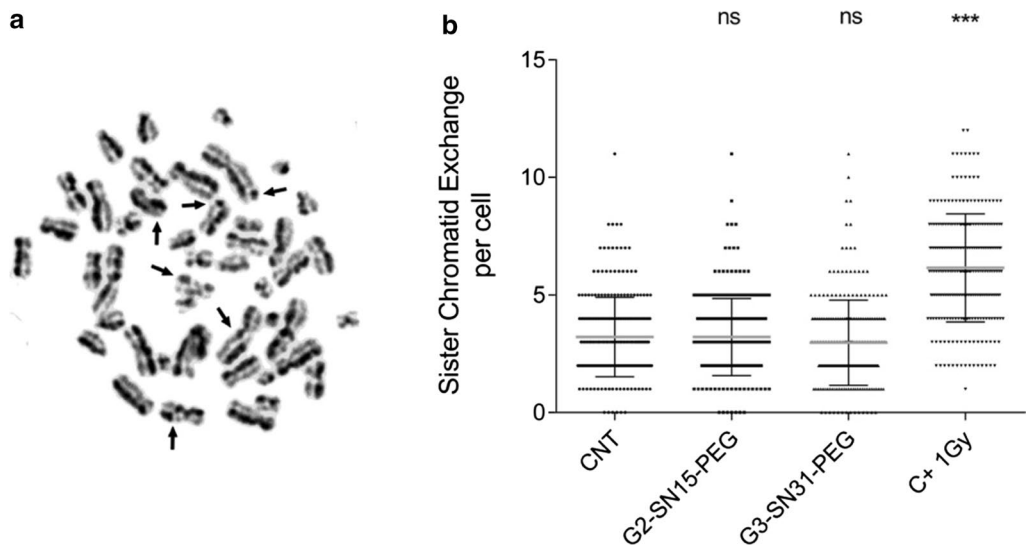

Fig. 2 Genotoxicity of carbosilane cationic dendrimers. Quantification of the number of sister-chromatid exchange per cell in PBMCs non-treated, PBMCs treated with G2-SN15-PEG 10 μM, G3-SN31-PEG 5 μM or 1 Gy of radiation for 72 h. **a** Images of random field obtained from the SCE assay after FPG staining. Arrows indicated the sister-chromatid exchange. **b** Analysis of the SCE assay. Data are represented as dot plots of five individual experiments (50 mitosis analysis per healthy donor). *C + 1 Gy* 1 Gy radiation control, *NT* non-treated. (*p < 0.05; **p < 0.01; ***p < 0.001)

Table 1 Analysis of the genotoxicity of the dendrimers

Treatment	SCE (mean ± SD)	P value	n
CNT	3.22 ± 1.69	-	250
G2-SN-15-PEG	3.22 ± 1.65	1.000	250
G3-SN31-PEG	2.98 ± 1.82	0.1272	250
C + 1 Gy	6.15 ± 2.29	< 0.0001	250

measuring the particle zeta potentials (ZP) and the particle size distribution by dynamic light scattering (DLS).

The positive values obtained from the study of the surface charge by ZP measurements confirmed the cationic density of the periphery of the nanoparticles. As shown in Table 2, G2-SN15-PEG dendrimer presents the highest potential value (52,5 mV), which entails high electrical stability. For its part, G3-SN31-PEG presents a moderate value (30,24 mV), which still represents good stability.

The formation of dendriplexes with hsa-miR-29a-3p led to a change in the ZP values of both dendrimers. More precisely, there is a decrease of the potential value when complexing G2-SN15-PEG dendrimer with the miRNA, whereas there is an increase of the value when forming the dendriplex from G3-SN31-PEG which suggests that the correct formation of the dendriplex took place.

Results obtained from the study of the particle size distribution by DLS (Table 3) suggest aggregation or self-assembly for G2-SN15-PEG (302,95 nm). On the contrary, much lower values were obtained for G3-SN31-PEG dendrimer (4,93 nm) indicating that this one could be described as a single molecule. As for hsa-miR-29a-3p, its size was found with low aggregation degree (14 nm). In terms of dendriplexes formed with G2-SN15-PEG or G3-SN31-PEG dendrimers and hsa-miR-29a-3p, both presented moderate aggregation values (around 30 and 40 nm, respectively). All these values supported with data obtained in electrophoresis assays, confirm the correct formation and stability of complexes.

Internalization assay of the dendrimers

The progressive entry of G2-SN15-PEG FITC and G3-SN31-PEG FITC dendrimers in PBMCs and U87MG-$CD4^+CCR5^+$ cell line was determined by confocal microscopy and flow cytometry. For confocal microscopy cells were treated with dendrimers, (5 and 1 μM for PBMCs or 1 and 0.5 μM for U87MG-$CD4^+CCR5^+$ cell line), for 1 h, 2 h or 6 h. Results show a notable difference in the uptake of both dendrimers in CD3 positive cells. In terms of G2-SN15-PEG FITC, there was no differences in the uptake among the studied times, after 1 h of incubation around 90% of PBMCs were positive for dendrimer presence inside the host cell and differences were not detected in the entry percentage at 1, 2 or 6 h. Likewise, when PBMCs were treated with G3-SN31-PET FITC no differences in the uptake at different time points were detected. However, this G3-SN31-PEG FITC showed a percentage of positivity much lower than the previous dendrimer, only around 16% of positive cells (Fig. 5a, b).

U87MG-$CD4^+CCR5^+$ cells were treated with G2-SN15-PEG FITC 1 μM or G3-SN31-PEG FITC

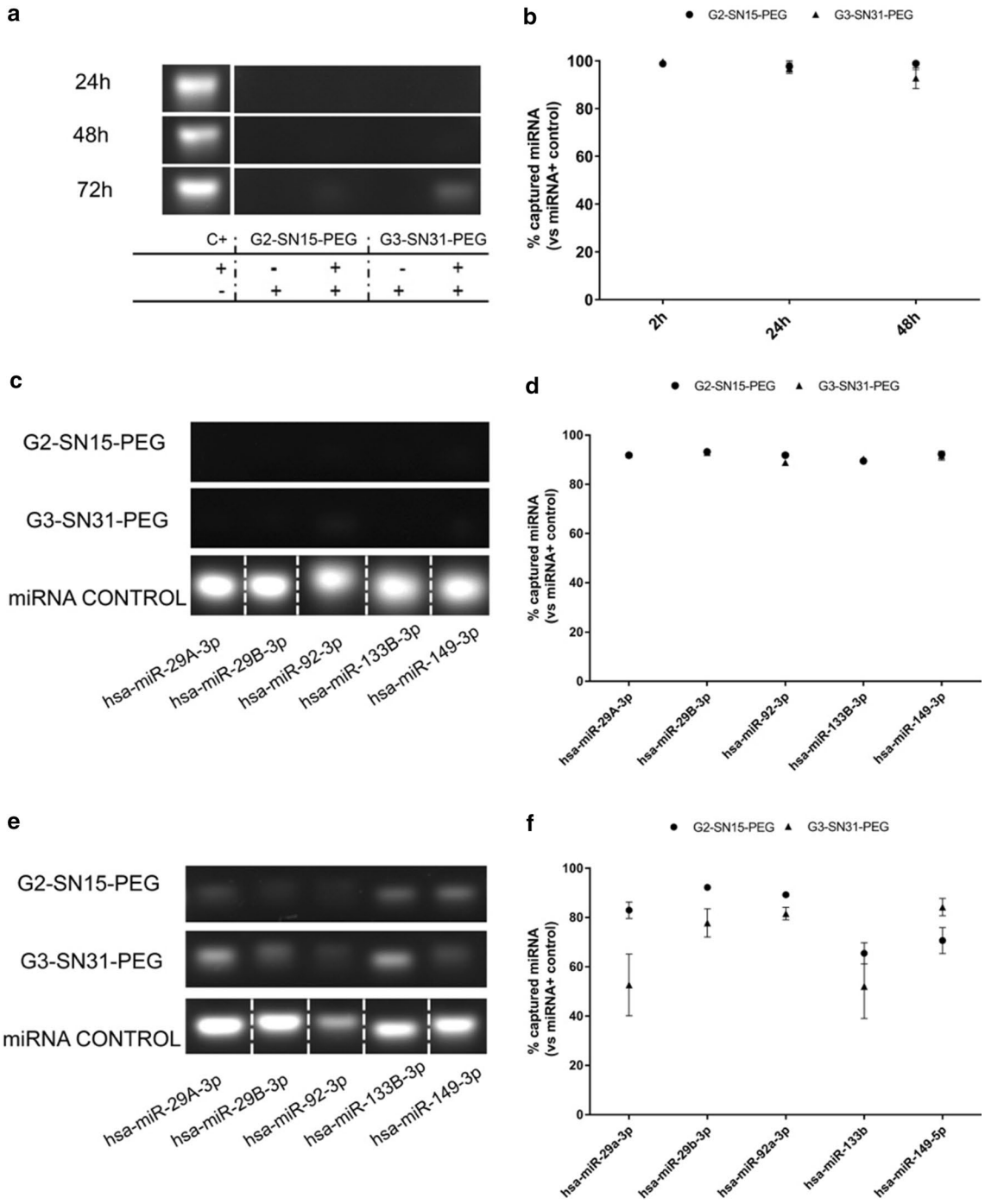

Fig. 3 Dendriplexes characterization. **a** Two per cent agarose gel electrophoresis showing the formation of different dendriplexes after 2 h, 24 h or 48 h of incubation of control microRNA with G2-SN15-PEG 10 μM and G3-SN31-PEG 5 μM dendrimers. b Percentage of microRNA captured *vs.* miRNA control after 2, 24 or 48 h of incubation. **c** Formation of dendriplexes with anti-HIV-1 microRNAs (hsa-miR-29a-3p, hsa-miR-29b-3p, hsa-miR-92a-3p, hsa-miR-133b and hsa-miR-149-5p) and G2-SN15-PEG (10 μM) and G3-SN31-PEG (5 μM) dendrimers after 2 h of incubation. **d** Percentage of microRNA captured *vs.* miRNA control after 2 h of incubation. **e** Formation of dendriplexes with anti-HIV-1 microRNAs and G2-SN15-PEG (5 μM) and G3-SN31-PEG (1 μM) dendrimers. **f** Percentage of microRNA captured *vs.* miRNA control

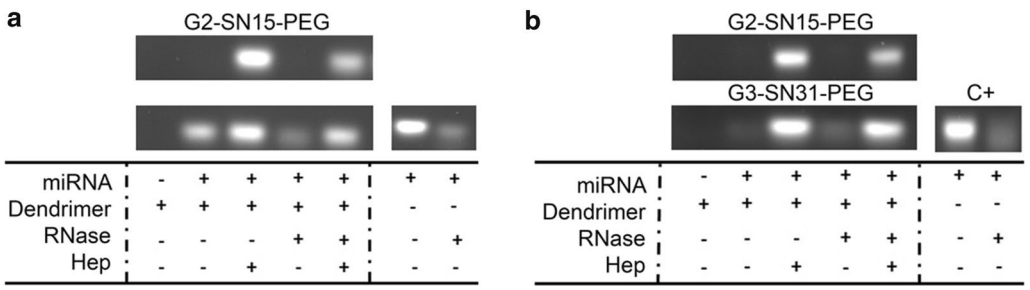

Fig. 4 Heparin competition and RNase protection assays. Dendriplexes were prepared with miRNA control 2 h before being treated with heparin and/or RNases. Dendrimers concentrations were **a** G2-SN15-PEG 10 μM and G3-SN31-PEG 5 μM or **b** G2-SN15-PEG 5 μM and G3-SN31-PEG 1 μM

Table 2 ZP values (mV) for dendrimers and dendriplexes formed with G2-SN15-PEG and G3-SN31-PEG and hsa-miR-29a-3p

Compound	Zeta potential (mV)
G2-SN15-PEG	52.5 ± 0.42
G2-SN15-PEG + hsa-miR-29a-3p	49.45 ± 1.62
G3-SN31-PEG	30.6 ± 0
G3-SN31-PEG + hsa-miR-29a-3p	32.24 ± 2.37

Table 3 Measure of hydrodynamic size for dendrimers and dendriplexes formed with G2-SN15-PEG, G3-SN31-PEG and hsa-miR-29a-3p

Compound	Hydrodynamic size (diameter, nm)
G2-SN15-PEG	302.95 ± 14.78
G2-SN15-PEG + hsa-miR-29a-3p	30.19 ± 2.88
G3-SN31-PEG	4.93 ± 0.26
G3-SN31-PEG + hsa-miR-29a-3p	41.1 ± 2.88
hsa-miR-29a-3p	14.42 ± 4.16

0.5 μM and the internalization was again studied by confocal microscopy (Fig. 6a) and flow cytometry (Fig. 6b). In this case we can observe again a differential entry between G2-SN15-PEG FITC and G3-SN31-PEG FITC dendrimers and an increase in the number of positive cells along the selected time points. After 1 h of incubation, both dendrimers were found in the outside part of the cell membrane, due to the fact that both dendrimers co-localize with F-actin and flow cytometry indicated that 40% of cells were positive for G2-SN15-PEG FITC whereas only 20% of cells where positive for G3-SN31-PEG FITC. However, after 2 h of incubation we observed a notable increase inside cells and positivity values raised to 50 and 45%, respectively, suggesting that both dendrimers need at least 2 h for internalize into U87MG-CD4$^+$CCR5$^+$ cells.

Our results indicate that both G2-SN15-PEG FITC and G3-SN31-PEG FITC dendrimers are capable of entering inside of PBMCs and U87MG-CD4$^+$CCR5$^+$ cells in less than 6 h, showing that both dendrimers could be used as delivery systems.

HIV-1 inhibition activity of the dendriplexes

To determine the anti-HIV-1 activity of dendriplexes, inhibition experiments were performed using non-labelled dendrimers, with the objective that these dendrimers could be used as a possible therapy. PBMCs or U87MG-CD4$^+$CCR5$^+$ cells were infected with R5-HIV-1NL$_{(AD8)}$ and treated with dendriplexes after 2 h of incubation of G2-SN15-PEG or G3-SN31-PEG dendrimer and the anti-HIV-1 miRNAs at concentrations of 10 and 5 μM for PBMCs or 5 and 1 μM for U87MG-CD4$^+$CCR5$^+$, respectively. Then, 72 h after R5-HIV-1NL$_{(AD8)}$ infection, supernatants of PBMCs or U87MG-CD4$^+$CCR5$^+$ cells were collected and titrated on TZM.bl cells to quantify R5-HIV-1NL$_{(AD8)}$ infection by luciferase activity measurements. Non-treated samples were used as uninfected control. The treatment of PBMCs with G2-SN15-PEG or G3-SN31-PEG dendrimer caused around 80 or 45% of HIV-1 reduction, regarding the control of infection. This inhibition was even greater when PBMCs were treated with dendriplexes formed with anti-HIV-1 miRNAs and both G2-SN15-PEG or G3-SN31-PEG dendrimer showing a significant increase of inhibition reaching values of 96 and 73% reduction of HIV-1 infection, respectively (Fig. 7a).

Treatment of U87MG-CD4$^+$CCR5$^+$ cells (Fig. 7b) with G2-SN15-PEG FITC 1 μM or G3-SN31-PEG dendrimer caused a significant inhibition of HIV-1 infection, around 40%, in agreement with previously mentioned in the bibliography.34 Moreover, the treatment with some of the dendriplexes produced an increase of HIV-1 inhibition, for example

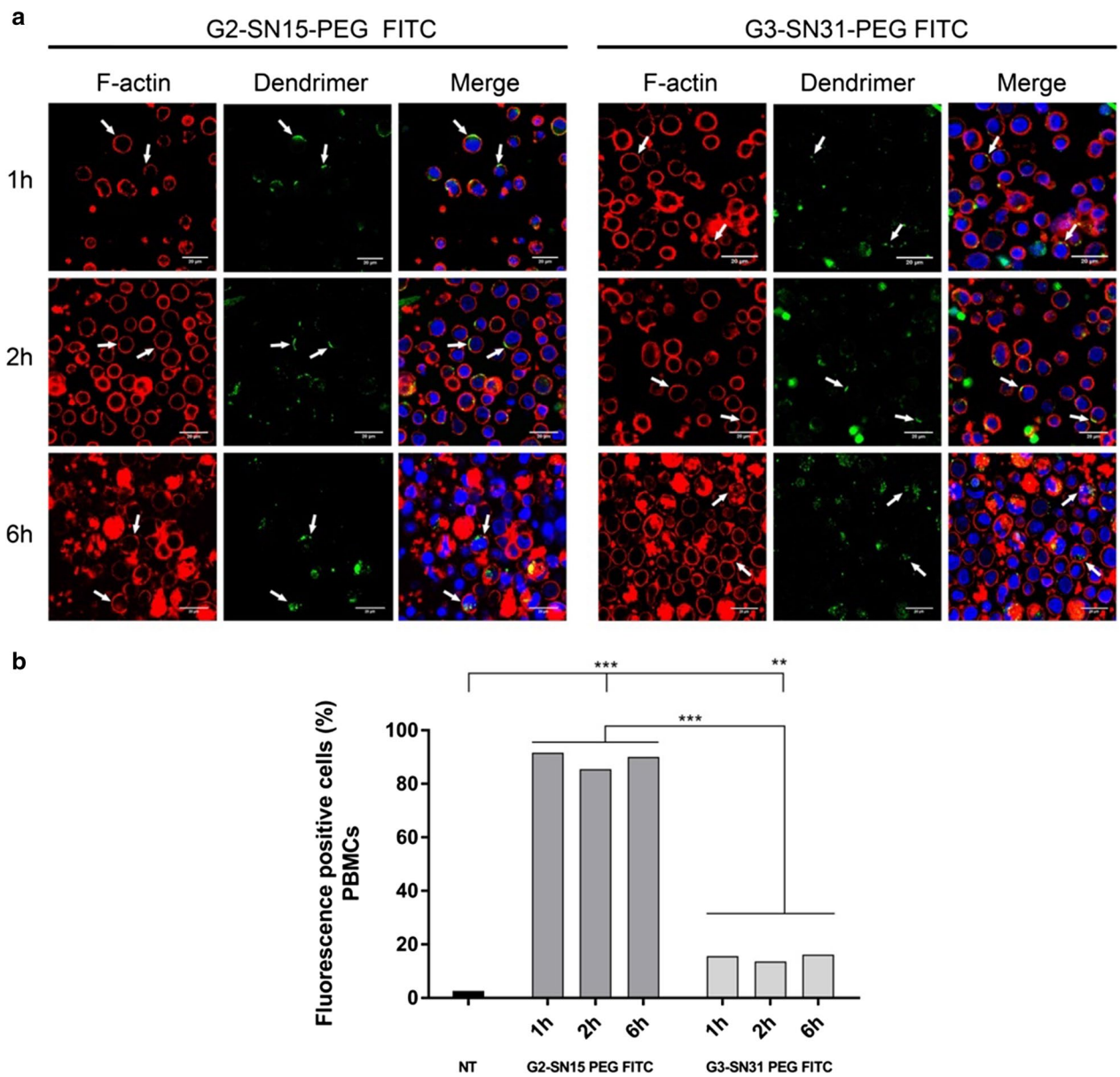

Fig. 5 Internalization of cationic carbosilane dendrimers in PBMCs. Confocal microscopy images of PBMCs treated for 1, 2 or 6 h with 5 μM G2-SN15-PEG FITC-dendrimer and 1 μM G3-SN31-PEG FITC-dendrimer (**a**). PBMCs were fixed and stained with Phalloidin (red, actin filaments) and DAPI (blue, nucleus). Confocal images of random field (**b**). Entry of FITC labeled dendrimers into PBMCs observed by flow cytometry at 1, 2 and 6 h post-treatment. *DAPI* 4′,6-Diamidino-2-phenylindole dihydrochloride

hsa-miR-29A-3p with G2-SN15-PEG or G3-SN31-PEG dendrimer. As expected, this increase was not significant regarding the inhibition resulting from the treatment with only G2-SN15-PEG or G3-SN31-PEG dendrimer, suggesting that dendriplexes cause a significant inhibition of R5-HIV-1 infection only in specific cell lines.

Discussion

Combinations of antiretroviral therapies have been a major step towards controlling HIV-1 infection, suppressing viral load to undetectable levels, and reducing mortality and morbidity associated with HIV-1 infection [38, 39]. These treatments are unable to overcome the main problems that infection still entails: the existence of

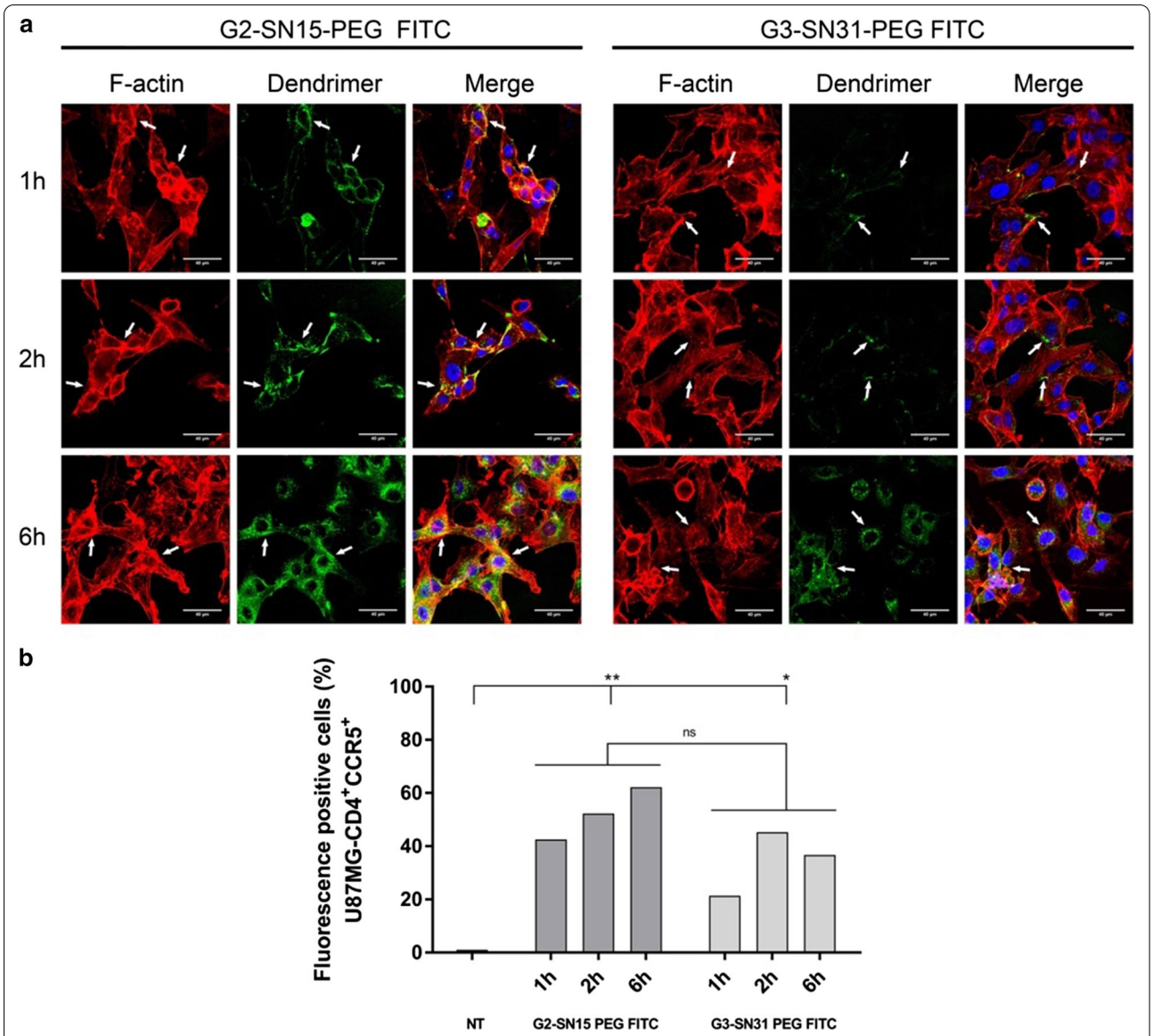

Fig. 6 Internalization of cationic dendrimers in U87MG-CD4$^+$CCR5$^+$ cells. Confocal microscopy images of U87MG-CD4$^+$CCR5$^+$ cells treated for 1, 2 or 6 h with G2-SN15-PEG FITC 1 µM and G3-SN31-PEG FITC 0.5 µM (green) FITC-labeled dendrimers. Cells were fixed and stained with Phalloidin (red, actin filaments) and DAPI (blue, nucleus). **a** Confocal images of random field. **b** Entry of FITC labeled dendrimers into PBMCs observed by flow cytometry at 1, 2 and 6 h post-treatment. *DAPI* 4′,6-Diamidino-2-phenylindole dihydrochloride

stable viral reservoirs and appearance of resistant strains [40–43]. The use of small RNAs is a powerful approach to target these problems, since a broad range of miRNAs has a negative impact on HIV-1 replication [28–30]. The delivery of miRNAs to infected cells constitutes a boundary for its efficient application. Nanotechnology is a strategy to address this issue, since it has previously shown to efficiently deliver small RNA molecules or small miRNAs [12–14]. Our group has carried out wide research about this topic, specifically related to the use of dendrimers in the context of HIV-1 infection [18, 23, 44, 45]. These three-dimensional hyperbranched nanostructures have modifiable edges which promote, for example, the formation of dendriplexes through the interplay among these edges, when positively charged, and the negatively charged backbone of small RNAs. We have analyzed the potential therapeutic effect of the use of four novel cationic dendrimers as delivery systems for different anti-HIV-1 miRNAs to control HIV-1 progression in PBMCs and U87MG-CD4$^+$CCR5$^+$ cells.

The initial phase of this study was to determine the biocompatibility of dendrimers on PBMCs and

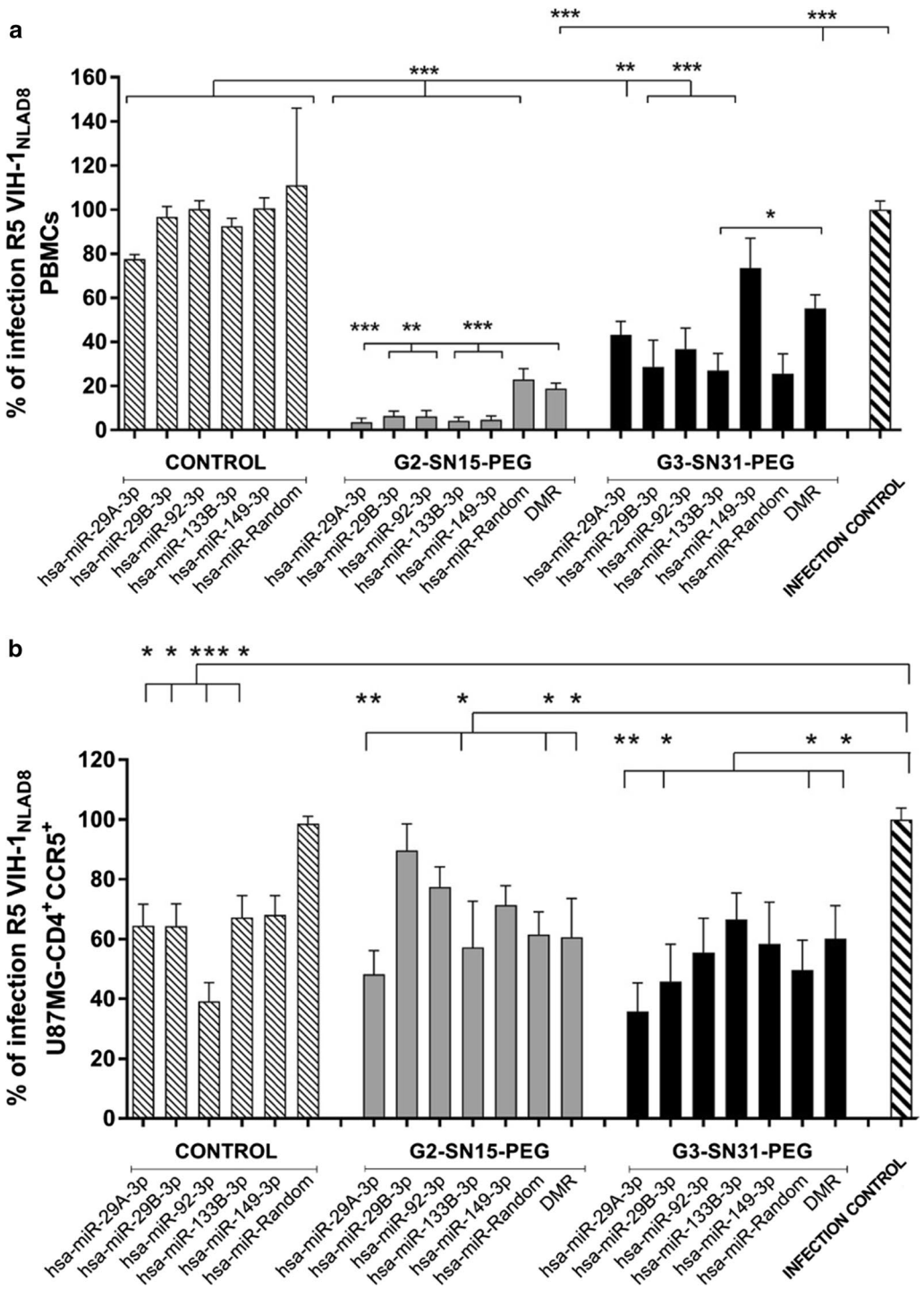

Fig. 7 HIV-1 inhibition of dendriplexes. Quantification of R5-HIV-1 infection in **a** PBMCs and **b** U87MG-CD4^{+}CCR5^{+} cells treated with dendriplexes. Infection was measured by titration of supernatants on TZM.bl cell line. Infection was inferred from the measurement of luciferase activity 48 h post-titration and was represented as fold change of percentage from HIV-1 infection control. Dendriplexes were formed with non-labeled G2-SN15-PEG or G3-SN31-PEG cationic dendrimer and control or anti-HIV-1 microRNAs (hsa-miR-29a-3p, hsa-miR-29b-3p, hsa-miR-92a-3p, hsa-miR-133b and hsa-miR-149-5p). Data are represented as mean ± SD of three individual experiments performed in triplicate. DMR: dendrimer. (*$p < 0.05$; **$p < 0.01$; ***$p < 0.001$)

U87MG-CD4$^+$CCR5$^+$ cell line. Cationic dendrimers interact with cell surface, which is negatively charged, producing nanoscale pores in the membrane increasing its permeability. This interaction affects the integrity of membrane depending on different characteristics of dendrimers, such as molecular size or presence of fluorescent markers that could lead to cell death [46]. Therefore, our four dendrimers were conjugated with PEG to mask some cationic groups reducing the toxicity and immunogenicity, and improving solubility, drug loading and drug delivery [32].

Cytotoxicity analysis, performed by MTT assay showed that G3-SN31-PEG FITC dendrimer had the highest toxicity rates followed by G2-SN15-PEG FITC, G3-SN31-PEG and G2-SN15-PEG dendrimers, respectively. As expected, our results show that larger molecular sizes and introduction of fluorescent labels enhance the cytotoxicity of compounds. Studies of genotoxicity, based on SCE assay, showed that non-labelled dendrimers can be used in vivo, did not cause genetic toxicity. It is important to note that these dendrimers could be not used if they affect the host genome and produced genetic changes. The fact that selected miRNAs are naturally present on host cell makes unnecessary to study genotoxicity of these dendrimers.

The capability of different PEGylated cationic dendrimers to complex with various miRNAs to form dendriplexes using the maximum non-toxic working concentrations was studied. Dendriplexes were formed by electrostatic interactions among positively charged functional groups at periphery of dendrimers and negatively charged backbone of small miRNAs [47]. G2-SN15-PEG and G3-SN31-PEG dendrimers can efficiently form dendriplexes after 2 h of incubation with different miRNA in agarose gel electrophoresis.

We also analyzed whether dendrimers conferred protection to miRNAs from RNase-mediated degradation and if dendrimer-miRNA bound could be disengaged in order to enable its binding mRNA. RNase protection assay showed that miRNAs are completely recovered from dendriplex after incubation with RNases, indicating that dendrimer-miRNA complex protects miRNAs from degradation. Moreover, dendriplexes can be completely dissociated when dealing with a binding site competitor, such as heparin. Moreover, dendrimer-miRNAs complex will act in case of piercing of plasmatic membrane of host cell, because heparin assay recreates this situation caused by the disparity in the number of charges due to different environments between cytoplasm and extracellular fluids, thus proving that dendrimers release complexed miRNA when internalizing in the host cell.

To evaluate how the addition of the miRNAs affects the properties of the dendrimer we studied the surface charge and stability by measuring the particle zeta potentials (ZP) and the particle size distribution by dynamic light scattering (DLS). Results indicated that both dendrimers are stable, and their surface charges are positive in solution. In addition, results showed a fall of the ZP value in third-generation dendrimer (G3-SN31-PEG) compared to second-generation dendrimer (G2-SN15-PEG), which can be explained on the basis of a more effective wrapping of the PEG moiety, because PEGylation reduces charge density, as previously described elsewhere [48]. When studying the effect of the complexation of miRNAs, values showed a small change of ZP values, confirming the formation of the dendriplexes without affecting the stability of the particles.

In terms of the particle size distribution, G2-SN15-PEG dendrimer was found to form aggregates probably due to a reorganization over time owing to interactions between different molecules when it is in solution. On the other hand, G3-SN31-PEG dendrimer was described as a single molecule and hsa-miR-29a-3p also presented low aggregation values. It would be expected for the hydrodynamic size of the complexes to be superior to that of the individual dendrimers as discrete particles. However, when forming the dendriplex with G2-SN15-PEG dendrimer aggregation values were lower, which could be explained because the introduction of the miRNA into the medium leads to more favorable electrostatic binding and contributes to more stable systems in solution without the need for aggregation by the dendrimer. The nanoconjugate formed with G3-SN31-PEG dendrimer and hsa-miR-29a-3p presented the expected increase in the hydrodynamic size after the formation of the complex. Changes in particle size distribution of the dendrimers, along with data obtained in electrophoresis assays, confirm the correct formation and stability of complexes.

The internalization of both FITC-labelled dendrimers in PBMCs and U87MG-CD4$^+$CCR5$^+$ cells confirm that these dendrimers could be used as carriers. Cationic dendrimers cross cell membranes with different effectiveness depending on dendrimer properties such as size or surface charge and cellular features such as and membrane chemical composition. These elements determine the affinity with which dendrimers are bound to cell surface: higher amounts of positive charges entail stronger interactions that lead to longer resident times on membrane and, thus, slower internalization [49]. This fact has been reflected in our results, where we can observe a higher internalization of G2-SN15-PEG FITC dendrimer in both cell lines studied compared to G3-SN15-PEG FITC dendrimer, probably due to a higher affinity with cell surface produced by the presence of more positive charges being a bigger molecule.

Regardless of this result, both dendrimers are able to internalize into host cells in less than 6 h and these two dendrimers present a resembling behavior inside the cells, showing that both dendrimers can be used as delivery systems.

After demonstrating that G3-SN31-PEG FITC and G2-SN15-PEG FITC dendrimers form stable dendriplexes that confer protection to different miRNAs and that can be efficiently delivered, we studied their anti-HIV-1 activities. This activity was tested in R5-HIV-1$NL_{(AD8)}$ infected PBMCs and U87MG-$CD4^+CCR5^+$ cells to determine whether the conjugation of both G3-SN31-PEG and G2-SN15-PEG non-labelled dendrimers with cellular anti-HIV-1 miRNAs improved the therapeutic effect. Our results showed that both dendrimers are able to significantly inhibit HIV-1 infection in both PBMCs and U87MG-CD4 + CCR5 cells. However, inhibition with dendriplexes was only significantly improved when treating PBMCs suggesting a specific behavior depending on cell lineage. The selected miRNAs cannot decrease the HIV-1 infection by themselves in PBMCs. They need the formation of complexes with dendrimers. The main objective was to prove that these novel cationic dendrimers can be used as delivery agents in order to replace current methods and develop a safer method with possible in vivo perspectives. Our results could fill the gap between the in vitro delivery researches and the possibility of implementing this technology in clinic, developing a new "from bench to patient" safe and effective technology.

Conclusion

In conclusion, the PEGylated carbosilane dendrimers G2-SN15-PEG and G3-SN31-PEG are valid delivery systems for miRNAs. Formation of dendriplexes provides miRNAs with protection against degradation and enables delivery to different cells. These dendriplexes specifically and significantly improve the anti-R5-HIV-1 activity of miRNAs, being good candidates to be used therapeutically to address the main problems that the HIV-1 infection still entails.

Methods

Cell lines

TZM.bl cell line (NIH AIDS Research and Reference Reagent Program, Germantown, MD, USA) is a human cervical epithelial carcinoma cell (HeLa cell line), that expresses CD4 receptor and CCR5 co-receptor and contains β-galactosidase and luciferase genes under control of long terminal repeat (LTR) regions of HIV-1 promoter [50]. U87MG-$CD4^+CCR5^+$ (NIH AIDS Research and Reference Reagent Program, Germantown, MD, USA) is a human astrocytoma (glioblastoma) cell line derived from U87MG to express CD4 receptor and CCR5 and CXCR4 co-receptors.

TZM-bl cell line was cultured in Dulbecco's Modified Eagle's Medium (DMEM) (Biochrom GmbH, Berlin, Germany) supplemented with 5% heat-inactivated fetal bovine serum (FBS) (Biochrom GmbH, Berlin, Germany), 2 mM L-glutamine (Lonza, Base, Switzerland) and a cocktail of antibiotics (125 mg/ml ampicillin, 125 mg/ml cloxacillin and 40 mg/ml gentamicin (Normon, Madrid, Spain)) at 37ºC with 5% CO2. U87MG-$CD4^+CCR5^+$ cell line was maintained in DMEM supplemented with 10% FBS, 2 mM L-glutamine and the aforementioned antibiotic cocktail at 37ºC with 5% CO2.

Primary cells

Buffy coats, acquired from healthy anonymous donors from the Transfusion Centre of Madrid (Madrid, Spain) following the current legislation, were used to obtain PBMCs on a Ficoll-Hypaque density gradient (Rafer) according to standard procedures of Spanish HIV HGM BioBank [51].

After the isolation, PBMCs were cultured (5×10^6/mL) in RPMI 1640 (Biochrom GmbH, Berlin, Germany) supplemented with 10% FBS, 2 mM L-glutamine, the aforesaid cocktail of antibiotics, 60 IU/mL of interleukin-2 (IL-2, Bachem, Budendorf, Switzerland) and 2 µg/mL of phytohemagglutinin (PHA) (Remel, Dartford, Kent, UK).

Viral isolates

Viral stock of CCR5-tropic R5-HIV-1$NL_{(AD8)}$ laboratory isolate was obtained by transient transfection with $pNL_{(AD8)}$ plasmid (NIH AIDS Research and Reference Reagent Program, Germantown, MD, USA) into HEK-293 T cell line (ATCC, Manassas, VA, USA). Viral stock was clarified by centrifugation and the viral titter was later evaluated using an HIV-1 p24gag enzyme-linked Immunosorbent assay (ELISA) kit (INNOTEST HIV, Antigen mAb, Innogenetics, Ghent, Belgium), as previously reported [52].

MicroRNAs

Five cellular miRNAs reported to have anti-HIV-1 activity were selected based on their homology with HIV-1 genome: hsa-miR-29a-3p, hsa-miR-29b-3p, hsa-miR-92a-3p, hsa-miR-133b and hsa-miR-149-5p (QUIAGEN, Hilden, Germany) [33, 34]. We also selected one miRNA with random sequence but similar length and no activity against HIV-1 as a negative control (QUIAGEN, Hilden, Germany). Sequence, HIV-1 genome target and effect on HIV-1 replication are shown in Table 4. Stock solutions of miRNAs (66,7 µM) and working concentrations (6670 nM) were prepared in nuclease-free water (Promega, Madrid Spain) and stored at − 20ºC.

Table 4 Sequence, HIV-1 target and effect on HIV-1 replication of selected anti-HIV-1 microRNAs and control microRNA

Name	Sequence	HIV-1 genome target	Effect on HIV-1 replication
miR-29a-3p	UAGCACCAUCUGAAAUCGGUUA	*Nef*/3'UTR	Negative
miR-29b-3p	UAGCACCAUUUGAAAUCAGUGUU	*Nef*/3'UTR	Negative
miR-92a-3p	UAUUGCACUUGUCCCGGCCUGU	*Pol*	Negative
miR-133b	UUUGGUCCCCUUCAACCAGCUA	*Env*	Negative
miR-149-5p	UCUGGCUCCGUGUCUUCACUCCC	*Gag*	Negative
miR-Control	UCACCGGGUGUAAAUCAGCUUG	-	None

Dendrimers and reagents

PEGylated cationic dendrimers G2-SN15-PEG and G3-SN31-PEG and their FITC-labelled forms were synthesized and tested according to the methods described by Dendrimers for Biomedical Applications Group of University of Alcalá (Madrid, Spain). Stock solutions of dendrimers (1 mM) and subsequent dilutions for working concentrations were prepared in nuclease-free water (Promega, Madrid Spain). The schematic structures of PEGylated cationic carbosilane dendrimers are represented in Fig. 8.

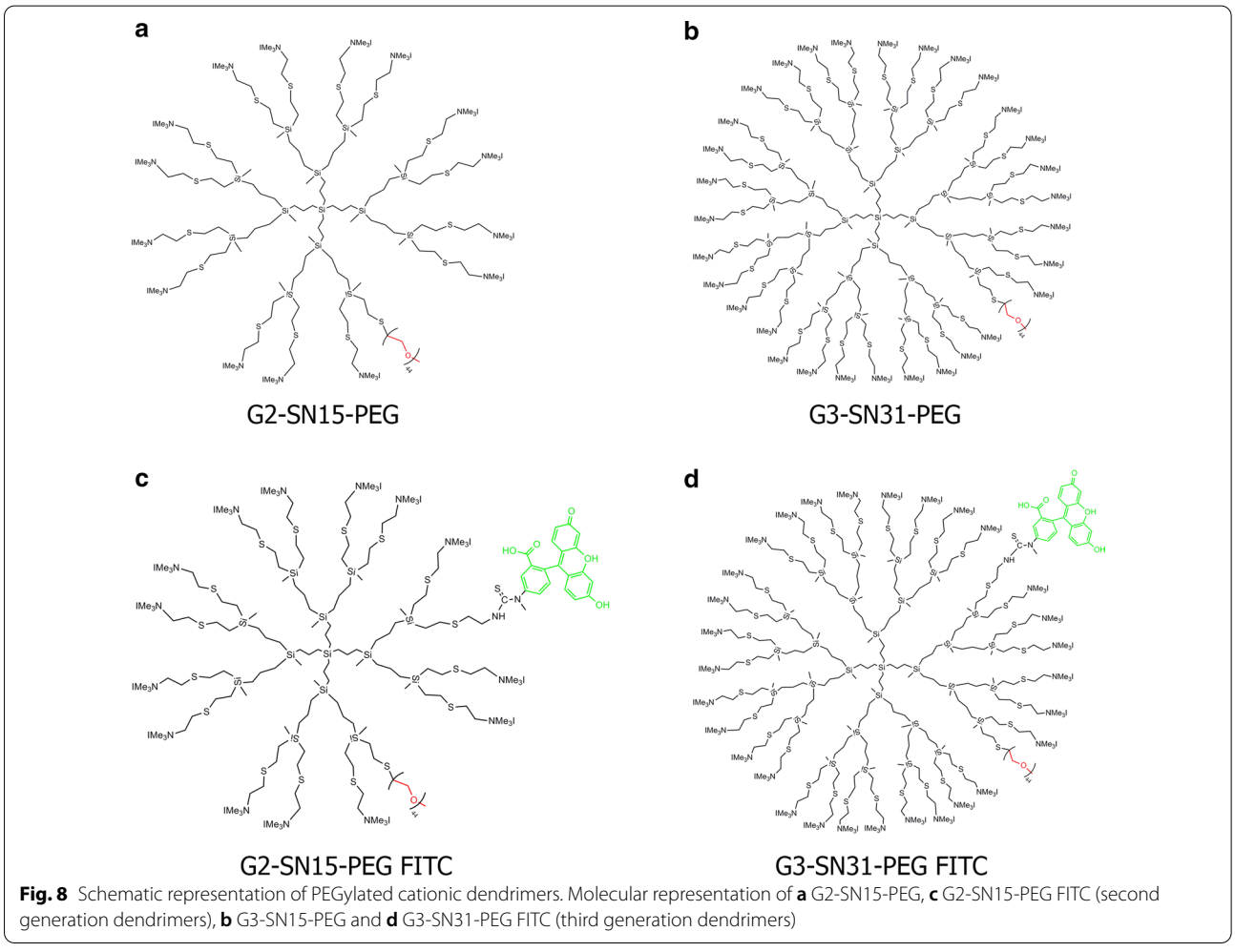

Fig. 8 Schematic representation of PEGylated cationic dendrimers. Molecular representation of **a** G2-SN15-PEG, **c** G2-SN15-PEG FITC (second generation dendrimers), **b** G3-SN15-PEG and **d** G3-SN31-PEG FITC (third generation dendrimers)

Mitochondrial activity assay

Mitochondrial activity was determined by the 3-(4–5-dimethylthiazol-2-yl)-2,5-diphenyltetrazolium bromide (MTT) assay (Sigma, St Louis, MO, USA) following manufacturer's instructions to establish the mitochondrial toxicity of the dendrimers. Briefly, 2×10^5 PBMCs or 7.5×10^3 U87MG-CD4$^+$CCR5$^+$ cells/well were seeded in 96-well plates and treated with different concentrations of dendrimers for 72 h. After incubation, culture medium was discarded and a 200 µL of a mixture of MTT/Opti-MEMTM solution (1:11) (Thermo Fisher Scientific, Waltham, MA, USA) was added. After 2 h, the reaction was stopped by removing the solution and dissolving the formazan crystals in 200 µL of dimethyl sulfoxide (DMSO, Honeywell, Charlotte, NC, USA) and absorbance was recorded in a Synergy 4 plate reader (BioTek, Winooski, VT, USA) at 490 nm. Ten per cent DMSO was used as cellular death control and culture medium as non-treated control. All measurements were performed in triplicate three times.

Genotoxicity of dendrimers

To assess the genotoxicity of non-labelled G2-SN15-PEG and G3-SN31-PEG dendrimers sister chromatids exchange (SCE) assay was performed in PBMCs. Cells were treated with G2-SN15-PEG 10 µM or G3-SN31-PEG 5 µM for 72 h. Radiation at 1 Gy was used as genotoxic positive control and non-treated cells were used as control of genetic viability. Cell cultures were then treated with 25 µM bromodeoxyuridine (BrdU) (Thermo Fisher Scientific, Waltham, MA, USA) to monitor second divisions. After 70 h, 0.1 µM/mL colcemid (Thermo Fisher Scientific, Waltham, MA, USA), a mitosis inhibitor, was added to cultures and, 2 h after, metaphases were extended and analyzed by fluorescence plus Giemsa (FPG). Briefly, cells were centrifuged 10 min at 600 g and the supernatant was discarded and 10 mL of 5.6 µg/mL potassium chloride (Merck KGaA, Darmstadt, Germany) was added. Cells were then centrifuged 10 min at 600 g, the supernatant was discarded, and the pellet was fixed with methanol/glacial acetic acid (3:1) (PanReac AppliChem, Madrid, Spain). This procedure was repeated 3 more times and the resulting metaphases were dropped over slides (Thermo Fisher Scientific, Waltham, MA, USA).

After 48 h maturing at 56ºC, slides were immersed in Hoechst solution (Sigma, St Louis, MO, USA) for 30 min, washed with water and immersed in McIlvaine buffer (0.55 mL citric acid plus 19.45 mL di-Sodium hydrogen phosphate) (Merck KGaA, Darmstadt, Germany), for 40 min in a thermostatic plate at 56ºC 5 cm away from UV light. Slides were then washed and stained with Giemsa (Merck KGaA, Darmstadt, Germany) for 7 min. Images were obtained with a Leica DM 5000 B Microscope and analyzed with Cytovision® software (Leica, Wetzlar, Germany).

Dendriplexes formation

Dendrimer-miRNA complexes were formed mixing the maximum non-toxic concentration of the different cationic dendrimers with 100 nM of the desired miRNAs in nuclease-free water (Promega, Madrid, Spain). The formation and stability of dendriplexes were evaluated by agarose gel electrophoresis after 2, 24 and 48 h of incubation at room temperature (RT). Samples were treated with Blue/Orange Loading Dye 6X (Promega, Madrid, Spain) and loaded on a gel with 2% agarose (Sigma, St Louis, MO, USA) and 0.01% GelRed® (Biotium, Fremont, CA, USA) in Tris–acetate-EDTA (TAE) buffer (PanReac AppliChem, Darmstadt, Germany) at 120 mV for 40 min on a PowerPac Universal power supply (Bio-Rad Laboratories, Hercules, CA, USA).

Heparin competition assay and RNase protection

Heparin exclusion and RNase protection assays were performed to test the capacity to disengage miRNAs from the complex and whether the formation of dendriplexes confers protection against RNases, respectively. Dendriplexes were formed within 2 h of incubation and were treated with 0.2 UI/µL of heparin (Lab Ramón Sala, Barcelona, Spain) for 5 min at RT and/or 1 µg/µL of RNase (Promega, Madrid, Spain) for 10 min at RT and loaded as described before.

Zeta potential and dynamic light scattering

Surface charge and stability of the dendrimers and dendriplexes were studied by measuring the zeta potential (ZP) and their distribution analyzed measuring the hydrodynamic size (diameter) by dynamic light scattering (DLS).

Dendrimer and dendriplexes samples were prepared in nuclease-free water (Promega, Madrid, Spain) using the maximum non-toxic concentrations (G2-SN15-PEG 10 µM and G3-SN15-PEG 5 µM) and hsa-miR-29A-3p (100 nM). For ZP, samples were loaded into folded capillary cells and measured using a voltage of 100 V. For DLS, samples were loaded into quartz cuvettes with pathlength 10 mm. Measurements were performed at 25ºC with a Zetasizer Nano ZS spectrometer (Malvern Instrument, Malvern, UK). Three measurements with fourteen cycles were made for each sample.

Confocal microscopy

Internalization of the dendrimers into cells was analyzed by confocal microscopy with a Leica TSC SPE Confocal Microscope (Leica, Wetzalar, Germany).

PBMCs were seeded at a density of 1×10^6 cells/well in 24-well plates and U87MG-CD4$^+$CCR5$^+$ cells were seeded at 7.5×10^3 cells in 12 mm circle cover slips (Thermo Fisher Scientific, Waltham, MA, USA) pretreated for 24 h with poly-L-Lysine (Sigma, St Louis, MO, USA). Cells were treated with the fluorescent dendrimers for 1 h, 2 h or 6 h at 37ºC. After incubation, handling PBMCs as suspension cells and U87MG-CD4$^+$CCR5$^+$ as adherent cells, cells were rinsed twice with 3% bovine serum albumin (BSA, Sigma, St Louis, MO, USA) phosphate buffered saline (PBS, Lonza, Base, Switzerland), fixed with 4% paraformaldehyde (PFA, Panreac, Barcelona, Spain) and permeabilized with 0.1% Triton 100X (Sigma, St Louis, MO, USA) for 15 min. Cells were then incubated with Alexa Fluor® 555 Phalloidin (Thermo Fisher Scientific, Waltham, MA, USA) for 1 h at RT for actin labelling and then rinsed with PBS 3% BSA. Lastly, cells were incubated with 4′,6-Diamidino-2-phenylindole dihydrochloride (DAPI, Sigma, St Louis, MO, USA) for nuclear visualization and mounted in microscope slides (Dako, Carpinteria, CA, USA) with fluorescent mounting media (Dako, Carpinteria, CA, USA).

Flow cytometry

The internalization of FITC labelled dendrimers was confirmed by flow cytometry. Briefly, 1×10^6 PBMCs or 1.5×10^4 U87MG-CD4$^+$CCR5$^+$ cells/well were seeded in 24-well plates and treated with the fluorescent dendrimers for 1, 2 or 6 h at 37ºC. After incubation, adherent cells were removed by trypsinization and rinsed with PBS 3% BSA. PBMCs were incubated with anti-CD3-PC5 (Beckman Coulter, Brea, CA, USA) for 30 min at RT and then rinsed with PBS 3% BSA. Viability was assessed in both cell lines with 7-Aminoactinomycin D (7-AAD) (Sigma, St Louis, MO, USA) following manufacturer's instructions in both cell lines. Lastly, cells were fixed with 4% PFA. Measurements were analyzed using Kaluza software (Beckman Coulter, Brea, CA, USA).

HIV-1 inhibition activity of the dendriplexes

Inhibition experiments were carried out to test the anti-R5-HIV-1 activity of the different dendriplexes. PBMCs were seeded at a density of 1×10^6 cells/well in 24-well plates and U87MG-CD4$^+$CCR5$^+$ at 7.5×10^3 cells/well in 96-well plates. Afterwards, cells were infected with R5-HIV-1NL$_{(AD8)}$ strain (15 ng p24/10^6 cells) and treated with the desired dendriplexes previously incubated for 2 h to allow the complex formation. 72 h after the infection, supernatants were collected and titrated or frozen at − 80 ºC.

Supernatant titration

Viral infectivity was inferred by luciferase activity measurements performed following supernatant titration on TZM.bl cells with the previously collected supernatants. TZM.bl cells were seeded at a density of 1×10^4 cells/well in 96-well plates. Subsequently, medium was removed and replaced with 100 µL of new medium and 100 µL of supernatants from PBMCs or U87MG-CD4$^+$CCR5$^+$ infected and treated cells. 48 h post-titration, medium was removed, and cells were lysed with 50 µL of the Cell Culture Lysis 5X Reagent (Promega, Madrid Spain) for 30 min at 4ºC. Finally, 25 µL of the lysates were transferred to a white clear bottom plate and 25 µL of Luciferase Assay Reagent (Promega, Madrid, Spain) were added right before reading the luciferase activity in a Synergy 4 plate reader at a 135/200 nm.

Statistics

GraphPad software Prism v.5.0 (GraphPad Software, San Diego, CA, USA) was used for the different statistical analysis performed. Data with three replicates are displayed as bars ± SD. A p-value of ≤ 0.05 was considered to be statistically significant ($^*p < 0.05$; $^{**}p < 0.01$; $^{***}p < 0.001$).

Acknowledgements

We would like to thank Vanessa Cañadilla Martín (Consejería de Educación e Investigación de la Comunidad de Madrid y Fondo Social Europeo (Grant nº.: PEJ-2018-TL/BMD-11529)) and Patricia Pola for their expert technical assistance.

Authors' contributions

Study Design and Supervision: MFMA, JJL Experimental design: RII, RRE, MDM, GR* LCT*, MFJ* (*provided the dendrimers), MFMA, JJL. Data acquisition: RII, RRE, MDM. Data analysis: RII, RRE, MDM, MFMA, JJL. Manuscript writing: RII, RRE, MFMA, JJL Manuscript editing: RII, RRE, MFMA, JJL. All authors read and approved the final manuscript.

Funding

This work was (partially) supported by the RD16/0025/0019 projects as part of Acción Estratégica en Salud, Plan Nacional de Investigación Científica, Desarrollo e Innovación Tecnológica (2013–2016) and cofinanced by Instituto de Salud Carlos III (ISC-III-Subdirección General de Evaluación) and Fondo Europeo de Desarrollo Regional (FEDER), RETIC PT17/0015/0042, Fondo de Investigación Sanitaria (FIS) (PI19/01638, PI17/01115), EPIICAL project, CTQ2017-86224-P (MINECO), Comunidad de Madrid (B2017/BMD-3703; B2017/BMD-3733) and and project SBPLY/17/180501/000358 JCCM. CIBER-BBN is an initiative funded by the VI National R&D&i Plan 2008–2011, Iniciativa Ingenio 2010, the Consolider Program, and CIBER Actions and financed by the ISC-III with assistance from the European Regional Development Fund (PIE14/00061). This work has been supported partially by a EUROPARTNER: Strengthening and spreading international partnership activities of the Faculty of Biology and Environmental Protection for interdisciplinary research and innovation of the University of Lodz Programme: NAWA International Academic Partnership Programme. This article/publication is based upon work from COST Action CA 17140 "Cancer Nanomedicine from the Bench to the Bedside" supported by COST (European Cooperation in Science and Technology). Programa de Investigación de la Consejería de Sanidad de la Comunidad de Madrid to JLJ.

Availability of data and materials
Not applicable.

Declarations

Ethics approval and consent to participate
Not applicable.

Consent for publication
Not applicable.

Competing interests
The authors declare that they have no competing interests.

Author details
[1]Laboratorio InmunoBiología Molecular, Hospital General Universitario Gregorio Marañón (HGUGM), Instituto Investigación Sanitaria Gregorio Marañón (IiSGM), Spanish HIV HGM BioBanco, Madrid, Spain. [2]Plataforma de Laboratorio (Inmunología), HGUGM, IiSGM, Spanish HIV HGM BioBank, Madrid, Spain. [3]Laboratorio Dosimetría Biológica, HGUGM, IiSGM, Madrid, Spain. [4]Departmento Química Orgánica Y Química Inorgánica E Instituto de Investigación Química "Andrés M. del Río" (IQAR), Universidad de Alcalá (IRYCIS), Campus Universitario, 28871 Madrid, Spain. [5]Networking Research Center On Bioengineering, Biomaterials and Nanomedicine (CIBER-BBN, Madrid, Spain.

Received: 17 January 2021 Accepted: 18 May 2021
Published online: 28 May 2021

References

1. Bissel SJ, Wiley CA. Human immunodeficiency virus infection of the brain: pitfalls in evaluating infected/affected cell populations. Brain Pathol. 2004;14(1):97–108.
2. Zayyad Z, Spudich S. Neuropathogenesis of HIV: from initial neuroinvasion to HIV-associated neurocognitive disorder (HAND). Curr HIV/AIDS Rep. 2015;12(1):16–24.
3. A I. Guidelines for the use of antiretroviral agents in adults and adolescents living with HIV. . Department of Health and Human Services; 2019 [updated 10 July 2019]. https://aidsinfo.nih.gov/guidelines/html/1/adult-and-adolescent-arv/0.
4. EAC S. Guidelines for the clinical management and treatment of HIV-infected adults in Europe. 2018. https://www.eacsociety.org/guidelines/.
5. Diallo M, Adekpedjou R, Ahouada C, Ngangue P, Ly BA. Impact of pre-antiretroviral therapy CD4 counts on drug resistance and treatment failure: a systematic review. AIDS Rev. 2020;22(2):78–92.
6. Inzaule SC, Jordan MR, Bello G, Wadonda-Kabondo N, Mounerou S, Mbulli IA, et al. High levels of resistance to nucleoside/nucleotide reverse transcriptase inhibitors in newly diagnosed antiretroviral treatment-naive children in sub-Saharan Africa. AIDS. 2020;34(10):1567–70.
7. Sylla M, Dolo O, Maiga AI, Traore FT, Coulibaly YA, Togo J, et al. Second-line antiretroviral therapy failure and characterization of HIV-1 drug resistance patterns in children in Mali. Arch Pediatr. 2019;26(5):254–8.
8. Cantero-Perez J, Grau-Exposito J, Serra-Peinado C, Rosero DA, Luque-Ballesteros L, Astorga-Gamaza A, et al. Resident memory T cells are a cellular reservoir for HIV in the cervical mucosa. Nat Commun. 2019;10(1):4739.
9. Chatzidimitriou D, Tsotridou E, Grigoropoulos P, Skoura L. HIV-1: towards understanding the nature and quantifying the latent reservoir. Acta Virol. 2020;64(1):3–9.
10. Reeves DB, Duke ER, Wagner TA, Palmer SE, Spivak AM, Schiffer JT. A majority of HIV persistence during antiretroviral therapy is due to infected cell proliferation. Nat Commun. 2018;9(1):4811.
11. Wallet C, De Rovere M, Van Assche J, Daouad F, De Wit S, Gautier V, et al. Microglial cells: the main HIV-1 reservoir in the brain. Front Cell Infect Microbiol. 2019;9:362.
12. Dahlman JE, Barnes C, Khan O, Thiriot A, Jhunjunwala S, Shaw TE, et al. In vivo endothelial siRNA delivery using polymeric nanoparticles with low molecular weight. Nat Nanotechnol. 2014;9(8):648–55.
13. Ratajczak K, Krazinski BE, Kowalczyk AE, Dworakowska B, Jakiela S, Stobiecka M. Optical biosensing system for the detection of survivin mRNA in colorectal cancer cells using a graphene oxide carrier-bound oligonucleotide molecular beacon. Nanomaterials (Basel). 2018;8(7):510.
14. Song WJ, Du JZ, Sun TM, Zhang PZ, Wang J. Gold nanoparticles capped with polyethyleneimine for enhanced siRNA delivery. Small. 2010;6(2):239–46.
15. Stobiecka M, Hepel M. Double-shell gold nanoparticle-based DNA-carriers with poly-L-lysine binding surface. Biomaterials. 2011;32(12):3312–21.
16. Cena-Diez R, Martin-Moreno A, de la Mata FJ, Gomez-Ramirez R, Munoz E, Ardoy M, et al. G1–S4 or G2–S16 carbosilane dendrimer in combination with Platycodin D as a promising vaginal microbicide candidate with contraceptive activity. Int J Nanomedicine. 2019;14:2371–81.
17. Genebat M, Tarancon-Diez L, Pulido I, Alvarez-Rios AI, Munoz-Fernandez MA, Ruiz-Mateos E, et al. Hepatitis C virus and cumulative infections are associated with atherogenic cardiovascular events in HIV-infected subjects. Antiviral Res. 2019;169:104527.
18. Guerrero-Beltran C, Rodriguez-Izquierdo I, Serramia MJ, Araya-Duran I, Marquez-Miranda V, Gomez R, et al. Anionic carbosilane dendrimers destabilize the GP120-CD4 complex blocking HIV-1 entry and cell to cell fusion. Bioconjug Chem. 2018;29(5):1584–94.
19. Relano-Rodriguez I, Juarez-Sanchez R, Pavicic C, Munoz E, Munoz-Fernandez MA. Polyanionic carbosilane dendrimers as a new adjuvant in combination with latency reversal agents for HIV treatment. J Nanobiotechnology. 2019;17(1):69.
20. Sepulveda-Crespo D, de la Mata FJ, Gomez R, Munoz-Fernandez MA. Sulfonate-ended carbosilane dendrimers with a flexible scaffold cause inactivation of HIV-1 virions and gp120 shedding. Nanoscale. 2018;10(19):8998–9011.
21. Bermejo JF, Ortega P, Chonco L, Eritja R, Samaniego R, Mullner M, et al. Water-soluble carbosilane dendrimers: synthesis biocompatibility and complexation with oligonucleotides; evaluation for medical applications. Chemistry. 2007;13(2):483–95.
22. Gonzalo T, Clemente MI, Chonco L, Weber ND, Diaz L, Serramia MJ, et al. Gene therapy in HIV-infected cells to decrease viral impact by using an alternative delivery method. ChemMedChem. 2010;5(6):921–9.
23. Perise-Barrios AJ, Jimenez JL, Dominguez-Soto A, de la Mata FJ, Corbi AL, Gomez R, et al. Carbosilane dendrimers as gene delivery agents for the treatment of HIV infection. J Control Release. 2014;28(184):51–7.
24. Weber N, Ortega P, Clemente MI, Shcharbin D, Bryszewska M, de la Mata FJ, et al. Characterization of carbosilane dendrimers as effective carriers of siRNA to HIV-infected lymphocytes. J Control Release. 2008;132(1):55–64.
25. Palmerston Mendes L, Pan J, Torchilin VP. Dendrimers as nanocarriers for nucleic acid and drug delivery in cancer therapy. Molecules. 2017;22(9):1401.
26. Balasubramaniam M, Pandhare J, Dash C. Are microRNAs important players in HIV-1 infection? An update. Viruses. 2018;10(3):110.
27. Gulyaeva LF, Kushlinskiy NE. Regulatory mechanisms of microRNA expression. J Transl Med. 2016;14(1):143.
28. Huang J, Wang F, Argyris E, Chen K, Liang Z, Tian H, et al. Cellular microRNAs contribute to HIV-1 latency in resting primary CD4+ T lymphocytes. Nat Med. 2007;13(10):1241–7.
29. Nathans R, Chu CY, Serquina AK, Lu CC, Cao H, Rana TM. Cellular microRNA and P bodies modulate host-HIV-1 interactions. Mol Cell. 2009;34(6):696–709.
30. Swaminathan G, Navas-Martin S, Martin-Garcia J. MicroRNAs and HIV-1 infection: antiviral activities and beyond. J Mol Biol. 2014;426(6):1178–97.
31. Whitehead KA, Langer R, Anderson DG. Knocking down barriers: advances in siRNA delivery. Nat Rev Drug Discov. 2009;8(2):129–38.
32. Suk JS, Xu Q, Kim N, Hanes J, Ensign LM. PEGylation as a strategy for improving nanoparticle-based drug and gene delivery. Adv Drug Deliv Rev. 2016;99(Pt A):28–51.
33. Ahluwalia JK, Khan SZ, Soni K, Rawat P, Gupta A, Hariharan M, et al. Human cellular microRNA hsa-miR-29a interferes with viral nef protein expression and HIV-1 replication. Retrovirology. 2008;23(5):117.
34. Houzet L, Klase Z, Yeung ML, Wu A, Le SY, Quinones M, et al. The extent of sequence complementarity correlates with the potency of cellular miRNA-mediated restriction of HIV-1. Nucleic Acids Res. 2012;40(22):11684–96.
35. Gonzalez-Beltran F, Morales-Ramirez P. In vivo repair during G1 of DNA lesions eliciting sister chromatid exchanges induced by

methylnitrosourea or ethylnitrosourea in BrdU substituted or unsubstituted DNA in murine salivary gland cells. Mutat Res. 1999;425(2):239–47.
36. Gonzalez-Beltran F, Morales-Ramirez P. Repairability during G1 of lesions eliciting sister chromatid exchanges induced by methylmethanesulfonate or ethylmethanesulfonate in bromodeoxyuridine-substituted and unsubstituted DNA strands. Mutagenesis. 2003;18(1):13–7.
37. Matsuoka A, Lundin C, Johansson F, Sahlin M, Fukuhara K, Sjoberg BM, et al. Correlation of sister chromatid exchange formation through homologous recombination with ribonucleotide reductase inhibition. Mutat Res. 2004;547(1–2):101–7.
38. Laskey SB, Siliciano RF. A mechanistic theory to explain the efficacy of antiretroviral therapy. Nat Rev Microbiol. 2014;12(11):772–80.
39. Saylor D, Dickens AM, Sacktor N, Haughey N, Slusher B, Pletnikov M, et al. HIV-associated neurocognitive disorder–pathogenesis and prospects for treatment. Nat Rev Neurol. 2016;12(4):234–48.
40. Blankson JN, Persaud D, Siliciano RF. The challenge of viral reservoirs in HIV-1 infection. Annu Rev Med. 2002;53:557–93.
41. Clutter DS, Jordan MR, Bertagnolio S, Shafer RW. HIV-1 drug resistance and resistance testing. Infect Genet Evol. 2016;46:292–307.
42. Pierson T, McArthur J, Siliciano RF. Reservoirs for HIV-1: mechanisms for viral persistence in the presence of antiviral immune responses and antiretroviral therapy. Annu Rev Immunol. 2000;18:665–708.
43. Taylor BS, Hammer SM. The challenge of HIV-1 subtype diversity. N Engl J Med. 2008;359(18):1965–6.
44. Rodriguez-Izquierdo I, Natalia C, Garcia F, Los Angeles Munoz-Fernandez M. G2–S16 sulfonate dendrimer as new therapy for treatment failure in HIV-1 entry inhibitors. Nanomedicine. 2019;14(9):1095–107.
45. Sepulveda-Crespo D, Serramia MJ, Tager AM, Vrbanac V, Gomez R, De La Mata FJ, et al. Prevention vaginally of HIV-1 transmission in humanized BLT mice and mode of antiviral action of polyanionic carbosilane dendrimer G2–S16. Nanomedicine. 2015;11(6):1299–308.
46. Jain K, Kesharwani P, Gupta U, Jain NK. Dendrimer toxicity: let's meet the challenge. Int J Pharm. 2010;394(1–2):122–42.
47. Liu X, Rocchi P, Peng L. Dendrimers as non-viral vectors for siRNA delivery. New J Chem. 2012;36(2):256–63.
48. Somani S, Laskar P, Altwaijry N, Kewcharoenvong P, Irving C, Robb G, et al. PEGylation of polypropylenimine dendrimers: effects on cytotoxicity, DNA condensation, gene delivery and expression in cancer cells. Sci Rep. 2018;8(1):9410.
49. Albertazzi L, Serresi M, Albanese A, Beltram F. Dendrimer internalization and intracellular trafficking in living cells. Mol Pharm. 2010;7(3):680–8.
50. Wei X, Decker JM, Liu H, Zhang Z, Arani RB, Kilby JM, et al. Emergence of resistant human immunodeficiency virus type 1 in patients receiving fusion inhibitor (T-20) monotherapy. Antimicrob Agents Chemother. 2002;46(6):1896–905.
51. Garcia-Merino I, de Las CN, Jimenez JL, Gallego J, Gomez C, Prieto C, et al. The Spanish HIV BioBank: a model of cooperative HIV research. Retrovirology. 2009;9(6):27.
52. Garcia-Broncano P, Cena-Diez R, de la Mata FJ, Gomez R, Resino S, Munoz-Fernandez MA. Efficacy of carbosilane dendrimers with an antiretroviral combination against HIV-1 in the presence of semen-derived enhancer of viral infection. Eur J Pharmacol. 2017;15(811):155–63.

Publisher's Note

pharmaceutics

MDPI

Article

Prevention of *Herpesviridae* Infections by Cationic PEGylated Carbosilane Dendrimers

Elena Royo-Rubio [1,2], Vanessa Martín-Cañadilla [1,2], Marco Rusnati [3], Maria Milanesi [3], Tania Lozano-Cruz [4,5], Rafael Gómez [4,5], José Luís Jiménez [2] and Maria Ángeles Muñoz-Fernández [1,*]

1 Laboratorio InmunoBiologia Molecular, Instituto Investigacion Sanitaria Gregorio Maranon (IiSGM), Hospital General Universitario Gregorio Maranon (HGUGM), 28009 Madrid, Spain; elena.royo@iisgm.com (E.R.-R.); vanessa.canadilla@iisgm.com (V.M.-C.)
2 Plataforma de Laboratorio (Inmunologia), HGUGM, IiSGM, Spanish HIV HGM BioBank, 28009 Madrid, Spain; jjimenezf.hgugm@salud.madrid.org
3 Department of Molecular and Translational Medicine, University of Brescia, 25123 Brescia, Italy; marco.rusnati@unibs.it (M.R.); m.milanesi006@unibs.it (M.M.)
4 Departmento Quimica Organica y Quimica Inorganica, Instituto de Investigacion Quimica "Andres M. del Rio" (IQAR), Universidad de Alcalá (IRYCIS), Campus Universitario, 28871 Madrid, Spain; tania.lozano@uah.es (T.L.-C.); rafael.gomez@uah.es (R.G.)
5 Networking Research Center on Bioengineering, Biomaterials and Nanomedicine (CIBER-BBN), 28029 Madrid, Spain
* Correspondence: mmunoz.hgugm@gmail.com or mmunoz.hgugm@salud.madrid.org

Abstract: Infections caused by viruses from the *Herpesviridae* family produce some of the most prevalent transmitted diseases in the world, constituting a serious global public health issue. Some of the virus properties such as latency and the appearance of resistance to antiviral treatments complicate the development of effective therapies capable of facing the infection. In this context, dendrimers present themselves as promising alternatives to current treatments. In this study, we propose the use of PEGylated cationic carbosilane dendrimers as inhibitors of herpes simplex virus 2 (HSV-2) and human cytomegalovirus (HCMV)infections. Studies of mitochondrial toxicity, membrane integrity, internalization and viral infection inhibition indicated that G2-SN15-PEG, G3-SN31-PEG, G2-SN15-PEG fluorescein isothiocyanate (FITC) labeled and G3-SN31-PEG-FITC dendrimers are valid candidates to target HSV-2 and HCMV infections since they are biocompatible, can be effectively internalized and are able to significantly inhibit both infections. Later studies (including viral inactivation, binding inhibition, heparan sulphate proteoglycans (HSPG)binding and surface plasmon resonance assays) confirmed that inhibition takes place at first infection stages. More precisely, these studies established that their attachment to cell membrane heparan sulphate proteoglycans impede the interaction between viral glycoproteins and these cell receptors, thus preventing infection. Altogether, our research confirmed the high capacity of these PEGylated carbosilane dendrimers to prevent HSV-2 and HCMV infections, making them valid candidates as antiviral agents against *Herpesviridae* infections.

Keywords: *Herpesviridae*; cationic dendrimers; HSPG; VHS-2 infection; HCMV infection; nanotechnology; inhibition

Citation: Royo-Rubio, E.; Martín-Cañadilla, V.; Rusnati, M.; Milanesi, M.; Lozano-Cruz, T.; Gómez, R.; Jiménez, J.L.; Muñoz-Fernández, M.Á. Prevention of *Herpesviridae* Infections by Cationic PEGylated Carbosilane Dendrimers. *Pharmaceutics* **2022**, *14*, 536. https://doi.org/10.3390/pharmaceutics14030536

Academic Editor: Melgardt de Villiers

Received: 31 January 2022
Accepted: 23 February 2022
Published: 28 February 2022

1. Introduction

Herpesviridae is a large family of enveloped double-stranded DNA viruses that comprises a wide variety of herpesviruses with different biological characteristics, but that have in common basic properties such as their ability to infect animals (including humans), their morphology, their genetic complexity and a high regulated transcription [1].

The International Committee on Taxonomy of Viruses (ICTV) established the division of this family in three subfamilies: (i) *Alfaherpesviridae*, (ii) *Gammaherpesviridae*, and (iii) *Betaherpesviridae* [2]. In turn, they are divided into different subtypes, including herpes simplex

virus 1 and 2 (HSV-1 and HSV-2), Epstein–Barr virus (EBV), varicella zoster virus (VZV), or human cytomegalovirus (HCMV). Those are among the most widespread pathogens in the word; in fact, more than 90% of adults have been infected with one of these subtypes [3,4]. These viruses are able to infect a wide range of cells and the pathogenesis of the infection can range from mild lytic infections to severe persistent and latent infections with many recurrences, and there is still no cure [5].

One of the most prevalent infections is the one produced by HSV-2 which, according with the latest available data, affects nearly 500 million people, mainly women from Africa, aged between 15 to 49 years old [6]. This infection, almost entirely sexually transmitted, produces symptoms such as ulcers on the external genitalia and perineum, dysuria, and painful inguinal lymphadenopathy. Other rare complications caused by HSV-2 infection are lip lesions, herpetic hepatitis, or aseptic meningitis [7]. Another concerning infection is the one produced by HCMV; transmission of this virus may occur transplacentally, through breastfeeding, by intimate contact or transplantation [8]. Congenital infection is estimated in between 0.7 and 5% of all births, and is the leading cause of neurological impairment in infants, including hearing and vision loss, microcephaly, or developmental and motor delay. In adults, HCMV is mainly asymptomatic but can lead to life-threatening diseases in immunocompromised individuals, producing manifestations such as mononucleosis-like syndrome, tissue-invasive disease, neutropenia, interstitial pneumonia or autoimmune phenomena (vasculitis, scleroderma, systemic lupus erythematosus, etc.) [9].

Virions of the *Herpesviridae* family have four main shared structural components: a core in which the dsDNA is wrapped, encased in an icosahedral capsid composed of 12 pentameric and 150 hexameric capsomers, coated with a tegument formed by variable amounts of globular material and an envelope surrounding the structure formed by different proteins and glycoproteins in a lipidic bilayer [10]. Initial contact between viral envelope glycoproteins (mainly gB, gH and gL) and cell membrane takes place usually through different types of cell proteoglycans, usually heparan sulphate proteoglycans (HSPGs) [11]. This occurs between the negatively charged sulphated groups of the heparin-like glycosaminoglycan (GAG) chains of HSPGs and stretches of basic amino acids (referred as heparin-binding domains) present within the viral glycoproteins [11–13]. This first association with HSPGs usually favours the following binding of the virus to its specific entry receptor and hence infection. Herpesviruses have extensive cell tropism, with a wide variety of entry routes that depend on viral determinants and cell types; however, in all cases, these interactions trigger conformational changes which lead to membrane fusion and subsequent viral entry [14].

Currently, there is no treatment that completely clearances HSV-2 and HCMV, mainly due to the capacity of these viruses to establish latent infections in the host and to the appearance of resistance against these drugs. Ongoing therapies for HSV-2 infections are based on nucleoside analogues to inhibit DNA polymerases, such as acyclovir, valacyclovir, or famciclovir in order to control viral replication, disease progression, recurrences and transmission [15]. Related to HCMV, infants with congenital CMV infection and people with immunodeficiencies are mostly treated with ganciclovir or its pro-drug valganciclovir, other inhibitors of DNA polymerases based on nucleoside analogues [16]. These treatments have proved effective in the prevention and treatment of different CMV infections, including retinitis, gastrointestinal manifestations, pneumonia, polyradiculopathy or mononeuritis [17].

The absence of a definitive therapy, the fact that herpesviruses have a broad cell tropism, and the appearance of resistances against existing treatments makes it mandatory to develop new therapeutic approaches to face the present situation. Our group has carried out broad research focused on the use of nanotechnology against viral infections [18–21]. Specifically, these works are based on the use of dendrimers, which are three-dimensional hyperbranched molecules formed by a nuclear core around which branched units (named dendrons) are built; these dendrons present diverse functional groups on their periphery, which endow unique physicochemical characteristics [22,23]. These molecules are charac-

terized by a controlled synthesis, high biocompatibility, low polydispersity or polyvalency which make them better instruments than other polymers to face viral infections [24,25]. In this work, we present the use of four PEGylated cationic carbosilane dendrimers (PCCDs), G2-SN15-PEG, G3-SN31-PEG, G2-SN15-PEG-FITC and G3-SN31-PEG-FITC, which are characterized by the presence of positively charged functional terminal groups and PEGylation residues [26]. These two features make them great candidates to be used against *Herpesviridae* infections due to their improved biocompatibility and the positive charges at the periphery which can bind to HSPGs, thus masking these receptors and preventing further viral infections [27]. Hence, the objective of this work is to develop a new promising therapy against HSV-2 and HCMV infections based on the use of PCCDs as inhibitors of the interaction between viral glycoproteins and cell HSPGs.

2. Materials and Methods

2.1. Cell Lines

The Vero cell line, a fibroblast-like kidney cell from the African green monkey, was obtained from the American Type Culture Collection (ATCC) (CCL-81^{TM}, ATCC, Manassas, VA, USA). Cells were cultured in Dulbecco's modified Eagle's medium (DMEM) (Biochrom GmbH, Berlin, Germany) supplemented with 5% heat-inactivated fetal bovine serum (FBS) (Biochrom GmbH, Berlin, Germany), 2 mM L-glutamine (Lonza, Base, Switzerland), and a cocktail of antibiotics formed by 125 mg/mL ampicillin, 125 mg/mL cloxacillin and 40 mg/mL gentamicin (Normon, Madrid, Spain).

The MRC-5 cell line, a human fibroblast lung cell, was obtained from ATCC (CCL-171^{TM}, ATCC, Manassas, VA, USA). This cell line was maintained in Eagle's minimum essential medium (EMEM) (ATCC, Manassas, VA, USA) supplemented with 10% FBS, 2 mM L-glutamine, and the previously mentioned cocktail of antibiotics. Both cell lines were cultured at 37 °C with 5% CO_2.

2.2. Viral Isolates

Viral strain HSV-2_{333} (GenBank accession number LS480640, NIH, Bethesda, MD, USA) and $HCMV_{AD-169}$ (ATCC VR-538^{TM}, ATCC, Manassas, VA, USA) were grown and propagated in Vero and MRC-5 cells, respectively, and titrated by plaque assay with serial dilutions as previously described [28,29]. After ultracentrifugation, stock aliquots were stored at −80 °C.

2.3. Dendrimers and Reagents

PEGylated cationic carbosilane dendrimers (PCCDs)—G2-SN15-PEG and G3-SN31-PEG—and their FITC-labelled forms were synthesized according to methods reported by Dendrimers for Biomedical Applications Group of the University of Alcalá (Alcalá de Henares, Madrid, Spain) [26]. Stock solutions of dendrimers (1 mM) and their subsequent dilutions were prepared with nuclease-free water (Promega, Madrid, Spain). Table 1 includes a brief description of these dendrimers.

Table 1. Characterization of PEGylated cationic carbosilane dendrimers.

Nomenclature	Molecular Formula	Functional Groups	Molecular Weight (g/mol)
G2-SN15-PEG	$C_{190}H_{438}I_{15}N_{14}O_{17}S_{16}Si_{13}$	NMe_3 and PEG	5987.31
G3-SN31-PEG	$C_{420}H_{969}I_{31}N_{31}O_{44}S_{32}Si_{29}$	NMe_3 and PEG	12,926.92
G2-SN15-PEG FITC	$C_{209}H_{445}I_{14}N_{16}O_{22}S_{17}Si_{13}$	NMe_3, PEG and FITC	6221.74
G3-SN31-PEG FITC	$C_{439}H_{969}I_{30}N_{32}O_{49}S_{33}Si_{29}$	NMe_3, PEG and FITC	13,161.34

Acliclovir 50 mg (Selleckchem, Houston, TX, USA) was purchased as a lyophilised product and reconstituted into a 10 mM dilution with dimethyl sulfoxide (DMSO, Honeywell, Charlotte, NC, USA). Ganciclovir 500 mg (Hoffmann-La Roche, Basel, Switzerland) was also purchased as a lyophilised product and reconstituted into a 5.4 mg/mL dilution with nuclease-free water (Promega, Madrid, Spain).

Heparin (13.6 kDa) was obtained from Laboratori Derivati Organici Spa (Milan, Italy). Heparinase II from *Flavobacterium heparinum* was obtained from Merck KGaA (Merck Group, Darmstadt, Germany).

2.4. Mitochondrial Activity Assay

Evaluation of the dendrimer-induced mitochondrial toxicity was done by the MTT assay (Sigma, St Louis, MO, USA). This assay, based on the reduction of the 3-(4-5-dimethylthiazol-2-yl)-2,5-diphenyltetrazolium bromide (MTT) into formazan crystals, allows determination of the cellular mitochondrial metabolism. Briefly, following manufacturer's instructions, Vero and MRC-5 cells were seeded at a density of 1.5×10^4 cells/well into 96-well plates. After incubating cells for 24 h at 37 °C, cells were treated with different concentrations of PCCDs for 48 h and 6 days, respectively, to ensure that this treatment would not affect viability during inhibition experiments. After incubation, the medium was discarded and a solution formed by MTT (5 mg/mL) and Opti-MEM^{TM} (Thermo Fisher Scientific, Waltham, MA, USA) (1:11) was added. Two hours later, the reaction was stopped by removing the solution and dissolving formazan crystals in DMSO (Honeywell, Charlotte, NC, USA). Absorbance was recorded in a Synergy 4 plate reader (BioTek, Winooski, VT, USA) at 490 nm. Culture medium was used as non-treated control and DMSO 10% as cellular death control. Measurements were performed in triplicate.

2.5. Membrane Integrity Assay

Determination of cellular toxicity was done by the lactate dehydrogenase (LDH) CytoTox 96® Non-Radioactive Cytotoxicity assay (Promega, Spain, Madrid). Shortly, following manufacturer's instructions, both cell lines were seeded at a density of 1.5×10^4 cells/well into 96-well plates. Then, 24 h after, cells were treated with increasing concentrations of PCCDs for 48 h (Vero cells) and 6 days (MRC-5 cells), again to ensure no toxicity during inhibition experiments. Afterwards, cells were lysed for 45 min at 37 °C in 0.9% Triton X-100 (Promega, Madrid, Spain). Then, 50 µL of LDH reagent (Promega, Spain, Madrid) were added and incubated in the dark for 30 min at room temperature. Absorbance was recorded in a Synergy 4 plate reader at 490 nm. The culture medium was used as a non-treated control. Measurements were performed in triplicate.

2.6. Confocal Microscopy

Internalization of cationic dendrimers into Vero and MRC-5 cells was studied by confocal microscopy using a Leica TSC SPE Confocal Microscope (Leica, Wetzalar, Germany). Vero and MRC-5 cells were seeded at a density of 1.75×10^5 and 8×10^4 cells, respectively, in 12 mm circle cover slips (Thermo Fisher Scientific, Waltham, MA, USA) pre-treated with poly-L-Lysine (Sigma, St Louis, MO, USA). Cells were treated with the maximum non-toxic concentrations of FITC-labelled PCCDs (G2-SN15-PEG FITC and G3-SN31-PEG FITC) for 2 h, 6 h and 24 h at 37 °C. After incubation, cells were rinsed with 3% bovine serum albumin (BSA, Sigma, St Louis, MO, USA) phosphate buffered saline (PBS, Lonza, Base, Switzerland). Cell fixation was performed with 4% paraformaldehyde (PFA, Panrea, Barcelona, Spain) for 15 min and permeabilization with 0.1% Triton 100X (Sigma, St Louis, MO, USA) for 15 min. Actin labelling was carried out by incubating cells with Alexa Fluor® 555 Phalloidin (Thermo Fisher Scientific, Waltham, MA, USA) for 1 h at room temperature (RT). Following two rinses with 3% BSA PBS, cells were incubated with 4′,6-Diamidino-2-phenylindole dihydrochloride (DAPI, Sigma, St Louis, MO, USA) for nuclear visualization. Lastly, cells were mounted in microscope slides (Dako, Carpinteria, CA, USA) with fluorescent mounting media (Dako, Carpinteria, CA, USA). ImageJ (National Institutes of Health, Bethesda, MD, USA) was used to analyse the images.

2.7. Flow Cytometry

Flow cytometry was used to confirm the internalization of FITC labelled dendrimers into both cell lines. Briefly, Vero and MRC-5 cells were seeded at a density of 1.75×10^5

and 6×10^4 cells, respectively, in 24 well-plates and treated with 1 μM G2-SN15-PEG FITC and 0.5 μM G3-SN31-PEG FITC for 1 h, 2 h, 6 h and 24 h. Viable cells were identified using LIVE/DEAD™ Fixable Aqua Dead Cell Stain (Thermo Fisher Scientific, Waltham, MA, USA). Lastly, cells were fixed with 3% paraformaldehyde. Flow cytometry was performed on a Galios (Beckman Coulter, Brea, CA, USA). Kaluza software 2.1 (Beckman Coulter, Brea, CA, USA) was used for the analysis of the measurements.

2.8. Inhibition Assay

The antiviral activity of the different dendrimers was evaluated performing inhibition experiments by plaque reduction assay. In-brief, Vero and MRC-5 cells were seeded at a density of 1.75×10^5 and 6×10^4 cells/well in 24-well plates, respectively, and incubated at 37 °C for 24 h. Both cell lines were then treated with increasing concentrations from 0.2 μM to the maximum non-toxic of G2-SN15-PEG and G3-SN31-PEG dendrimers for 1 h. In addition, increasing concentrations (from 0.2 μM to 10 μM) of reference treatments Acyclovir or Ganciclovir were used for comparison with current reference treatments. Afterwards, pre-treated Vero and MRC-5 cells were infected with the viral strains HSV-2_{333} and $HCMV_{AD\text{-}169}$, respectively, at a multiplicity of infection (MOI) of 0.001. Three hours after infection, cells were washed with PBS to remove unabsorbed viruses. HSV-2 infection remained in DMEM supplemented with 2% FBS and 0.4% IgG (Berigloblin P, CSL Behring, King of Prussia, PA, USA) for 48 h. HCMV infection remained in EMEM supplemented with 2% FBS for 6 days. Then, medium was removed and both cell lines were stained with 300 mg/L Methylene Blue (Sigma, St Louis, MO, USA) for 30 min (Vero) and 3 h (MRC-5). Inhibition was determined as the reduction of the plaques formed with treatments regarding the infection control. Non-infected and non-treated samples were used as non-treated (NT) and infection controls (IC), respectively.

2.9. Viral Inactivation Assay

To determine if the observed inhibition is a result of the direct interaction of PCCDs with HSV-2 or HCMV, a viral inactivation assay was performed. Briefly, Vero and MRC-5 cells were seeded at a density of 1.75×10^5 and 6×10^4 cells/well in 24-well plates, respectively, and incubated at 37 °C for 24 h. Then, G2-SN15-PEG or G3-SN31-PEG dendrimers at 1 μM were incubated with 175 pfu/mL or 60 pfu/mL of cell free HSV-2_{333} and $HCMV_{AD\text{-}169}$, respectively, for 2 h at 37 °C. After incubation, the mixture was centrifuged at 12,000 rpm for 1 h at 4 °C and the supernatant was discarded; then, the pellet was rinsed with PBS and centrifuged again at 12,000 rpm for 1 h at 4 °C. Afterwards, the supernatant was discarded and replaced either with fresh DMEM supplemented with 2% FBS and added to Vero cells, or fresh EMEM supplemented with 2% FBS and added to MRC-5 cells. Infections were revealed as previously described. Viral disruption positive control was obtained with Triton X-100 at 0.1% and a culture medium was used as a negative control.

2.10. Binding Inhibition Assay

To resolve if the observed HSV-2 or HCMV inhibition is a result of the blockade of cell membrane viral-receptors by PCCDs, a binding inhibition study by plaque reduction assay was performed. Briefly, Vero and MRC-5 cells were seeded at a density of 1.75×10^5 and 6×10^4 cells/well in 24-well plates, respectively, and incubated at 37 °C for 24 h. Then, cells were pre-cooled at 4 °C for 15 min and treated with 1 μM G2-SN15-PEG or G3-SN31-PEG dendrimers for 1 h at 4 °C. Subsequently, cells were infected with 175 pfu/mL or 60 pfu/mL of HSV-2_{333} and $HCMV_{AD\text{-}169}$, respectively, for 2 h at 4 °C. Afterwards, inoculum was discarded and replaced either with fresh DMEM supplemented with 2% FBS and 0.4% IgG in Vero cells, or fresh EMEM supplemented with 2% FBS in MRC-5 cells. Infections were revealed as previously described. Culture medium was used as a negative control.

2.11. HSPG Binding Assay

Heparin competition assay was carried out to study the interactions between PCCDs and HSPGs. To do so, cells were seeded in 24-well plates and incubated for 2 h at 4 °C in PBS with 1 μM G2-SN15-PEG or 0.5 μM G3-SN31-PEG dendrimers in the absence or presence of 10 μg/mL of heparin, a structurally similar molecule [30]. In additional experiments, cells were incubated for 1 h at 37 °C with dendrimers at the same concentration and washed with PBS containing 2.0 M NaCl, known to disrupt the binding to HSPGs [31]. Along with these experiments, cells were pre-treated with 200 mU/mL of heparinase II, acknowledged to inhibit HSPG-dependent binding [32], (Merck Group, Darmstadt, Germany) for 2 h at 37 °C, before incubating for 1 h at 37 °C with dendrimers at this concentration. Assessment of the amounts of cell-associated dendrimers after these studies was done by evaluating the mean fluorescence intensity (MFI) of dendrimers in cells by flow cytometry, as described in its corresponding section.

2.12. Surface Plasmon Resonance

Surface plasmon resonance (SPR) was conducted to study the capacity of dendrimers to bind to heparin/HSPGs. Measurements were performed on a BIAcore X100 instrument (Cytiva, Marlborough, MA, USA) using a research grade sensor chip SA (Cytiva, Marlborough, MA, USA) whose surface consists of a carboxy methylated dextran matrix pre-immobilized with streptavidin. One cell of the sensor chip was conditioned with three consecutive 1-min injections of 1.0 M NaCl in 50 mM NaOH; then, heparin biotinylated at its reducing end diluted in 10 mM HEPES buffer, pH 7.4, containing 150 mM NaCl, 3 mM EDTA, and 0.005% surfactant P20 (HBS-EP) was injected for 8 min at a flow rate of 10 μL/min, allowing the immobilization of 134.1 resonance units (RU) (equal to 9.8 fmol/mm^2) of the GAG. Then, the heparin-containing flow cell was over-coated by injecting biotinylated BSA re-suspended in HBS-EP for 8 min at a flow rate of 10 μL/min, allowing immobilization of 104 RU (equal to 1.6 fmol/mm^2) of the protein, expected to help mask the residual aspecific negatively charged binding site available on the surface. The remaining flow cell of the sensor chip was coated only with biotinylated BSA protein as described above, allowing the immobilization of 569.2 RU (equal to 8.6 fmol/mm^2) of protein, and used to evaluate the nonspecific binding and for blank subtraction. For the study of their interaction with heparin, dendrimers G2-SN15-PEG and G3-SN31-PEG were re-suspended in HBS-EP and injected at increasing concentrations over the heparin and control BSA flow cells for 3 min (to allow their association with immobilized molecules) and then washed. After every run, the sensor chip was regenerated by injection of 2.0 M NaCl to detach the dendrimers that tend to remain bound to the biosensor surfaces. The dissociation constant (Kd, that is inversely proportional to the affinity binding) was calculated by fitting with the Scatchard's equation for the plot of RU measured at equilibrium as a function of the ligand concentration in solution. All fitting was performed by a least-square minimization procedure based on the Levemburg–Marquardt algorithm. To evaluate the specificity of the binding of the compounds to surface-immobilized heparin, the compounds (0.75 μM) were injected onto the biosensor in the presence of a molar excess (5 mg/mL) of free heparin.

2.13. Statistics

The different statistical analyses were performed using GraphPad software Prism v.5.0 (GraphPad Software, San Diego, CA, USA). Data were obtained from two or three independent experiments performed by duplicate or triplicate. Data with two or three replicates are displayed as bars ± SD. A p-value of ≤ 0.05 was considered statistically significant (* $p < 0.05$; ** $p < 0.005$; *** $p < 0.001$).

3. Results

3.1. Cytotoxicity of the Dendrimers on Vero and MRC-5 Cell Lines

Evaluation of the cytotoxicity of the different dendrimers (G2-SN15-PEG, G3-SN31-PEG, G2-SN15-PEG FITC and G3-SN31-PEG FITC) in both cell lines was assessed by

nificant (* $p < 0.05$; ** $p < 0.005$; *** $p < 0.001$).

3. Results

3.1. Cytotoxicity of the Dendrimers on Vero and MRC-5 Cell Lines

Evaluation of the cytotoxicity of the different dendrimers (G2-SN15-PEG, G3-SN31-PEG, G2-SN15-PEG FITC and G3-SN31-PEG FITC) in both cell lines was assessed by mitochondrial toxicity determination by the MTT assay and by membrane integrity by the LDH assay. Briefly, in both assays, Vero and MRC-5 cells were treated with increasing concentrations of dendrimers from 0.01 to 30 µM for 48 h and 6 days, respectively. Concentrations were considered non-toxic when the survival rate was ≥80%.

Results obtained from the MTT assay (Figure 1A,B) were more restrictive than those obtained from the LDH assay (Figure 1C,D), therefore we considered those results for the determination of the working concentrations. Non-toxic concentrations of the dendrimers for both cell lines are as follows: 1 µM, 1 µM, 1 µM and 0.5 µM for G2-SN15-PEG, G3-SN31-PEG, G2-SN15-PEG FITC and G3-SN31-PEG FITC, respectively.

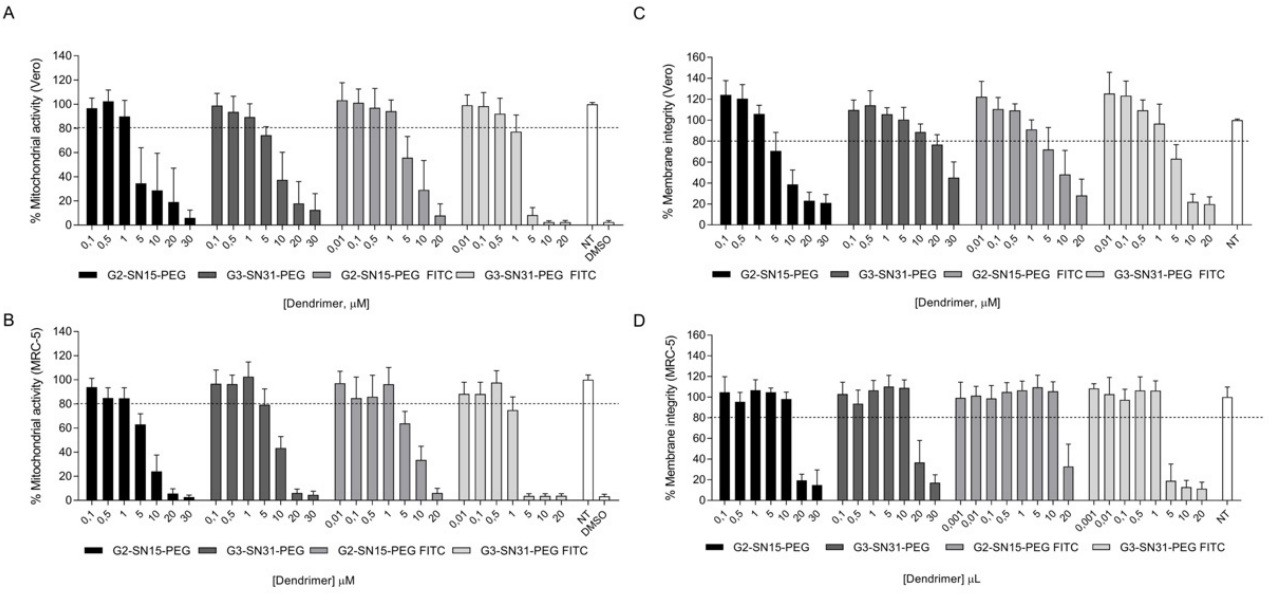

Figure 1. Cytotoxicity of dendrimers by 3-(4-5-dimethylthiazol-2-yl)-2,5-diphenyltetrazolium bromide (MTT) and lactate dehydrogenase (LDH) assay. (**A**,**B**) MTT assay; (**C**,**D**) LDH assay. (**A**,**C**) Vero and (**B**,**D**) MRC-5 cells were treated with increasing concentrations of dendrimers G2-SN15-PEG, G3-SN31-PEG, G2-SN15-PEG fluorescein isothiocyanate (FITC) labeled and G3-SN31-PEG FITC from 0.01 to 30 µM. Non-toxic concentrations were established when cell viability was ≥80%. Culture medium was used as cell viability control and DMSO 10% was used as death control. Data are represented as mean ± SD of three individual experiments performed in triplicate. NT: non-treated; DMSO: dimethylsulfoxide.

Figure 1. Cytotoxicity of dendrimers by 3-(4-5-dimethylthiazol-2-yl)-2,5-diphenyltetrazolium bromide (MTT) and lactate dehydrogenase (LDH) assay. (**A**,**B**) MTT assay; (**C**,**D**) LDH assay. (**A**,**C**) Vero and (**B**,**D**) MRC-5 cells were treated with increasing concentrations of dendrimers G2-SN15-PEG, G3-SN31-PEG, G2-SN15-PEG fluorescein isothiocyanate (FITC) labeled and G3-SN31-PEG FITC from 0.01 to 30 µM. Non-toxic concentrations were established when cell viability was ≥80%. Culture medium was used as cell viability control and DMSO 10% was used as death control. Data are represented as mean ± SD of three individual experiments performed in triplicate. NT: non-treated; DMSO: dimethylsulfoxide.

3.2. Internalization Study into Vero and MRC-5 Cells

We examined the capacity of FITC-labelled dendrimers to internalize into Vero and MRC-5 cell lines by confocal microscopy and flow cytometry. The sequence of the internalization process was studied by incubating both cell lines with either 1 µM G2-SN15-PEG FITC or 0.5 µM G3-SN31-PEG FITC dendrimers for 1 h, 2 h, 6 h or 24 h. To deepen its distribution, in confocal microscopy studies, actin filaments and the nucleus were labelled with phalloidin and DAPI, respectively.

Entry analyses of both cell lines indicated that the G2-SN15-PEG FITC dendrimer has faster uptake dynamics than the G3-SN31-PEG FITC dendrimer, since it showed a significant increase of fluorescent positive cells after the first hour of incubation compared with the control (14% in Vero and 26% in MRC5) (Figures 2a and 3a). In addition, the amount of positive fluorescent marks from both dendrimers showed an important increase along time points. The increment of signal in Vero cells from 1 h to 24 h from the G2-SN15-PEG FITC dendrimer was evident (45%), whilst for the G3-SN31-PEG FITC dendrimer it was not so remarkable (20%). In MRC-5 cells, both dendrimers showed a 30% increase in the number of positive cells from the first time point studied to the last.

icant increase of fluorescent positive cells after the first hour of incubation compared with the control (14% in Vero and 26% in MRC5) (Figures 2a and 3a). In addition, the amount of positive fluorescent marks from both dendrimers showed an important increase along time points. The increment of signal in Vero cells from 1 h to 24 h from the G2-SN15-PEG FITC dendrimer was evident (45%), whilst for the G3-SN31-PEG FITC dendrimer it was not so remarkable (20%). In MRC-5 cells, both dendrimers showed a 30% increase in the number of positive cells from the first time point studied to the last.

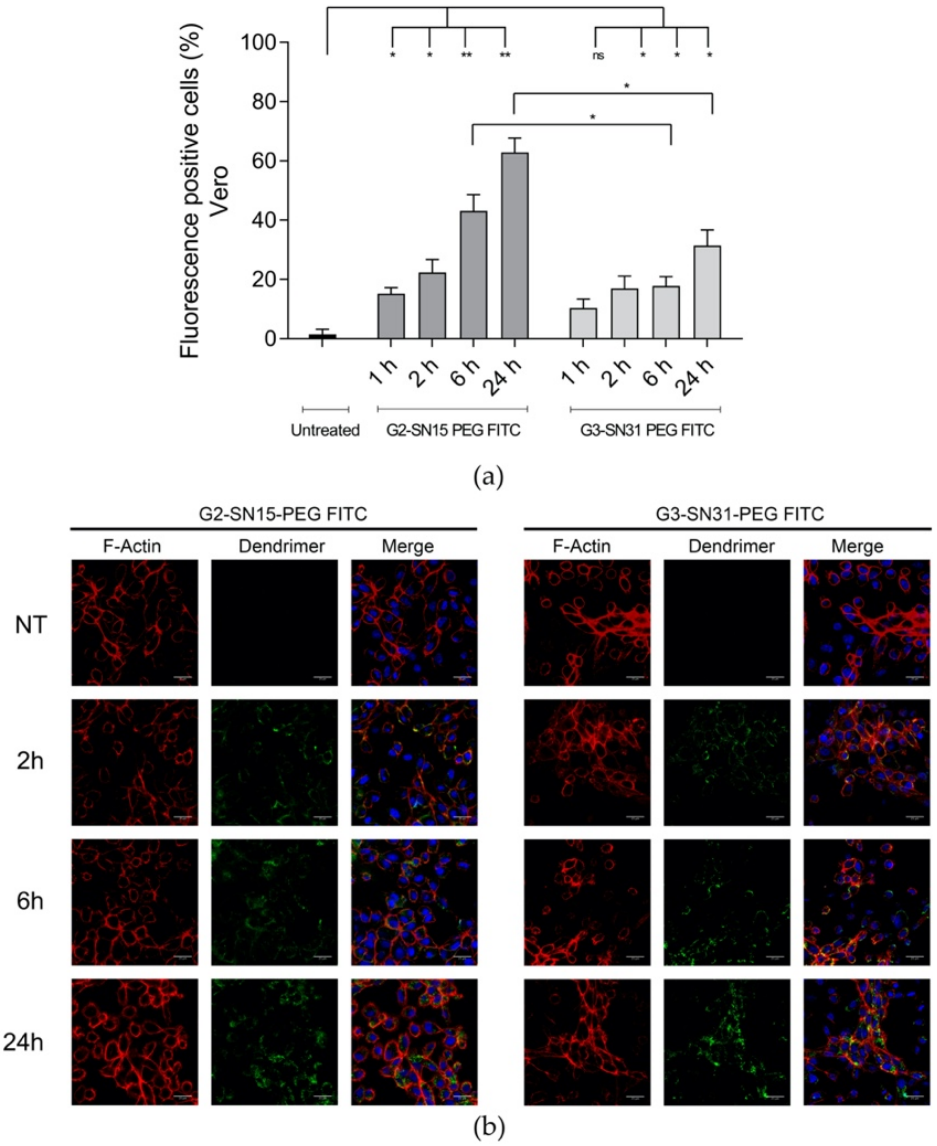

Figure 2. Internalization study of cationic dendrimers into Vero cells. (**a**) Percentage of FITC-positive cells observed by flow cytometry 1 h, 2 h, 6 h and 24 h post-treatment. Data are represented as mean ± SD of two individual experiments. (**b**) Representative confocal images of cells incubated with 1 µM G2-SN15-PEG FITC and 0.5 µM G3-SN31-PEG FITC dendrimers (green) for 2 h, 6 h or 24 h. Phalloidin was used to mark actin filaments (red) and DAPI for nucleus (blue). Scale bars indicate a length of 25 µm. (* $p < 0.05$; ** $p < 0.01$; ns: non-significant). DAPI: 4′,6-diamidino-2-phenylindole dihydrochloride.

Figure 2. Internalization study of cationic dendrimers into Vero cells. (**a**) Percentage of FITC-positive cells observed by flow cytometry 1 h, 2 h, 6 h and 24 h post-treatment. Data are represented as mean ± SD of two individual experiments. (**b**) Representative confocal images of cells incubated with 1 µM G2-SN15-PEG FITC and 0.5 µM G3-SN31-PEG FITC dendrimers (green) for 2 h, 6 h or 24 h. Phalloidin was used to mark actin filaments (red) and DAPI for nucleus (blue). Scale bars indicate a length of 25 µm. (* $p < 0.05$; ** $p < 0.01$; ns: non-significant). DAPI: 4′,6-diamidino-2-phenylindole dihydrochloride.

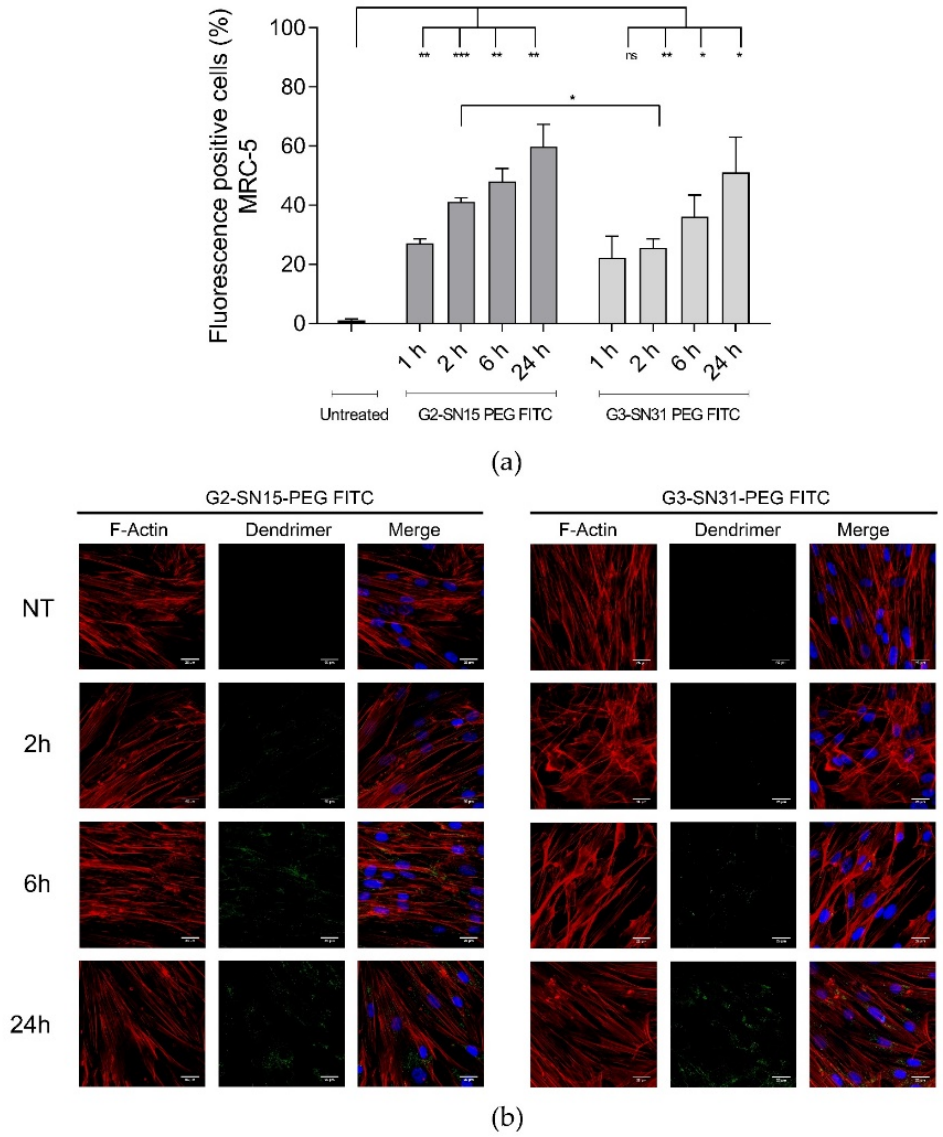

Figure 3. Internalization study of cationic dendrimers into MRC-5 cells. (**a**) Percentage of FITC-positive cells observed by flow cytometry 1 h, 2 h, 6 h and 24 h post-treatment. Data are represented as mean ± SD of two individual experiments. (**b**) Representative confocal images of cells incubated with 1 µM G2-SN15-PEG FITC and 0.5 µM G3-SN31-PEG FITC dendrimers (green) for 2 h, 6 h or 24 h. Phalloidin was used to mark actin filaments (red) and DAPI for nucleus (blue). Scale bars indicate a length of 25 µm. (* $p < 0.05$; ** $p < 0.01$; *** $p < 0.001$; ns: non-significant). DAPI: 4′,6-diamidino-2-phenylindole dihydrochloride.

A more detailed study of the fluorescent distribution in both Vero and MRC-5 cells indicated that both dendrimers have a modified distribution pattern depending on the time elapsed from the initial distribution: short times of incubation showed peripheral distribution (co-localizing with F-actin), while longer times showed dendrimers to be in more internal regions with a punctate intracellular distribution (Figures 2b and 3b). To summarize, both dendrimers can rapidly interact with the surface of both cell lines and be internalized into both Vero and MRC-5 cell lines, where they remain concentrated in a granular manner.

3.3. Anti-HSV-2 and HCMV Activity of the Dendrimers

Inhibition experiments were performed to determine the antiviral activity of the non-labelled dendrimers from HSV-2 and HCMV infections. Vero and MRC-5 cell lines were

treated with increasing concentrations of G2-SN15-PEG and G3-SN31-PEG dendrimers from 0.2 μM to the maximum non-toxic concentration (1 μM) one hour prior to infection with 0.001 MOI of $HSV\text{-}2_{333}$ and $HCMV_{AD\text{-}169}$. In addition, Acyclovir and Ganciclovir were used to compare our results with these reference treatments. After 48 h (Vero) and 6 days (MRC-5) of incubation, lysis plaques were revealed by methylene blue staining.

Results shown in Figure 4a,b indicate that both G2-SN15-PEG and G3-SN31-PEG dendrimers are able to inhibit HSV-2 and HCMV infections at the maximum non-toxic concentrations. In both cases, the G3-SN31-PEG dendrimer presented better inhibition results at all tested concentrations, achieving values of 99% and 86% for HSV-2 and HCMV, respectively, at the maximum non-toxic concentration. Interestingly, both dendrimers present significantly better inhibition results than the actual reference treatments Acyclovir and Ganciclovir at their maximum non-toxic concentration.

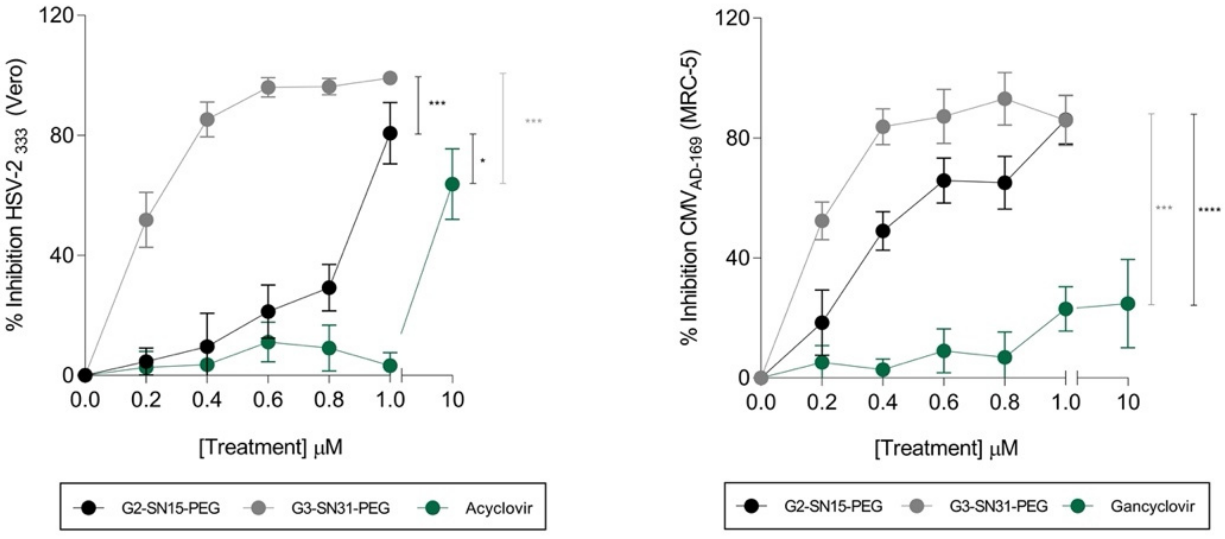

Figure 4. Antiviral activity of cationic dendrimers. Inhibition of herpes simplex virus-2 (HSV-2) (a) and human cytomegalovirus (HCMV) (b) infections by increasing concentrations of G2-SN15-PEG and G3-SN31-PEG dendrimers in Vero and MRC-5 cell lines, respectively. Acyclovir or Ganciclovir were used for comparison with reference treatments. Infection was measured by plaque reduction assay. Data are represented as mean ± SD of three individual experiments performed in triplicate (* $p < 0.05$; *** $p < 0.001$; **** $p < 0.0001$).

3.4. Cationic Dendrimers Prevent HSV-2 and HCMV at First Infection Stages

After demonstrating that both dendrimers have anti-HSV-2 and anti-HCMV activity, we proceeded to delve into the mechanism through which they carried out this activity. To do so, we studied two different mechanisms: viral inactivation (VI) and binding inhibition (BI). Briefly, for viral inactivation, dendrimers were incubated with cell-free HSV-2 or HCMV for 2 h at 37 °C. After two rounds of ultracentrifugation, the supernatant was added to cells. For binding inhibition, cells were pre-cooled at 4 °C for 15 min and treated with dendrimers for 1 h at 4 °C, then cells were infected for 2 h at 4 °C. After (Vero) and 6 days (MRC-5) of incubation, lysis plaques were revealed by methylene blue staining.

Figure 5a,b indicate that both dendrimers can significantly inhibit viral binding to both cell lines, obtaining similar inhibition values as the ones obtained in the antiviral activity study. On the other hand, G2-SN15-PEG and G3-SN31-PEG dendrimers are only able to inactivate HCMV and obtain lower inhibition values. These results suggest that inhibition is achieved at the first infection stages, most probably by impeding viral attachment to the cell membrane, thus preventing infection.

inhibition is achieved at the first infection stages, most probably by impeding viral attachment to the cell membrane, thus preventing infection.

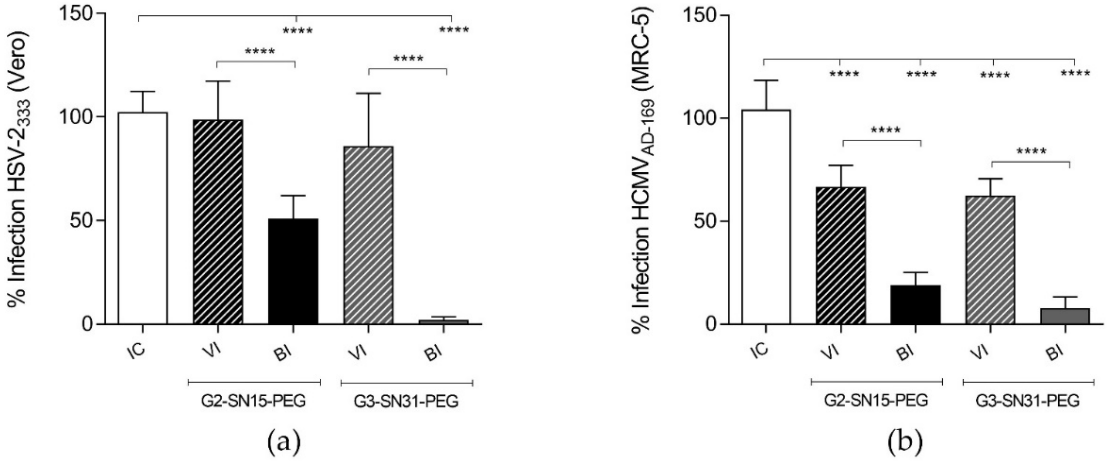

Figure 5. Antiviral mechanism of PEGylated cationic dendrimers. Effect of cationic dendrimers G2-SN15-PEG and G3-SN31-PEG at the maximum non-toxic concentration on HSV-2 (**a**) and HCMV (**b**) infectivity and binding. Viral inactivation (VI) and binding inhibition (BI) assays were performed, and results were measured by plaque reduction assay. Data are represented as mean ± SD of three individual experiments performed in triplicate. **** $p < 0.001$.

3.5. Determination of Surface Membrane Interactions

Due to the cationic nature of PCCDs, we wondered if their inhibition potential depends on their capacity to bind to anionic HSPGs, hence preventing the binding of the virus to these receptors. To evaluate this possibility, different binding assays were carried out, starting with a competition assay with heparin, a structural analogue of HSPGs. Briefly, cells were treated with G2-SN15-PEG or G3-SN31-PEG dendrimers in the absence or presence of heparin. Alternatively, cells were treated with those dendrimers and washed with 2 M NaCl, a treatment known to detach basic proteins bound to heparin/HSPGs [27]. In other experiments, cells were pre-treated with heparinase II before incubation with dendrimers. After performing these assays, either the percentage of fluorescence positive cells or the mean fluorescence intensity (MFI) of the dendrimers was measured to infer the remaining amounts of cell-associated dendrimers.

Results shown in Figure 6a,b demonstrate that HSPGs play a prominent role in the interaction of PCCDs with the cell surface. This can be observed in the remarkable drop in the number of cell-associated dendrimers (both G2-SN15-PEG FITC and G3-SN31-PEG FITC dendrimers) in both cell lines after treatment with heparin. These interactions were also partially disrupted when washing with 2 M NaCl, but, despite a remarkable reduction of the number of cell-associated dendrimers in all samples, differences were only significant for the G2-SN15-PEG FITC dendrimer in the Vero cell line and for the G3-SN31-PEG FITC dendrimer in the MRC-5 cell line. In the heparinase assay, Figure 6c,d indicates a notable decrease of binding capacity of dendrimers after treatment with heparinase II, observed in the notorious decline of the MFI in every sample; however, this decrease was only statistically significant for the G2-SN15-PEG FITC in the Vero cell line.

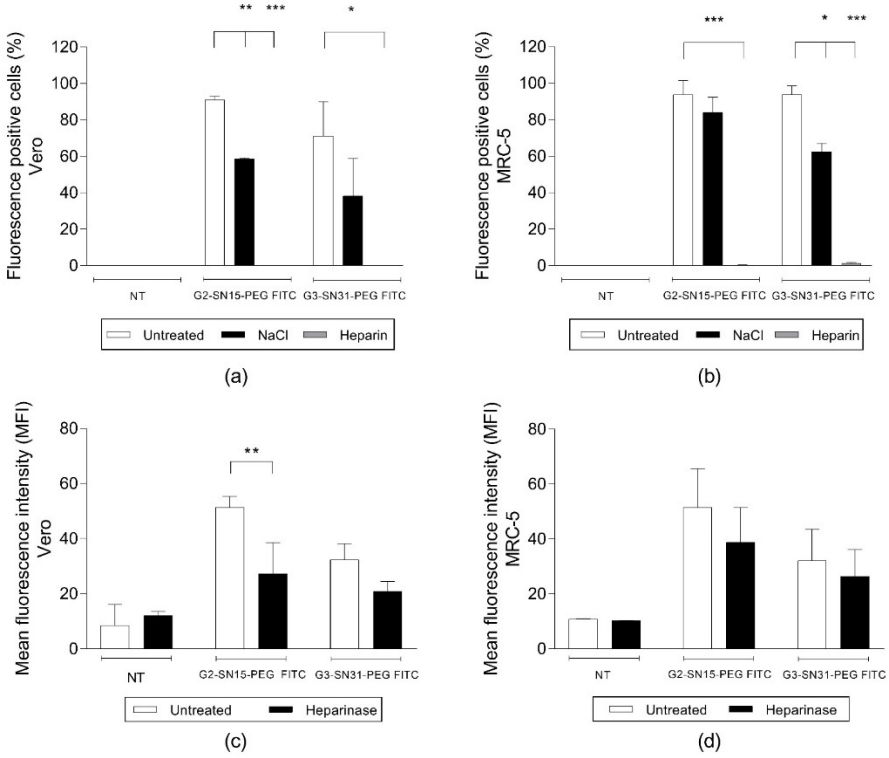

Figure 6. Interaction of cationic dendrimers with cell surface heparan sulphate proteoglycans (HSPGs). Fluorescent positive cells and mean fluorescence intensity of G2-SN15-PEG FITC and G3-SN31-PEG FITC dendrimers measured by flow cytometry in Vero (**a**,**c**) and MRC-5 (**b**,**d**) cells. Heparin competition assay, NaCl wash, and heparinase II treatment experiments were performed to determine the interaction of PEGylated cationic carbosilane dendrimers (PCCDs) with cell surface HSPGs. Data are represented as mean ± SD of two individual experiments * $p < 0.05$; ** $p < 0.01$; *** $p < 0.001$.

Due to the strong structural analogy existing between heparin and HSPGs, a surface plasmon resonance (SPR) biosensor containing immobilized heparin represents a simplified "cell-free" model that resembles the interaction of proteins or synthetic compounds to cell-associated HSPGs in vivo [33] that we have thus exploited to additionally evaluate the heparin/HSPGs binding capacity of PCCDs. As shown in Figure 7a,b, despite a significant aspecific binding to the BSA-containing surface (here used as a negative control), both dendrimers showed a significant specific binding to surface-immobilized heparin. The overlay of blank-subtracted sensorgrams obtained by injecting the dendrimers at increasing concentrations onto the sensor chip demonstrated a dose-response binding. Additionally, it is apparent that the binding of the dendrimers to heparin is very stable since they do not detach spontaneously from heparin at the end of the injection phase and can be removed only by a high salt washing (Figure 7c,d). From these sensorgrams, the values of binding at equilibrium of the dendrimers were used to obtain the dose-response curves shown in Figure 7e,f, and to calculate Kd values. Both G2-SN15-PEG and G3-SN31-PEG dendrimers bind surface-immobilized heparin in a saturable manner with a relatively high affinity (Kd in the high nanomolar, Table 2). The specificity of the binding is demonstrated by the fact that a molar excess of heparin completely abolishes the binding of the dendrimers to surface-immobilized heparin (Figure 7e,f).

Pharmaceutics **2022**, *14*, x FOR PEER REVIEW 13 of 17

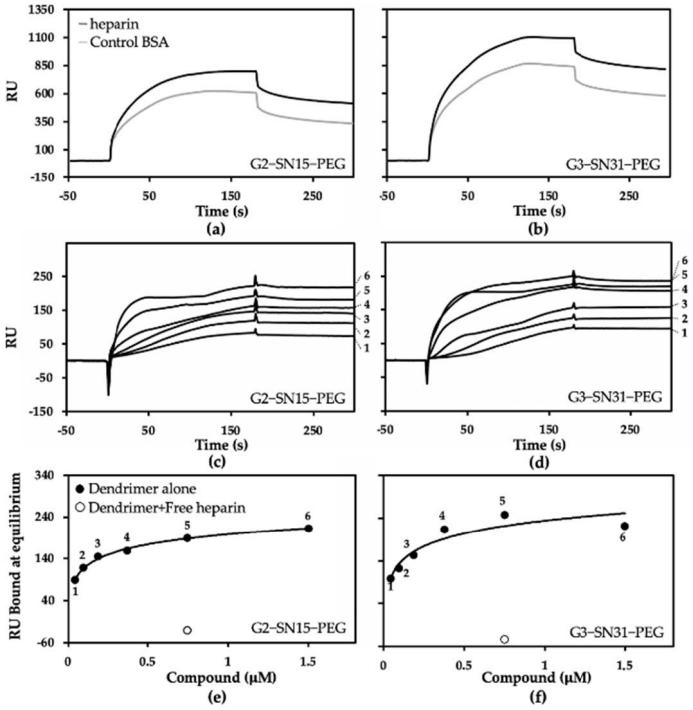

Figure 7. Surface plasmon resonance (SPR) analysis of G2-SN15-PEG- and G3-SN31-PEG-heparin interaction. (**a**,**b**) Sensorgrams showing the binding of G2-SN15-PEG and G3-SN31-PEG dendrimers (0.75 μM) to the heparin- or BSA-coated flow cells. (**c**,**d**) Blank-subtracted sensorgram overlays showing the specific binding of increasing concentrations of the dendrimers (1: 0.047 μM; 2: 0.094 μM; 3: 0.188 μM; 4: 0.375 μM; 5: 0.75 μM; 6: 1.5 μM) to surface-immobilized heparin. The response (in resonance units, RU) was recorded as a function of time. (**e**,**f**) Saturation curves obtained using the values of RU bound at equilibrium from panels (**c**,**d**). Result of the competition assay with free heparin is also reported.

Table 2. Kd values of the interactions of G2-SN15-PEG and G3-SN31-PEG dendrimers to heparin. Data corresponds to mean ± SEM of three individual experiments.

Dendrimer	Kd (nM) at Equilibrium
G2-SN15-PEG	368.3 ± 108.1
G3-SN31-PEG	186.7 ± 82.6

4. Discussion

Years of research on the host entry mechanism of viruses from the *Herpesviridae* family has led to the conclusion that, despite the extensive cell tropism that they exhibit, host cell infection takes place through a conserved mechanism [4]. The entry machinery is formed by a conserved core fusion machinery (formed the heterodimer gH-gL and the fusion protein gB) and by divergent proteins such as gD for HSV-2 or gO for HCMV [34,35]. The latter act as ligands that bind to different host cell receptors, being the first step of the entry process the interaction with distinct classes of HSPGs located on the exterior surface of target cells [36]. This critical role makes HS a therapeutic target to develop novel inhibitors of HS-mediated binding and subsequent infection of herpesviruses.

In this sense, we have studied the therapeutic effect of the use of the novel G2-SN15-PEG and G3-SN31-PEG dendrimers to prevent HSV-2 and HCMV infections based on their specific structures. Two characteristics of the periphery of these PCCDs makes them relevant candidates: (i) the presence of positively charged functional groups, which compete for electrostatic binding with viral glycoproteins; and (ii) the presence of PEGylation residues, which improves the biocompatibility of the dendrimers, thus reducing toxicity [37,38].

The initial phase of this study was the assessment of the cytotoxicity of dendrimers in both Vero and MRC-5 cell lines, and to do so, MTT and LDH assays were performed. Toxicity of PCCDs is a consequence of the positively charged groups in their periphery, which interacts with the negatively charged cell membrane producing nanoscale pores that affect its integrity to a point that depends on characteristics of dendrimers such as their molecular weight or the presence of fluorescent labels [39]. Masking of some of these peripheric groups was achieved by conjugation of the dendrimers with polyethylene glycol (PEG), which has previously proved to reduce immunogenicity and toxicity [40]. Results of our studies indicated that some concentrations, despite not compromising membrane integrity, had negative effects on mitochondrial activity; therefore, we selected the values from the MTT assay greater than 80% as working concentrations. No notable differences between G2-SN15-PEG, G3-SN31-PEG and G2-SN15-PEG FITC dendrimers were observed. However, G3-SN31-PEG FITC was the dendrimer presenting the highest toxicity, suggesting that larger molecular sizes and the addition of this fluorescent label enhanced the cytotoxicity of this nanostructure.

The next step was to examine the capacity of FITC-labelled dendrimers to internalize into both cell lines by confocal microscopy and flow cytometry. Entry analyses revealed that the G2-SN15-PEG FITC dendrimer has faster uptake dynamics in both cell lines than the G3-SN31-PEG FITC dendrimer; in addition, the amount of positive fluorescent marks from both dendrimers presented an important increase along time points. Study of the fluorescent distribution showed that short times of incubation resulted in peripheral distribution, while longer times suggested that dendrimers were in more internal regions in a granular manner. This agrees with previous studies demonstrating that the size and surface charge of dendrimers influence their effectiveness of crossing cell membranes [41,42]. Our results reflect that the presence of more positive charges in the G3-SN31-PEG FITC dendrimer for being a larger molecule entailed higher affinity and stronger interactions with the cell surface, leading to longer resident times on the cell membrane, resulting in slower internalization.

We next delved into the ability of dendrimers to inhibit HSV-2 and HCMV infections. Antiviral activity studies revealed that both studied PCCDs can inhibit these infections, with better inhibition performance than the actual reference treatments Acyclovir and Ganciclovir. In addition, we investigated the mechanism through which inhibition was achieved and results demonstrate that both dendrimers can significantly inhibit viral binding to Vero and MRC-5 cell lines; however, they are only able to directly neutralize HCMV itself and with lower inhibition values. All these results together indicate that dendrimers perform inhibition at the first stages of the infection. The fact that the G3-SN31-PEG FITC dendrimer, which has longer resident times on the cell membrane, shows better inhibition results supports this idea that inhibition is achieved by impediment of viral attachment to the cell membrane, thereby preventing further infection.

To determine how the impediment of viral attachment takes place, we performed different analysis of the interactions of PCCDs with the receptors involved in the first stages of infection of viruses from the *Herpesviridae* family, namely the HS chains of HSPGs [36]. To do so, we started with a cell culture-based heparin competition assay, followed by 2M NaCl washing, heparinase II treatment, and "cell free" surface plasmon resonance. The first assay is based on the fact that heparin is a GAG with a similar structure to HS, thus likely able to act as an antagonist of HSPGs present on cell membranes for the binding to cationic dendrimers, leading to the observed absence of cell-associated PCCDs in both cell lines [30]. In addition, the disruption of this dendrimer-cell membrane interaction was also noticed both in Vero and MRC-5 cell lines when washing with 2.0 M NaCl, a treatment known to remove cationic molecules from cell membrane HSPGs [27]. Furthermore, digestion of the GAG moiety of HSPGs by heparinase II also lead to a notable decrease of the capacity of PCCDs to bind to cells, determined by the shift in fluorescence intensity of dendrimers in both cell lines. However, it is important to mention that there might be alternative binding sites for the dendrimers which would explain the residual amounts

of dendrimers associated to cells after the performed treatments. On the other hand, SPR analysis demonstrated that these dendrimers are effectively able to bind surface-immobilized heparin (here used as a surrogate of cell-associated HSPGs) in a stable and specific way, hence with a relatively high affinity.

5. Conclusions

In conclusion, we can state that G2-SN15-PEG and G3-SN31-PEG dendrimers are promising therapies to face HSV-2 and HCMV infections. Biocompatibility and entry studies confirmed the suitability of these dendrimers to be used in target cells of these infections. Binding assays confirm that the studied dendrimers effectively compete with HSV-2 and HCMV for adsorption on the receptors involved in the first stages of infection of susceptible cells, leading to the impediment of viral attachment and thus producing the inhibition of these viral infections.

Author Contributions: Conceptualization, M.Á.M.-F. and J.L.J.; methodology, E.R.-R., V.M.-C., M.M., R.G. and T.L.-C.; software, M.R. and M.M.; validation, M.Á.M.-F., J.L.J. and M.R.; formal analysis, M.Á.M.-F., J.L.J., E.R.-R. and M.R.; investigation, M.Á.M.-F., J.L.J., E.R.-R., V.M.-C.; M.R., M.M., R.G. and T.L.-C.; resources M.Á.M.-F. and J.L.J.; data curation, M.Á.M.-F., J.L.J., E.R.-R., V.M.-C.; M.R. and M.M.; writing—original draft preparation, M.Á.M.-F., J.L.J. and E.R.-R.; writing—review and editing, M.Á.M.-F., J.L.J., E.R.-R., M.R., R.G. and T.L.-C.; provision of dendrimers, R.G. and T.L.-C.; supervision, M.Á.M.-F. and J.L.J.; project administration, M.Á.M.-F. and J.L.J.; funding acquisition, M.Á.M.-F. and J.L.J. All authors have read and agreed to the published version of the manuscript.

Funding: This research was funded by Instituto de Salud Carlos III and Fondo Europeo de Desarrollo Regional (FEDER), RETIC PT17/0015/0042, Fondo de Investigaciones Sanitarias (FIS) (grant number PI19/01638) and the EPIICAL project. This work has been partially supported by a EUROPARTNER: Strengthening and spreading international partnership activities of the Faculty of Biology and Environmental Protection for interdisciplinary research and innovation of the University of Lodz Programme: NAWA International Academic Partnership Programme. This article/publication is based upon work from COST Action CA 17140 "Cancer Nanomedicine from the Bench to the Bedside" supported by COST (European Cooperation in Science and Technology).

Institutional Review Board Statement: Not applicable.

Informed Consent Statement: Not applicable.

Data Availability Statement: Not applicable.

Acknowledgments: We would like to thank R. Samaniego from the Confocal Unit of HGUGM for confocal samples analysis, and L. Diaz of the Flow Cytometry Unit for her technical assistance as flow cytometry technician.

Conflicts of Interest: The authors declare no conflict of interest.

References

1. Ryan, K.J.; Ahmad, N.; Alspaugh, J.A.; Drew, W.L.; Lagunoff, M.; Pottinger, P.; Reller, L.B.; Reller, M.E.; Sterling, C.R.; Weissman, S. *Ryan & Sherris Medical Microbiology*; McGraw-Hill Education: New York, NY, USA, 2021.
2. ICTV. Virus Taxonomy: 2020 Release. Available online: https://talk.ictvonline.org/taxonomy/ (accessed on 30 November 2021).
3. Lan, K.; Luo, M.H. Herpesviruses: Epidemiology, pathogenesis, and interventions. *Virol. Sin.* **2017**, *32*, 347–348. [CrossRef] [PubMed]
4. Sathiyamoorthy, K.; Chen, J.; Longnecker, R.; Jardetzky, T.S. The COMPLEXity in herpesvirus entry. *Curr. Opin. Virol.* **2017**, *24*, 97–104. [CrossRef]
5. Gatherer, D.; Depledge, D.P.; Hartley, C.A.; Szpara, M.L.; Vaz, P.K.; Benko, M.; Brandt, C.R.; Bryant, N.A.; Dastjerdi, A.; Doszpoly, A.; et al. ICTV Virus Taxonomy Profile: Herpesviridae 2021. *J. Gen. Virol.* **2021**, *102*, 001673. [CrossRef] [PubMed]
6. WHO. Herpes Simplex Virus. Available online: https://www.who.int/news-room/fact-sheets/detail/herpes-simplex-virus (accessed on 30 November 2021).
7. Loeffelholz, M.J.; Hodinka, R.L.; Young, S.A.; Pinsky, B. *Clinical Virology Manual*, 5th ed.; American Society Microbiology Press: Washington, DC, USA, 2016.

8. Stockdale, L.; Nash, S.; Nalwoga, A.; Painter, H.; Asiki, G.; Fletcher, H.; Newton, R. Human cytomegalovirus epidemiology and relationship to tuberculosis and cardiovascular disease risk factors in a rural Ugandan cohort. *PLoS ONE* **2018**, *13*, e0192086. [CrossRef] [PubMed]
9. Varani, S.; Landini, M.P. Cytomegalovirus-induced immunopathology and its clinical consequences. *Herpesviridae* **2011**, *2*, 6. [CrossRef] [PubMed]
10. Dietrich, M.L.; Schieffelin, J.S. Congenital Cytomegalovirus Infection. *Ochsner J.* **2019**, *19*, 123–130. [CrossRef] [PubMed]
11. Gomez Toledo, A.; Sorrentino, J.T.; Sandoval, D.R.; Malmstrom, J.; Lewis, N.E.; Esko, J.D. A Systems View of the Heparan Sulfate Interactome. *J. Histochem. Cytochem.* **2021**, *69*, 105–119. [CrossRef] [PubMed]
12. Heldwein, E.E. gH/gL supercomplexes at early stages of herpesvirus entry. *Curr. Opin. Virol.* **2016**, *18*, 1–8. [CrossRef] [PubMed]
13. Osterrieder, K. *Cell Biology of Herpes Viruses*, 1st ed.; Springer: Cham, Switzerland, 2017; p. 224.
14. Connolly, S.A.; Jardetzky, T.S.; Longnecker, R. The structural basis of herpesvirus entry. *Nat. Rev. Microbiol.* **2021**, *19*, 110–121. [CrossRef] [PubMed]
15. Workowski, K.A.; Bachmann, L.H.; Chan, P.A.; Johnston, C.M.; Muzny, C.A.; Park, I.; Reno, H.; Zenilman, J.M.; Bolan, G.A. Sexually Transmitted Infections Treatment Guidelines, 2021. *MMWR Recomm. Rep.* **2021**, *70*, 1–187. [CrossRef] [PubMed]
16. Zachary, K.C. Ganciclovir and Valganciclovir: An Overview. Available online: https://www.uptodate.com/contents/8342 (accessed on 30 November 2021).
17. Al-Badr, A.A.; Ajarim, T.D.S. Ganciclovir. *Profiles Drug Subst. Excip. Relat. Methodol.* **2018**, *43*, 1–208. [CrossRef] [PubMed]
18. Cena-Diez, R.; Vacas-Cordoba, E.; Garcia-Broncano, P.; de la Mata, F.J.; Gomez, R.; Maly, M.; Munoz-Fernandez, M.A. Prevention of vaginal and rectal herpes simplex virus type 2 transmission in mice: Mechanism of antiviral action. *Int. J. Nanomed.* **2016**, *11*, 2147–2162. [CrossRef]
19. Guerrero-Beltran, C.; Prieto, A.; Leal, M.; Jimenez, J.L.; Munoz-Fernandez, M.A. Combination of G2-S16 dendrimer/dapivirine antiretroviral as a new HIV-1 microbicide. *Future Med. Chem.* **2019**, *11*, 3005–3013. [CrossRef]
20. Rodriguez-Izquierdo, I.; Gasco, S.; Munoz-Fernandez, M.A. High Preventive Effect of G2-S16 Anionic Carbosilane Dendrimer against Sexually Transmitted HSV-2 Infection. *Molecules* **2020**, *25*, 2965. [CrossRef] [PubMed]
21. Sepulveda-Crespo, D.; de la Mata, F.J.; Gomez, R.; Munoz-Fernandez, M.A. Sulfonate-ended carbosilane dendrimers with a flexible scaffold cause inactivation of HIV-1 virions and gp120 shedding. *Nanoscale* **2018**, *10*, 8998–9011. [CrossRef] [PubMed]
22. Dias, A.P.; da Silva Santos, S.; da Silva, J.V.; Parise-Filho, R.; Igne Ferreira, E.; Seoud, O.E.; Giarolla, J. Dendrimers in the context of nanomedicine. *Int. J. Pharm.* **2020**, *573*, 118814. [CrossRef] [PubMed]
23. Wu, L.P.; Ficker, M.; Christensen, J.B.; Trohopoulos, P.N.; Moghimi, S.M. Dendrimers in Medicine: Therapeutic Concepts and Pharmaceutical Challenges. *Bioconjug. Chem.* **2015**, *26*, 1198–1211. [CrossRef] [PubMed]
24. Janaszewska, A.; Lazniewska, J.; Trzepinski, P.; Marcinkowska, M.; Klajnert-Maculewicz, B. Cytotoxicity of Dendrimers. *Biomolecules* **2019**, *9*, 330. [CrossRef] [PubMed]
25. Relano-Rodriguez, I.; Munoz-Fernandez, M.A. Emergence of Nanotechnology to Fight HIV Sexual Transmission: The Trip of G2-S16 Polyanionic Carbosilane Dendrimer to Possible Pre-Clinical Trials. *Int. J. Mol. Sci.* **2020**, *21*, 9403. [CrossRef]
26. Royo-Rubio, E.; Rodriguez-Izquierdo, I.; Moreno-Domene, M.; Lozano-Cruz, T.; de la Mata, F.J.; Gomez, R.; Munoz-Fernandez, M.A.; Jimenez, J.L. Promising PEGylated cationic dendrimers for delivery of miRNAs as a possible therapy against HIV-1 infection. *J. Nanobiotechnol.* **2021**, *19*, 158. [CrossRef] [PubMed]
27. Donalisio, M.; Quaranta, P.; Chiuppesi, F.; Pistello, M.; Cagno, V.; Cavalli, R.; Volante, M.; Bugatti, A.; Rusnati, M.; Ranucci, E.; et al. The AGMA1 poly(amidoamine) inhibits the infectivity of herpes simplex virus in cell lines, in human cervicovaginal histocultures, and in vaginally infected mice. *Biomaterials* **2016**, *85*, 40–53. [CrossRef] [PubMed]
28. Guerrero-Beltran, C.; Garcia-Heredia, I.; Cena-Diez, R.; Rodriguez-Izquierdo, I.; Serramia, M.J.; Martinez-Hernandez, F.; Lluesma-Gomez, M.; Martinez-Garcia, M.; Munoz-Fernandez, M.A. Cationic Dendrimer G2-S16 Inhibits Herpes Simplex Type 2 Infection and Protects Mice Vaginal Microbiome. *Pharmaceutics* **2020**, *12*, 515. [CrossRef]
29. Relano-Rodriguez, I.; Espinar-Buitrago, M.S.; Martin-Canadilla, V.; Gomez-Ramirez, R.; Jimenez, J.L.; Munoz-Fernandez, M.A. Nanotechnology against human cytomegalovirus in vitro: Polyanionic carbosilane dendrimers as antiviral agents. *J. Nanobiotechnol.* **2021**, *19*, 65. [CrossRef]
30. Meneghetti, M.C.; Hughes, A.J.; Rudd, T.R.; Nader, H.B.; Powell, A.K.; Yates, E.A.; Lima, M.A. Heparan sulfate and heparin interactions with proteins. *J. R. Soc. Interface* **2015**, *12*, 0589. [CrossRef] [PubMed]
31. Bugatti, A.; Paiardi, G.; Urbinati, C.; Chiodelli, P.; Orro, A.; Uggeri, M.; Milanesi, L.; Caruso, A.; Caccuri, F.; D'Ursi, P.; et al. Heparin and heparan sulfate proteoglycans promote HIV-1 p17 matrix protein oligomerization: Computational, biochemical and biological implications. *Sci. Rep.* **2019**, *9*, 15768. [CrossRef]
32. Alekseeva, A.; Urso, E.; Mazzini, G.; Naggi, A. Heparanase as an Additional Tool for Detecting Structural Peculiarities of Heparin Oligosaccharides. *Molecules* **2019**, *24*, 4403. [CrossRef]
33. Rusnati, M.; Bugatti, A. Surface Plasmon Resonance Analysis of Heparin-Binding Angiogenic Growth Factors. *Methods Mol. Biol.* **2016**, *1464*, 73–84. [CrossRef] [PubMed]
34. Agelidis, A.M.; Shukla, D. Cell entry mechanisms of HSV: What we have learned in recent years. *Future Virol.* **2015**, *10*, 1145–1154. [CrossRef] [PubMed]
35. Nishimura, M.; Mori, Y. Entry of betaherpesviruses. *Adv. Virus Res.* **2019**, *104*, 283–312. [CrossRef] [PubMed]

36. Koganti, R.; Memon, A.; Shukla, D. Emerging Roles of Heparan Sulfate Proteoglycans in Viral Pathogenesis. *Semin. Thromb. Hemost.* **2021**, *47*, 283–294. [CrossRef] [PubMed]
37. Dogra, P.; Martin, E.B.; Williams, A.; Richardson, R.L.; Foster, J.S.; Hackenback, N.; Kennel, S.J.; Sparer, T.E.; Wall, J.S. Novel heparan sulfate-binding peptides for blocking herpesvirus entry. *PLoS ONE* **2015**, *10*, e0126239. [CrossRef] [PubMed]
38. Suk, J.S.; Xu, Q.; Kim, N.; Hanes, J.; Ensign, L.M. PEGylation as a strategy for improving nanoparticle-based drug and gene delivery. *Adv. Drug Deliv. Rev.* **2016**, *99*, 28–51. [CrossRef]
39. Mignani, S.; Rodrigues, J.; Roy, R.; Shi, X.; Cena, V.; El Kazzouli, S.; Majoral, J.P. Exploration of biomedical dendrimer space based on in-vivo physicochemical parameters: Key factor analysis (Part 2). *Drug Discov. Today* **2019**, *24*, 1184–1192. [CrossRef] [PubMed]
40. Thakur, S.; Kesharwani, P.; Tekade, R.K.; Jain, N.K. Impact of pegylation on biopharmaceutical properties of dendrimers. *Polymer* **2015**, *59*, 67–92. [CrossRef]
41. Heyder, R.S.; Zhong, Q.; Bazito, R.C.; da Rocha, S.R.P. Cellular internalization and transport of biodegradable polyester dendrimers on a model of the pulmonary epithelium and their formulation in pressurized metered-dose inhalers. *Int. J. Pharm.* **2017**, *520*, 181–194. [CrossRef] [PubMed]
42. Salatin, S.; Maleki Dizaj, S.; Yari Khosroushahi, A. Effect of the surface modification, size, and shape on cellular uptake of nanoparticles. *Cell Biol. Int.* **2015**, *39*, 881–890. [CrossRef] [PubMed]

FACULTAD DE CIENCIAS
UNIVERSIDAD AUTÓNOMA DE MADRID

IIG-M

Molecular

SaludMadrid

Hospital General Universitario
Gregorio Marañón